Université du Québec
Institut National de la Recherche Scientifique
Centre Energie, Matériaux et Télécommunications

ELECTROCHEMICALLY EXFOLIATED GRAPHENE OXIDES (EGO): ELECTROCHEMICAL PROPERTIES AND APPLICATIONS IN APTASENSORS AND SUPERCAPACITORS

Par

Yuting Lei

Thèse présentée pour l'obtention du grade de Philosophiae Doctor (Ph.D.)
en sciences de l'énergie et des matériaux

Jury d'évaluation

Président du jury et examinateur interne	Prof. Mohamed Mohamedi INRS-ÉMT
Examinateur externe	Prof. Dominic Rochefort Université de Montréal
Examinateur externe	Prof. Philippe Dauphin Ducharme Université de Sherbrooke
Directeur de recherche	Prof. Ana C. Tavares INRS-ÉMT
Codirecteur de recherche	Prof. Jonathan Perreault INRS-AFSB

ACKNOWLEGMENTS

First of all, I would like to extend my sincere gratitude to my supervisor, Prof. Ana C. Tavares, for her patience, motivation, teaching, and continuous support throughout my Ph.D. study. The guidance she provided throughout my research and writing was very helpful. My heartfelt gratitude goes out to her for providing me with opportunities to advance myself, such as attending international conferences, seminars, workshops, and internships, and ensuring I competed in various awards. I have greatly benefited from her advice both in terms of my research and my career. As her student, I feel extremely fortunate.

Meanwhile, I would like to extend my sincere gratitude to my co-supervisor, Prof. Jonathan Perreault, for providing me with substantial guidance and support throughout my Ph.D. journey. Whenever I got stuck, he was always patient and willing to help. He also encouraged me to participate in various awards programs. His presence as my co-supervisor has been a great privilege for me.

I would like to thank the members of my thesis committee Prof. Mohamed Mohamedi, Prof. Dominic Rochefort, and Prof. Philippe Dauphin Ducharme for offering me precious comments and valuable time.

My appreciation goes out to all the lovely members of my group as well. I am honored to be a member of such an inspiring, hardworking, and supportive group. I especially thank Dr. Benjamin D. Ossonon for training me to start my research and suggesting good ideas for my experiments, thank Jiyun Chen for helping me with my experiments, and thank Dr. Cybelle Palma de Oliveira Soares for training and helping me to start my experiments. I also want to thank members of the co-lab, Prof. Marcos R. V. Lanza, Pierre-Luc Trahan, Kamar Daou, Ludmila dos Santos Madalena and Fausto Eduardo Bimbi Junior for their help and for providing me with samples for my research. It is an honor and a pleasure to work with them.

In appreciation, I thank Prof. Mohamedi, Mohamed, Prof. Shuhui Sun, and Prof. Mohamed Siaj for the inspiring classes and presentations given by them. I would like to thank Prof. Mohamedi, Mohamed, and Prof. Fiorenzo Vetrone, for the inspiring conversations with them. Additionally, I would like to thank the technicians and administrators at INRS-EMT for being so courteous and helpful, especially Christophe Chabanier, Catalin Harnagea, Sylvain Gingras, Hélène Tanguay, Michelle Marcotte, and Geneviève Quintal.

Furthermore, I feel lucky to have been able to share life and feelings with many friends at the INRS-EMT center, particularly, Xu Na, Ruiqi Yang, Mengyang Fan, Xin Liu, Minghui Hao, Xianglei

Liu, Ting Yu, Qingzhe Zhang, Xin Chai, Xin Tong, Yong Wang, Chen Wang, Cheng Jiang, Yinming Lai, Qiliang Wei, Fang Dong, Fan Yang, Pei You, Xiaoying Zheng, Faying Li, Wanting He, Daling Cui, and many others.

I would like to thank Jean-Philippe Masse and Gwenal Chamoulaud for their assistance and support throughout the characterization of my samples. As well, I am grateful to Dr. José Miguel García-Martín and Dr. Yves Huttel for their reception and help during my internship in Madrid.

Last but not least, I want to extend my deepest gratitude to my family, my mother Kexian Luo, and father Gang Lei. Words cannot express how grateful I am to my parents, and all the family members for their unconditional love, understanding, and support during my life. I would like to thank Li Shi for his company in my life in Montreal. Although their names never appear in my work, their contributions are undeniable. I love you all.

ABSTRACT

Graphene and its related materials have been extensively studied in recent years due to their unique properties, including high electrical conductivity, high specific surface area, and tunable chemistry (e.g., surface functional groups and heteroatoms doping). Graphene oxide (GO) materials are abundant in surface functional groups like hydroxyl, epoxy, carbonyl, and carboxyl, making them easily functionalize with other molecules or nanoparticles to form new compounds and composites with improved properties. As a result, GO and its composites have been used in a wide variety of applications, including (bio)sensors, supercapacitors, etc. The electrochemical exfoliation of graphite provides a low-cost, quick, and environmentally friendly method for synthesizing GO materials. Electrochemically exfoliated graphene oxide (EGO) materials can be synthesized with a variety of properties (amounts and types of functional groups, defect density, layer density, flake size) by changing the experimental conditions during the electrochemical exfoliation, such as voltage and electrolyte. Moreover, the method can also prepare EGO-based composites or modify EGO surfaces with other molecules in one step. However, as EGO's physicochemical properties have a profound effect on its electrochemical properties, it can be challenging to synthesize and select the correct EGO for a target application. It is therefore crucial to identify a method of selecting EGO materials and to understand the mechanism of graphite electrochemical exfoliation so as to control the structural properties of resulting EGO materials.

First, EGO materials were produced by electrochemical exfoliation of graphite in 0.1 M H_2SO_4, and the effect of the electric field (applied voltage divided by electrode distance) was studied. Raman and XPS analysis revealed two different regimes during synthesis: slow exfoliation kinetics at low voltage vs high $OH^{\bullet}$ radical concentrations at high voltage. Then, we used a platform based on the self-assembly of EGO sheets onto the surface of a glassy carbon electrode (GCE) through a *p*-aminophenyl (AP) linker for the systematic electrochemical characterization of the EGO materials by cyclic voltammetry in 1 mM $[Fe(CN)_6]^{3-/4-}$ to determine electrochemical surface area (ESA) and standard rate constant of electron transfer (k^0). The two parameters scale with each other and are sensitive to the type of EGO, confirming the suitability of the platform used in this work to characterize the EGO materials.

Second, electrochemical cocaine aptasensors based on EGO flakes were investigated. We examined the influence of the following parameters on the sensor's performance: i) the terminal group of the aptamer ($-NH_2$ vs -OH); ii) functionalization of EGO with the aptamer by physical adsorption and covalent immobilization; iii) electrochemical properties of EGO, such as ESA and k^0. The results demonstrate that NH_2-modified cocaine aptamer adsorbed very rapidly and

strongly on EGO flake surfaces, not only making fabrication of the sensing platform simple and quick, but also having very good reproducibility, shelf-life stability, and high sensitivity to cocaine detection, with a 50 nM detection limit. Further, it verified that EGO materials with higher ESA and k^0 exhibit better sensing performance.

Third, electrochemical exfoliation of graphite in the presence of 4-aminebenzoic acid (4-ABA) is used as one-step method to prepare EGO materials functionalized with aminobenzoic acid (EGO-ABA), and their applications to oxygen reduction reaction (ORR) and supercapacitors have been studied. Based on electrochemical studies, EGO-ABA catalysts showed better ORR activity in alkaline medium compared to EGO because of their high oxygenation density, and lower selectivity for the 2-electron process as their carbonyl group content is low. In contrast to EGO, EGO-ABA materials also have a greater specific capacitance, and the materials prepared from exfoliation in 5-ABA/0.1 M H_2SO_4 have a 3x greater specific capacitance than EGO. In addition, the electrode material showed a remarkable cycling capability, losing only 19.4% after 5000 cycles at 50 mVs^{-1}.

Keywords: electrochemically exfoliated graphene oxide (EGO), self-assembly of EGO flakes, electrochemical surface area (ESA), standard rate constant of electron transfer (k^0), electrochemical aptasensor, physical adsorption method, NH_2-modified aptamer, amine oxidation, aminobenzoic acid, supercapacitors.

RÉSUMÉ

Le graphène et ses matériaux associés ont été largement étudiés ces dernières années en raison de leurs propriétés uniques, notamment une conductivité électrique élevée, une surface spécifique élevée et une chimie accordable (par exemple, les groupes fonctionnels de surface et le dopage des hétéroatomes). Les matériaux d'oxyde de graphène (GO) sont abondants dans les groupes fonctionnels de surface du graphène comme l'hydroxyle, l'époxy, le carbonyle et le carboxyle, ce qui les rend facilement fonctionnalisés avec d'autres molécules ou nanoparticules pour former de nouveaux composés et composites aux propriétés améliorées. En conséquence, le GO et ses composites ont été utilisés dans une grande variété d'applications, y compris les (bio)capteurs, les supercondensateurs, etc. L'exfoliation électrochimique du graphite fournit une méthode peu coûteuse, rapide et respectueuse de l'environnement pour synthétiser les matériaux GO. Les matériaux d'oxyde de graphène exfoliés électrochimiquement (EGO) peuvent être synthétisés avec une variété de propriétés (quantités et types de groupes fonctionnels, densité de défauts, densité de couches, taille des flocons) en modifiant les conditions expérimentales pendant l'exfoliation électrochimique, telles que la tension et l'électrolyte. De plus, le procédé peut également préparer des composites à base d'EGO ou modifier des surfaces d'EGO avec d'autres molécules en une seule étape. Cependant, comme les propriétés physicochimiques de l'EGO ont un effet profond sur ses propriétés électrochimiques, il peut être difficile de synthétiser et de sélectionner l'EGO correct pour une application cible. Il est donc crucial d'identifier une méthode de sélection des matériaux EGO et de comprendre le mécanisme d'exfoliation électrochimique du graphite afin de contrôler les propriétés structurelles des matériaux EGO résultants.

Tout d'abord, les matériaux EGO ont été produits par exfoliation électrochimique du graphite dans 0,1 M H_2SO_4, et l'effet du champ électrique (tension appliquée divisée par la distance de l'électrode) a été étudié. Les analyses Raman et XPS ont révélé deux régimes différents lors de la synthèse : une cinétique d'exfoliation lente à basse tension et une cinétique plus rapide à haute tension accompagnée des concentrations élevées de radicaux $OH^{\bullet}$. Ensuite, nous avons utilisé une plateforme basée sur l'auto-assemblage de feuilles EGO sur la surface d'une électrode de carbone vitreux (GCE) avec un lieur *p*-aminophényl (AP) pour la caractérisation électrochimique systématique des matériaux EGO par voltamétrie cyclique en 1 mM $[Fe(CN)_6]^{3-/4-}$ pour déterminer la surface électrochimique (ESA) et la constante de vitesse standard du transfert d'électrons (k^0). Les deux paramètres évoluent l'un avec l'autre et sont sensibles au type d'EGO, confirmant la pertinence de la plate-forme utilisée dans ce travail pour caractériser les matériaux EGO.

Deuxièmement, un aptasenseur électrochimique de cocaïne basé sur des matériaux EGO a été conçu et étudié. Nous avons examiné l'influence des paramètres suivants sur les performances du capteur : i) le groupe terminal de l'aptamère (-NH_2 vs -OH) ; ii) la fonctionnalisation d'EGO avec l'aptamère par adsorption physique et immobilisation covalente ; iii) les propriétés électrochimiques d'EGO, telles que ESA et k^0. Les résultats démontrent que l'aptamère de cocaïne modifiée par NH_2 s'adsorbe très rapidement et fortement sur les surfaces des flocons d'EGO, rendant non seulement la fabrication de la plateforme de détection simple et rapide, mais lui conférant aussi une très bonne reproductibilité, une stabilité de durée de conservation et une sensibilité élevée à la détection de cocaïne, avec une limite de détection de 50 nM. En outre, nous avons démontré que les matériaux EGO avec un ESA et un k^0 plus élevés présentent de meilleures performances de détection.

Troisièmement, l'exfoliation électrochimique du graphite en présence d'acide 4-aminobenzoïque (4-ABA) est utilisée comme méthode en une étape pour préparer des matériaux EGO fonctionnalisés avec de l'acide aminobenzoïque (EGO-ABA) et leurs applications à la réaction de réduction de l'oxygène (ORR) et les supercondensateurs ont été étudiés. Sur la base d'études électrochimiques, les catalyseurs EGO-ABA ont montré une meilleure activité ORR en milieu alcalin par rapport à l'EGO en raison de leur densité d'oxygénation élevée et d'une sélectivité plus faible pour le processus à deux électrons car leur teneur en groupes carbonyle est faible. Contrairement à l'EGO, les matériaux EGO-ABA ont également une plus grande capacité spécifique, et les matériaux préparés à partir d'une exfoliation dans 5-ABA/0,1 M H_2SO_4 ont une capacité spécifique trois fois supérieure à l'EGO. De plus, le matériau d'électrode a montré une capacité de cyclage remarquable, ne perdant que 19,4 % de sa capacité après 5000 cycles à 50 mVs^{-1}.

Mots clés : oxyde de graphène exfolié électrochimiquement (EGO), auto-assemblage de flocons d'EGO, surface électrochimique (ESA), constante de vitesse standard de transfert d'électrons (k^0), aptasenseur électrochimique, méthode d'adsorption physique, aptamère modifié par NH_2, oxydation des amines, acide aminobenzoïque, supercondensateurs.

SOMMAIRE RÉCAPITULATIF

I. Introduction

Le graphène et ses matériaux associés ont été largement étudiés ces dernières années en raison de leurs propriétés uniques, notamment une conductivité électrique élevée et une surface spécifique élevée. En conséquence, les applications basées sur ces matériaux, dont l'oxyde de graphène (GO), sont nombreuses, notamment dans le domaine de l'électrochimie, comme les biocapteurs et les supercondensateurs.

Les GO sont composés de couches de graphène modifiées avec des groupes fonctionnels oxygénés, tels qu'hydroxyle, époxy, carbonyle et carboxyle, ce qui leur permet d'être dispersés dans les solvants polaires et de fonctionner avec d'autres molécules ou nanoparticules pour créer des composés et composites améliorés. Diverses procédures peuvent être utilisées pour préparer les matériaux GO, y compris des méthodes chimiques et des méthodes d'exfoliation mécaniques, chimiques ou électrochimiques. Les méthodes d'exfoliation mécanique et chimique sont simples et peu coûteuses, mais présentent un problème de reproductibilité et d'évolutivité. La synthèse chimique de GO (connue sous le nom de méthode Hummers) implique l'oxydation du graphite dans un mélange d'acides concentrés et d'oxydants forts efficaces mais toujours laborieux et chronophages. Par rapport à ces méthodes, l'exfoliation électrochimique du graphite fournit une méthode peu coûteuse, rapide et respectueuse de l'environnement pour synthétiser les matériaux GO. En bref, il consiste en un système à deux électrodes utilisant du graphite comme électrode de travail et une contre-électrode immergée dans un électrolyte. Lorsqu'une différence de potentiel est appliquée entre les électrodes immergées dans un électrolyte aqueux, l'eau est réduite à la cathode générant du H_2, et des radicaux hydroxyles se forment à l'anode. Ces radicaux attaquent l'électrode de graphite et facilitent l'intercalation des ions des électrolytes au sein des couches graphitiques, entraînant la formation de flocons qui se dispersent dans l'électrolyte. La poudre d'EGO est facilement récupérée après filtration, lavée et lyophilisée. De plus, le procédé peut également préparer des composites à base d'EGO ou modifier des surfaces d'EGO avec d'autres molécules en une seule étape. En modifiant les conditions d'exfoliation électrochimique, telles que la tension et l'électrolyte, des matériaux EGO avec une variété de propriétés (quantités et types de groupes fonctionnels, densité de défauts, densité de couches et taille de flocons) peuvent être obtenus. Malgré cela, les propriétés physicochimiques de l'EGO ont une profonde influence sur ses performances électrochimiques, ce qui peut rendre difficile la synthèse et la sélection du bon EGO pour un usage particulier. Par conséquent, pour mieux appliquer les matériaux EGO dans une application cible, une meilleure compréhension des

mécanismes d'exfoliation électrochimique du graphite pour contrôler leurs propriétés structurelles et électrochimiques est cruciale.

Cependant, très peu de travaux rapportent l'influence des paramètres expérimentaux sur les défauts structuraux des EGO, leur composition de surface et leur nombre de couches de même que sur leurs propriétés électrochimiques, y compris la constante de vitesse standard de transfert d'électrons (k^0) et la surface électrochimique (ESA). L'ESA, une propriété de base d'une interface électrifiée, est la surface du matériau d'électrode disponible pour transférer des électrons vers et depuis l'électrolyte. Le k^0 est un paramètre très important lié à la cinétique de l'électrode et mesure la "facilité cinétique" du transfert d'électrons d'un couple redox à la surface d'une électrode : plus k^0 est élevé, plus vite l'équilibre sera atteint. Généralement, les matériaux carbonés avec plus d'arêtes auront des valeurs k^0 et ESA plus élevées car le nombre de couches peut augmenter les sites du plan de bord qui ont un taux de transfert d'électrons hétérogène plus rapide que le plan de base, mais l'influence des groupes fonctionnels oxygénés n'est pas encore claire. Par exemple, Chou et *al.* ont montré que l'augmentation des groupes carboxyle sur des nanotubes de carbone à paroi unique après activation électrochimique peut augmenter la valeur de k^0 pour le couple redox $[Fe(CN)_6]^{3-/4-}$. Ji et *al.* ont constaté que la valeur k^0 diminuait en augmentant les groupes contenant de l'oxygène sur le plan de base des électrodes en graphite pyrolytique oxydées pendant 12 h à l'air et des nanotubes de carbone à parois multiples oxydés à l'air pendant plus d'une semaine. Pumera et *al.* ont constaté que les groupes contenant de l'oxygène jouent un rôle majeur sur les sites aux bords des parois des nanotubes de carbone multiparois et ont un impact favorable sur la valeur de k^0 pour le couple $[Fe(CN)_6]^{3-/4-}$ redox. Plus tard, Ambrosi et *al.* ont comparé la valeur de k^0 pour $[Fe(CN)_6]^{3-/4-}$ pour l'oxyde de graphite, l'oxyde de graphène, l'oxyde de graphène réduit thermiquement, l'oxyde de graphène réduit chimiquement et l'oxyde de graphène réduit électrochimiquement immobilisé sur GCE par la méthode de coulée en goutte, et ont trouvé un k^0 inférieur lorsque des groupes fonctionnels oxygénés sont présents. Cependant, le type et la teneur des groupes fonctionnels oxygénés ne sont pas pris en compte dans leur discussion.

De plus, les recherches sur l'EGO en tant que matériaux pour les transducteurs dans un biocapteur sont rares. Généralement, un biocapteur se compose d'un transducteur et d'un bio-récepteur. Pour les biocapteurs électrochimiques, les biorécepteurs tels que les enzymes, les anticorps, les aptamères, etc. reconnaissent l'analyte cible, et l'électrode convertit l'événement de reconnaissance en un signal électrique mesurable. Les nanomatériaux à base de graphène, notamment le graphène (G), le GO et le GO réduit (rGO), sont généralement utilisés comme

matériaux d'électrode dans les transducteurs pour améliorer les performances analytiques du capteur. Leurs propriétés électrochimiques (valeurs ESA et k^0) peuvent avoir une influence sur les performances de détection électrochimique. En outre, la capacité à fonctionnaliser la surface des matériaux à base de graphène avec des aptamères et d'autres éléments de détection repose sur les propriétés physicochimiques des matériaux, telles que la composition de la surface et la taille de la feuille. Selon la littérature antérieure, les méthodes d'adsorption physique et d'immobilisation chimique sont souvent utilisées pour les anticorps et l'ADN. L'immobilisation chimique implique la formation d'une liaison covalente stable entre le biorécepteur et la surface du transducteur, telle que la liaison carboxamide formée après la réaction entre les groupes amine et carboxyle. La méthode d'adsorption physique utilise les interactions d'empilement pi-pi entre les brins d'ADN et la surface des matériaux à base de graphène et les forces électrostatiques entre les groupes fonctionnels du bio-récepteur et ceux des matériaux à base de graphène. Malgré la simplicité de cette méthode, elle est utilisée moins fréquemment, car elle rapporte généralement une adhérence plus faible et moins de contrôle sur l'orientation des biomolécules, conduisant à une stabilité et une sensibilité inférieures par rapport aux méthodes d'immobilisation chimique. Récemment, Eissa et *al.* ont rapporté que la réponse des aptasenseurs de la toxine microcystine-LR préparés par adsorption physique s'est avérée améliorée avec l'augmentation de la taille de la feuille GO (de 0, 22 à > 100 µm). Pendant ce temps, les feuilles GO de petite taille (<2,5 µm) offraient de meilleures performances de détection par la méthode de fixation covalente. Comme peu de recherches existent sur les biocapteurs électrochimiques basés sur les matériaux EGO, les performances de détection électrochimique de matériaux EGO fonctionnalisés avec des biorécepteurs, tel qu'un aptamère, doivent encore être explorées.

D'un autre côté, les matériaux EGO ont une plus faible densité de groupes fonctionnels oxygénés (C/O > 4) par rapport aux méthodes chimiques (e.g. méthode de Hummers : C/O $\approx$ 2), une propriété qui peut être bénéfique à l'électrochimie de dispositifs tels que les supercondensateurs. Les supercondensateurs sont des systèmes de stockage de charge caractérisés par une densité de puissance élevée et une charge-décharge rapide. De plus, ils sont respectueux de l'environnement en raison des faibles émissions de CO_2 et ont une durée de vie plus longue que les batteries. Ils peuvent être utilisés comme dispositifs complémentaires aux batteries conventionnelles dans des applications qui nécessitent des impulsions de puissance de pics, ou pour alimenter des dispositifs électroniques extensibles et portables. Les pseudo-condensateurs, un type spécifique de supercondensateurs, sont basés sur le stockage de charge impliquant des

réactions redox de surface rapides à l'interface électrode/électrolyte, et les matériaux GO présentent un intérêt potentiel en tant que matériaux d'électrode pour cette technologie. La présence de groupes oxygénés fonctionnels à la surface du GO empêche le réempilement des couches et l'agglomération des flocons, un inconvénient important associé à l'utilisation de feuilles de graphène. Ces groupements fonctionnels améliorent également la mouillabilité de l'électrode par l'électrolyte et peuvent participer à des processus redox réversibles, augmentant ainsi la pseudocapacité. Cependant, le groupe fonctionnel oxygéné abaisse la conductivité électrique des matériaux GO, leur contenu doit donc être optimisé. Les matériaux EGO avec différentes quantités et types de groupes fonctionnels d'oxygène peuvent être obtenus rapidement par des méthodes d'exfoliation électrochimique, ce qui pourrait être un avantage pour les supercondensateurs. De plus, en changeant d'électrolyte ou en ajoutant des précurseurs dans l'électrolyte, il est possible de synthétiser des matériaux EGO avec différents composites et/ou groupes fonctionnels en une seule étape comme le dopage hétéroatome (par exemple F, N, P, S), la fonctionnalisation par aryl diazonium, ou l'utilisation hybrides de nanoparticules, etc., rendant les matériaux EGO idéaux pour l'étude des supercondensateurs. L'influence des quantités ou des types de groupes fonctionnels/composites de matériaux EGO sur la capacité peut être explorée.

II. Objectifs

Ce travail de thèse porte sur la synthèse de matériaux EGO et leurs applications électrochimiques dont les biocapteurs électrochimiques et le stockage d'énergie (supercondensateurs). L'objectif de recherche comprend : i) synthétiser une série de matériaux EGO obtenus dans différentes conditions expérimentales (tension appliquée, distance entre les électrodes et réduction thermique ultérieure) et étudier systématiquement leurs propriétés structurelles et électrochimiques; ii) étudier les performances électrochimiques d'aptasenseurs basées sur des matériaux EGO; iii) réaliser l'exfoliation électrochimique de graphite dans de l'acide sulfurique 0,1 M contenant de l'acide 4-aminobenzoïque (4-ABA) pour obtenir une série de matériaux EGO fonctionnalisés avec l'acide aminobenzoïque (EGO-ABA) en une seule étape, et pour étudier le rôle des groupes fonctionnels vers les supercondensateurs. Trois projets connexes sont mis en œuvre pour atteindre ces objectifs :

1) Caractérisation électrochimique de matériaux de type graphène obtenus par exfoliation électrochimique de graphite.

Dans le premier projet, nous avons utilisé une plateforme basée sur l'auto-assemblage de feuilles d'EGO sur la surface d'une électrode de carbone vitreux (GCE, 3 mm de diamètre) via un lieur *p*-aminophényl (AP) pour la caractérisation électrochimique systématique des matériaux EGO. Les électrodes EGO/AP/GCE sont caractérisées électrochimiquement par voltamétrie cyclique (CV) dans 1 mM $[Fe(CN)_6]^{3-/4-}$ couple redox pour déterminer le k^0 par la méthode de Nicholson, et l'ESA par l'équation de Randles-Sevcik. Ces deux paramètres sont corrélés avec la morphologie, la composition et les défauts structuraux des EGO étudiés par microscopie électronique à balayage (SEM), microscopie électronique à transmission (TEM), diffraction des rayons X (XRD), spectroscopie Raman et par spectroscopie photoélectronique à rayons X (XPS).

2) Aptasenseur de cocaïne électrochimique simple et efficace à base d'oxyde de graphène exfolié électrochimiquement.

Dans le deuxième projet, nous avons démontré la pertinence et les avantages d'utiliser des matériaux EGO qui ont de meilleures propriétés électrochimiques du premier projet pour la fabrication d'aptasenseurs électrochimiques. Des aptamères de cocaïne déjà publiés avec des groupes terminaux amine (aptamère-NH_2) ont été fonctionnalisés sur la surface EGO sur des électrodes de carbone vitreux par des méthodes d'adsorption physique et d'immobilisation chimique par la formation de liaisons carboxamide entre les groupes carboxyle des EGO et les groupes amine des aptamères. Les électrodes ont été caractérisées par CV et voltamétrie à onde carrée (SWV) dans 1 mM $[Fe(CN)_6]^{3-/4-}$ couple redox après chaque modification, et leurs performances de détection ont été étudiées et comparées.

3) Synthèse en une étape d'oxyde de graphène fonctionnalisé avec l'acide aminobenzoïque par exfoliation électrochimique du graphite pour supercondensateurs.

Dans le troisième projet, en ajoutant différentes quantités d'acide 4-aminobenzoïque (4-ABA) dans un électrolyte H_2SO_4 (0,1 M), nous avons fabriqué les matériaux EGO fonctionnalisés avec l'acide aminobenzoïque (EGO-ABA) par synthèse en une étape. Au cours de ce processus en une étape, le graphite est électrochimiquement oxydé et exfolié pour former des feuilles d'EGO, tandis que les groupes amines du 4-ABA sont oxydés en radicaux, suivis de la formation de liaisons covalentes entre les carbones sp^2 (sur le plan de base EGO) et les radicaux dérivés d'amines. Les matériaux EGO-ABA sont caractérisés par la spectroscopie infrarouge à transformée de Fourier (FT-IR), SEM, XPS, XRD et Raman. Le mécanisme de réaction du processus d'exfoliation électrochimique et le rôle des groupes fonctionnels des matériaux EGO-ABA pour les supercondensateurs ont été étudiés.

III. Réalisation du premier projet : Caractérisation électrochimique de matériaux de type graphène obtenus par exfoliation électrochimique de graphite.

III.1. Section expérimentale

III.1.1. Synthèse de l'EGO

Une feuille de graphite (7,5 cm × 2 cm × 0,05 cm) a été utilisée comme anode et connectée à la borne positive de l'alimentation en courant continu. Une maille de Pt (6 cm^2) a été utilisée comme cathode. Les deux électrodes ont été immergées dans un électrolyte H_2SO_4 (0,1 M) et la distance entre elles a été maintenue constante (4 ou 6 cm). L'exfoliation électrochimique a commencé immédiatement après l'application de la différence de potentiel entre les électrodes (6, 8, 10, 12 V). Les feuilles d'EGO ont été recueillies par filtration sous vide à travers un filtre à membrane MF-Millipore avec une taille de pores de 0,22 µm et lavées plusieurs fois avec de l'eau millipore. La poudre EGO a été dispersée dans de l'eau et soniquée pendant 90 min pour maximiser l'exfoliation. Les poudres EGO ont été obtenues après lyophilisation. Les échantillons sont nommés en fonction de la tension appliquée et de la distance entre les électrodes de graphite et de Pt, telles que 6V6cm. Un échantillon supplémentaire a été obtenu après réduction de la poudre EGO (8V6cm) à 900°C dans Ar (appelée (R)8V6cm). Le tableau S4.1 résume les conditions expérimentales utilisées pour la synthèse des matériaux EGO. Des suspensions d'EGO (0,05 mg mL^{-1}) soniquées pendant 3 h ont été préparées pour les études électrochimiques (échantillons nommés par exemple EGO6V6cm-3h). Les techniques SEM, TEM et XRD, de même que les spectroscopies Raman et XPS ont été utilisées pour caractériser les EGO et les poudres EGO-3h.

III.1.2. Modification d'électrodes en carbone vitreux avec un film mince d'EGO

Le **schéma 4.1** illustre la procédure utilisée pour assembler les EGO sous forme de films minces à la surface d'électrodes en carbone vitreux (GCE). Tout d'abord, la surface d'un GCE est modifiée avec un film de *p*-nitrophényle (film NP) en utilisant la chimie du diazonium (0,15 mM $NaNO_2$ + 0,15 mM 4-nitroaniline) dans 0,5 M HCl par voltamétrie cyclique, balayant le potentiel de 0 V à -0,6 V vs Ag/AgCl à 0,05 V s^{-1} et pendant 3 cycles, **schéma 4.1a**. Ensuite, le film NP est réduit électrochimiquement en film *p*-aminophényl (film AP) dans du KCl (0,1 M) par CV de 0 V à -1,3 V vs Ag/AgCl à 0,05 V s^{-1} et pendant 3 cycles, **schéma 4.1b**. Enfin, le GCE modifié avec AP-

film est incubé dans la dispersion EGO (0,05 mg mL^{-1} pendant 20 minutes, permettant aux feuilles EGO de s'auto-assembler sur la surface du GCE via le lieur AP-film, **schéma 4.1c**. Les CV en présence de couple redox $[Fe(CN)_6]^{3-/4-}$ 1 mM dans KCl 0,1 M ont été enregistrés à 0,1 V s^{-1} après chaque étape pour suivre la modification de surface du GCE, **schéma 4.1d**.

III.2. Résultats et discussion

Les images TEM (**Figure 4.1a et Figure S2**) montrent que les flocons d'EGOs sont composés de multicouches. Les flocons obtenus à 6V ont un plus grand nombre de couches (8 ~ 11) par rapport à ceux obtenus à 8 à 12V (3 ~ 7 couches). Les images SEM (**Figure 4.2**) montrent que la taille de la feuille augmente avec la tension appliquée. Ceci est probablement lié à la cinétique d'exfoliation qui est lente à 6 V (4 heures pour ≈0,67 g) mais devient plus rapide lorsque la tension augmente (1 heure pour ≈0,68 g à 12 V). À des tensions plus basses, les radicaux hydroxyle et les anions sulfate de l'électrolyte s'intercalent lentement entre les feuilles de graphite, et le gaz libéré (SO_2, CO_2, O_2) lors de l'exfoliation aide à la fracturation de l'EGO en petits flocons. En revanche, lorsqu'une haute tension est appliquée, les ions sulfate et les molécules d'eau s'intercalent rapidement et le long des feuilles de graphite, ce qui donne de grandes feuilles d'EGO exfoliées (**Figure 4.1b**). Pour l'analyse XPS, les spectres C 1s (**Figure S4.6**) ont été déconvolués en cinq pics identifiés comme carbone graphitique C-C et C=C à 284,5 eV, C-OH à 285,8 eV, C-O-C à 286,8 eV et C=O à 288 eV, ainsi que le O-C=O à 289 eV. Les pourcentages atomiques relatifs (at%) des espèces carbonées ont été quantifiés, seul les at% des groupes C-OH et C-O-C varie avec la tension appliquée, **Figure 4.3b et c**. Le rapport C-OH/C at% augmente de 6V6cm à 12V6cm, ce qui est attribué à une concentration croissante en radicaux OH avec la tension et à l'attaque subséquente des couches graphitiques. Le rapport C-O-C/C at% montre une dépendance en forme de U avec la tension appliquée en raison de deux régimes différents : une cinétique d'exfoliation plus lente, plus des flocons plus petits et plus épais à une tension plus faible, et une concentration élevée de radicaux OH et des flocons plus gros à une tension plus élevée. Pour l'analyse par spectroscopie Raman, le rapport entre l'intensité des bandes D et G (I_D/I_G) liée à la densité de défauts des matériaux de graphène a été calculé (**Figure 4.4b**). Il augmente systématiquement de 0,5 à 0,9 avec la tension appliquée au-dessus de 8 V, montrant que le degré d'oxydation des quelques couches EGO-3h augmente avec le champ électrique appliqué.

Afin d'évaluer l'impact des conditions d'exfoliation sur les propriétés électrochimiques des électrodes à base d'EGO, une série de CV a été enregistrée à différentes vitesses de balayage (entre 20 mV s^{-1} et 200 mV s^{-1}) en utilisant $[Fe(CN)_6]^{3-/4-}$ comme sonde redox. Comme le montre la **Figure 4.5**, l'ESA des électrodes à base d'EGO a été calculée selon l'équation de Randles-Sevcik, qui varie entre 0,065 cm^2 et 0,082 cm^2 et montre une dépendance du type volcanique avec la tension, avec un maximum entre 8 et 10V. Le k^0 a été évalué par la méthode de Nicholson, qui varie entre 0,05 et 0,13 cm s^{-1} montrant ainsi une dépendance du volcan avec la tension. Le k^0 le plus élevé est obtenu lorsque la tension appliquée est de 8 ou 10 V. Il existe une relation linéaire entre les valeurs de k^0 et ESA pour les électrodes modifiées EGO, et les EGO 8V6cm et 10V6cm conduisent aux électrodes à couche mince avec le plus haut ESA (0,08 cm^2) et k^0 le plus élevé (0,13 cm s^{-1}).

Les valeurs ESA et k^0 ont été corrélées avec l'I_D/I_G et le ratio at% de groupes fonctionnels oxygénés, une corrélation n'a été trouvée qu'entre les valeurs ESA et k^0 et le rapport C-O-C/C at%. Comme le montre la **Figure 4.6**, pour les échantillons avec peu de couches ($\leqslant$ 7 couches), l'ESA diminue avec l'augmentation du nombre de défauts (I_D/I_G et C-O-C/C at% ratio), ce qui peut être attribué à une diminution de la conductivité électrique. La dépendance de k^0 avec le rapport I_D/I_G et C-O-C/C at% montre clairement que trop peu ou trop de défauts ont un impact négatif sur ce paramètre. Lorsque le nombre de couches augmente à 7 ou plus, le k^0 diminue considérablement même si le rapport I_D/I_G est faible. La valeur ESA est également faible. Ces résultats montrent clairement que lorsque le nombre de couches et la structure d'EGO sont similaires, la densité de groupes C-O-C est le principal facteur altérant les valeurs de k^0 et ESA.

A des fins de comparaison, une série d'électrodes ont également été préparées par un procédé de coulée en goutte et les électrodes ont été caractérisées électrochimiquement comme ci-dessus. Comme le montre la **Figure S4.10**. Les valeurs de l'ESA sont d'environ 0,11 cm^2 qui sont très similaires à celle du GCE nu, les valeurs de k^0 varient entre 0,03 et 0,04 cm s^{-1} sans tendance claire entre elles, et aucune corrélation ne peut être établie avec les propriétés physico-chimiques. Ces résultats confirment que la méthodologie proposée est valable pour le criblage de matériaux de type graphène.

IV. Réalisation du deuxième projet : Aptasenseur de cocaïne électrochimique simple et efficace à base d'oxyde de graphène exfolié électrochimiquement

IV.1. Section expérimentale

IV.1.1. Fabrication et caractérisation électrochimique de l'aptasenseur de cocaïne basée sur EGO.

Le **schéma 5.1** illustre les procédures utilisées pour fabriquer l'aptasenseur de cocaïne électrochimique à base d'EGO pour les méthodes d'adsorption physique et d'immobilisation covalente. Dans un premier temps, 8 µL de suspension EGO 10V6cm (0,4 mg mL^{-1} soniqué pendant 3 h) ont été déposés sur la surface d'une GCE (3 mm de diamètre) et séchés à température ambiante (21±1°C). Ensuite, l'électrode modifiée (GCE/EGO) a été incubée dans la solution d'aptamère de cocaïne avec des groupes terminaux amine (6 µL d'aptamère-NH_2 1 µM dans du KCl 0,05 M, pH = 7), 10 minutes pour le temps optimisé. L'électrode modifiée avec l'aptamère-NH_2 (GCE/EGO/Apt-NH_2) a ensuite été immergée dans 6 µL de solution de BSA à 0,1 %, 30 minutes pour le temps optimisé, afin de bloquer la surface de l'électrode et d'éviter une adsorption non spécifique. Enfin, l'électrode bloquée (GCE/EGO/Apt-NH_2/BSA) a été incubée dans 8 µL de solutions de cocaïne de concentrations variables pendant 30 minutes pendant le temps optimisé (GCE/EGO/Apt-NH_2/BSA/Co).

Pour la méthode d'immobilisation covalente, une étape supplémentaire a été ajoutée à la procédure de fabrication. L'électrode GCE/EGO a été incubée dans 8 µL d'une solution 50 µM N,N,N',N'-tétraméthyl (succinimido) tétrafluoroborate d'uronium (TSTU) et 4-diméthylaminopyridine (DMAP) pendant 1 heure pour former le lieur (GCE /EGO/linker). Ensuite, l'électrode a été incubée dans la solution d'aptamère-NH_2 (GCE/EGO/linker/Apt-NH_2) pendant 10 minutes, la solution de BSA (GCE/EGO/linker/Apt-NH_2/BSA) pendant 30 minutes, et enfin, la solution de cocaïne (GCE/EGO/linker/Apt-NH_2/BSA/Co) pendant 30 minutes.

Pour suivre la modification de surface du GCE, des CV et des voltammogrammes à onde carrée (SWV) ont été enregistrés après chaque étape avec au moins trois électrodes dans 1 mM $[Fe(CN)_6]^{3-/4-}$ couple redox dans 0,1 M KCl. Les CV ont été enregistrés de -0,2 V à 0,6 V avec une fréquence de balayage de 0,1 V s^{-1}, et les SWV de -0,2 V à 0,8 V avec une fréquence de 25 Hz.

La XPS a été utilisée pour confirmer la fixation chimique de l'aptamère-NH_2 sur la surface des flocons d'EGO lors de la fabrication du capteur. Les tests de radioactivité ont été utilisés pour vérifier si la liaison de la cocaïne avec l'aptamère affectait son adhésion à la surface de l'EGO.

IV.2. Résultats et discussion

D'après le CV (**Figure 5.1a**) de chaque étape de modification par méthode d'adsorption physique, le courant a augmenté après dépôt d'EGO sur le GCE en raison de l'augmentation de l'ESA et du k^0 de l'électrode, puis a diminué après incubation dans une solution avec l'aptamère-NH_2 et du BSA en raison du blocage de la surface. Enfin, le courant a de nouveau augmenté car la configuration aptamère-NH_2 a été modifiée après liaison avec la molécule de cocaïne. La SWV est utilisée pour quantifier la variation relative des pics du courant (Δi) après chaque étape de modification (**Figure 5.1b et Figure S5.1**). Le temps d'incubation de l'aptamère de cocaïne-5'-NH_2, de la BSA et de la cocaïne a été optimisé. Le Δi pour l'étape de modification de l'aptamère-NH_2 (GCE/EGO/Apt-NH_2) était constant après 10 minutes, indiquant que l'aptamère-NH_2 peut être adsorbé très rapidement sur l'EGO (**Figure 5.1c**). La surface a été bloquée par BSA (**Figure 5.1d**) après 30 minutes. La liaison entre l'aptamère-NH_2 et la molécule de cocaïne est terminée après 30 minutes (**Figure 5.1e**).

La même expérience a été menée pour étudier l'effet du groupe terminal de l'aptamère en utilisant l'aptamère de cocaïne non modifiée qui a un groupe terminal OH (aptamère-OH). Comme la **Figure 5.2a** montre, la valeur Δi de l'électrode GCE/EGO avec l'aptamère-OH a diminué légèrement moins que celle de l'aptamère-NH_2, mais a diminué de façon spectaculaire après incubation dans la BSA, montrant qu'une plus grande surface a été bloquée par la BSA et l'aptamère-OH couvrait moins de surface que l'aptamère-NH_2. Enfin, l'électrode ayant l'aptamère-NH_2 a permis une meilleure détection de la cocaïne (**Figure 5.2b**). Les aptamères avec des groupes fonctionnels NH_2 terminaux sont susceptibles de mieux fonctionner sur les biocapteurs, car les groupes amine chargés positivement interagissent électrostatiquement avec les EGO chargés négativement, ce qui entraîne une adhérence plus stable des aptamères aux EGO. De plus, pour vérifier si les changements induits par la cocaïne ont été déclenchés par des aptamères libérés de la surface ou par un changement conformationnel de l'aptamère à la surface, un test de radioactivité utilisant des aptamères-NH_2 radiomarqués au ^{32}P a été effectué. Le résultat (**Figures S5.2-S5.4**) montre qu'aucun aptamère-NH_2 de cocaïne n'a été libéré de la surface de l'EGO après la liaison avec la cocaïne, même en essayant de dépouiller les surfaces EGO des aptamères en utilisant une DNase. Ces tests démontrent que l'EGO a une forte capacité d'adsorption pour les aptamères modifiés avec le groupe terminal NH_2 ainsi que pour les séquences d'ADN plus petites.

Pour la méthode d'immobilisation covalente, la même concentration d'aptamère-NH_2 et le même temps d'incubation que dans la méthode d'adsorption physique ont été utilisés pour comparer correctement ces deux méthodes. Il convient de noter que l'adsorption physique des aptamères

sur la surface de l'électrode ne peut être évitée pendant le processus d'immobilisation covalente, en raison de l'adsorption rapide et forte de l'aptamère-NH_2 sur l'EGO. L'analyse XPS a été utilisée pour étudier le processus d'immobilisation covalente par la réaction TSTU/DMAP dans une solution aqueuse, qui consiste en la formation de liaisons carboxamide entre les groupes carboxyle des EGO et les groupes amine des aptamères (**Schéma S5.1**). D'après les spectres C 1s, **Figure S5.5b-e**, les intensités relatives des pics C=O/C=N et O-C=O/N-C=O ont augmenté après la fonctionnalisation avec le lieur et l'aptamère-NH_2. D'après les spectres N 1s, **Figure 5.3**, la liaison N-(C=O) est apparue en raison de la formation de l'azote succinimidyle du lieur dans l'électrode GCE/EGO/lieur. Après incubation avec l'aptamère de cocaïne, des liaisons amine et amide ont été observées correspondant aux aptamères-NH_2 de cocaïne et aux liaisons carboxamide formées entre l'EGO et les aptamères, respectivement, mais aucune liaison N-(C=O) n'a été trouvée pour l'électrode GCE/EGO/Apt-NH_2. Ces résultats démontrent une modification d'électrode réussie via la méthode d'immobilisation covalente.

En comparant les méthodes d'immobilisation covalente et d'adsorption physique, leurs valeurs de Δi (**Figure 5.4a**) sont presque les mêmes après fonctionnalisation avec les aptamères-NH_2 de cocaïne et BSA. Le Δi a également été calculé après incubation dans des solutions de cocaïne à différentes concentrations (0,05 µM à 100 µM) pour obtenir des courbes d'étalonnage (**Figure 5.4b**). La limite de détection (LOD) a été calculée à environ 50 nM pour les deux méthodes. De plus, un test de durée de conservation a également été effectué, les aptasenseurs construits ont été stockés à 4 °C pendant 14 jours, et ils ont maintenu 98,7% et 98,4% de leur réponse initiale pour l'adsorption physique et les méthodes d'immobilisation covalente, respectivement, **Figure 5.5**. Les résultats confirment l'excellente capacité de l'EGO à adsorber l'aptamère à sa surface, montrant que l'aptasenseur à base d'EGO présentait une bonne stabilité. Comparé à d'autres aptasenseurs électrochimiques de cocaïne (Tableau S5.3), ce capteur électrochimique basé sur EGO présente de bonnes performances mais est surtout plus simple et plus rapide à préparer. Dans le cadre de l'évaluation de l'aptasenseur proposé, la sélectivité a également été évaluée pour s'assurer qu'elle n'était pas affectée par d'autres problèmes de sélectivité en plus de ceux liés à cet aptamère.

Enfin, différents matériaux EGO (du 1er projet) ont également été utilisés pour fabriquer l'aptasenseur de cocaïne par la méthode d'adsorption physique afin d'étudier l'influence de leurs propriétés électrochimiques (ESA et k^0) sur les performances de détection. Toutes ces électrodes modifiées ont été testées sous la même concentration de 1 µM de cocaïne. Selon les valeurs Δi associées à chaque étape de modification d'électrode et de détection de cocaïne (**Figure S5.10**),

les différents EGO présentent des performances de détection différentes. Comme prévu, les valeurs Δ*i* après détection de 1 µM de cocaïne augmentent avec l'ESA et le k^0 respectifs, et l'électrode modifiée EGO 10V6cm a présenté le Δ*i* le plus élevé par rapport aux autres EGO signalés, indiquant les meilleures performances de détection (**Figure 5.7**).

V. Réalisation du troisième projet : Synthèse en une étape d'oxyde de graphène fonctionnalisé avec l'acide aminobenzoïque par exfoliation électrochimique du graphite pour supercondensateurs.

V.1. Section expérimentale

V.1.1. Préparation d'oxyde de graphène fonctionnalisé par l'acide aminobenzoïque (EGO-ABA)

Dans un système à deux électrodes, une feuille de graphite (7,5 cm × 2 cm × 0,05 cm) a été utilisée comme anode et une maille de Pt (6 cm^2) a été utilisée comme cathode. Les deux électrodes ont été immergées dans un électrolyte H_2SO_4 (0,1 M) avec différentes concentrations d'acide 4-aminobenzoïque (4-ABA, 0, 5, 10, 20, 40 mM) et connectées à l'alimentation en courant continu. La longueur de graphite dans l'électrolyte était de 5 cm. La distance entre les deux électrodes était de 6 cm. La tension appliquée était de 8 V. Après l'exfoliation, les feuilles d'EGO ont été lavées avec de l'eau millipore et recueillies par filtration sous vide à travers un filtre à membrane MF-Millipore avec une taille de pores de 0,22 µm. Du papier pH a été utilisé pour vérifier la présence d'acide résiduel. Lorsque le pH du filtrat incolore s'est avéré être d'environ 5-6, indiquant que l'électrolyte d'acide sulfurique et l'adduit produit par les réactions secondaires ont été éliminés. Les poudres EGO et EGO-ABA ont ensuite été dispersées dans l'eau par ultrasons pendant 90 min pour maximiser l'exfoliation. La dispersion a été lyophilisée et les poudres ont été stockées pour une utilisation ultérieure. Les échantillons sont nommés en fonction de la concentration en acides 4-aminobenzoïques, tels qu'EGO (0 mM de 4-ABA) et EGO-ABA-5 (5 mM de 4-ABA). Les observations expérimentales lors de la synthèse ont été résumées dans le tableau 6.1.

Les matériaux EGO et EGO-ABA ont été caractérisés par Fourier Transform Infrared (FT-IR), XPS, XRD et SEM.

V.1.2. Préparation et caractérisation électrochimique d'électrodes à base d'EGO-ABA pour l'étude ORR

Des études électrochimiques dans du KOH (0,1 M) ont été menées sur un disque de GCE (diamètre de 5 mm) et sur une électrode annulaire à disque rotatif en carbone vitreux (RRDE) recouverte de couches de catalyseur EGO ou EGO-ABA. Les encres catalytiques ont été préparées en dispersant 10 mg d'EGO ou d'EGO-ABA dans 525 µL d'alcool isopropylique et 25 µL de solution de résine perfluorée Nafion® à 5 % en poids. Ensuite, les encres ont été soniquées pendant 1 heure. Les disques ont été recouverts d'un volume approprié de l'encre catalytique pour obtenir une charge de catalyseur de 463,8 µg cm^{-2}, et séchés à température ambiante. Les électrodes GCE / RRDE recouvertes de matériaux EGO, une contre-électrode (Pt) et une électrode de référence au calomel saturé (SCE) étaient toutes logées dans une cellule électrochimique à un seul compartiment. La voltamétrie cyclique a d'abord été réalisée sur le GCE dans un électrolyte N_2 saturé à 50 mV s^{-1} de 0,4 V à -1,4 V vs SCE et 20 cycles ont été enregistrés pour chaque matériau. Pour les études ORR, le RRDE et le protocole suivant ont été utilisés : i) trois CV de 0,4 V à -1,4 V vs SCE ont été enregistrés à 50 mVs^{-1} ; ii) des voltammogrammes à balayage linéaire (LSV) entre -0,10 V et -1,35 V vs SCE ont été enregistrés dans un électrolyte N_2 saturé à 5 mVs^{-1} faisant varier la vitesse de rotation de 1600, 900, 400, 225 à 100 tr/min ; iii) la saturation de l'électrolyte avec O_2 et les procédures i) et ii) ont été effectuées à nouveau. Le potentiel de l'anneau a été fixé à une valeur constante de 1,2 V vs SCE pour oxyder le H_2O_2 formé sur l'électrode à disque, permettant sa quantification. Avant les expériences LSV, le cycle Pt a été activé par CV dans un électrolyte N_2 saturé à 500 mV s^{-1} (15 CV) de 0,4 V à -0,9 V vs SCE. Afin de calculer le nombre d'électrons impliqués pendant l'ORR et le pourcentage de H_2O_2 électrogénéré, les équations 6.6 et 6.7 ont été utilisées respectivement.

V.1.3. Préparation et caractérisation électrochimique d'électrodes à base d'EGO-ABA pour supercondensateurs

Des mousses de nickel (NF) ont été utilisées comme supports pour la fabrication des électrodes EGO et EGO-ABA. Les matériaux à base d'EGO et le liant PTFE (90 :10 wt% ratio, 90 mg de matériaux de graphène et 10 mg de PTFE) ont été mélangés dans un petit volume (2 ml) d'éthanol sous sonication jusqu'à ce qu'une dispersion homogénéisée soit obtenue. Ensuite, la mousse de Ni (1 cm^2) a été enduite par de simples étapes répétitives de revêtement par trempage dans des encres EGO et séchée à 60 ° C sous vide pendant une nuit. La charge en matière active (environ 1,5 à 2,0 mg) a été calculée à partir de la différence de poids de la mousse de nickel avant et après revêtement déterminée par une balance de haute précision (précision 0,0001 mg). Le comportement électrochimique des électrodes NF à base d'EGO a été étudié par CV dans une configuration à trois électrodes, où du papier carbone (CP) et une SCE ont été utilisés comme

contre-électrodes et électrodes de référence, respectivement. Les études électrochimiques ont été réalisées dans l'électrolyte KOH (6 M) et la vitesse de balayage variait entre 5 et 100 mV s^{-1}. La capacité spécifique (Cs) d'EGO/NF et EGO-COOH/NF a été évaluée à partir des CV en utilisant la charge voltamétrique cathodique (Q) intégrée dans la fenêtre de potentiel 0 à -1,15 V vs SCE en utilisant l'équation 6.11.

V.2. Résultats et discussion

V.2.1. Synthèse et caractérisation physico-chimique des EGO et EGO-ABA

Lors de l'exfoliation électrochimique de graphite dans du H_2SO_4 (0,1 M) avec différentes concentrations de 4-ABA (entre 0 et 40 mM), l'eau est réduite à la cathode générant du H_2 et des radicaux hydroxyles se forment à l'anode. Ces radicaux attaquent l'électrode de graphite, facilitent l'intercalation des ions de l'électrolyte dans les couches graphitiques, et les gaz libérés (SO_2, CO_2) aident à la formation des flocons EGO et EGO-ABA. Pendant ce temps, la coloration de l'électrolyte indique l'oxydation du 4-ABA (Réaction 1) qui entre en compétition avec l'oxydation du graphite. Ainsi, la formation d'un composé azoïque a lieu lors de l'exfoliation et entre en compétition avec la fonctionnalisation du 4-ABA sur le plan basal de l'EGO (Réactions 2 et 3). Lorsque la concentration de 4-ABA dans l'électrolyte augmente, plus la valeur du courant initial est faible, plus l'électrolyte vire rapidement au violet autour de l'électrode de graphite jusqu'à ce qu'il devienne finalement brun, et plus le temps d'exfoliation est long (tableau 6.1).

La **Figure 6.1** montre les spectres de FT-IR de l'EGO, de l'EGO-ABA-5 et de l'EGO-ABA-20. Le spectre d'EGO affiche les bandes associées aux vibrations d'étirement C-O-C (1284 cm^{-1}), C-OH (1370 cm^{-1}), C=O (1680 cm^{-1}) et une large bande provenant des vibrations d'étirement OH autour de 3000 cm^{-1}. Les pics correspondant aux modes de flexion aromatiques C-H (770 cm^{-1}) et aux vibrations de déformation N-H (amine secondaire, à 700 cm^{-1}) apparaissent dans les spectres des échantillons EGO-ABA et leur intensité augmente avec la concentration de 4-ABA. La même tendance se retrouve pour la bande C=O. De plus, pour EGO-ABA-20 et 40 (**Figure S6.1a**), les pics correspondant aux vibrations d'étirement C-N (environ 1410 cm^{-1}) et aux vibrations d'étirement des composés azoïques N=N (1516 cm^{-1}) sont observés. Enfin, les pics correspondant aux vibrations d'étirement NH_2 asymétriques et symétriques (amine primaire, autour de 3400 cm^{-1}, voir le spectre FTIR du 4-ABA dans la **Figure S4.1b**) sont absents des spectres des EGO-ABAs. L'analyse FT-IR confirme que l'EGO a été fonctionnalisé avec du 4-

ABA et que des composés azoïques se sont formés lorsque la concentration de 4-ABA était supérieure à 20 mM.

Les spectres de XPS (**Figure 6.2a**) montrent les pics attendus de C 1s, N 1s et O 1s à 285, 400 et 532 eV, respectivement ; et le pic N 1s plus intense pour EGO-ABA-20 et EGO-ABA-40. Le spectre C 1s (**Figure S6.2a**) a été déconvolué en cinq pics identifiés comme du carbone graphitique : C-C et C=C (284,5 eV), C-OH (285,8 eV), C-O ou C-N (286,8 eV), C=O (288 eV) et O-C=O (289 eV). Le spectre N 1s (**Figure S2b**) a été ajusté en 3 pics : C–N (399,8 eV), N–H (401,7 eV) et =N- (398,6 eV), la présence de groupes =N- confirme que le 4-ABA a subi une réaction secondaire conduisant à la formation de composés diazoïques. Les différents groupes fonctionnels et les espèces carbonées et azotées associées ont été quantifiés et les pourcentages atomiques (at%) sont présentés dans les **Figures 6.2b-e**. Comme prévu, ces rapports at% augmentent avec la concentration croissante de 4-ABA dans l'électrolyte, indiquant une fonctionnalisation réussie de la surface EGO avec 4-ABA, mais ont atteint un plateau pour [4-ABA] $\geqslant$ 20 mM. Toutes les parcelles sauf celle pour C-OH ont un point d'inflexion à 10 mM de 4-ABA. D'après les **Figures 6.2d et e**, on peut conclure que la plupart des espèces N sont sous la forme de liaisons N-C avec de petites quantités de liaisons N-H et =N-. De plus, les rapports at% de toutes les autres espèces C et N diminuent de 5 à 10 mM de 4-ABA, à l'exception des espèces C-OH/C-N. Ces tendances suggèrent que la fonctionnalisation d'EGO par greffage oxydatif de 4-ABA domine jusqu'à 10 mM, après quoi la fonctionnalisation d'EGO par adsorption physique de 4-ABA et des composés diazoïques domine. Par conséquent, 5 à 10 mM de 4-ABA semblent être la concentration appropriée pour conduire simultanément l'exfoliation du graphite et le greffage de 4-ABA sur la surface de l'EGO, tandis que trop de 4-ABA augmente l'apparition de réactions secondaires et ralentit le processus d'exfoliation.

Les EGO et EGO-ABA ont été caractérisées par XRD, les diagrammes XRD (**Figure 6.3a**) montrent les caractéristiques typiques des matériaux de graphène avec un pic de diffraction de haute intensité à 26,5 ° attribué au plan (002) du graphite. La position du pic de diffraction ne varie pas significativement avec l'étendue de la fonctionnalisation, et elle correspond à un espacement moyen des réseaux de 0,3587 nm. La valeur d'espacement du réseau et l'absence de pic de diffraction de l'oxyde de graphène (généralement à 10°) suggèrent que les matériaux EGO ont un faible degré d'oxydation et que le 4-ABA se trouve sur la surface externe des flocons EGO.

La spectroscopie Raman a été utilisée pour caractériser les défauts structuraux des EGO et EGO-ABA, le rapport entre l'intensité des bandes D et G (I_D/I_G) a été calculé (**Figure 6.3b**), il est de

0,52 ± 0,02 pour EGO et varie entre 0,68 ± 0,01 pour EGO-ABA-5 et 0,55 ± 0,08 pour EGO-ABA-40. Le résultat indique que les EGO-ABA ont plus de défauts que l'EGO, et l'EGO-ABA-5 semble avoir le plus grand nombre de défauts. Ces résultats sont cohérents avec les autres résultats expérimentaux indiquant que le greffage oxydatif du 4-ABA est favorisé à de faibles concentrations de l'amine et que la présence de 4-ABA dans l'électrolyte entrave l'oxydation et l'exfoliation du graphite.

Selon les images SEM (**Figure S6.3**), la taille de la feuille d'EGO est supérieure à celle d'EGO-ABA. Cela peut s'expliquer par la lente cinétique d'exfoliation en présence de 4-ABA, où la lente intercalation des anions sulfates entre les feuillets de graphite combinée à l'évolution des gaz SO_2, CO_2 lors de l'exfoliation conduit à la formation de l'EGO-ABA avec des flocons plus petits.

V.2.2. Caractérisation électrochimique des EGO et EGO-ABA et leurs performances pour la réduction de l'oxygène en peroxyde d'hydrogène

CV dans 0,1 M KOH a été utilisé pour évaluer le comportement électrochimique des couches minces EGO et EGO-ABA déposées sur la surface d'un GCE. Comme la **Figure 6.4a** et la **Figure S6.4a** montrent, le CV de EGO/GCE dans du 0,1 M KOH saturé en N_2 n'a qu'un seul pic cathodique large (~ -0,30 V) et un pic anodique large (~ -0,50 V) correspondant à les réactions redox réversibles des groupes fonctionnels oxygénés; tandis que les CV des EGO-ABAs/GCE ont une paire supplémentaire étroite et bien définie de pics anodiques et cathodiques (~ -0,90 V et -0,85 V, respectivement) correspondant à l'oxydation/réduction des groupes amines secondaires (-NH-). La charge voltamétrique totale (Q_{total}) a été tracée en fonction de [4-ABA] (**Figure 6.4b**), on peut apprécier que l'électrode à base d'EGO-ABA-5 a le Q_{total} le plus élevé indiquant que ce matériau a la plus grande surface électrochimique. Une tendance similaire a été trouvée pour la charge faradique ($Q_{Faradic}$) comme la **Figure S6.5** montre.

Pour évaluer l'activité électrocatalytique et la sélectivité de l'EGO et des EGO-ABA pour l'ORR, un ensemble de courbes de polarisation RRDE a été enregistré dans 0,1 M KOH en O_2 et N_2 saturé. Les courants de disque sont constitués de deux ondes de réduction, la première ayant un plateau de courant limite entre -0,50 ~ -0,85 V et la seconde commençant à des potentiels plus négatifs (autour de -1,00 V). Ces LSV indiquent que l'ORR passe par le processus à deux électrons avec la formation de l'anion hydroperoxyde (équation 6.1) suivi d'un second processus à deux électrons conduisant à la formation de l'anion hydroxyle (équation 6.2). Le potentiel d'apparition, ici défini comme le potentiel nécessaire pour atteindre un courant de -0,1 mA, est plus positif pour l'EGO-ABA par rapport à l'EGO indiquant une activité ORR plus élevée après

fonctionnalisation, **Figure 6.5a (encart)**. De plus, l'intensité du courant augmente également de l'EGO à l'EGO-ABA-10, diminuant ensuite pour des concentrations supérieures d'ABA, confirmant l'activité ORR la plus élevée pour ce catalyseur. L'activité plus élevée de l'EGO-ABA est clairement liée à une quantité plus élevée de groupes fonctionnels COOH, C=O et C-O-C par rapport à l'EGO (voir **Figure 6.2**).

La sélectivité des catalyseurs EGO et EGO-ABA vis-à-vis de l'électrogénération de H_2O_2 a été évaluée par l'analyse des courants de disque et d'anneau, et les équations (6.3) et (6.4) ont été utilisées pour estimer le nombre d'électrons échangés (*n*) pendant ORR et le rendement en espèces de peroxyde (HO_2^-), respectivement. La valeur *n* est proche de 2,4 pour l'EGO et elle augmente jusqu'à 2,7 pour l'EGO-ABA, **Figure 6.5b**. Cela indique que l'ORR procède principalement par la voie $2e^-$ avec la production de HO_2^- sur EGO et EGO-ABA. Cependant, la sélectivité en H_2O_2 diminue significativement après la modification de surface de l'EGO par le 4-ABA (**Figure 6.5c**), selon la tendance suivante : EGO (81,6%) > EGO-ABA-10 (71,2%) > EGO-ABA-5 ≈ EGO-ABA-20 ≈ EGO-ABA-40 (64–66%). La haute sélectivité de l'EGO est probablement associée à la quantité relativement faible de groupes C=O sur des éclats de grande taille également caractérisés par une faible densité de défauts sur le plan basal. À mesure que la quantité et la densité des groupes C=O augmentent dans la série EGO-ABA, la sélectivité diminue. Par rapport à la littérature, l'EGO préparé dans ce travail a une sélectivité plus élevée pour H_2O_2, mais une sélectivité plus faible.

V.2.3. Performances des EGO et EGO-ABA pour les supercondensateurs

La **Figure 6.6a** montre les CV des électrodes EGO et EGO-ABA dans du 6 M KOH collecté à la vitesse de balayage de 50 mV s^{-1} de 0 à -1,15 V. Les EGO-ABA montrent une réponse de courant importante avec des pics redox prononcés dans la gamme de potentiel de -0,3 à -1 V liée à l'oxydation et à la réduction des groupes fonctionnels (équations 6.8 - 6.10). L'intensité du courant est la plus élevée pour EGO-ABA-5, puis elle diminue pour EGO-ABA-10 et EGO-ABA-40. Les pics sont moins visibles sur l'EGO non modifié qui montre un CV de forme quasi rectangulaire et symétrique typique d'un comportement capacitif à double couche. Premièrement, la faible teneur en 4-ABA dans le milieu réactionnel pourrait conduire à un greffage uniforme des molécules d'ABA sur l'EGO et pourrait supprimer l'agrégation des feuilles d'oxyde de graphène et faciliter la réactivité redox, comme illustré sur la **Figure 6.6a** pour l'EGO-ABA-5. En outre, cela pourrait améliorer la mouillabilité de surface et la surface accessible de l'électrode conduisant à une pseudocapacité plus élevée (**Figure 6.5a**). Cependant, la quantité excessive de 4-ABA lors de la synthèse conduit à une réaction entre les amines et à l'adsorption de ces produits sur la surface

de l'EGO. Cela entrave le chemin de porosité dans les feuilles de graphène, est défavorable au transport rapide des ions électrolytes et affecte même négativement les performances électrochimiques globales des échantillons, comme la **Figure 6.6a** pour EGO-ABA-40 montre.

Des CV ont également été enregistrés à différentes vitesses de balayage (**Figure S6.7**) pour déterminer la capacité spécifique de chaque électrode. La **Figure 6.6b** montre la variation des capacités spécifiques qui diminuent progressivement avec l'augmentation de la vitesse de balayage. Cependant, les capacités d'EGO et EGO-ABA-5 à 5 mV s^{-1} sont inférieures à celles à 10 et 20 mV s^{-1}, ce qui est inhabituel, indiquant que la surface des électrodes est moins accessible au taux de balayage le plus bas. D'autres études ont rapporté des tendances similaires avec des matériaux en carbone et il a été proposé que la structure des matériaux s'effondre lors d'un balayage à faible taux de balayage ou d'une charge à faible densité de courant. De plus, la capacité des EGO-ABA est supérieure à celle de l'EGO puis diminue progressivement avec l'augmentation de la concentration en amine dans le milieu réactionnel de 5 à 40 mM. Les groupes fonctionnels oxygène (**Figure 6.2c**) en plus de participer aux processus redox rapides qui fournissent la pseudocapacité, jouent un rôle très important dans les processus de charge/décharge car ils rendent la surface interne de la matrice de graphène accessible aux ions de l'électrolyte.

La capacité de cyclage étendue a été réalisée pour l'électrode EGO-ABA-5 en enregistrant jusqu'à 5000 cycles à 50 mV s^{-1}. Comme la **Figure 6.7** montre, l'électrode a conservé 80,6 % de la capacité initiale après 5 000 cycles dans du 6 M KOH. Cette diminution de la capacité peut être attribuée à la désorption des molécules d'ABA attachées de manière non covalente qui sont faiblement liées à la surface de l'EGO. Dans tous les cas, le test de cyclage prolongé démontre la remarquable durabilité électrochimique de ce matériau d'électrode et son potentiel d'utilisation dans les supercondensateurs.

VII. Conclusion

Dans cette thèse, nous avons étudié la synthèse de matériaux EGO dans plusieurs conditions différentes, analysé leurs propriétés physicochimiques et électrochimiques et les avons appliquées à des aptasenseurs électrochimiques et à des supercondensateurs.

Tout d'abord, une série des EGO ont été synthétisés dans 0,1 M H_2SO_4 sous différents effets du champ électrique (tension appliquée divisée par la distance entre les électrodes). D'après les résultats de la caractérisation physico-chimique, les groupements fonctionnels oxygénés situés

au plan basal (C-OH et C-O-C) sont fortement influencés par les conditions d'exfoliation, et leur vitesse dépend de deux régimes différents : la cinétique d'exfoliation et les concentrations en radicaux OH•. En utilisant la sonde redox $[Fe(CN)_6]^{3-/4-}$, les EGO assemblés sur GCE via un lieur de film AP ont été caractérisés électrochimiquement, montrant qu'une haute densité de groupes C-O-C a un impact néfaste sur les valeurs ESA et k^0 pour quelques couches ($\leqslant$ 7 couches) EGO. Les EGO obtenus à 8 - 10 V et 6 cm ont fourni l'ESA (0,08 cm^2) et le k^0 (0,13 cm^{-1}) les plus élevés. Sur la base de la plateforme proposée, d'excellentes corrélations peuvent être établies entre les matériaux de type graphène préparés par exfoliation électrochimique du graphite et leurs propriétés électrochimiques, structurelles et chimiques.

Ensuite, des aptasenseurs électrochimiques basés sur des flocons d'EGO de grande taille et un aptamère de cocaïne publiée ont été étudiés. Les résultats ont démontré que l'aptamère de cocaïne, en particulier avec le groupe terminal $-NH_2$, peut être adsorbé rapidement (10 minutes) sur la surface du GCE modifié par EGO grâce à une méthode d'adsorption physique, résultant en un moyen facile, rapide et rentable de fabriquer la plateforme de détection, qui est importante pour les applications industrielles. Il a également montré une bonne reproductibilité, une durée de conservation et une sensibilité intéressante, avec une limite de détection de 50 nM. De plus, une valeur ESA et k^0 plus élevée de l'EGO 10V6cm offre de meilleures performances de détection que les autres EGO, ce qui prouve à quel point les propriétés électrochimiques des matériaux jouent un rôle crucial dans les performances de détection. La plateforme simple EGO/aptamère-NH_2 est censée être applicable à la fabrication de biocapteurs similaires.

Enfin, en faisant varier la concentration de 4-ABA (entre 0 et 40 mM) dans l'électrolyte H_2SO_4 (0,1 M) pendant l'exfoliation électrochimique du graphite, différentes quantités d'oxyde de graphène exfolié électrochimiquement fonctionnalisés par l'acide aminobenzoïque (EGO-ABA) ont été synthétisés en une seule étape. Il a été constaté que la présence de 4-ABA réduisait les taux d'exfoliation ainsi que plusieurs réactions qui se produisent simultanément et entrent en compétition : (1) oxydation électrochimique du graphite opposée à l'oxydation du 4-ABA ; (2) greffage EGO-ABA contre la formation de colorant azoïque. Le 4-ABA doit être limité à 10 mM pour favoriser le greffage sur les surfaces EGO. Par rapport à l'EGO nu, les EGO-ABA ont montré des tailles de flocons plus petites et une densité plus élevée de groupes fonctionnels oxygénés. Les EGO et EGO-ABA ont ensuite été testés en milieu alcalin pour l'ORR et les supercondensateurs. Par rapport à l'EGO, les catalyseurs EGO-ABA ont une activité plus élevée pour l'ORR en H_2O_2 en raison de leur densité de groupes fonctionnels oxygénés plus élevée. Cependant, une teneur plus faible en groupes carbonyle de l'EGO nu lui a valu une plus grande

sélectivité pour le processus à deux électrons. Pour les supercondensateurs, les EGO-ABA avaient une capacité spécifique accrue par rapport à l'EGO, augmentant d'un facteur 3 pour les matériaux préparés par exfoliation dans 5 mM 4-ABA/0,1 M H_2SO_4. Le matériau d'électrode a également montré une capacité de cyclage impressionnante après 5000 cycles à 50 mVs^{-1}, avec une perte de seulement 19,4 %.

VIII. Composition de la thèse

Cette thèse se compose de huit chapitres. Le premier chapitre est une introduction générale. Le deuxième chapitre présentera une revue générale des matériaux de graphène, y compris les matériaux GO et EGO, le aptasenseur électrochimique et les supercondensateurs y seront introduits. Le troisième chapitre présentera les méthodes de caractérisation de base utilisées dans cette thèse, puis démontrera les méthodes de synthèse des matériaux EGO et la préparation d'électrodes à base d'EGO pour les caractérisations et applications électrochimiques. Le quatrième chapitre présente notre article sur la caractérisation électrochimique des matériaux EGO. Le cinquième chapitre décrit nos travaux sur l'aptasenseur de cocaïne électrochimique fabriqué à partir de matériaux EGO. Le sixième chapitre décrira la synthèse en une étape de matériaux EGO fonctionnalisés par l'acide 4-aminobenzoïque (EGO-ABA) et leur application aux supercondensateurs. Le septième chapitre présentera quelques travaux en cours et à venir sur la synthèse de matériaux EGO décorés de nanoparticules d'or (EGO-Au NP) et leur caractérisation électrochimique. Dans le dernier chapitre, quelques conclusions seront tirées et quelques perspectives seront discutées.

TABLE OF CONTENTS

LIST OF FIGURES

LIST OF TABLES

LIST OF ACRONYMS AND ABBREVIATIONS

Δi	Relative variation of the current
0D	Zero-dimensional
1D	One-dimensional
2D	Two-dimensional
3D	Three-dimensional
4-ABA	4-aminobenzoic acid
AP	*p*-aminophenyl
AP-film	*p*-aminophenyl film
Apt	Cocaine aptamer
Aptamer-NH_2	Cocaine aptamer with amine terminal groups
Aptamer-OH	Cocaine aptamer with hydroxyl terminal groups
at%	Atomique percentage
Au NPs	Gold nanoparticles
BSA	Bovine serum albumin
CNT	Carbon nanotube
Co	Cocaine
CP	Carbon paper
Cs	Specific capacitance
CV	Cyclic voltammetry/voltammogram
CVD	Chemical vapor deposition
DC	Direct current
DMAP	4-dimethylaminopyridine
DPV	Differential pulse voltammetry
EDLC	Electric double-layer capacitor
EG	Exfoliated graphene
EGO	Electrochemically exfoliated graphene oxide
EGO-ABA	4-aminobenzoic acid functionalized EGO
EGO-Au NPs	Gold nanoparticles decorated EGO
EGO-membrane	EGO synthesis with membrane
EIS	Electrochemical impedance spectroscopy
ESA	Electrochemical surface area
FLG	Few layer graphene
FT-IR	Fourier Transform Infrared Spectroscopy
FWHM	Full width at half maximum
GCE	Glassy carbon electrode
GFNs	Graphene-family nanomaterials
GIC	Graphene-intercalated compound
GO	Graphene oxide
HOPG	Highly ordered pyrolytic graphite

Ils	Ionic liquids
i_p	Peak current
k^0	Standard rate constant of electron transfer
LOD	Limit of detection
LSV	Linear sweep voltammetry/voltammogram
NF	Nickel foams
NP-film	*p*-nitrophenyl film
ORR	Oxygen reduction reaction
PBS	Phosphate buffer saline
PC	Propylene carbonate
PTFE	Poly(tetrafluoroethylene)
Q	Charge
rGO	Reduced graphene oxide
RRDE	Glassy carbon rotating disk ring electrode
SC	Supercapacitors
SCE	Saturated calomel electrode
SEM	Scanning electron microscope
SI	Supporting information
SLG	Single layer graphene
SWV	Square-wave voltammetry/voltammogram
T	Temperature
TEM	Transmission electron microscopy
THC	Tetrahydrocannabinol
TSTU	N,N,N',N'-tetramethyl (succinimido) uronium tetrafluoroborate
XPS	X-ray photoelectron spectroscopy
XRD	X-ray powder diffraction

1. GENERAL INTRODUCTION

Graphene-based materials have been extensively investigated in recent years because of their tunable chemistry (e.g., surface functional groups and heteroatoms doping), high surface area and good electrical conductivity. [1-2] Graphene oxide (GO) materials consist of graphene layers modified with oxygen functional groups such as hydroxyl and epoxy groups mostly located on the basal plane, with smaller amounts of carbonyl and carboxylic groups at the edges. [3] These oxygen functional groups confer to GO flakes a good dispensability in polar solvents, [4] biocompatibility and affinity for specific biomolecules. [5-6] They also provide chemical flexibility to GO which can, for example, be used as cross-linker between a substrate and molecules of interest through π-π stacking, electrostatic interactions or chemical bonds. [5, 7-8] For these reasons GO and its composites have been used in a broad range of applications, [9-11] especially in the electrochemistry field [6, 10] including (bio)sensors, [8, 12] supercapacitors, [1] electrogeneration of hydrogen peroxide, [13-14] etc.

Generally, GO materials are prepared using chemical methods such as the modified Hummers method, [15] followed by a thermal treatment, [16-17] by electrochemical reduction [18] or by hydrothermal treatment [19] to partially remove the functional groups and to obtain reduced graphene oxide (rGO). Electrochemical exfoliation of graphite is an environmentally friendly and low-cost method that offers the possibility of synthesizing GO materials in few hours. [20-23] These materials are usually referred as electrochemically exfoliated graphene oxide (EGO). Briefly, it consists of a two-electrode system using graphite as the working electrode and a counter electrode immersed in an electrolyte. When a potential difference is applied between the electrodes immersed in an aqueous electrolyte, water is reduced at the cathode generating H_2 and hydroxyl radicals are formed at the anode. [20] These radicals attack the graphite electrode, and facilitate the intercalation of ions from electrolyte within the graphitic layers, resulting in the formation of flakes that are dispersed in the electrolyte. [20] In addition, depending on the electrolyte used, the method may also allow the preparation of EGO-based composites [24-25] or the surface modification of EGO with other molecules in a one-step process. [26-27] Therefore, a wide range of EGO materials with different properties (amounts and types of functional groups, density of defects, number of layers, flake sizes, composites) can be easily synthesized by varying the experimental conditions during the electrochemical exfoliation, such as applied voltage and electrolyte. [23] Compared to the chemical methods (e.g. Hummers' method: C/O $\approx$ 2), [15] the EGO materials obtained this way usually have a lower density of oxygenated functional groups (C/O > 4) [23] which could be of advantage for electrochemical applications, [16, 28] because the oxygenated

functional group may lower the electrical conductivity of the GO materials. [1] Since EGO's oxygenated groups are able to strongly affect its electrochemical properties, [10, 29] the synthesis and selection of an appropriate EGO for the target application is a challenge.

The thesis work focuses on the synthesis of EGO materials for different electrochemical applications including electrochemical biosensing and energy storage (supercapacitors). The research objective includes: i) synthesizing a series of EGO materials obtained under different experimental conditions (applied voltage, distance between the electrodes, and subsequent thermal reduction) and to systematically investigating their structural and electrochemical properties; ii) investigating the electrochemical apta-sensing performance based on EGO materials; iii) electrochemical exfoliation of graphite foil in 0.1 M sulfuric acid containing 4-aminobenzoic acid (4-ABA) to obtain a series of aminobenzoic acid functionalized EGO materials (EGO-ABA) in one-step, and to investigate the role of the functional groups towards the supercapacitors. Three related projects are implemented to achieve these objectives:

1) Electrochemical characterization of graphene-type materials obtained by electrochemical exfoliation of graphite foil.

Here, a platform based on the self-assembly of EGO sheets onto the surface of a glassy carbon electrode (GCE) through a p-aminophenyl (AP) linker is proposed for the systematic electrochemical characterization of the EGO materials.

2) Electrochemically exfoliated graphene oxide-based simple and efficient electrochemical cocaine aptasensor.

Here, we demonstrate the suitability and advantages of using the EGO materials which have better electrochemical properties from the first project for the fabrication of electrochemical aptasensors. This was achieved by physically adsorbing and chemically immobilizing a commercial cocaine aptamer with amine terminal groups (aptamer-NH_2) on the EGO surface, their sensing performances were investigated and compared.

3) One-step synthesis of aminobenzoic acid functionalized graphene oxide by electrochemical exfoliation of graphite for supercapacitors.

In this third project, the surface of EGO is modified by electrochemically grafted 4-amino benzoic acid (4-ABA) during the one-step synthesis, and the new materials investigated the role of the functional groups for supercapacitors.

This thesis consists of eight chapters. The first chapter is this general introduction. The second chapter will present a general review of the graphene materials including the GO and the EGO materials. Then, the electrochemical biosensor and supercapacitors will be introduced. The third chapter will introduce the basic characterization methods used in this thesis, and then demonstrate the methods to synthesize the EGO materials and the preparation of EGO based electrode for electrochemical characterizations and applications. The fourth chapter presents our article on the electrochemical characterization of EGO materials. The fifth chapter described our work on fabricated electrochemical cocaine aptasensor based on EGO materials. The sixth chapter will describe the one-step synthesis of 4-aminobenzoic acid functionalized EGO materials and their application to supercapacitors. The seventh chapter will introduce some ongoing and future works about the synthesis of gold nanoparticles decorated EGO (EGO-Au NPs) materials and their electrochemical characterization. In the last chapter, some conclusions will be drawn and some perspectives will be discussed.

2. LITERATURE REVIEW

2.1. Graphene materials

As reported in 2004, Andre Geim and Konstantin Novoselov included a method for micromechanical cleaving a single-layer of graphene (SLG) on sticky tape from highly ordered pyrolytic graphite (HOPG). Their pioneering experiments involving graphene won them the 2010 Nobel Prize in Physics. [30] Graphene has large theoretical specific surface area (2630 $m^2 g^{-1}$), [31] strong mechanical properties (1100 GPa Young's modulus), [32] high optical transmittance (97.7%), [33] remarkable thermal conductivity (~5000 $Wm^{-1}K^{-1}$), [34] and good electrical conductivity (3189 Scm^{-1}) [35] which can withstand 108 Acm^{-1} of current density. [36] Due to these excellent properties, graphene and its derivatives, referred to as graphene-family nanomaterials (GFNs), [37] have generated immense attention and have been extensively studied. The GFNs mainly includes graphene, graphene oxide (GO), and reduced graphene oxide (rGO). [37] GFNs have been used in various applications including nanoelectronics, [38-39] batteries, [40-42] drug delivery, [43-44] sensors [42, 45-46] and supercapacitors, [47-49] etc.

A graphene sheet comprises hexagonal honeycombs that are made of covalently bonded sp2-hybridized carbon atoms, which are arranged in two dimensions (2D). [50] Other carbon materials can be created by wrapping graphene as a basic building block, as shown in **Figure 2.1**: 1) zero-dimensional (0D) fullerenes, wrapped graphene sheets into spheres (Bucky Ball), 2) one-dimensional (1D) carbon nanotubes (CNTs), rolled graphene sheets into cylindrical structures, and 3) three-dimensional (3D) graphite, made by stacking graphene sheets. [51-52] Actually, the 3D graphitic carbon have existed since the 1500s, 0D fullerene and 1D CNT were found during the 1980s and 1990s (**Figure 2.1**). [53-54]

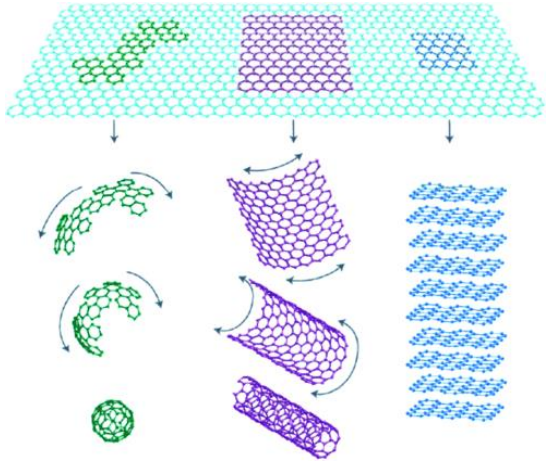

Figure 2.1. Schematic illustration of different carbon allotropes created from graphene: wrapped up into 0D buckyballs, rolled into 1D nanotubes, or stacked into 3D graphite. [52] (Copyright © 2007 Springer Nature)

Graphene with one, two, and three graphitic layers is called monolayer or SLG, bilayer graphene, and trilayer graphene, respectively. The term few layer graphene (FLG) and thick graphene are commonly used to describe graphene with more than five layers and up to 30 layers. [55] As shown in **Figure 2.2**, there is about 0.33 nm layer thickness and a distance of 0.142 nm between carbon atoms in graphene. [56]

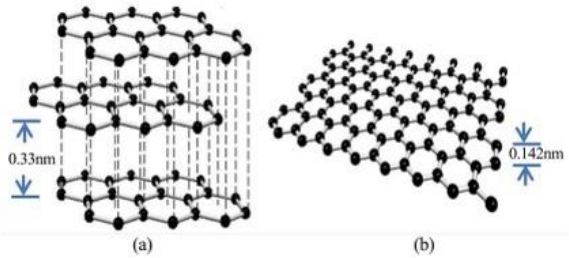

Figure 2.2. Schematic illustration of (a) trilayer and (b) monolayer of graphene from graphite.[56] (Copyright © 2015 John Wiley and Sons)

GO consists of layers of graphene sheets with oxygen functional groups on their surfaces and edges, including hydroxyl, epoxy, carbonyl, and carboxyl, etc. In general, most hydroxyl and epoxy groups are found on the basal plane, while carbonyl and carboxyl groups are found at the edges. [6, 12, 57] The layer thickness of GO can be more than 0.334 nm upon the oxidation degree of GO. [58] Compared to graphene, oxygen functional groups on GO may enhance the heterogeneous electron transfer rate and make GO exhibit better dispersion in water and many other solvent, better biocompatibility, and higher affinity for biomolecules. [45, 59] GOs can also be used as a cross-linker to bind with other molecules through the oxygen functional groups. [7-8] GO can be converted into rGO by removing most oxygenated functional groups through chemical, thermal, electrochemical and microwave treatments. [60-62] As a consequence, rGO sheets lose their hydrophilic properties. [63] **Figure 2.3** shows the different structures of graphene, GO and rGO.

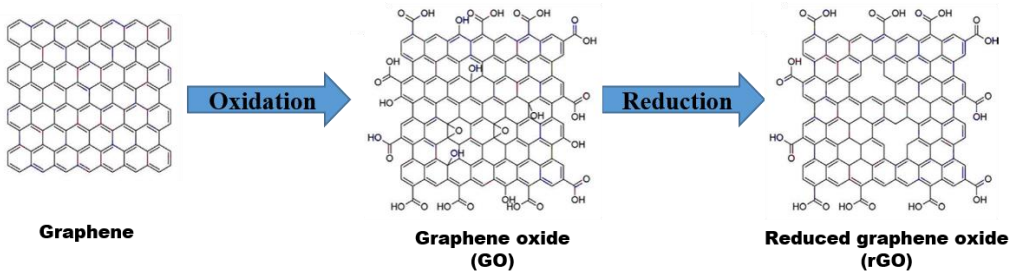

Figure 2.3. Schematic illustration of structures of graphene, graphene oxide (GO), and reduced graphene oxide (rGO). [63] (Copyright © 2010 Elsevier)

2.1.1. Synthesis of graphene materials

Over the last decade, a variety of approaches to graphene synthesis have been investigated. They can be divided into two types as shown in **Figure 2.4**: 1) top-down process and 2) bottom-up process. [64] The top-down approach considers graphene to be the structural motif of graphite and other carbon nanomaterials, which can be obtained by mechanical exfoliation, [30, 65-67] chemical exfoliation, [68] and chemical synthesis [58, 69-71]. Due to their simplicity and lower costs, top-down approaches are usually used to produce most commercial graphene products. In the bottom-up synthesis method, molecules grow into graphene sheets, such as pyrolysis of graphene, [72] epitaxial growth of graphene on silicon carbide surface, [73] chemical vapor deposition (CVD) of gaseous carbon precursors on a solid substrate [74-75] and other methods. They require complex infrastructure and operational conditions. Among all these synthesis methods, the most commonly used today are CVD [74-75], mechanical exfoliation, [30, 65-67] chemical exfoliation, [68] and chemical synthesis. [58, 69-71]

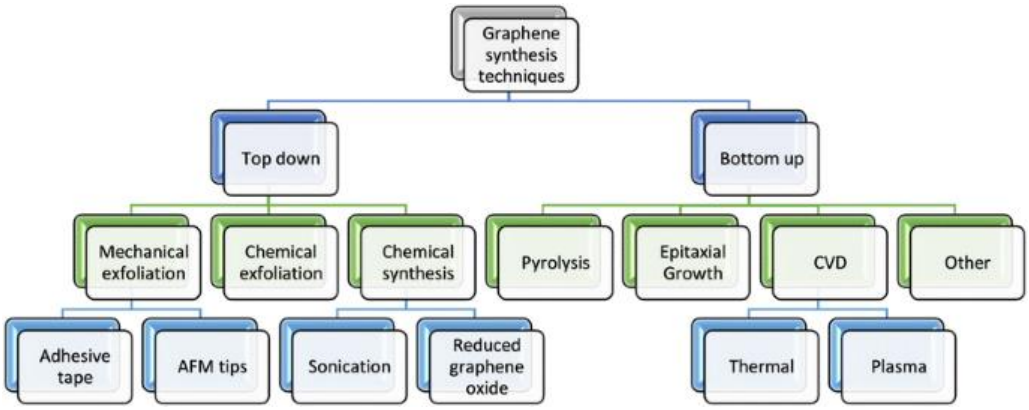

Figure 2.4. Schematic illustration of the graphene synthesis process flowchart. [76] (Open Access)

Due to its simplicity and relatively good control, CVD is popular for synthesizing graphene materials. [77-78] It comprises a step during which molecules are heated and gasified, to form a precursor. Once the precursors (in the form of solids, liquids, or gases) are thermally disintegrated, they are diffused over a substrate to form single or few layers of graphene. Graphene is typically deposited by CVD on transition-metal substrates, including Ni, [79] and Cu, [80] etc. [77-78] Despite the fact that CVD has overcome the scalability problems of mechanical exfoliation, it is still expensive: it requires sophisticated instruments and the graphene transfer process consumes lots of energy and time.

Mechanical exfoliation, which extracts graphene flakes from a preferred substrate, is the first method known. [30] This is a top-down nanotechnology technique that creates layered structures with transverse or longitudinal stresses. The graphite structure consists of layers of single-atomic graphene held together by weak van der Waals forces. The interlayer bond energy is 2 $eVnm^{-2}$ between each layer, and SLG can be separated from graphite with a force of about 300 nN μm^{-2}. [81] Through mechanical cleaving from graphitic materials like HOPG or natural graphite, SLG to FLG can be produced. [30, 65-67] This mechanical exfoliation process can be accomplished in several ways, including scotch tape, [30] electricity field, [66] and ultrasonication, [65] etc. Low-cost production of high-quality graphene can be achieved through this process. There is, however, a problem with the reproducibility and scalability of the exfoliation process. To produce high-quality graphene materials at large-scale for nanotechnology, further improvements are needed.

Chemical exfoliation of graphene flakes is also an effective method of obtaining a monolayer or few layers of graphene. In this method, alkali metals are added to a graphite dispersion, which reduces van der Waals forces between the layers by expanding their interlayer spacing and forming graphene-intercalated compounds (GICs). A few layers of graphene are produced by dispersing these in liquid through sonication. To form GICs, only alkali metals are appropriate because graphite's ionization potential differs from that of alkali metals'. A large amount of graphene materials can be produced at a low temperature with this method, but the produced graphene flakes can probably assemble back into graphite. [68, 82]

Chemical methods are widely used for synthesizing graphene materials, particularly GO. This method produces GO from graphite by oxidizing it with strong acids and oxidizing agents, such as concentrated sulfuric acid (H_2SO_4) and potassium permanganate ($KMnO_4$). [15, 71, 83] The oxidation degree of GO is controlled by stoichiometry, reaction conditions (temperature, pressure, etc.), as well as graphite type (HOPG, pure or natural graphite, etc.). [58, 84] The Brodie, [83] Staudenmaier, [71] and Hummers[15] methods or some modifications of these methods are usually used to produce GO. [85-86] **Figure 2.5** illustrates these three methods of producing GO from graphite. [87] As compared to the other methods, Hummers' method is faster, safer, and more effective, and is widely used today with a couple of modifications. Despite this, the process is still time-consuming, and labor-intensive, and toxic gases (including NO_2, N_2O_4, and ClO_2) are generated. [15, 85-86, 88]

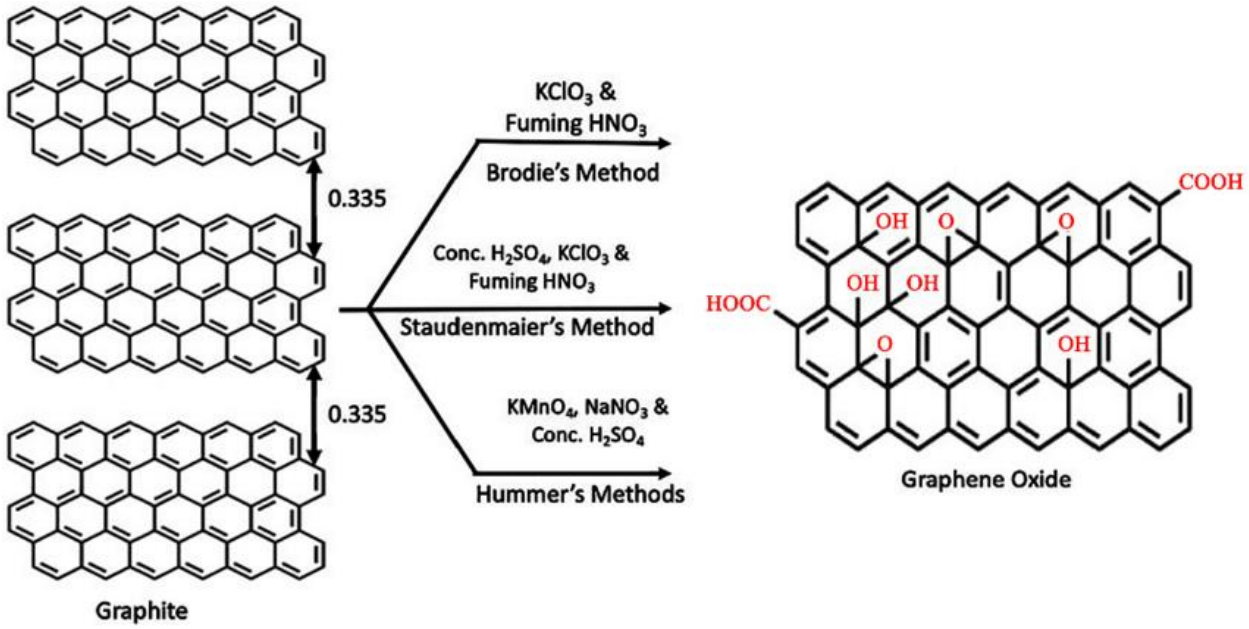

Figure 2.5. Schematic illustration of graphene oxide (GO) synthesis by Brodie, Staudenmaier, and Hummers' methods. [87] (Open Access)

2.2. Electrochemically exfoliated graphene oxide

In recent years, a simple method of producing graphene materials has emerged through the electrochemical exfoliation of graphite. [22, 89-90] In general, this process uses a two-electrode system, and a typical experimental arrangement includes: (a) a graphite working electrode, which can be made from graphite powder, foil, rod, flakes, or highly oriented pyrolytic graphite (HOPG); [27, 91-92] (b) a counter electrode such as platinum, carbon, or graphite; [91] (c) an electrolyte, which can be aqueous (such as salt solutions, acidic, or alkaline) or non-aqueous (ionic or organic liquids); [20, 27, 91] (d) a potentiostat or a direct current (DC) power supply. When graphite is exfoliated in liquid electrolytes under ambient conditions, oxygen is introduced into the carbon lattice of graphene, the graphene oxide materials obtained by this method are called electrochemically exfoliated graphene oxide (EGO).

2.2.1. Synthesis and mechanism

When a DC power supply applies a voltage, electrolyte molecules, ions, or co-intercalating species in electrolytes intercalate among the graphene layers of graphite and attack them, causing expansion and exfoliation of graphene layers, resulting in the formation of EGO flakes that are dispersed in the electrolyte. According to the power supply applied to graphite electrodes,

exfoliating graphite electrodes involves two types: anodic (uses a positive bias) and cathodic (uses a negative bias) exfoliations. [27, 91, 93] As shown in **Figure 2.6**, anodic exfoliation involves intercalating anions (e.g., SO_4^{2-}) in aqueous electrolyte, while cathodic exfoliation involves attracting positively charged ions (e.g., Li^+) in organic solvent.

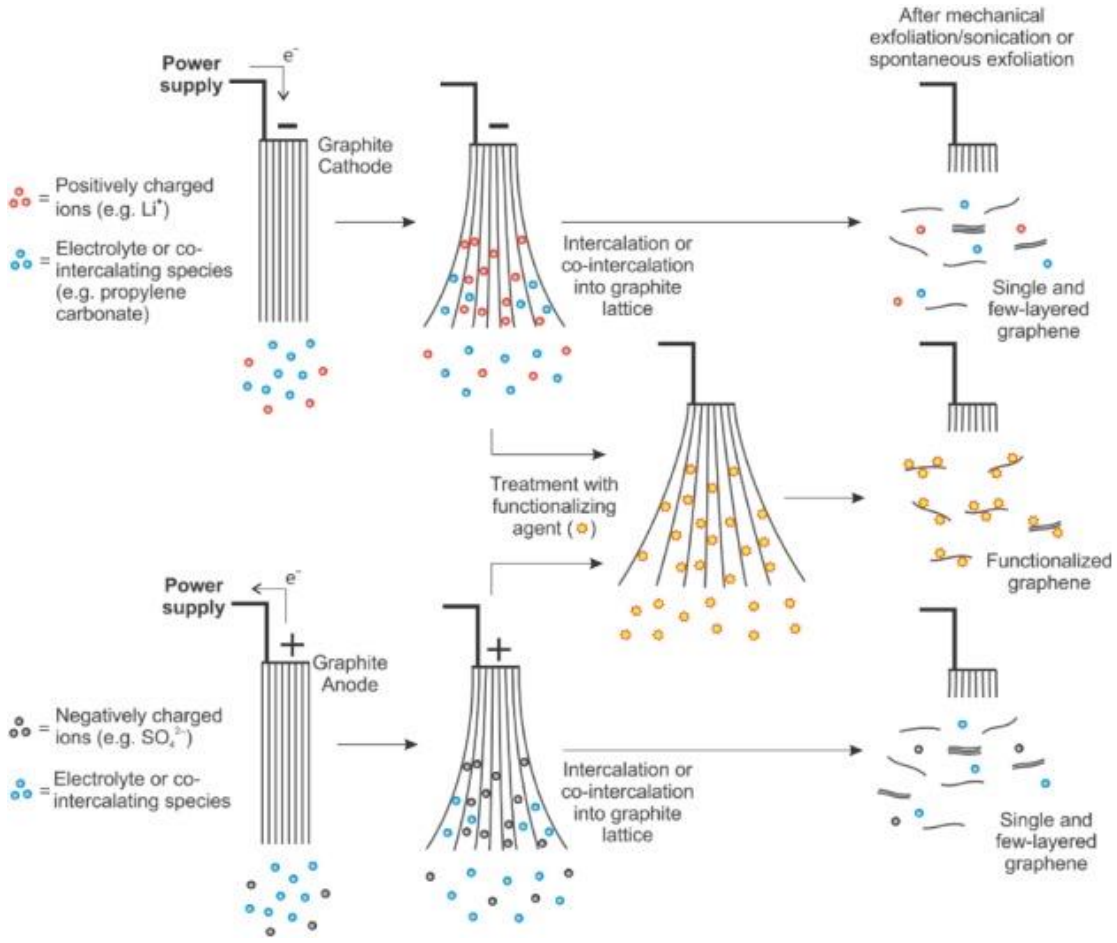

Figure 2.6. Schematic illustration of an overview of cathodic and anodic exfoliation of graphite. When a graphite working electrode is charged positively or negatively, oppositely charged intercalating ions are attracted to it. The presence of co-intercalating molecules is optional. Functionalization can be achieved either after exfoliation or during exfoliation by adding functionalizing agents. [93] (Copyright © 2015 Elsevier)

Different exfoliation methods may result in different electrochemical exfoliation mechanisms. Parvez et *al.* [20] presented a mechanism for anodic exfoliation in $(NH_4)_2SO_4$ aqueous solutions. As illustrated in **Figure 2.7a**, when water is electrolyzed, hydroxyl ions are formed, and these strong nucleophiles attack sp^2 carbons at graphite grain boundaries and edges to form vicinal OH groups (**Figure 2.7b**, reaction 1). Epoxide rings are formed when OH groups interact with each other (**Figure 2.7b**, reaction 2). By further oxidation, OH groups can be dissociated into carbonyl groups (**Figure 2.7b**, reaction 3). As a result, graphite layers at the edges depolarize and expand,

allowing sulfate ions (SO_4^{2-}) to intercalate, possibly even more water molecules. There are other reactions that may occur alongside graphite oxidation, including CO_2 and O_2 evolution in reactions 4 and 5 of **Figure 2.7b**, these gases facilitate the graphite layer exfoliation. The decomposition of SO_4^{2-} during exfoliation can generate various gaseous products, including SO_2, O_2, and H_2, that can also increase graphite interlayer spacing.

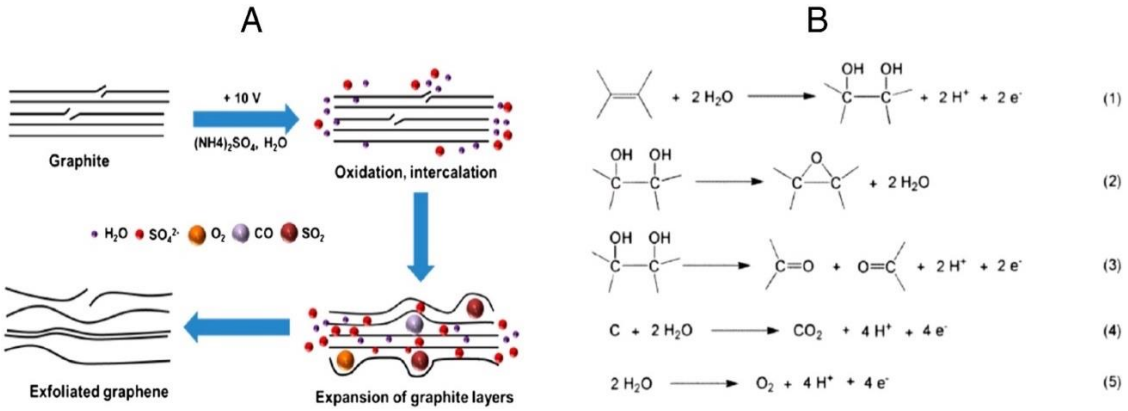

Figure 2.7. (a) Schematic illustration of the mechanism of electrochemical exfoliation in $(NH_4)_2SO_4$ aqueous solution. (b) Schematic illustration of the electrochemical oxidation of a graphite electrode. [20] (Copyright © 2014 American Chemical Society)

For cathodic exfoliation, Wang et *al.* provide a mechanism for graphite exfoliation by using positive ions (Li^+) as intercalating agents in an organic solvent (propylene carbonate, PC). As shown in **Figure 2.8**, under sufficiently high voltages, Li^+ ions and PC will co-intercalate into negatively charged graphite layers, forming propylene gas that will assist graphite expansion. [94] Compared to anodic electrochemical exfoliation, intercalation, and expansion efficiencies, less damage was done to the graphene sp^2 structure.

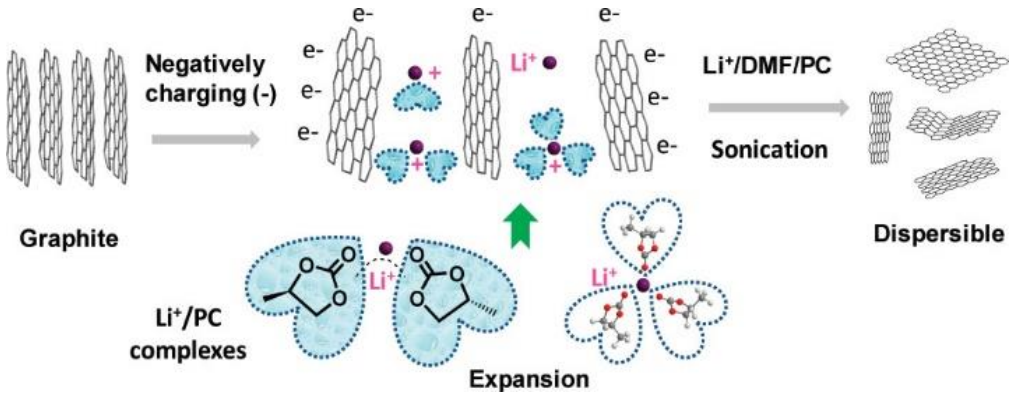

Figure 2.8. Schematic illustration of exfoliation of graphite through intercalation of Li^+ Complexes. [94] (Copyright © 2011 American Chemical Society)

Through the control of exfoliation parameters, such as voltage (current), the distance between two electrodes, graphite electrode, and electrolyte, the EGO materials with different amounts of oxygen functional groups, defect densities, layer numbers, and lateral sizes can be obtained. Further, during electrochemical exfoliation, chemical reactions can be carried out with functionalizing agents to achieve in situ chemical doping (functionalization) of EGO materials, as shown in **Figure 2.9**. [20, 22-23, 25-27, 57, 93, 95-96]

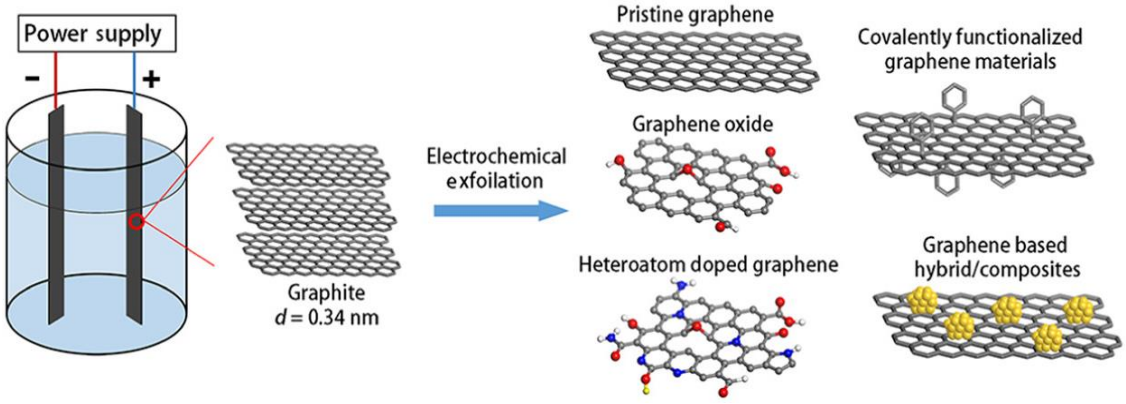

Figure 2.9. Schematic illustration of graphite electrochemically exfoliated to produce various graphene materials.[27] (Open Access)

2.2.2. Influence of the exfoliation process parameters

2.2.2.1. Graphite electrode

In electrochemical exfoliation, graphite electrodes are usually either natural graphite foils, rods, or highly oriented pyrolytic graphite (HOPG). [27, 91-92] As ions intercalate between graphene layers during exfoliation, they will be affected by graphite electrodes' microstructures, including their thickness, composition, defects, and pretreatment, etc. Munuera *et al.* found that graphite foils have fewer voids, folds, and wrinkles enabling graphite to exfoliate easily and prevent damage caused by oxidation, and thus produce better graphene materials than those obtained from HOPG electrodes. [97] According to Fuertes *et al.*, compared with thin graphite foils or flacks, thick graphite rods or sheets typically exfoliate more slowly, which promotes graphite oxidation, leading to getting more hydrophilic graphene materials. [98] In the study of Chen *et al.*, nanoclay in pencil cores assisted electrochemical exfoliation of pencil cores and in-situ functionalization processes to produce graphene materials. [99] Also, graphite electrodes pretreatment or appropriate interactions may be helpful in generating desirable graphene materials. For example, according to Fang *et al.*, before electrochemical exfoliation in acid electrolytes, pretreatment with alkaline

solutions significantly reduces graphite oxidation, either because the pretreatment in NaOH increased the interlayer spacing in graphite, or because the H_2O produced by the neutralization reaction between NaOH and H_2SO_4 in graphene layers. [100]

From these studies, it is recommended that the electrochemical exfoliation of defective, thin, and small graphite electrodes could be more efficient to yield graphene materials with less damage which caused by oxidative reactions.

2.2.2.2. Voltage (Current)

The voltage or current plays an important role in electrochemical exfoliation kinetics. In the study of Su *et al.*, graphite flake was exfoliated in H_2SO_4 solution under +1 V first, followed by ramping up to +10 V. When the voltages were less than +10 V, they observed a slow and inefficient exfoliation process. [22] For another example, Srivastava et *al.* used a chronoamperometry technique to compare five voltage values from 2 to 10 V for the electrochemical exfoliation of graphite rods in 0.1 M sodium saccharin solution. Their results indicate that higher voltage potentials might result in graphene materials with higher defect densities and O contents due to intensified oxidation.[101]

According to these results, the graphite electrode can be exfoliated more quickly under higher voltage, and the graphene materials obtained will have more oxygenated functional groups.

2.2.2.3. Electrode distance

In recent research, Liang *et al.* [102] found that the distance between two electrodes (electrode distance) can influence insertion speed, direction, and exfoliation kinetic rates. They obtained the following different microstructures of graphene materials by modifying electrode distance during the exfoliation of graphite papers in 1M $(NH_4)_2SO_4$ at the presence of 0.1 wt% H_2O_2 : at a short electrode distance of 3 cm, high-quality exfoliated graphene with the size above 5 μm and thickness below 5 layers was produced; when the electrode distance increased to 30 cm, exfoliated graphene quantum dots (EGQD) with the size below 5 nm were prepared; when the distance between 3 and 30 cm, EGO (with ca. 15% oxygen content) was obtained. Further, when electrode distance is increased, graphene materials yield decreases.

According to their results, a short electrode distance promotes insertion speed and exfoliation kinetics, while a long electrode distance promotes oxidation.

2.2.2.4. Electrolyte

An electrochemical exfoliation of graphite can be achieved with different electrolytes, including acids, alkaline, inorganic/organic salts, organic solvent, or a mixture of them, etc. [27, 93, 97] Among them, organic solvents (e.g. PC or dimethyl sulfoxide) are used to exfoliate graphite cathodically, and the graphene materials obtained are usually less damaged but the yield is low. [94, 103-104] Other electrolytes are used for anodic exfoliation.

Aqueous acids, [27, 95, 105-107] particularly H_2SO_4, are the most commonly used electrolyte, since SO_4^{2-} ions have a similar ionic size to graphite d-spacing (0.34 nm), making them relatively easy to intercalate. [106] However, the anions intercalate and decompose at such a fast rate in acidic electrolytes that graphene materials synthesized may have a large number of layers and small lateral sizes. Additionally, highly acidic conditions can further accelerate the oxidation of graphite electrodes, leading to exfoliated graphene materials with increased defects and oxygen groups. [27, 95, 105-107]

Graphite has also been electrochemically exfoliated with alkaline solutions. [108-111] Habibulla Imran *et al.* have electrochemically exfoliated graphite rod (pencil) to obtain EGO materials in 3 different electrolytes: HCl, NaOH, and phosphate buffer saline (PBS, pH 7.4). Among them, the exfoliation in NaOH solution had the lowest yield. [108] In the study of Rao *et al.*, H_2O_2 was added to the NaOH electrolyte, the reaction of H_2O_2 and hydroxyl ions (HO^-) generated the nucleophilic O_2^{2-} ions which are important for the intercalation of graphite, making the electrochemical exfoliation process more efficient. [109]

Besides the acid and alkaline solution, electrolytes can be prepared using organic or inorganic salts, such as ionic liquids (ILs), or sulfate salts, etc. [20, 112-117] ILs have been used as electrolytes in several early studies to exfoliate graphite, but graphene materials generally produce low yields. [115-117] In the study of Parvez *et al.*, [20] exfoliations in various sulfate salts (Na_2SO_4, $(NH_4)_2SO_4$, and K_2SO_4) under neutral pH conditions were compared. It was found that $(NH_4)_2SO_4$ is the best electrolyte for producing graphene products that have large lateral sizes (>5 mm) and a high C/O ratio (17.2). The electrolyte concentration effects were also investigated. By increasing $(NH_4)_2SO_4$ concentration from 0.01 M to 1.0 M, graphene production increased from 5 wt.% to 75 wt.%.

Further increases in concentration failed to increase the yield, possibly because the low water content in the $(NH_4)_2SO_4$ would decrease the formation of $HO^{\bullet}$ radicals, which reduce the oxidation and expansion of graphite edges. [20] Munuera *et al.* have exfoliated graphite in different sodium halides (NaCl, NaI, and NaBr) producing single and few layers of graphene materials with up to 16.7 C/O ratio, they found the hydrated halide anions are not only intercalated in graphite foil electrodes but also react with $HO^{\bullet}$ radicals, producing graphene materials with low O content. [114]

When graphite is anodically exfoliated in an aqueous electrolyte (such as sodium sulfate solution in **Figure 2.10a**), $HO^{\bullet}$ radicals are generated from water electrolysis, which leads to graphene materials oxidation. [118] In order to avoid this oxidation, electrolyte additives were used in some studies to neutralize or eliminate such radicals. [113, 118] As shown in **Figure 2.10b**, in the presence of readily oxidizable electrolytes, such as sodium benzenesulfonate which has low oxidation potential, the hydroxylate electrolyte formed during anodic oxidation, inhibiting graphene oxidation. In this way, the electrolyte protects graphene from oxidation by serving as a sacrificial agent. [118] On another side, oxidizing materials (such as Na_2WO_4, $NaNO_3$, and H_2O_2) [109, 119-120] and oxidative electrolytes (such as H_2SO_4, HNO_3, and $HClO_4$) [121-123] can be used to synthesize significantly oxidized graphene materials (with a C/O ratio smaller than 10). For example, Abdelkader *et al.* found a significant decrease in the C/O ratio of GO (from 7.6 to 4) when 0.2 M HNO_3 was added to 0.2 M sodium citrate electrolyte, because the $NO_2^{-\bullet}$ radicals from HNO_3 were highly oxidative, resulting in a significant increase in oxygenated functional groups. [123] According to Coroş *et al.*, GO with a low C/O ratio (0.81) was obtained from graphite rods exfoliated in the strongly oxidative H_2SO_4/HNO_3 (3:1) mixture. [121]

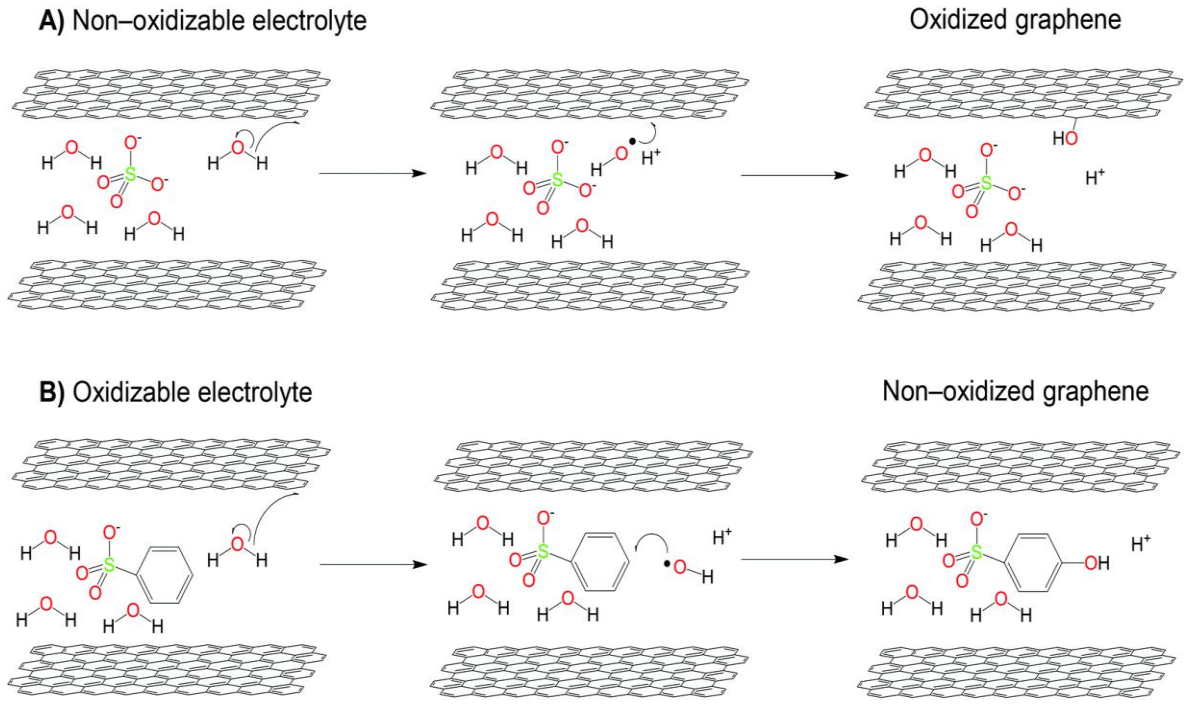

Figure 2.10. Schematic illustration of electrolyte roles. (A) In nonoxidizable electrolytes (such as Na_2SO_4), molecules of water would form reactive $OH^{\bullet}$ and $O^{\bullet}$ radicals which attach graphene layers. (B) An oxidizable electrolyte (such as sodium benzenesulfonate) would be used as a sacrificial agent in order to prevent graphene from oxidizing. [118] (Copyright © 2016 Royal Society of Chemistry)

2.2.3. Graphene composite synthesis by electrochemical exfoliation

A composite graphene material can be manufactured by electrochemically exfoliating graphite or chemically functionalizing electrochemically exfoliated graphene materials under ambient conditions., such as heteroatom (e.g. F, N, P ,S) doping graphene, [124-129] aryl diazonium functionalization graphene, [26, 130-131] and nanoparticle/graphene hybrids. [132-136]

Doping N into electrochemically exfoliated graphene materials can be achieved by adding urea, ammonia, azide, or glycine to electrolytes. [125, 128-129] As an example shown in **Figure 2.11a**, Yen *et al.* [125] generated an in situ hydrogen plasma using -60 V on a graphite cathode. The plasma discharge induced direct electron dissociation, resulting in $NH_3^{\bullet}$, $NH_2^{\bullet}$, and $NH^{\bullet}$ radicals when 2 M NH_4OH was added to a 2 M NaOH electrolyte. N-doped graphene materials with 0.71 at% N were obtained by reacting radicals containing N with electrochemically exfoliated graphene.

Various aryl groups can be grafted onto sp^2-hybridized carbon materials using diazonium chemistry. Many studies have demonstrated the aryl-functionalization approach during graphite exfoliation. [26, 130-131] With the presence of diazonium salts in electrolyte, positively charged aryl diazonium cations are reduced electrochemically to form aryl radicals, which attack graphite

electrodes resulting in the aryl diazonium functionalization of graphene materials. Meanwhile, the diazonium reduction generates N_2, which helps graphite expand and exfoliate. An example is given in **Figure 2.11b**, which shows that when 2-aminoanthraquinone (2-aminoAQ) was added to the 0.1 M H_2SO_4 electrolyte, aryl diazonium cations ($Ar\text{-}N_2^+$) spontaneously reacted with electrochemically exfoliated graphene sheets, AQ-grafted graphene materials were produced by Ossonon *et al.* [26]

Additionally, synthesizing nanoparticle/graphene hybrids in one-step electrochemical exfoliation of graphite has been studied. [132-136] In another study of Ossonon *et al.*, [132] graphene-manganese dioxide composites were prepared by electrochemical exfoliation of graphite in 0.1 M H_2SO_4 containing $KMnO_4$ at ambient temperature. As shown in **Figure 2.11c**, during exfoliation, as freshly exfoliated graphene (EG) sheets reduced the permanganate ions (MnO_4^-) spontaneously, MnO_2 nanoparticles were formed on EG sheets. [132]

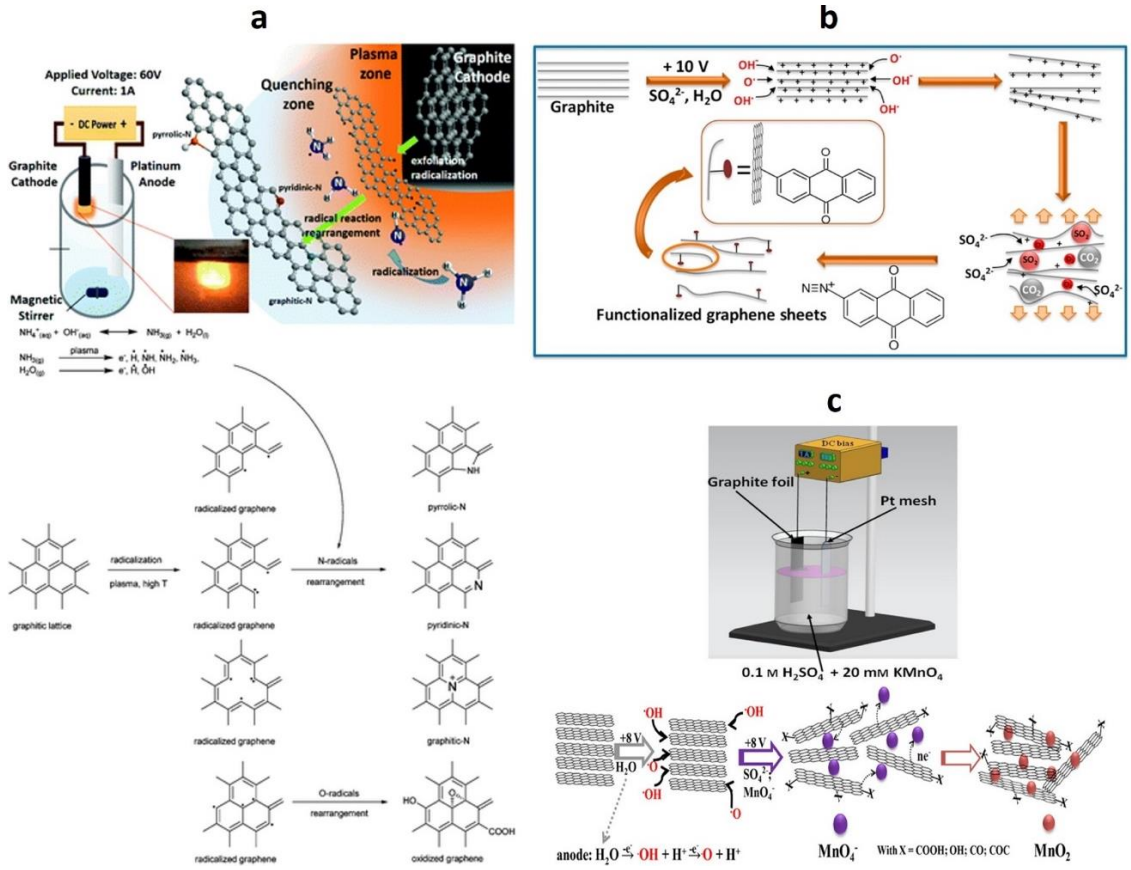

Figure 2.11. Schematic illustrations of (a) N-doped graphene prepared by the cathodic plasma process and its corresponding reactions with N-containing radicals, [125] (Copyright © 2017 Royal Society of Chemistry) (b) electrochemical exfoliation and functionalization of anthraquinone-grafted graphene sheets, [26] (Copyright © 2017 Elsevier) (c) graphene/MnO_2 composites composites preparation and its mechanism of functionalization and exfoliation. [132] (Open Access)

2.2.4. Summary

In conclusion, the electrochemical exfoliation of graphite process typically involves the following steps: (1) insertion and expansion of the graphite electrodes interlayer through the electrolyte species including ions, H_2O molecules, etc.; (2) graphite interlayer oxidation by oxygen radicals generated during electrolysis or by oxidative electrolyte radicals; (3) formation of abundant gases facilitating the exfoliation of graphite layers. The kinetics of these three procedures depend on the experimental conditions such as electrode materials, voltage applied, electrode distance, and electrolyte (component, concentration, temperature) etc. Different microstructures of exfoliated graphene materials (such as sheets size, number of layers, defects, C/O ratios, functional groups etc.) can be obtained by tuning the experimental conditions during the electrochemical exfoliation. Thus, the graphite exfoliation reaction needs to be further understood to control the structural properties of graphene materials for desirable applications.

2.3. Electrochemical applications of EGO

As a member of graphene-family nanomaterials (GFNs), EGO materials can also be widely used in different applications such as bioimaging, [137] energy storage, [95, 113, 129, 138] sensors [139] and energy storage, [120, 124, 127, 132] etc. Here, we focus on their application in electrochemical biosensors and supercapacitors.

2.3.1. Electrochemical biosensor

According to the definition, a sensor (or transducer) is a device to detect physical phenomena by converting them into electrical signals. The electrical signals that are produced are proportional to the physical quantity to be measured, which might be a force, a temperature, a pressure, or a light intensity, etc.[140] A biosensor converts biochemical phenomena into measurable signals using an analytical device. It consists of two principal components: a “bio-receptor” in which biomolecules recognize the target analytes and a "transducer" for converting the recognition into measurable signals. The bio-receptors include enzymes, antibodies, nucleic acids, etc.[141] The use of biosensors allows the testing of a wide range of samples, including body fluids, food, and environmental samples. The typical elements of a biosensor are shown in **Figure 2.12**: a) bio-receptors that detect analytes; b) electrical interfaces at which biological events occur and signals are generated; c) signal amplifiers that pick up signals from (b) and converted them to electronic

signals; d) signal processors that process the electronic signals; e) displays that present the data.[142]

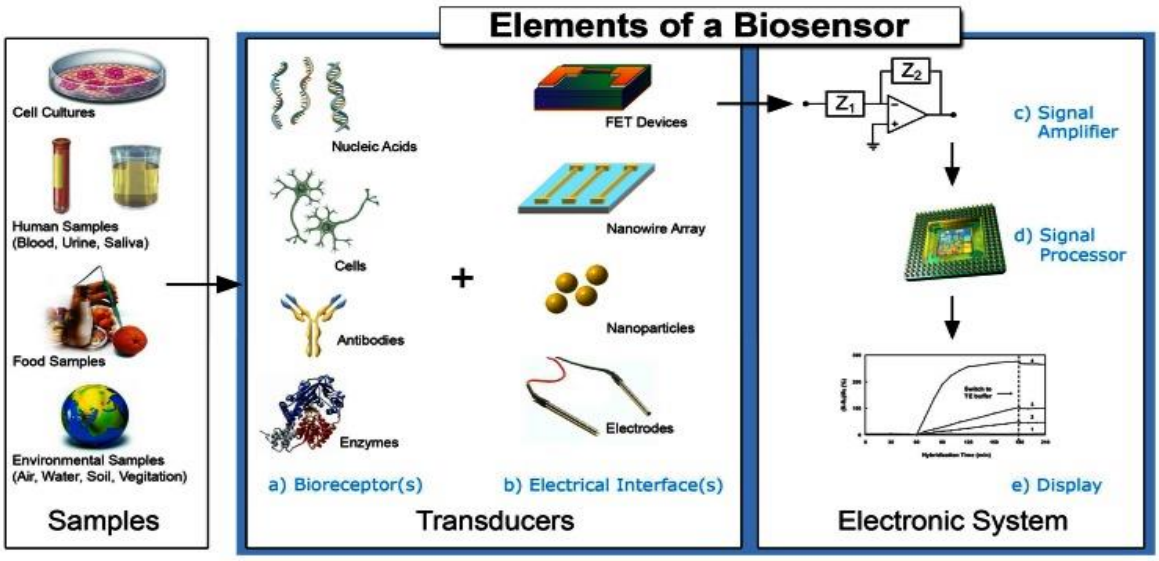

Figure 2.12. Schematic representation of elements and components of a typical biosensor. [142] (Open Access)

There are eight important parameters for biosensor characteristics: selectivity, sensitivity, linearity (concentration range), the limit of detection, time to response, lifetime, reproducibility, and stability.[141] To improve these parameters, the electrical interfaces of an electrochemical biosensor usually contain advanced nanomaterials such as graphene and nanoparticles. Using current flowing through the system, potential differences, or resistance differences between electrodes (electrical interfaces) from oxidation and reduction reactions involving electrochemical species, an analyte can be quantified. There are several redox couples that can provide oxidation and reduction reactions, including $[Fe(CN)_6]^{3-/4-}$, $[Ru(NH_3)_6]^{3+/2+}$, and $Fe^{3+/2+}$, etc.[143] According to the recorded electrochemical signal (current, potential or resistance), the typically electrochemical characterization techniques are amperometric, potentiometric and impedimetric.[142] As electrochemical methods, cyclic voltammetry (CV), differential pulse voltammetry (DPV), square-wave voltammetry (SWV), and electrochemical impedance spectroscopy (EIS) are commonly used,[141] as shown in **Figure 2.13**.

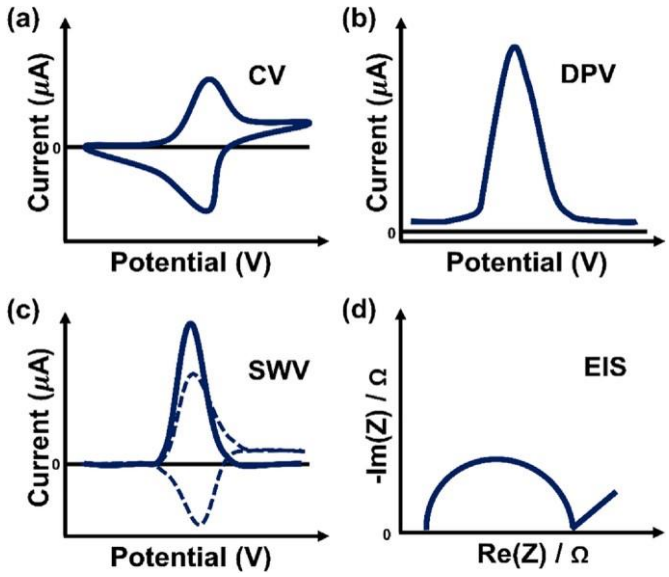

Figure 2.13. Schematic representation of commonly used electrochemical response: (a) cyclic voltammetry (CV), (b) differential pulse voltammetry (DPV), (c) square wave voltammetry (SWV), and (d) electrochemical impedance spectroscopy (EIS). [144] (Copyright © 2022 Springer Nature)

For the bio-receptor, enzymes, antibodies, and aptamers are frequently used. Among them, aptamers have recently received a lot of attention. Aptamers are short (15-100 bases) and single-stranded oligonucleotides that bind strongly and specifically with high affinity to their target molecules. Typically, they are selected in *vitro* using a method called SELEX (systematic evolution of ligands by exponential enrichment).[145-146] In comparison with antibodies which are costly and time-consuming to prepare, aptamers have considerable application potential because of their considerable advantages, including low cost, ease of synthesis, high thermal stability, and reversible denaturation, etc. An aptamer usually provides well-defined three-dimensional (3D) structures for the recognition of target molecules, which can be used to create aptasensors (sensors based on aptamers).[147-148]

For the transducer, various nanomaterials such as metal nanoparticles, graphene materials including CNTs, GO, rGO, etc.), or the mixture of them, are usually used for electrode fabrication due to their high surface area and conductivity. [5, 10, 149] Incorporating nanomaterials can increase the active surface area and/or promote the electron transfer reactions which enable a better electrochemical signal improving the sensibility, the speed and the detection limit of the biosensor, they may also have an influence on the stability.[148]

There is a considerable body of work on sensing platform based on graphene materials especially on GO.[5, 10] The oxygen functional groups on GO may enhance the heterogeneous electron

transfer rate and makes GO exhibit better dispersion in water, biocompatibility, and high affinity for specific biomolecules.[45, 59] Its properties make it suitable for integrating with a variety of biomolecules to create new biosensing systems, as shown in **Figure 2.14**. [5, 150] However, the way to functionalization of biomolecules on graphene materials may rely on their physico-chemical properties, such as surface composition and sheet size. [151-153] According to the previous literature, both physical adsorption and chemical immobilization methods are often used. [5, 154-156] In chemical immobilization, biomolecules and GO surfaces form a stable covalent bond, such as the carboxamide bond formed after the reaction between the amine and carboxyl groups. [154, 157] The physical adsorption method includes the pi-pi stacking interactions and the electrostatic forces between the biomolecules and the GO surface, and between their functional groups, respectively. [154, 158] The physical adsorption method is much simple than the chemical immobilization method. Still, its weaker adhesion and less control over the orientation of biomolecules may lead to lower stability and sensibility compared to chemical immobilization methods. [154, 158] In another hind, GO can indeed lose electrical conductivity due to covalent oxygenated functional groups. [159] Recently, Yet, Eissa *et al.* reported that the response of microcystin-LR toxin aptasensors prepared by physical adsorption was found to be enhanced with increasing GO sheet size. Meanwhile, small-sized GO sheets offered better sensing performance by the covalent attachment method. [151] The results indicate that GO's chemical and physical properties will affect its sensing performance significantly.

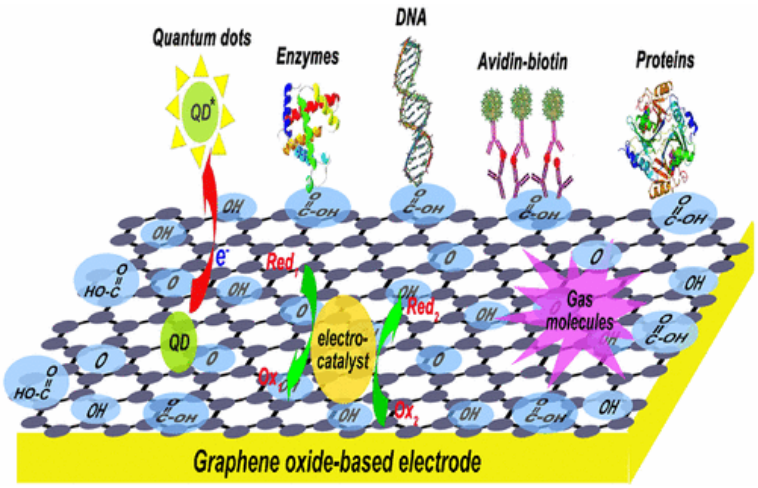

Figure 2.14. Schematic illustration of graphene oxide-based electrodes for electrochemical biosensor. [10] (Copyright © 2012 American Chemical Society)

As a wide range of EGO materials with different amounts and types of oxygenated groups, structural defects, and sheet sizes can be obtained easily and fast through the electrochemical

exfoliation of graphite by tuning the different parameters (the electrolyte, the voltage, and distance between two electrodes), this class of materials provide excellent opportunities to develop new sensing platform. However, with so many EGO materials available, what is the best one for your application? Electrochemical exfoliation can synthesize a wide range of EGO materials, a big advantage, but also a challenge in selecting the one that is suitable for a specific project.

2.3.2. Supercapacitors

Energy sources that are clean and sustainable, as well as technologies for energy conversion and storage, are becoming increasingly necessary as the global economy develops rapidly. As an alternative energy storage device, supercapacitors have gained significant attention due to their advantages such as high power density, quick charge-discharge, excellent energy density, long cycle lifetime, eco-friendliness, etc. [1, 160]

Generally, capacitors are devices that, by accumulating electric charges on two close surfaces that are insulated from each other, are capable of storing electrical energy in an electric field. This ability or "capacity" to store the electricity of a capacitor is represented by the capacitance, which is measured in Farad (F). It depends on the charge (Q) and the voltage (V) between the two surfaces or plates of the capacitor, as shown in equation (2.1) below: [161]

$$C = \frac{Q}{V} \qquad (2.1)$$

Supercapacitors (SCs), also called ultracapacitors, are capacitors with high capacity that can manage high power. However, the amount of charge they can store is usually 3~30 times less than batteries. [162] On the other hand, their output is lower than that of electrolytic capacitors.[163] As a result, they bridge the gap between electrolytic capacitors which have high power density (W kg $^{-1}$) to uptake or deliver energy and batteries which have high energy storage (Wh kg $^{-1}$). [162-163] It can be illustrated with a Ragone plot (**Figure 2.15**), which shows energy and power densities on horizontal and vertical axes. Nowadays, supercapacitors are commonly used for applications that require rapid charging and discharging cycles and high power density in order to provide fast power delivery, regenerative braking, and short-term energy storage for applications like automobiles, trains, elevators, etc. [162, 164]

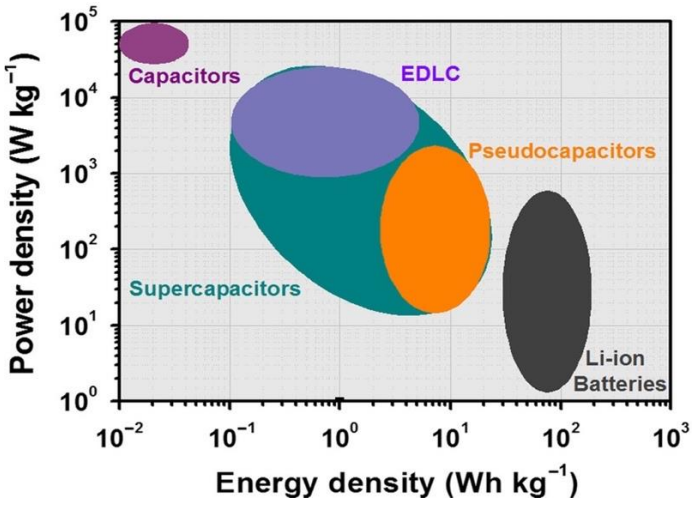

Figure 2.15. Ragone plot of different energy storage devices. [165] (Copyright © 2019 John Wiley and Sons)

In general, there are three types of supercapacitors based on storage mechanism or cell configuration, as shown in **Figure 2.16**: electric double-layer capacitors (EDLCs), pseudocapacitors, and asymmetric supercapacitors. [166] According to the cell composition, asymmetric supercapacitors can be classified into two capacitive electrodes and hybrid capacitors [167-168]

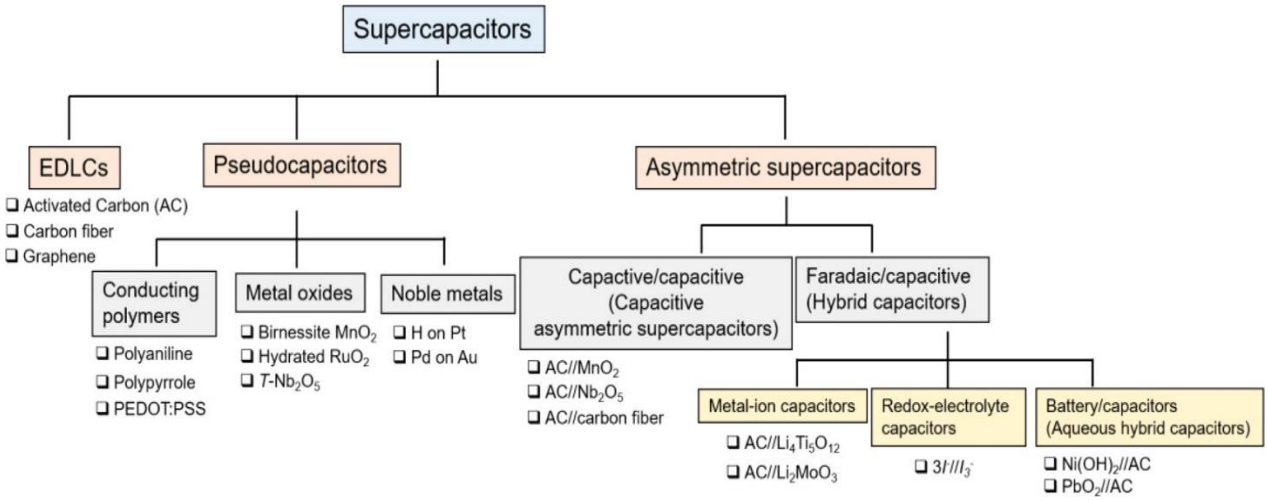

Figure 2.16. Schematic illustration of supercapacitors classification. [166] (Copyright © 2013 John Wiley and Sons)

EDLC and pseudocapacitors are distinguished based on their mechanism of charge storage (**Figure 2.17**). At the electrode/electrolyte interface, EDLC accumulates its electrical charge, while pseudocapacitors store their charge through fast surface redox reactions. [160, 169-171] Thus, carbon materials with a high specific surface area, high porosity to electrolyte ions, and good

electrochemical stability, often serve as active electrode materials in EDLCs, resulting in high capacitance. For EDLC electrodes, equation (2.2) can be used to estimate their capacitance: [172]

$$\mathrm{C} = \frac{\varepsilon_r \varepsilon_0}{d} A \qquad (2.2)$$

where ε_r is the relative permittivity of the liquid electrolyte, ε_0 is the permittivity of vacuum, d is the distance between the electrical double layers that separates charge effectively, A is the effective electrode surface area that is accessible to electrolyte ions.

The first experimental evidence of pseudocapacitivity was found in ruthenium dioxide (RuO_2). [173-174] Despite the fact that charge-transfer reactions on RuO_2 thin film electrodes are Faradaic reactions, the CV curve exhibits a similar shape to a typical capacitance curve. [175] Therefore, pseudocapacitance is defined as the capability of an electrode material to store charge through charge-transfer reactions across two layers but exhibit the electrochemical properties of a capacitive device. [176] Pseudocapacitance arises from a special relationship between charge acceptance and potential change, resulting capacitance to vary as shown in equation 2.3: [173]

$$\mathrm{C} = \frac{\mathrm{dQ}}{\mathrm{dV}} \qquad (2.3)$$

It is possible to obtain electrochemical capacitance by a variety of Faradaic mechanisms with different materials, [171] as shown in **Figure 2.17b–d**: (1) underpotential deposition, in which ions deposit at reversible redox potentials on metal–electrolyte interfaces (such as H^+ on Pt); [177-178] (2) redox pseudocapacitance, that reduced species are electrochemically absorbed on/near the surface of oxidized species or some conducting polymers (such as RuO_2); [179] (3) intercalation pseudocapacitance, ions are intercalated into redox-active materials without undergoing a crystallographic phase change (such as Nb_2O_5). [180] Briefly, their electrodes are based on conducting polymer, metal oxide, and functionalized porous carbons materials, which can have fast and reversible redox reactions to store charge via Faradaic processes, increasing the pseudocapacitance. [162-163, 166, 171, 175] As shown in **Figure 2.18**, the cyclic voltammogram of an ideal EDLC shows no redox reactions on its electrode surface, which is different from the one recorded with pseudocapacitors. [181]

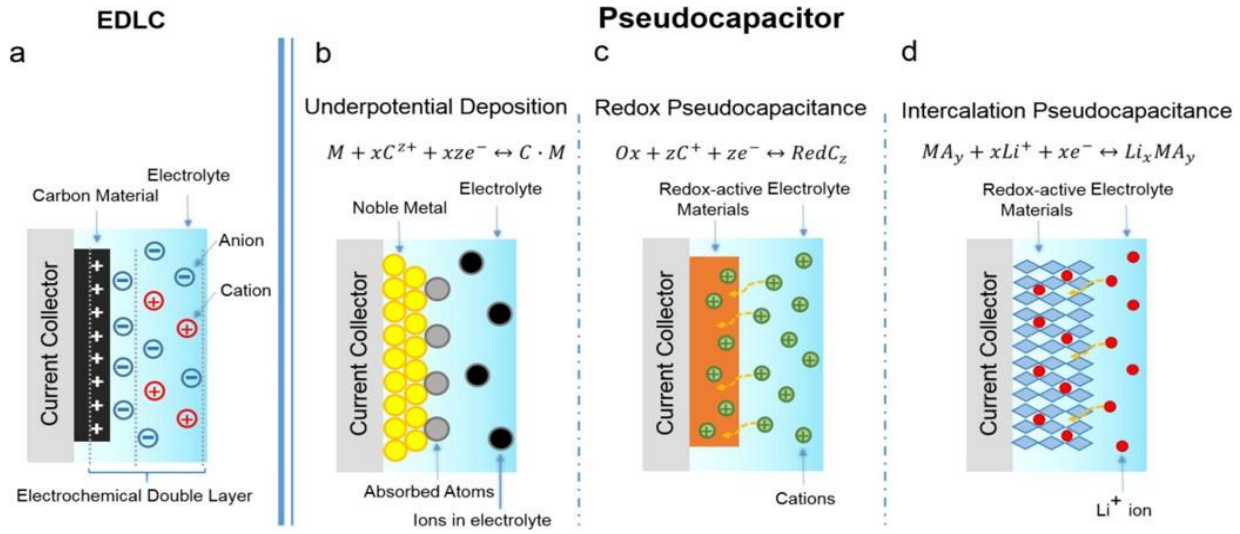

Figure 2.17. Schematics presentation of charge-storage mechanisms for (a) an electric double-layer capacitor (EDLC) and (b–d) different types of pseudocapacitors: (b) underpotential deposition, (c) redox pseudocapacitor, and (d) ion intercalation pseudocapacitor. [171] (Copyright © 2018 American Chemical Society)

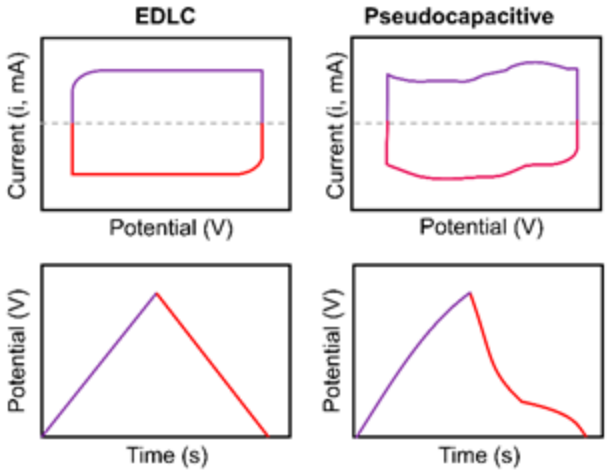

Figure 2.18. Schematic cyclic voltammograms and corresponding charge-discharge curves of electric double-layer capacitor (EDLC) and pseudocapacitor. [182] （Open Access）

With their high specific surface area, suitable pore sizes, enhanced electron conductivity, and ease of chemical processing, graphene materials and their composites are more and more used for supercapacitors' electrode fabrication. Especially graphene, rGO, and CNTs are ideal for EDLCs electrodes. [183-185] In contrast, the oxygen functional groups of GO may decrease its electrical conductivity, but they can improve wettability with the electrolyte, as well as causing the pseudocapacitance to increase. [1, 186-188] Thus, the content of oxygen functional groups of GO materials should be optimized. EGO materials synthesized by electrochemical exfoliation method

have a lower density of oxygenated functional groups (C/O > 4) [23] compared to the chemical methods (e.g. Hummers' method: C/O $\approx$ 2), [15] which could be an advantage for supercapacitors. [16, 28] In addition, as mentioned before, by changing electrolyte or adding precursors in the electrolyte, it is possible to synthesize EGO materials with different composites and/or functional groups in one step such as heteroatom (e.g. F, N, P ,S) doping, [124-129] aryl diazonium functionalization, [26, 130-131] and nanoparticle hybrids etc., [132-136] making them ideal for studying supercapacitors. The influence of the amounts or kinds of functional groups/composites of EGO materials on capacitance can be explored.

3. SYNTHESIS AND METHODOLOGY

3.1. Materials and chemicals

Millipore water (18.2 MΩ cm) was used for washing all samples, electrodes, and preparing all aqueous solutions. Graphite foil (0.5 mm thick, 99.8%), potassium hexacyanoferrate ($K_4[Fe(CN)_6]\cdot 3H_2O$, 98.5 – 102.0%), and 4-aminobenzoic acid ($C_7H_7NO_2$, 99%) were purchased from Alfa Aesar. Potassium chloride (KCl, min. 99.5%) and magnesium chloride ($MgCl_2$, 99+%) were purchased from Bioshop. Potassium ferricyanide ($K_3[Fe(CN)_6]$, 99+%, for analysis) and tetrachloroauric (III) acid trihydrate ($HAuCl_4\cdot 3H_2O$) were purchased from Arcos. Bovine serum albumin (BSA, 20 mg/mL) was purchased from BioLabs. P-nitroaniline ($C_6H_6N_2O_2$, 99.5%), sodium nitrite ($NaNO_2$, ≥ 99%), hydrochloric acid (HCl, 37%), sulfuric acid (H_2SO_4, 95.0 - 98.0%), N,N,N',N'-tetramethyl (succinimido) uronium tetrafluoroborate (TSTU, 97%), 4-dimethylaminopyridine (DMAP, ≥99%), methyl benzoate ($C_6H_5COOCH_3$, 99%), kanamycin sulfate ($C_{18}H_{36}N_4O_{11}$ H_2O_4S), cocaine ($C_{17}H_{21}NO_4$,1.0 mg/mL in acetonitrile), and anhydro ecgonidine methyl ester ($C_{10}H_{15}NO_2$, 1.0 mg/mL in acetonitrile) were purchased from Sigma. Cocaine aptamers were purchased from AlphaDNA (Montreal, Canada). The cocaine aptamer sequence was 5′- AGACAAGGAAAATCCTTCAATGAAGTGGGTCG-3′, named as Aptamer-OH (Apt-OH). The sequence of the cocaine aptamer modified with an amine group (Aptamer-NH_2, Apt-NH_2) was 5′-C6-NH_2-AGACAAGGAAAATCCTTCAATGAAGTGGGTCG-3′. Potassium hydroxide (KOH, >99.99%), isopropyl alcohol (99.5%), ethanol (91.5%) and methanol (92%) were purchased from Fisher Scientific. The 5 wt% Nafion® suspensions and Nafion membrane were purchased from Ion Power, Inc. Poly(tetrafluoroethylene) (PTFE) binder was purchased from Aldrich Chemical Company, Inc. High grade nickel foam (99.8% purity) was purchased from KUNHEWUHUA, China. Glassy carbon electrodes (GCE, 3mm), Ag/AgCl reference electrodes and Pt electrodes were purchased from CH Instruments, Inc. from the USA.

3.2. Synthesis of EGO materials

3.2.1. Synthesis of EGO

A graphite foil (7.5 cm × 2 cm × 0.05 cm) was used as anode and connected to the positive terminal of the direct current (DC) power supply. A Pt mesh (6 cm^2) was used as the cathode. Both electrodes were immersed into 0.1 M H_2SO_4 electrolyte and the distance between them kept constant (4 or 6 cm). The electrochemical exfoliation started immediately after applying the potential difference between the electrodes (6, 8, 10, 12 V). The EGO sheets were collected by vacuum filtration through a MF-Millipore membrane filter with 0.22 μm pore size and washed several times with Millipore water to remove the residual acid, which was verified with pH paper. The EGO powder was then dispersed in water by ultrasonication for 90 min to maximize the exfoliation. EGO powders were made from the dispersion after freeze-drying.

The samples are named according to the applied voltage and the distance between the graphite and Pt electrodes, such as 6V6cm. An additional sample was obtained after reducing the EGO 8V6cm powder at 900 °C in Ar named (R)8V6cm.

3.2.2. One-step synthesis of 4-aminobenzoic acid functionalized EGO (EGO-ABA)

In a two-electrodes system, a graphite foil (5 cm (in the electrolyte) × 2 cm × 0.05 cm) was used as anode and a Pt mesh (6 cm^2) was used as cathode. Both electrodes were immersed into 0.1 M H_2SO_4 electrolyte with different concentration of 4-aminobenzoic acid (4-ABA, 0, 5, 10, 20, 40 mM) and connected to the DC power supply. The distance between the two electrodes was 6 cm. After applying a potential difference of 8 V, the electrochemical exfoliation of graphite started immediately. After the exfoliation, the EGO sheets were washed with Millipore water and collected by vacuum filtration through a MF-Millipore membrane filter with 0.22 μm pore size. pH paper was used to verify the presence of residual acid. After several washes with water and vacuum filtration, the pH of the colorless filtrate was found to be around 5-6, indicating that the sulfuric acid electrolyte and the adduct produced by the side reactions have been removed. The EGO and EGO-ABA powders were then dispersed in water by ultrasonication for 90 min to maximize the exfoliation. After the dispersion was freeze-dried, the EGO and EGO-ABA powders were obtained.

The samples are named according to the concentration of 4-aminobenzoic acid, such as EGO (0 mM of 4-ABA) and EGO-ABA-5 (5 mM of 4-ABA).

3.2.3. One-step synthesis of EGO with gold nanoparticle

EGO with gold nanoparticle (EGO-Au) NPs materials were synthesized in a H-type cell, a proton exchange Nafion membrane (N117) was used to separate the electrolyte in the sides of graphite foil and Pt electrode. In the side of graphite foil, chloroauric acid ($HAuCl_4$) was added in the sulfuric acid electrolyte. The proton exchange Nafion membrane was used to avoid the gold ions deposition on the Pt electrode during the electrochemical exfoliation. Due to the H-type cell, the distance between graphite and Pt electrodes was kept at 7 cm. Graphite in the electrolyte has a width of 2 cm and a length of 4.5 cm. The following parameters were investigated during the electrochemical exfoliation: voltage applied, concentration of H_2SO_4 and $HAuCl_4$. Other observations including the electrolyte temperature, the time of exfoliation of the graphite foil (4.5 cm × 2 cm × 0.05 cm), the color of the membrane after exfoliation were noted.

3.2.4. EGO synthesized with membrane

For comparison, four EGO-membrane samples were synthesized in H-type cell with Nafion membrane and without chloroauric acid. The Nafion membrane N115 used for one of the samples is slightly thinner than the commonly used Nafion membrane N117. These samples are named according to the Nafion membrane, the concentration of the sulfuric acid electrolyte, and the voltage applied, such as EGO-N117-05M15V.

3.3. Morphology and structure characterization

In this part, various analytical techniques are used for the morphological, structural, and compositional characterization of EGO materials are introduced.

3.3.1. Scanning electron microscope

A scanning electron microscope (SEM) uses high-energy electrons (0.2 ~ 40 keV) to scan the sample's surface in order to create high-resolution images. An electron gun emits a thin beam (0.4 ~5 nm) of electrons as a probe. As the electron beam interacts with atoms on and near a sample's surface (10 nm), it produces secondary electrons, backscattered electrons, and characteristic X-rays etc. (**Figure 3.1**), which are amplified, detected, and converted into electrical signals that reveal the sample's topography, morphology, and composition. [189-190]

In this thesis, the SEM morphologies and images of the EGO materials were characterized and obtained with a Tescan Vega 3 microscope operating at 20.0 keV incident energy in INRS-EMT.

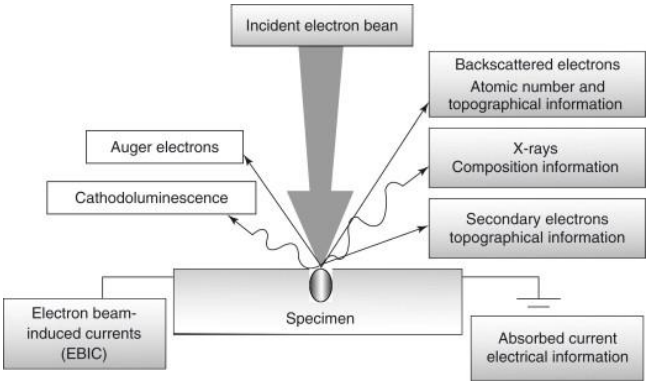

Figure 3.1. Schematic illustration of the signal generated by the interaction of the incident electron beam with the sample in a scanning electron microscope.[190] (Copyright © 2005 Elsevier)

3.3.2. Transmission electron microscopy

Transmission electron microscope (TEM) is an advanced and powerful technique to analyze materials' composition, morphology, and electronic structure from the interactions between energetic electrons and samples. High-voltage (~200 kV) electron beams are emitted from an electron gun and focused onto a sample by electromagnetic lenses. When the electron beam passes through a sample, it produces different kinds of radiation as shown in **Figure 3.2**. The detector can analyze these electrons, then translate them into a contrasted image. TEM can be used to evaluate the morphology, the flake and edge sizes, number of layers of the EGO materials.[191-192]

In this thesis, the EGO samples were characterized using a JEOL-2100F operated at 200 kV at the Center for Characterization of Microscopic Materials, at Ecole Polytechnique de Montreal.

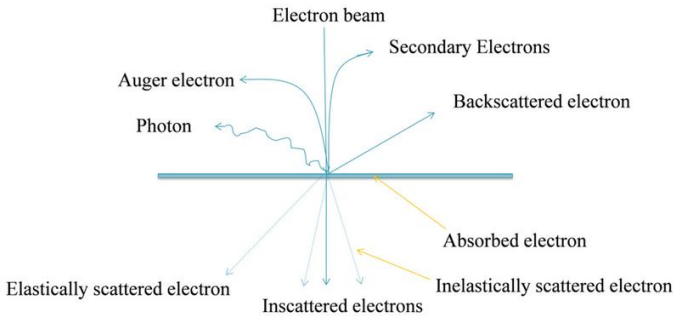

Figure 3.2. Schematic illustration of the signal generated by the interaction of the incident electron beam with the sample in a transmission electron microscope. [192] (Open Access)

3.3.3. X-ray powder diffraction

An X-ray powder diffraction (XRD) technique is usually used to characterize the crystal structure. Atoms are arranged in parallel planes in crystals by a distance d, also called the interplanar distance. When examining crystals, XRD can reveal their composition, phase, orientation, and lattice parameters. According to Bragg's law (equation 3.1), when X-rays strike the crystalline sample at an angle, they are scattered by the sample (**Figure 3.3**). [193]

$$n\lambda = 2dsin\theta \quad (3.1)$$

where *n* is an integer of the incident wave, *λ* is the wavelength of the X-ray beam, *d* is the spacing distance between diffracting crystal planes, and *θ* is the incident angle of the beam.

In this thesis, the bulk structure of EGO materials was characterized by Bruker D8 X-ray diffractometer with Cu-Kα radiation (λ = 1.54178 Å) at INRS-EMT, with a step size of 0.02° and a scan time of 4 s/step.

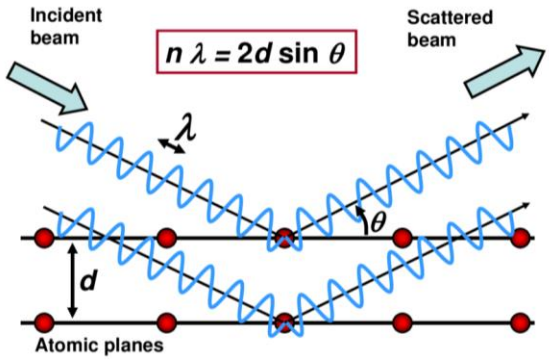

Figure 3.3. Schematic illustration of X-ray diffraction principle. [194] (Open Access)

3.3.4. X-ray photoelectron spectroscopy

X-ray photoelectron spectroscopy (XPS) is an analytical technique that provides information about the chemical state, electronic state, and surface composition of materials. As shown in **Figure 3.4**, when monochromatized X-ray beams emitted from Al Kα (with E_{photon}=1486.6eV) or Mg Kα (with E_{photon}=1253.6eV) interact with the atoms of a sample, the photoelectrons will be emitted through the photoelectric effect from the top of the sample (1~10 nm). Photoelectrons can be used to determine binding energy by measuring their kinetic energy, electrons emitted from

different orbitals of different elements have different binding energies, making their XPS spectrums have distinctive peaks. Thus, surface elements can be identified and quantified based on the intensity and energy of the peaks (except hydrogen). The following equation 3.2 can be used to determine the binding energy:

$$E_B = h\nu - E_K - \phi \qquad (3.2)$$

where E_B is the binding energy, E_K is the kinetic energy of the photoelectron, $h\nu$ is the X-ray energy, and ϕ is the work function.

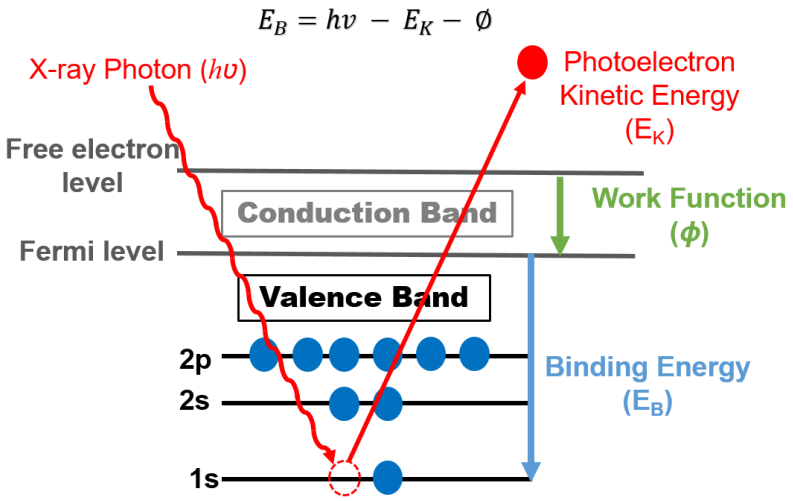

Figure 3.4. Schematic illustration of the principle of X-ray photoelectron spectroscopy.

Since graphene materials have only a few layers thick, XPS is an ideal tool for studying them. [195] In this thesis, XPS analysis was carried out on the VG Escalab 200i-XL equipped with a hemispherical analyzer (pass energy = 20 eV) and a multi-channel detector, applying a Twin Anode Al Kα X-Ray Source at 15 kV and 20 mA. The base pressure inside the spectrometer during analysis was less than 7×10^{-10} torr. A 284.5 eV binding energy for the C 1s peak was used as the internal standard. By using Casa XPS software, spectra were peak-fit using Lorentzian and Gaussian curves after Shirley-type background subtraction. During the deconvolution of C 1s spectra, the number and the full width at half maximum (FWHM) of peaks was fixed to 5 and 1.2 eV, respectively. The atomic sensitivity factors were applied to normalize peak areas. [196]

3.3.5. Raman spectroscopy

The Raman spectroscopy technique is typically used to determine molecules' vibrational modes (rotational and other low-frequency modes may also be seen). It relies on Raman scattering, the inelastic scattering of photons. When a laser light (visible, near-infrared, near-ultraviolet, or X-ray lasers) is applied to a sample, laser light scatters and interacts with molecular vibrations, phonon or other excitations, causing the laser photon energy to be shifted upward or downward. As shown in **Figure 3.5a**, if we plot the intensity of scattered light as a function of its energy shift (Raman spectrum), several peaks (or bands) may appear. When the incident light energy is equal to the scattered light energy, then the intensity is maximum. The energy shift corresponds to the Raman active phonon if the peak is a result of light interacting with a lattice vibration (a phonon). Due to the conservation of energy, the energy difference represents energy absorbed by the sample. Thus, a sample can be identified by Raman spectroscopy (**Figure 3.5b**). [197] Carbon materials are typically characterized by Raman spectroscopy because it is an inexpensive, fast, non-destructive, and high-resolution technique. [198]

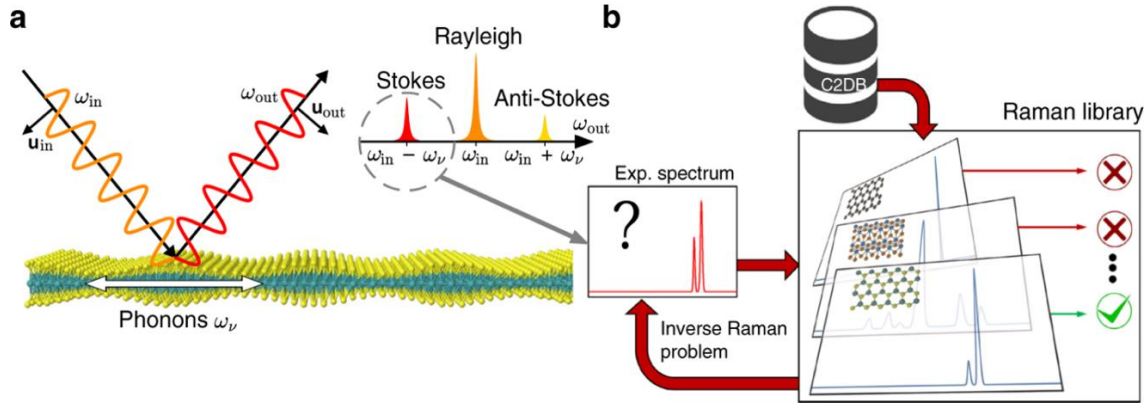

Figure 3.5. (a) Schematic illustration of Raman scattering processes: incident photons of polarization (u_{in}) and frequency (ω_{in}) are scattered into u_{out} and ω_{out} under emission (or absorption) of a phonon with frequency ω_v. (b) Schematic illustration of an experimental spectrum and the Raman library based on C2DB (Computational 2D Materials Database) for Raman spectrum identification.[197] (Open Access)

In this thesis, Raman spectra were recorded on a Raman microscope (Renishaw, inVia, at University of Québec at Montreal) with a laser source of 532 nm. The laser beam was focused on samples with a spot size of 1 µm in diameter, and at least 5 spectra were recorded for each EGO materials' film obtained by vacuum filtration.

3.3.6. Fourier Transform Infrared Spectroscopy

Fourier Transform Infrared Spectroscopy (FT-IR) is a powerful analytical technique used to identify and study the chemical composition of solids, liquids, and gases. It can be seen in **Figure 3.6** that a blackbody radiator, which emits infrared radiation, produces a beam of radiation that is directed into an interferometer, which measures the energy transmitted to the sample. Specific wavelengths of energy are absorbed by the sample surface during interferogram transmission or bounce. After passing through the detector, the energy signals are further processed by the computer in order to undergo Fourier transformation. Using the resulting spectrum, the molecular structure of a sample can be determined by identifying its functional groups and chemical bonds.[199]

In this thesis, FT-IR spectra of the powder samples were measured in the region 4000–600 cm^{-1} on a Nicolet FT-IR spectrophotometer at University of Québec at Montreal.

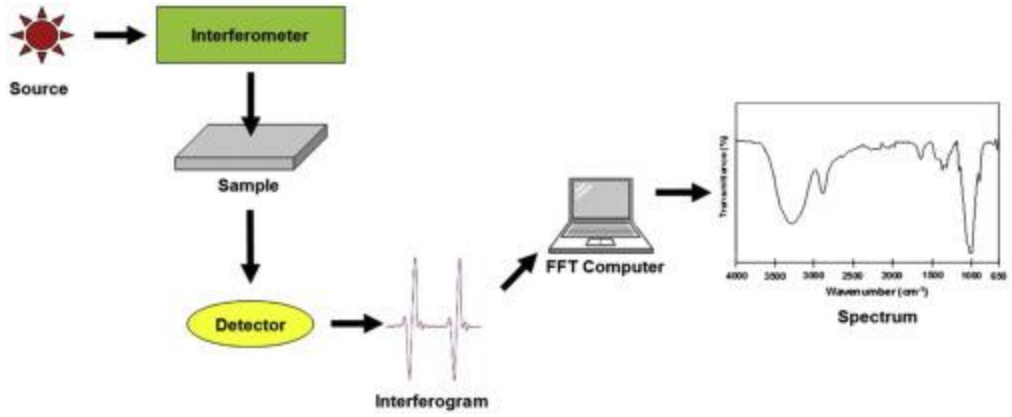

Figure 3.6. Schematic illustration of Fourier Transform Infrared Spectroscopy processes.[199] (Copyright © 2021 Elsevier)

3.4. Electrochemical characterization of EGO

In this part, the preparation of thin film of EGO materials on glassy carbon electrode for the electrochemical characterization is described, and the calculations for the determination of the electrochemical properties electrochemical surface area (ESA) and the standard rate constant of electron transfer (k^0) are explained.

3.4.1. Preparation of thin film of EGO materials on glassy carbon electrode

First, the surface of a glassy carbon electrode (GCE) is modified with a *p*-nitrophenyl film (NP-film) using diazonium chemistry (0.15 mM $NaNO_2$ + 0.15 mM 4-nitroaniline) in 0.5 M HCl by cyclic

voltammetry, scanning the potential from 0 V to -0.6 V vs Ag/AgCl at 0.05 V s^{-1} and for 3 cycles. Then, the NP-film is electrochemically reduced to the *p*-aminophenyl film (AP-film) in 0.1 M KCl by CV from 0 V to -1.3V vs Ag/AgCl at 0.05 V s^{-1} and for 3 cycles. Finally, the GCE modified with AP-film is incubated in the EGO materials dispersion (0.05 mg mL^{-1}, previously sonicated for 3 hours for 20 minutes, allowing the EGO sheets to auto-assemble on the surface of the GCE through the AP-film linker. The CVs in the presence of 1 mM $[Fe(CN)_6]^{3-/4-}$ redox couple in 0.1M KCl were recorded at 0.1 V s^{-1} after each step to follow the surface modification of the GCE.

For comparison purposes, the GCE electrodes were also modified by drop-casting the EGO dispersions (8 uL, 0.05 mg/mL, previously sonicated for 3 hours) on their surface followed by drying at room temperature. These electrodes were also characterized by cyclic voltammetry at different scan rates (between 20 mV/s and 200 mV/s) in 1 mM $[Fe(CN)_6]^{3-/4-}$ redox couple in 0.1 M KCl.

The electrochemical measurements were carried out with a Metrohm Autolab potentiostat / galvanostat PGSTAT101, and a conventional three-electrode cell equipped with a 3 mm bare GCE or modified with the EGO flakes as the working electrode, a Pt wire as the counter electrode, and an Ag/AgCl (1M KCl) as the reference electrode. The GCE and the reference electrode were purchased from CHI. All the GCE electrodes were cleaned by polishing with 1 mm, 0.3 mm and 0.05 mm alumina particles respectively on a cloth and washed with Millipore water before use. At least three EGO-based electrodes of each type were characterized electrochemically.

3.4.2. Determination of the electrochemical surface area and standard rate constant of electron transfer

In order to evaluate the impact of the exfoliation conditions on the electrochemical properties of the EGO-based electrodes, a series of CVs were recorded at different scan rates (between 20 mV/s and 200 mV/s) using $[Fe(CN)_6]^{3-/4-}$ as redox probe to investigate the ESA and the k^0. The ESA, a basic property of an electrified interface, is the area of the electrode material available to the transfer of electrons to and from the electrolyte [200]. The k^0 is a very important parameter related to the electrode kinetics and measures the “kinetic facility” of the electron transfer of a redox couple on the surface of an electrode: the higher is k^0 the faster the equilibrium will be attained [201].

The ESA was calculated according to the Randles-Sevcik equation [202]:

$$i_p = 0.4463nFAC(\frac{nFvD}{RT})^{1/2} \quad (3.3)$$

where: i_p is the peak current; *n* is the number of electrons transferred in the redox event (1 in the case of $[Fe(CN)_6]^{3-/4-}$ redox couple); *A* is the electrode area in cm^2; *F* is the Faraday constant (96485 $Cmol^{-1}$); *D* is the diffusion coefficient of $[Fe(CN)_6]^{3-/4-}$ in 0.1 M KCl (7.4×10^{-6} cm/s)[203]; *C* is the $[Fe(CN)_6]^{3-/4-}$ concentration (10^{-6} mol cm^{-3}); *v* is the scan rate in V s^{-1}; *R* is the gas constant (8.314 J K^{-1} mol^{-1}); *T* is the temperature in K. The peak current was plotted as a function of the square root of the scan rate, and the ESA for each EGO-based electrode calculated from the slope.

The k^0 was evaluated by the Nicholson method [204]. For peak-to-peak separation values in the cyclic voltammograms under 200 mV the following equation is used [204-205]:

$$k^0 = \left[\frac{\pi DnvF}{RT}\right]^{1/2}\psi \quad (3.4)$$

where k^0 is the standard rate constant in cm s^{-1}; π is the mathematical constant; ψ is the Nicholson dimensionless number which is a function of the peak-to-peak separation (ΔE_p); *F* is the Faraday constant (96485 C mol^{-1}).

The Nicholson dimensionless number can be calculated using the following function [205]:

$$\psi = (-0.6288+0.0021\,X)/(1-0.017\,X) \quad (3.5)$$

where the *X* indicates $\Delta E_p \times n$ expressed in mV. When the peak separation is higher than 200 mV, a more suitable relationship has been proposed by Klingler and Kochi [201]:

$$k^0 = 2.18[D\alpha nvF/(RT)]^{1/2}exp[-(\alpha^2 nF/RT)\Delta Ep] \quad (3.6)$$

where α is the transfer coefficient. Combining equations (3.4), (3.5) and (3.6), k^0 can be calculated.

3.5. Fabrication of electrodes based on EGO materials for electrochemical applications

In this part, electrodes based on EGO materials were prepared for the electrochemical aptasensing application and supercapacitors.

3.5.1. Fabrication of electrochemical cocaine aptasensor based on EGO

The EGO-based electrochemical cocaine aptasensor were fabricated by both physical adsorption and covalent immobilization methods. First, 8 µL of EGO suspension (0.4 mg/mL sonicated for 3h) were deposited on the surface of a glassy carbon electrode (GCE, 3 mm diameter) and dried at room temperature (21±1° C). Next, the modified electrode (GCE/EGO) was incubated in the cocaine aptamer-NH_2 solution (6 µL of 1 µM cocaine aptamer in 0.05 M KCl, pH = 7), 10 minutes for the optimized time. The cocaine aptamer-NH_2 modified electrode (GCE/EGO/Apt-NH_2) was then immersed in 6 µL of 0.1% BSA solution, 30 minutes for the optimized time, to block the electrode's surface and to avoid nonspecific adsorption. Finally, the blocked electrode (GCE/EGO/Apt-NH_2/BSA) was incubated in 8 µL cocaine solutions of varying concentrations for 30 minutes for the optimized time, (GCE/EGO/Apt-NH_2/BSA/Co). For the covalent immobilization method, a supplementary step was added to the fabrication procedure. The GCE/EGO electrode was incubated in 8 µL of a 50 µM N,N,N',N'-tetramethyl (succinimido) uronium tetrafluoroborate (TSTU) and 4-dimethylaminopyridine (DMAP) solution for 1 hour to form the linker (GCE/EGO/linker). [206-207] Subsequently, the electrode was incubated in the cocaine aptamer-NH_2 solution (GCE/EGO/linker/Apt-NH_2) for 10 minutes, the BSA solution (GCE/EGO/linker/Apt-NH_2/BSA) for 30 minutes, and lastly, the cocaine solution (GCE/EGO/linker/Apt-NH_2/BSA/Co) for 30 minutes.

Before use, all the GCE electrodes were cleaned by cloth polishing with 1 mm, 0.3 mm and 0.05 mm alumina particles, respectively, and washed with Millipore water. The modified electrodes were also washed with Millipore water after each modification step. To follow the surface modification of the GCE, cyclic voltammograms (CVs) and square wave voltammograms (SWVs) were recorded after each step with at least three electrodes. The electrodes were also washed with Millipore water after each characterization step. A traditional three-electrode cell equipped with the bare or modified CGE as the working electrode, a Pt wire as the counter electrode, and an Ag/AgCl (1 M KCl) reference electrode was used. The GCE, Pt wire and the reference electrode were purchased from CH Instruments. All electrochemical measurements were conducted at room temperature in the presence of 1 mM $[Fe(CN)_6]^{3-/4-}$ inner-sphere redox couple in 0.1 M KCl, which is very sensitive to the surface structure of carbon materials. [207] The CVs were recorded from -0.2 V to 0.6 V with a scan rate of 0.1V s^{-1}, and the SWVs from -0.2 V to 0.8 V with a frequency of 25 Hz. A Metrohm Autolab potentiostat PSTAT302 controlled by NOVA 2.1.2 (Ecochemie) was used.

Physicochemical characterization of the electrodes was done by XPS and by radioactivity tests. XPS was used to confirm the chemical attachment of the aptamer-NH_2 on the surface of the EGO flakes during the sensor fabrication. The radioactivity tests were used to verify the adhesion of

the aptamer to the EGO surface after binding with cocaine. The experimental details can be found in the supporting information section of chapter 5.

3.5.2. Fabrication of EGO-ABA based electrodes for supercapacitors

Nickel foams (NF) were used as supports for the fabrication of EGO and EGO-ABA electrodes. The EGO-based materials and PTFE binder (90:10 wt.% ratio, 90 mg of graphene materials and 10 mg of PTFE) were mixed in a small volume (2 mL) of ethanol under sonication until a homogenized dispersion is obtained. Then, the NF (1 cm^2) was coated by simple repetitive dip-coating steps into EGO inks and drying at 60 °C under vacuum overnight. The active material loading (around 1.5 − 2.0 mg) was calculated from the weight difference of the nickel foam before and after coating determined by high precision weighing balance (accuracy 0.0001 mg).

The electrochemical behavior of EGO-based NF electrodes was investigated by cyclic voltammetry in a three-electrode configuration, where carbon paper (CP) and a saturated calomel electrode (SCE) were employed as counter and reference electrodes, respectively. The electrochemical studies were carried out in 6 M KOH electrolyte and the scan rate varied between 5 and 100 mV s^{-1} [208]. The specific capacitance (Cs) of EGO/NF and EGO-COOHs/NF was evaluated from the cyclic voltammograms using the cathodic voltammetric charge (Q) integrated in the 0 to -1.15 V vs SCE potential window by using equation 3.7 [24]:

$$Cs = \frac{Q}{m\Delta V} \qquad (3.7)$$

where Cs is the specific capacitance (in F g^{-1}), Q is the charge (in C), ΔV is the potential window (in V), and m is the mass of active material (in g).

A Princeton applied research 273A and an Autolab PGSTAT128N potentiostats were used to conduct the electrochemical tests.

4. ELECTROCHEMICAL CHARACTERIZATION OF GRAPHENE-TYPE MATERIALS OBTAINED BY ELECTROCHEMICAL EXFOLIATION OF GRAPHITE

CARACTERISATION ELECTROCHIMIQUE DES MATERIAUX DE TYPE GRAPHENE OBTENUS PAR EXFOLIATION ELECTROCHIMIQUE DU GRAPHITE

Authors:

Yuting Lei[a], Benjamin D. Ossonon[a], Jiyun Chen[a], Jonathan Perreault[b] and Ana C. Tavares[a]*

[a] Institut National de la Recherche Scientifique – Energie, Matériaux et Télécommunications (INRS-EMT), 1650 Boulevard Lionel-Boulet, J3X 1S2, Varennes, Québec, Canada

[b] Institut National de la Recherche Scientifique – Armand-Frappier Santé Biotechnologie (INRS-AFSB), 531 Boulevard des Prairies, H7V 1B7, Laval, Québec, Canada

Publication: Journal of Electroanalytical Chemistry

Publication Date: Accepted 16 February 2021

Volume 887, Pages 115084

DOI: https://doi.org/10.1016/j.jelechem.2021.115084

Contribution of authors:

This research was conceptualized and designed by Yuting Lei, Dr. Benjamin D. Ossonon, and Prof. Ana Tavares. Under the guidance of Dr. Benjamin D. Ossonon, Yuting Lei prepared all samples, conducted most of the physicochemical characterizations, and conducted all electrochemical characterizations. Jiyun Chen carried out XRD characterizations and analyses, as well as helped to draw the scheme. All the experimental results were discussed with Dr. Benjamin D. Ossonon, and Prof. Ana Tavares. The manuscript was written by Yuting Lei, and it was commented on and revised by Dr. Benjamin D. Ossonon, Prof. Jonathan Perreault, and Prof. Ana Tavares. This work was financially supported by Prof. Jonathan Perreault and Prof. Ana Tavares' grants.

4.1. Abstract:

The oxygenated functional groups of graphene oxide (GO) allow for its dispersion in water, biocompatibility and influence the heterogeneous electron transfer rate of redox processes. Therefore, it's important to determine the experimental conditions leading to GO materials with the desired electrochemical properties for a given application. Herein, few layers electrochemically exfoliated graphene oxide (EGO) flakes were prepared by electrochemical exfoliation of graphite in 0.1 M H_2SO_4 and the effect of the electric field (applied voltage divided by the distance between the electrodes) was investigated. Raman and XPS analysis evidence two different regimes during the synthesis: slow kinetics of exfoliation at low voltage vs high concentration of $OH^{\bullet}$ radicals at high voltage. The EGO sheets were successfully assembled on a glassy carbon electrode through an aminophenyl-film linker and characterized by cyclic voltammetry in 1 mM $[Fe(CN)_6]^{3-/4-}$ to determine electrochemical surface area (ESA) and standard rate constant of electron transfer (k^0). The two parameters scale with each other and are sensitive to the type of EGO, confirming the suitability of the platform used in this work to characterize the EGO materials. The highest ESA (0.08 cm^2) and the high k^0 (0.13 cm^{-1}) were measured with EGO materials obtained at 8 – 10 V and 6 cm.

4.2. Introduction

Graphene and its related materials have been extensively studied in recent years because of their unique properties including high electrical conductivity and high specific surface area. [31, 209] Hence, many applications based on these materials including graphene oxide (GO) are booming, [5, 9] especially in the electrochemistry field. [6, 10] GO consists of graphene layers modified with oxygen functional groups such as hydroxyl and epoxy groups mostly located on the basal plane, with smaller amounts of carboxyl ketone at the edges. [3] These oxygen functional groups confer to GO flakes a good dispensability in polar solvents, [4] biocompatibility and affinity for specific biomolecules. [5-6] They also provide chemical flexibility to GO which can, for example, be used as cross-linker between a substrate and molecules of interest through π-π stacking, electrostatic interactions or chemical bonds. [5, 7-8]

There are various procedures to prepare graphene and GO materials. Single layer graphene can be obtained by micro-mechanical exfoliation of graphite [209] or by chemical vapor deposition [210]. Instead, GO materials are obtained through chemical methods such as the Hummers method [15, 86] or by electrochemically exfoliation of graphite. [20, 22, 26] The chemical synthesis of GO involves the oxidation of graphite in a mixture of concentrated acids and strong oxidants. [15, 86] The synthesis of electrochemically exfoliated graphene oxide (EGO) by electrochemical exfoliation of

graphite is more environmentally friendly, of lower-cost and offers the possibility of synthesizing larger amounts (in the order of grams) of EGO sheets in a shorter period of time (few hours depending on the voltage applied). [20, 22, 26] Briefly, it consists of a two-electrode system using graphite as the working electrode and a counter electrode immersed in an electrolyte. When a potential difference is applied between the electrodes immersed in an aqueous electrolyte, water is reduced at the cathode generating H_2 and hydroxyl radicals are formed at the anode. [20] These radicals attack the graphite electrode, and facilitate the intercalation of ions from electrolyte within the graphitic layers, resulting in the formation of flakes that are dispersed in the electrolyte. [20] The EGO powder is easily recovered after filtration, washed, and freeze-dried. [20, 22, 26] The electrolyte, the voltage and the distance between the two electrodes are variables associated with this method, making it very versatile.

A wide range of EGO materials with different amounts and types of oxygenated groups, structural defects, sheet sizes can in principle be obtained by this method. [20, 22, 26, 95] However, very few works report on the influence of the experimental parameters on the EGO structural defects, surface composition, number of layers, and on their electrochemical properties including electron transfer standard rate constant (k^0) and electrochemical surface area (ESA). One example is the work of Ambrosi et *al*.[95] where the electrochemical properties of EGO obtained by electrochemically exfoliated graphite with 10V and 2 cm in three different electrolytes (H_2SO_4, $LiClO_4$, Na_2SO_4) were investigated. The EGO flakes were dispersed in DMF and deposited on glassy carbon electrode (GCE) by drop-casting method. It was demonstrated that the EGO with highest defects (C/O ratio from XPS) has the fastest k^0 for $[Fe(CN)_6]^{3-/4-}$. Thus, in this work we synthesize a series of EGO materials obtained under different experimental conditions (applied voltage, distance between the electrodes, and subsequent thermal reduction) and their structural and electrochemical properties are investigated are systematic investigated.

It has been reported in the literature that multi-layered carbon materials have higher k^0 compared with mono-layer carbon materials because the number of layers can increase the edge-plane sites which have faster heterogeneous electron-transfer rate than the basal plan. [211-213] The presence of oxygen functional groups also changes the intrinsic properties of carbon materials. [213-216] However, different materials, approaches and conclusions on the influence of the oxygenated functional groups and defects on the k^0 values are reported in the literature. For example, Chou et *al.*[216] showed that increasing the carboxyl-containing groups on single-walled carbon nanotubes after electrochemical activation can increase the k^0 value for $[Fe(CN)_6]^{3-/4-}$ redox couple. Ji et *al.*[211] found that the k^0 value decreased by increasing the oxygen-containing groups on the basal plane of pyrolytic graphite electrodes oxidized for 12 h in air, and of multi-walled

carbon nanotubes oxidized in air for more than 1 week. Pumera et *al.*[215] found that oxygen-containing groups play a major role on edges-like sites at the walls of multiwalled carbon nanotubes, and have a favorable impact on the k^0 value for $[Fe(CN)_6]^{3-/4-}$ redox couple. Later, Ambrosi et *al*. [214] compared the k^0 value for $[Fe(CN)_6]^{3-/4-}$ for graphite oxide, graphene oxide, thermally reduced graphene oxide, chemically reduced graphene oxide and electrochemically reduced graphene oxide immobilized on GCE by drop-casting method, and found a lower k^0 when oxygenated functional groups are present. However, the type and content of the oxygenated functional groups are not considered in their discussion.

There are several methods available for depositing active materials on substrate electrodes, and they span from drop-casting, [95] electrodeposition, [217] self-assembly, [218] spin-coating, [219] etc. In this study, we use a platform based on the self-assembly of EGO sheets onto the surface of a GCE using a p-aminophenyl (AP) linker [8, 220] for the systematic electrochemical characterization of the EGOs. Compared to other methods, the self-assembly method can minimize the re-stacking of EGO, and offers a better control of the thickness and homogeneity of the EGO films on the electrode substrate. This is because the negatively charged EGO sheets are self-assembled on the positively charged electrode surface through the electrostatic interaction and π-π stacking between them. [8, 220] The EGO/AP/GCE electrodes are electrochemically characterized by cyclic voltammetry (CV) in 1 mM $[Fe(CN)_6]^{3-/4-}$ inner-sphere redox couple which is very sensitive to surface structure of carbon materials. [207] The standard rate constant (k^0) of electron transfer is determined by the Nicholson method, [204-205] and the electrochemical surface area (ESA) by the Randles-Sevcik equation. [202] These two parameters are correlated with the EGOs morphology, composition and structural defects investigated by Scanning electron microscopy (SEM), Transmission electron microscopy (TEM), X-ray diffraction (XRD), Raman spectroscopy and by X-ray photoelectron spectroscopy (XPS). With the proposed platform and methodology, a rational choice of EGO materials can be done targeting a specific electrochemical application. As it will be shown in the paper, this platform offers the capability to differentiate the electrochemical response of the different EGO materials, with a clear advantage compared with the drop-casting method.

4.3. Experimental methods

Details related to materials, instrumentation, and physicochemical characterization techniques of the EGO are presented in the supporting information (SI).

4.3.1. Synthesis of electrochemically exfoliated graphene oxide

A graphite foil (7.5 cm × 2 cm × 0.05 cm) was used as anode and connected to the positive terminal of the direct current power supply. A Pt mesh (6 cm^2) was used as the cathode. Both electrodes were immersed into 0.1 M H_2SO_4 electrolyte and the distance between them kept constant (4 or 6 cm). The electrochemical exfoliation started immediately after applying the potential difference between the electrodes (6, 8, 10, 12 V). The EGO sheets were collected by vacuum filtration through a MF-Millipore membrane filter with 0.22 μm pore size and washed several times with Millipore water to remove the residual acid, which was verified with pH paper. The EGO powder was then dispersed in water by ultrasonication for 90 min to maximize the exfoliation. The dispersion was freeze-dried, and the EGO powders stored for further use. The samples are named according to the applied voltage and the distance between the graphite and Pt electrodes, such as 6V6cm. An additional sample was obtained after reducing the EGO powder (8V6cm) at 900°C in Ar (named as (R)8V6cm). **Table S4.1** summarizes the experimental conditions used for the synthesis of the EGO materials, including the electric field values (applied voltage divided by the distance between electrodes), the exfoliation time, and the mass obtained. Fresh EGO suspensions (0.05 mg/mL) were prepared for the electrochemical studies. These were obtained after sonicating the EGO powders in water for 3h (samples referred for example as EGO6V6cm-3h). SEM, TEM, X-ray diffraction (XRD), Raman spectroscopy and XPS were used to characterize the as prepared EGOs and the EGO-3h powders. Free-standing films were prepared by vacuum filtration and used for Raman and XPS characterization.

4.3.2. Modification of glassy carbon electrodes with a thin film of EGO

Scheme 4.1 illustrates the procedure used to assemble the EGOs as thin films on the surface of glassy carbon electrodes (GCE). First, the surface of a GCE is modified with a *p*-nitrophenyl film (NP-film) using diazonium chemistry (0.15 mM $NaNO_2$ + 0.15 mM 4-nitroaniline) in 0.5 M HCl by cyclic voltammetry, scanning the potential from 0 V to -0.6 V vs Ag/AgCl at 0.05 V s^{-1} and for 3 cycles, **Scheme 4.1a**. Cyclic voltammetry was used to modify the glassy carbon electrode without passivating it with the NP-film [221] (**SI Figure S4.1**). Then, the NP-film is electrochemically reduced to the *p*-aminophenyl film (AP-film) in 0.1 M KCl by CV from 0 V to -1.3V vs Ag/AgCl at 0.05 V s^{-1} and for 3 cycles, **Scheme 4.1b**. Finally, the GCE modified with AP-film is incubated in the EGO dispersion (0.05 mg mL^{-1}, previously sonicated for 3 hours for 20 minutes, allowing the EGO sheets to auto-assemble on the surface of the GCE through the AP-film linker, **Scheme 4.1c.** The pH values of the EGO-3h dispersions were lower than 4.5, thus the negatively charged EGO sheets can auto-assembly on the positive charged AP-film (**SI Table S4.2**). The CVs in the

presence of 1 mM $[Fe(CN)_6]^{3-/4-}$ redox couple in 0.1M KCl were recorded at 0.1 V s^{-1} after each step to follow the surface modification of the GCE, **Scheme 4.1d**.

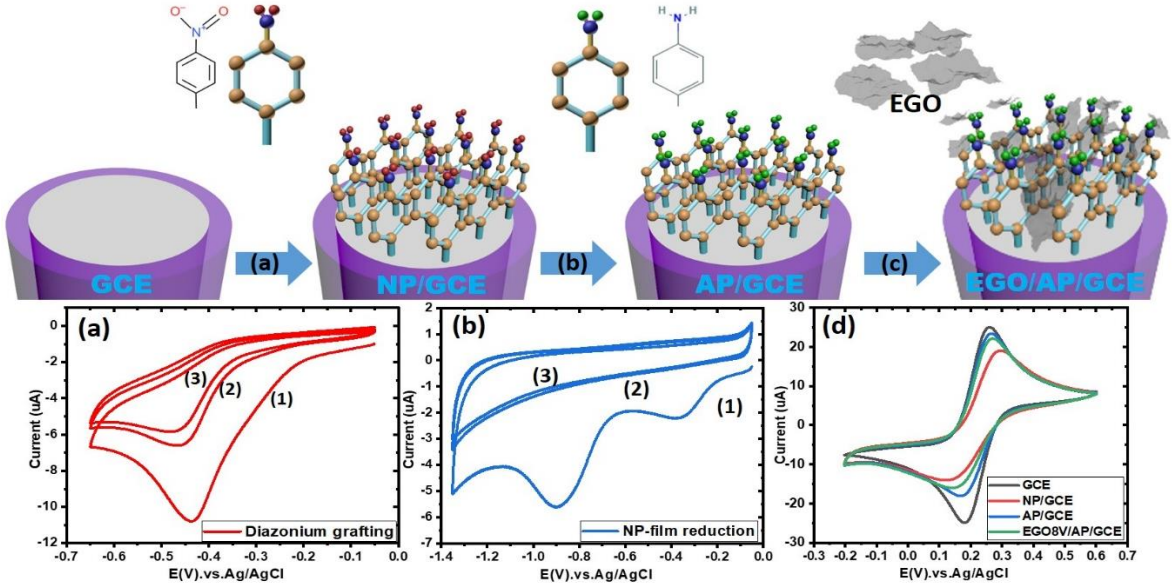

Scheme 4.1: Platform used for the electrochemical characterization of the EGOs. It consists of GCE modified with a p-aminophenyl (AP) linker, followed by self-assembly of the EGO sheets. (a) In-situ generated p-nitrophenyl (NP) diazonium cation in 0.5 M HCl is grafted on surface of GCE by cyclic voltammetry at 0.05 V s^{-1}. (b) Reduction of the NP-film to AP-film in 0.1 M KCl by cyclic voltammetry at 0.05 V s^{-1}. (c) The AP/GCE electrode is incubated in the EGO suspension. (d) Series of cyclic voltammograms recorded in the presence of 1 mM $[Fe(CN)_6]^{3-/4-}$ redox couple in 0.1 M KCl 0.1 V s^{-1} used to follow the modification of the electrodes.

For comparison purposes, the GCE electrodes were also modified by drop-casting the EGO dispersions (8 uL, 0.05 mg/mL, previously sonicated for 3 hours) on their surface followed by drying at room temperature. These electrodes were also characterized by cyclic voltammetry at different scan rates (between 20 mV/s and 200 mV/s) in 1 mM $[Fe(CN)_6]^{3-/4-}$ redox couple in 0.1 M KCl. The series of CVs recorded at different scan rates for the GCE and modified GCE electrodes were added to the Annex (Figure A4.11).

4.4. Results and discussions

4.4.1. Physicochemical characterization of EGO

The EGO materials were characterized by transmission electron and scanning electron microscopies, X-ray diffraction, Raman and X-ray photoelectron spectroscopies to evaluate the number of layers, the flakes size, the defects and the oxygenated functional groups, respectively. Since three hours of sonication were necessary to obtain homogenous suspension, this

physicochemical characterization was carried out on the EGOs before and after the 3 h sonication. It was found that the 3h sonication had no major influence on the physicochemical properties of the EGOs prepared in the work, except for the flakes size. Therefore, only data for samples after 3h of sonication (EGO-3h) is shown in the main paper. The results on the physical chemical characterization of the flakes before sonication are presented in the SI section.

Figure 4.1a and **SI Figure S4.2** show that the EGOs flakes are composed of multilayers. The flakes obtained at 6V have a larger number of layers (8 ~ 11) compared to those obtained at 8 to 12V (3 ~ 7 layers). High applied voltage promotes the intercalation of sulfate anions into the graphite layers as schematized in **Figure 4.1b**.

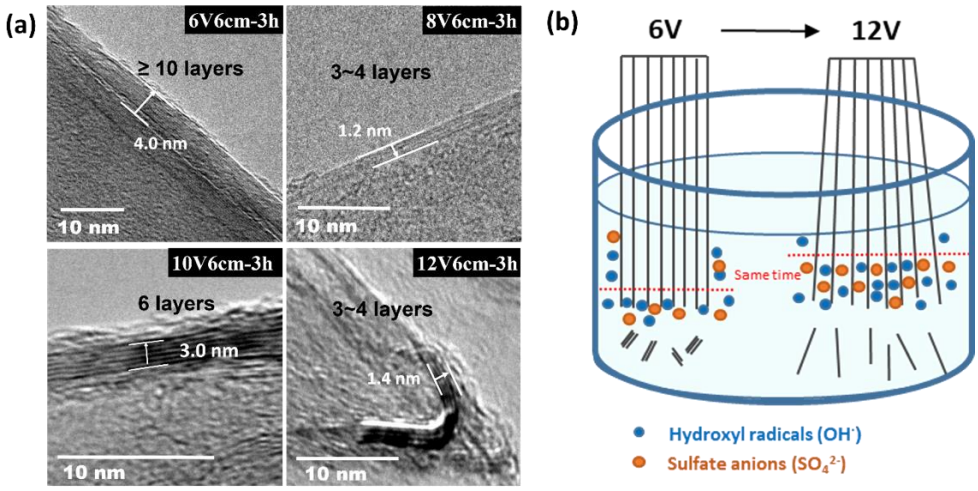

Figure 4.1. (a) TEM images for EGOs-3h. (b) Scheme illustrating the effect of the applied voltage on the number of layers and size of EGO flakes.

The typical morphology of graphene-type materials characterized by curled and overlapped flakes [26] was observed in all samples, **Figure 4.2**. Overall, the sheet size increases with the applied voltage (**SI Figure S4.3**). However, the sonication step breaks the flakes and the sizes of the flakes became more uniform. Although no systematic studies of the applied voltage on the sheet size are found in the literature, it was reported before that high bias voltage are required to exfoliate graphite in large particles. [22] This is probably related with the kinetics of exfoliation that is slow at 6 V (typically about 4 hours for ≈0.67 g, **SI Table S4.1**) but becomes faster as the voltage increases (typically about 1 hour for ≈0.68 g at 12 V). At lower voltages the hydroxyl radicals and sulfate anions from electrolyte intercalate slowly between the graphite sheets, and the gas released (SO_2, CO_2, O_2) during the exfoliation [20] assists the fracturing of the EGO in small flakes. In contrast, when a high voltage is applied, the sulfate ions and water molecules intercalate

quickly and along the graphite sheets, resulting in large exfoliated EGO sheets, see scheme in **Figure 4.1b**.

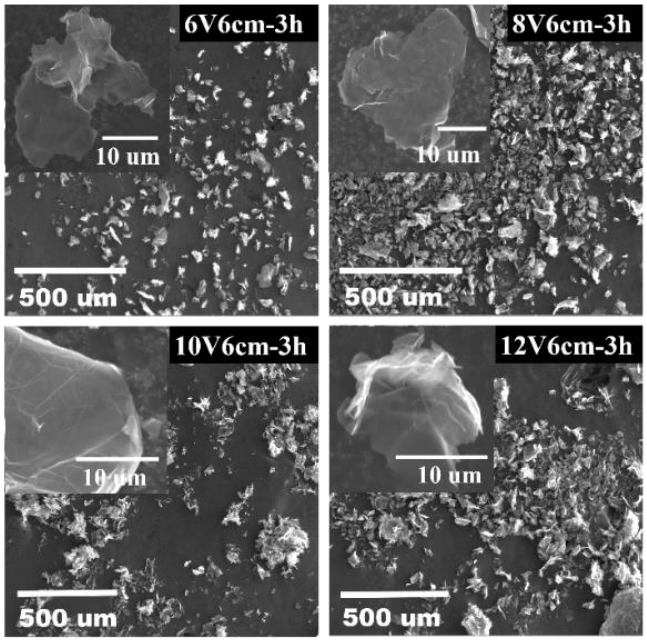

Figure 4.2. SEMs images of EGOs-3h exfoliated at different applied voltages.

Powder X-ray diffraction (XRD) was used to characterize the bulk structure of EGO materials. The XRD patterns (**SI Figure S4.4**) are those expected for few layer graphene materials with a low fraction of oxygenated functional groups: a high intensity diffraction peak attributed to the (002) plane of graphite is seen at 26.5°, and the diffraction peak of graphene oxide at 10° is absent. [222] The low intensity and broad wave centered at 12° comes from the sample holder.

XPS was used to investigate the surface composition of the EGOs. The XPS survey spectra (**SI Figure S4.5**) show the expected C 1s and O 1s peaks at ca. 285 and 532 eV, respectively. The peak S 2p (164 eV) was not detected, which indicates that the samples are free from sulfur containing species. Approximately 11.7 at% ~ 19.1 at% of oxygen is present in the EGOs after 3h of sonication (**SI Table S4.3**). As expected, the EGO (R)8V6cm has a much lower O at% content (about 4.4%). Compared with other graphene materials synthesized by electrochemically anodic exfoliation of graphite (**SI Table S4.4**), the EGOs prepared in this work have a higher O at% and a lower C/O at% ratio. In the present work, the graphite foil has been exfoliated in 0.1 M H_2SO_4 for long time (more than 1 h) to obtain 0.6 – 0.7 g of powder, whereas in most reported works the exfoliation was conducted for less than 20 mins. In addition, the use of high voltage in

dilute H_2SO_4 solution (0.1M) favors the production of hydroxyl radicals and the oxidation of the EGO flakes during the exfoliation process.[105]

The C 1s spectra **(SI Figure S4.6)** were deconvoluted into five peaks identified as graphitic carbon C-C and C=C at 284.5 eV, C-OH at 285.8 eV, C-O-C at 286.8 eV and C=O at 288 eV, as well as the O-C=O at 289 eV. [57] One example is given in **Figure 4.3a**. The hydroxyl (C-OH) and epoxy groups (C-O-C) are located on the graphene basal plan, and the carbonyl (C=O) and carboxyl (O-C=O) groups are located at the edges of graphene oxide sheets. [3] The relative percentages of the carbon species were quantified, and the results are reported in **Figures S4.6**, **4.3b** and **4.3c**. As expected, there is almost no noticeable variation of the C=O/C at% and the O-C=O/C at% ratios with the electric field (applied voltage or distance), **SI Figure S4.7**. Only the relative at% of C-OH and C-O-C groups varies with the applied voltage, **Figure 4.3b and 4.3c**. The C-OH/C at% ratio increases from 6V6cm to 12V6cm, which is attributed to an increasing concentration of OH radicals with the voltage [223] and subsequent attack of the graphitic layers. The C-O-C/C at% ratio shows a U-shape dependence with the applied voltage as the result of two different regimes: slower kinetics of exfoliation plus smaller and thicker flakes at lower voltage, and high concentration of OH radicals and larger flakes at higher voltage. As expected, EGO (R)8V6cm has a lower C-O-C/C at% ratio compared to the rest of the samples (**Figure 4.3c)**, and the few remaining oxygenated functional groups are mainly the C-OH groups (**Figure 4.3b and S4.7)**. These are the most difficult groups to reduce among all oxygenated functional groups, even after a thermal treatment in N_2 above 800 °C [224] or after vacuum heating treatment at 1000 °C [225].

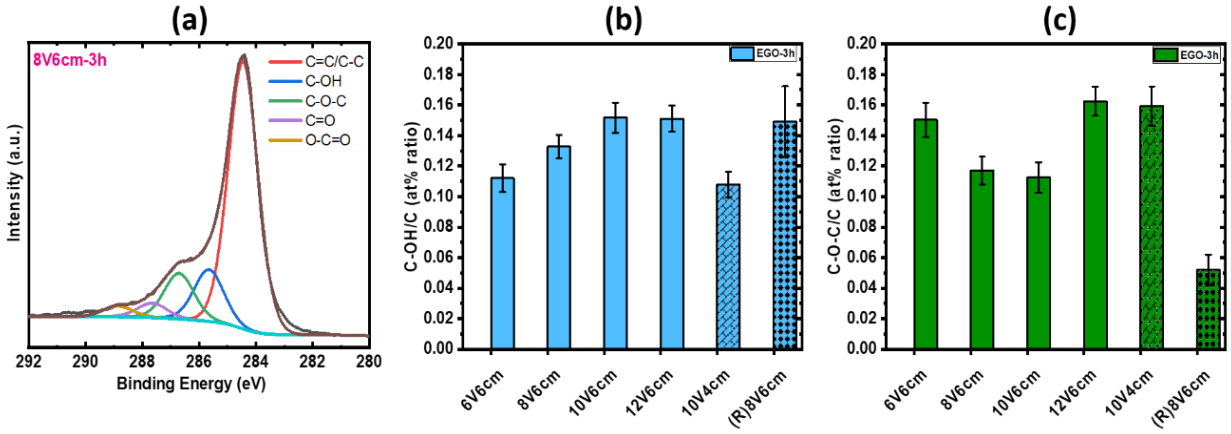

Figure 4.3. (a) C 1s spectrum for EGOs 10V6cm after 3 hours of sonication; (b) ratio between the atomic percentage of C-OH and total C (C-OH/C at% ratio) and (c) ratio between the atomic percentage of C-O-C and total C (C-O-C/C at% ratio) for the various EGOs after 3 hours of sonication.

Raman spectroscopy was used to characterize the structural defects of the samples in the form of free-standing films. Five Raman spectra were recorded for each sample and **Figure 4.4a** shows representative spectra. The strong G band at about 1600 cm^{-1} corresponds to the sp^2 carbon network in an infinite crystal. [226] The D band around 1350 cm^{-1} is related to defects such as vacancies, bonds disorder, edge defects, etc. [227] The 2D band which is related to the number of layers of graphene materials shifts from 2715.0 cm^{-1} to 2700.7 cm^{-1} when the voltage increases from 6 V to 12 V (SI Table S4.5) which is consistent with the decrease of the number of layers with increasing voltage. [228] The I_G/I_{2D} ratios vary from 2.4 to 3.1 (SI Table S4.6) consistent with EGOs materials composed of few layers. [229-230] However, it should be kept in mind that the Raman spectrum of graphene materials with more than 5 layers are hardly distinguishable from that of bulk graphite by using 2D band. [229-230] The intensity and width of the D+G (≈ 2950 cm^{-1}) and 2G (≈ 3171 cm^{-1}) bands increase with the voltage as the results of a higher degree of oxidation of the EGOs **(Figure 4.4a and SI Figure S4.8).** [231] Finally, the ratio between the intensity of the D and G bands (I_D/I_G) was calculated because it is a measure of the defects' density of graphene materials. [226, 232] As shown in **Figure 4.4b**, it increases systematically from 0.5 to 0.9 with the applied voltage above 8 V. These results show that the I_D/I_G ratio and the degree of oxidation of the few layers EGO-3h increase with the applied electric field. Consistent with the XPS data, the EGOs have a higher I_D/I_G ratio compared with other graphene materials synthesized by electrochemically anodic exfoliation of graphite (**Table S4.4**). As expected, the thermal treatment at high temperature (sample (R)8V6m-3h) reduces the I_D/I_G ratio, almost by half, and the D+G and 2G bands are absent from the spectrum indicating that this sample has fewer defects.

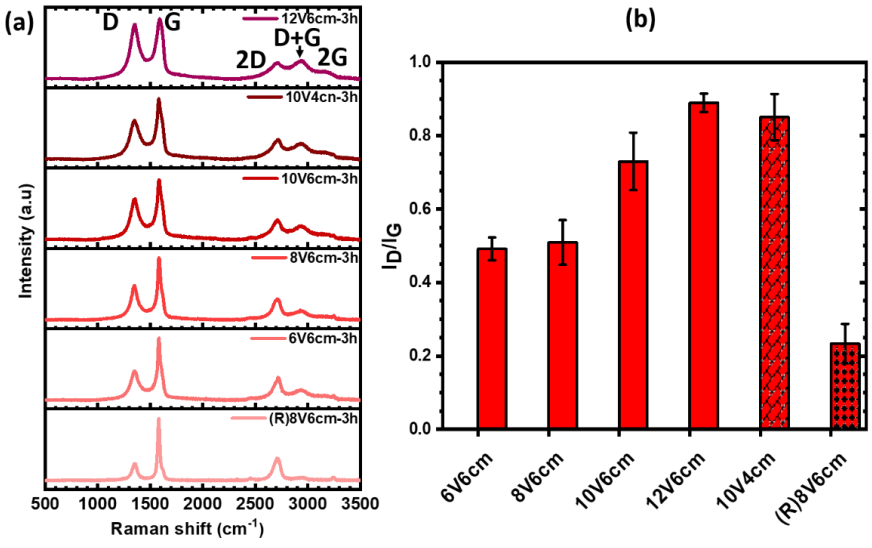

Figure 4.4. (a) Raman spectra of EGO samples after 3h of sonication; (b) Average I_D/I_G ratio obtained for the various EGO-3h.

4.4.2. Electrochemical characterization of the EGOs

The electrochemical surface area (ESA), a basic property of an electrified interface, is the area of the electrode material available to the transfer of electrons to and from the electrolyte. [200] The standard rate constant of electron transfer (k^0) is a very important parameter related to the electrode kinetics and measures the "kinetic facility" of the electron transfer of a redox couple on the surface of an electrode: the higher is k^0 the faster the equilibrium will be attained. [201] Generally, carbon materials with more edges will have higher k^0 and ESA values, but the influence of the oxygenated functional groups is not yet clear. [95, 211-216] In order to evaluate the impact of the exfoliation conditions on the electrochemical properties of the EGO-based electrodes, a series of CVs were recorded at different scan rates (between 20 mV/s and 200 mV/s) using $[Fe(CN)_6]^{3-/4-}$ as redox probe. The ESA was calculated according to the Randles-Sevcik equation [202]:

$$i_p = 0.4463nFAC(\frac{nFvD}{RT})^{1/2} \quad (4.1)$$

where: i_p is the peak current in A; n is the number of electrons transferred in the redox event (1 in the case of $[Fe(CN)_6]^{3-/4-}$ redox couple); A is the electrode area in cm^2; F is the Faraday constant (96485 C mol^{-1}); D is the diffusion coefficient of $[Fe(CN)_6]^{3-/4-}$ in 0.1 M KCl (7.4×10^{-6} cm s^{-1}); [203] C is the $[Fe(CN)_6]^{3-/4-}$ concentration (10^{-6} mol cm^{-3}); v is the scan rate in V s^{-1}; R is the gas constant (8.314 J K^{-1} mol^{-1}); T is the temperature in K. The peak current was plotted as a function of the square root of the scan rate, and the ESA for each EGO-based electrode calculated from the slope of the anodic peak current (SI **Figure S4.9** and **Table S4.7**).

The ESA values obtained for each electrode are shown in **Figure 4.5a**. Data for bare GCE and GCE modified with the AP-film are also included for comparison. The ESA of bare GCEs is about 0.108 cm^2 which is higher than their geometric area (0.07 cm^2). This means that the surface of these electrodes is not an ideal flat disk with a diameter of 3 mm. The ESA decreases to about 0.08 cm^2 after grafting the AP-film as expected from the partial blockage of the surface of electrode (See **SI Figure S4.1**). [233-234] The ESA of the EGO-based electrodes varies between 0.065 cm^2 to 0.082 cm^2 and shows a Volcano dependence with the voltage, with a maximum between 8 and 10V. The reduction of EGO 8V6cm at high temperature leads to intermediate ESA values characterized by the largest error bar. This material has fewer oxygenated functional groups to interact with amino groups of AP-film during the self-assembly of the sheets on the surface of the electrode. This results in a poor control of the degree of coverage of the electrode surface.

The k^0 was evaluated by the Nicholson method. [204] For the peak-to-peak separation values in the cyclic voltammograms under 200 mV the following equation is used: [204-205]

$$k^0 = \left[\frac{\pi D n v F}{RT}\right]^{1/2} \psi \qquad (4.2)$$

where k^0 is the standard rate constant in cm s^{-1}; π is the mathematical constant; ψ is the Nicholson dimensionless number which is a function of the peak-to-peak separation (ΔE_p); F is the Faraday constant (96485 C mol^{-1}).

The Nicholson dimensionless number [205] can be calculated using the following function:

$$\psi = (-0.6288+0.0021\,X)/(1-0.017\,X) \qquad (4.3)$$

where the X indicated $\Delta E_p \times n$ expressed in mV. When the peak separation is higher than 200 mV, a more suitable relationship has been proposed by Klingler and Kochi: [201]

$$k^0 = 2.18[D\alpha n v F/(RT)]^{1/2} exp[-(\alpha^2 n F/RT)\Delta Ep] \qquad (4.4)$$

where α is the transfer coefficient. Combining equations (4.2), (4.3) and (4.4), k^0 can be calculated and SI **Table S4.8** illustrate the results obtained for EGO 10V6cm. The variation of k^0 with the applied voltage is shown in **Figure 4.5b**. First, the k^0 value for GCE is similar to the results of Li *et al.*[235] which is around 0.025 cm s^{-1}, and it increased to 0.07 cm s^{-1} after modified with AP-film showing that the positively charged AP-film attracts the negatively charged ferricyanide ions and facilitates the electron transfer between electrode surface and the redox probe. [196] Then, after assembling with EGOs, the k^0 varies between 0.05 and 0.13 cm s^{-1} showing as well a volcano dependence with the voltage. The highest k^0 is obtained when the applied voltage is 8 or10 V. At last, the EGO (R)8V6cm has the lowest k^0 (0.04 cm s^{-1}). In addition, the k^0 of reduced EGO is very close to the one reported for reduced GO sheets obtained using hydrazine (0.049 cm s^{-1}). [235] As reported in **Figure 4.5c,** there is a linear relationship between k^0 and ESA values for the EGO-modified electrodes. From these results, it can be concluded that the EGOs 8V6cm and 10V6cm lead to the thin film electrodes with the highest ESA (0.08 cm^2) and highest k^0 (0.13 cm s^{-1}).

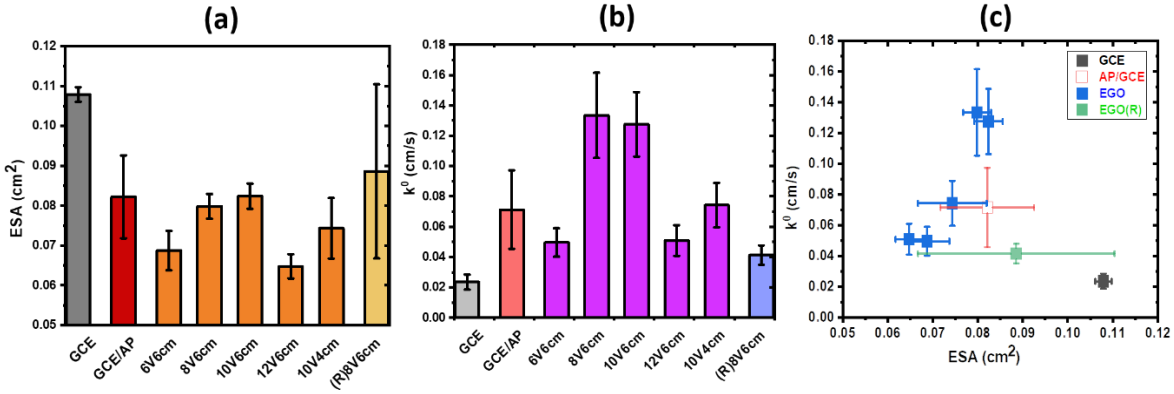

Figure 4.5. (a) Electrochemical surface area (ESA) and (b) standard rate constant (k^0) of the EGO-based electrodes; (c) correlation between the k^0 and ESA values.

To understand the trends reported in **Figure 4.5**, and the role of the oxygenated functional groups, the ESA and k^0 values were correlated with the I_D/I_G and the at% of oxygenated functional groups. Interestingly, among the oxygen functional groups, a correlation was found only between the ESA and k^0 values and the C-O-C/C at% ratio. These groups, together with the OH groups, are located at the basal plane of the EGO sheets and are the most abundant oxygenated functions on the flakes. All samples have 7 or less graphitic layers except for EGO-3h 6V6cm that has a higher number of layers. The sheet size of the EGO materials obtained in this work is relatively large which may explain the strong dependence of ESA and k^0 with this specific functional group.

As shown in **Figure 4.6**, for samples with few layers (≤ 7 layers), the ESA decreases with the increasing of number of defects (I_D/I_G and C-O-C/C at% ratio), which can be attributed to a decrease of the electrical conductivity. [57] The dependence of k^0 with the I_D/I_G and C-O-C/C at% ratio clearly shows that too few or too many defects have a negative impact on this parameter. In other words, the edge-like defects formed during the electrochemical exfoliation increase the k^0 values. [215] As mentioned above, the reduced EGO sample showed the lowest k^0 value pointing out the importance of the oxygenated functional groups of EGO to enhance the electron transfer between the electrolyte and the electrode. [216] However, too many defects, especially C-O-C groups, decrease the k^0 as already reported in literature. [214] When the number of layers increases to 7 or more, the k^0 decreases drastically even if the I_D/I_G ratio is low. The ESA value is also low. As shown in **Figure 4.6** this sample (EGO 6V6cm) also has a high density of C-O-C groups. These results clearly show that when the number layers and structure of EGO are similar, the density of C-O-C groups is the main factor impairing the k^0 and ESA values. Although, the contribution of the GCE's ESA to the overall ESA values found for the EGO-modified electrodes cannot not be totally excluded, the correlations shown in **Figure 4.5c**, **Figures 4.6 a and b** confirm that the proposed methodology is valid for the screening of graphene-type materials.

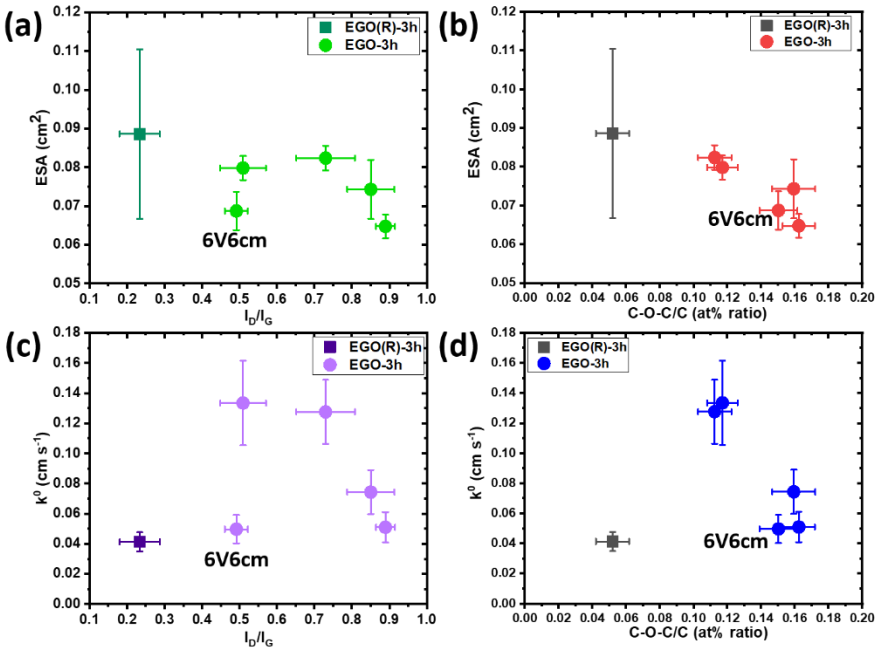

Figure 4.6. The electrochemical surface area according to (a) the ratio of I_D/I_G and (b) the C-O-C/C at% ratio. The standard rate constant of electron transfers according to (c) the ratio of I_D/I_G and (d) the C-O-C/C at% ratio.

For comparative purposes a series of electrodes were also prepared by drop-casting method and the electrodes electrochemically characterized as above. The ESA and k^0 values are reported in SI **Figure S4.10**. The ESA values are around 0.11 cm^2 which are very similar to that of the bare glassy carbon electrode. The k^0 values vary between 0.03 and 0.04 cm s^{-1} with no clear trend between them. Therefore, no correlation can be established between the physicochemical properties and the electrochemical response of the EGO materials. Poor distribution and random orientation of the flakes on the GCE averages out the intrinsic properties of the EGO flakes. We observed that the EGO flakes tend to go to the edges of the electrode because of the capillary force during the water evaporation, forming the so-called coffee ring effect. [236]

The self-assembly method has been successfully used to prepare electrochemical immunosensors using graphene oxide materials. [8, 218, 220] As shown in this work, this method also brings clear advantages in the electrochemical characterization of graphene-type materials prepared under similar conditions: the substrate electrodes are incubated in diluted suspensions and electrostatic forces direct the graphene-type flakes likely prevent their agglomeration. As a result, the k^0 and ESA respond to subtle variations in the structure and chemical composition of the flakes, and to the number of layers of the material. This method is however more laborious than the drop-casting method. Also, the graphene-type materials under investigation need to bear

charged species to interact electrostatically with the charged linker film during the self-assembly step.

4.5. Conclusion

In this work, EGO materials were prepared by electrochemical exfoliation of graphite in aqueous electrolyte. The effect of the electric field (applied voltage divided by the distance between the electrodes) on the defects of the EGO flakes were investigated by XPS and Raman spectroscopies. XPS analysis of the C 1s spectra uses curving fitting. Even if efforts are taken during the deconvolution of the spectra to obtain a set of results with a coherent physical meaning, caution is needed when using this data in correlations. Overall, the density of defects as determined by Raman spectroscopy (I_D/I_G) increases with the applied electric field. Moreover, mainly the density of oxygenated functional groups located at the basal plane (C-OH and C-O-C) is influenced by the exfoliation conditions, and is determined by the rate of two different regimes: the kinetics of exfoliation and the concentration of $OH^{\bullet}$ radicals. The electrochemical characterization using the $[Fe(CN)_6]^{3-/4-}$ redox probe of the EGO materials assembled on GCE through an AP-film linker revealed that the ESA and k^0 values of the EGO modified GCE electrode are sensitive to the intrinsic properties of the EGO flakes. More specifically, it is demonstrated that for a few layers (≤ 7 layers) EGO, a high density of C-O-C groups has a detrimental impact on ESA and k^0 values. When the number of layers of EGO is more than 10 layers, it becomes parameter having a negative impact on ESA and k^0 values. The platform proposed in this work allows an excellent correlation between the electrochemical, structural and chemical properties of the graphene-type materials prepared by electrochemical exfoliation of graphite. Overall, this study points forward for the advantages of the self-assembly method to investigate the electrochemical properties of graphene-based materials.

4.6. Supporting Information

4.6.1. Materials and Instrumentation

Materials. Graphite foil (0.5 mm thick, 99.8%) was purchased from Alfa Aesar. Millipore water (18.2 MΩ cm) was used for rinsing the EGOs samples and for preparation of all aqueous solutions. Potassium chloride (KCl, min. 99.5%) was purchased from Bioshop, potassium ferricyanide

($K_3[Fe(CN)_6]$, 99+%, for analysis) from Acrôs, potassium hexacyanoderrate ($K_4[Fe(CN)_6]\cdot 3H_2O$, 98.5 – 102.0%) from Alfa Aesar. P-nitroaniline ($C_6H_6N_2O_2$, 99.5%) from Aldrich, sodium nitrite ($NaNO_2$, ≥ 99%) from Sigma-Aldrich, hydrochloric acid (HCl, 37%) from Sigma-Aldrich, sulfuric acid (H_2SO_4, 95.0 - 98.0%) from Sigma-Aldrich.

Instrumentation. The electrochemical exfoliation of graphite was conducted with a DC Power supply (HY3005F-3) from Dr. Meter. Scanning Electron Microscopy (SEM) images were taken with a Tescan Vega 3 microscope operating at 20.0 keV incident energy. Transmission electron micrographs were obtained with a JEOL 2100F operated at 200 kV (Center for Characterization of Microscopic Materials, at Ecole Polytechnique de Montreal). The TEM samples were prepared by dipping the copper grids on the powder samples dispersed in methanol. The bulk structure of electrochemically exfoliated graphene oxide was characterized by X-ray diffraction (XRD) on Bruker D8 X-ray diffractometer with Cu-Kα radiation (λ = 1.54178 Å). Raman spectra were recorded on a Raman microscope (Renishaw, inVia, at University of Québec at Montreal) with a laser source of 532 nm. The laser beam was focused on the sample on a spot size of 1 μm in diameter, and at least 5 spectra were recorded for each EGO film. X-ray photoelectron spectroscopy (XPS) was performed with a VG Escalab 200i-XL equipped with a hemispherical analyzer (pass energy = 20 eV) and a multi-channel detector, applying a Twin Anode X-Ray Source at 15 kV and 20 mA. The base pressure inside the spectrometer during analysis was less than 7×10^{-10} torr. The binding energy of the C 1s peak at 284.5 eV was used as internal standard. The core level spectra were peak-fitted using Lorentzian and Gaussian curves after the Shirley type background subtraction, and Casa XPS software. During the deconvolution of C1s spectra, the number and the FWHM of peaks was fixed to 5 and 1.2 eV, respectively. Peak areas were normalized by appropriate atomic sensitivity factors.

The electrochemical measurements were carried out with a Metrohm Autolab potentiostat / galvanostat PGSTAT101, and a conventional three-electrode cell equipped with a 3 mm glassy carbon electrode (GCE) bare or modified with the EGO flakes as the working electrode, a Pt wire

as the counter electrode, and an Ag/AgCl (1M KCl) as the reference electrode. The GCE and the reference electrode were purchased from CHI. All the GCE electrodes were cleaned by polishing with 1 mm, 0.3 mm and 0.05 mm alumina particles respectively on a cloth and washed with Millipore water before use. At least three EGO-based electrodes of each type were characterized electrochemically.

4.6.2. Experimental conditions used for the synthesis of the EGOs

Table S4.1. Experimental conditions used for the synthesis of the EGOs and obtained mass

EGO	d (cm)	V_{app} (V)	E (V cm^{-1})	t_{exf} (min)	Thermal treatment	m_{EGO} (g)
6V6cm	6	6	1.00	> 360	-	0.67
8V6cm	6	8	1.33	≈ 150	-	0.65
10V6cm	6	10	1.67	≈ 100	-	0.65
12V6cm	6	12	2.00	≈ 60	-	0.68
10V4cm	4	10	2.50	≈ 90	-	0.73
(R)8V6cm	6	8	1.33	≈ 150	900 °C, 1 h	0.60

d - distance between graphite and Pt electrodes; V_{app} – applied voltage; E – electric field; t_{exf} – exfoliation time; m_{EGO} – mass of obtained EGO.

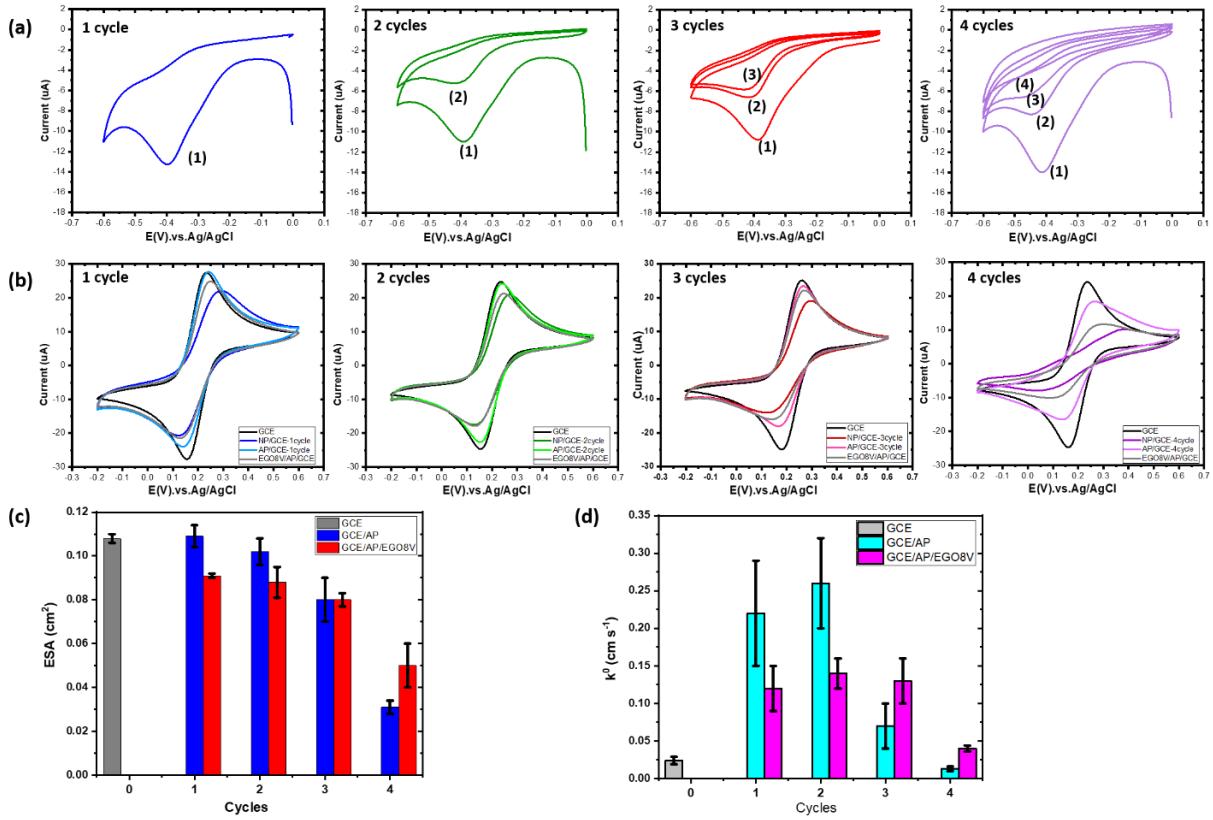

Figure S4.1. (a) In-situ generated p-nitrophenyl (NP) diazonium cation in 0.5 M HCl is grafted on surface of GCE by cyclic voltammetry at 0.05 V s^{-1} (the extent of grafting is varied through the number of cycles 1 to 4 cycles). (b) Series of cyclic voltammograms recorded in the presence of 1 mM $[Fe(CN)_6]^{3-/4-}$ redox couple in 0.1 M KCl 0.1 V s^{-1} used to follow the modification of the glassy carbon electrodes, including the grafting of the NP film, its reduction to AP form and incubation in the EGO 8V6cm suspension. (c) Electrochemical surface area (ESA) for AP-film and EGO 8V6cm modified electrodes as a function of the number of grafting cycles. (d) Electron transfer constant rate (k^0) for AP-film and EGO 8V6cm modified electrodes as a function of the number of grafting cycles.

The GCEs were modified with different amounts of NP-film (NP/GCE) by cyclic voltammetry (1 to 4 cycles, see **Figure. S4.1a**). After reduction of the NP-film to AP-film, the electrodes were further modified with the EGO 8V6cm thin layer (EGO8V/AP/GCE). The electrodes were characterized by cyclic voltammetry in the 1 mM $[Fe(CN)_6]^{3-/4-}$ in 0.1 M KCl to determine ESA and k^0, **Figure S4.1b**. As shown in the **Figures S4.1 c and d**, the ESA values tend to decrease with the extent of AP-film (number of cycles) and with the deposition of EGO flakes. As shown in the **Figure S4.1**, grafting of AP-film with 4 four cycles leads to the largest decrease in the ESA value, this is probably the best conditions to minimize the contribution of the GCE to the total ESA, but it blocks

severely the electron transfer and the k^0 values are too small to appreciate differences between electrodes.

Table S4.2. pH of 1 mM $[Fe(CN)_6]^{3-/4-}$ solution and EGO-3h dispersion.

Sample	pH
1mM $[Fe(CN)_6]^{3-/4-}$ (1M KCl)	6.0
EGO6V6cm	4.2
EGO8V6cm	4.5
EGO10V6cm	4.1
EGO12V6cm	4.2
EGO10V4cm	4.2
EGO(R)8V6cm	4.5

The pKa of aniline is 4.6, [237] meaning that the p-aminophenyl film (AP-film) can be protonated in the EGO-3h dispersions. The pH values measured for the EGO suspensions are lower than 4.5 indicating that the negatively charged EGO flakes can self-assemble on the positively charged AP-film on the electrode surface.

4.6.3. Physicochemical characterization of EGOs

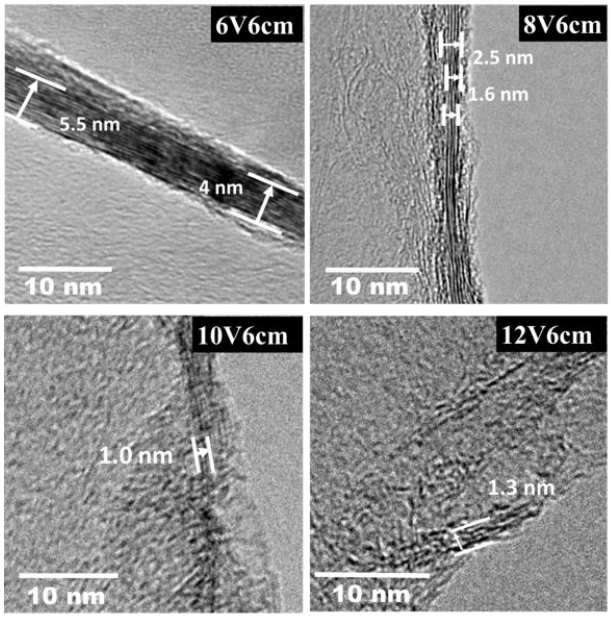

Figure S4.2. TEM images for EGO samples. The EGO flakes obtained at 6V have between 8 and 11 layers. The samples obtained at higher voltages (8 to 12 V) are composed of flakes formed by 3 to 7 layers.

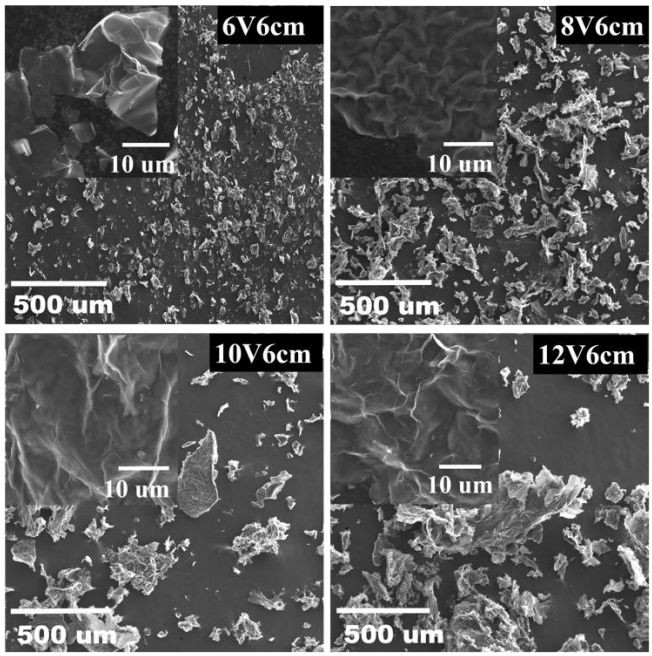

Figure S4.3. SEM images of EGO samples. EGOs sheets size increases with the applied voltage from 6V to 12V.

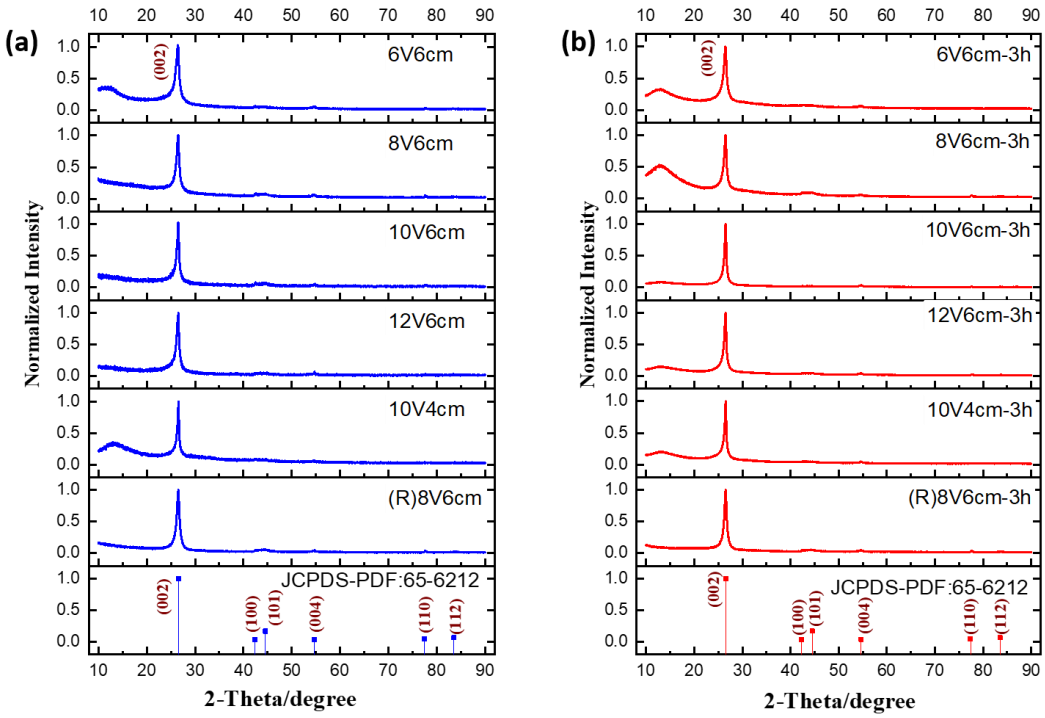

Figure S4.4. The powder XRD patterns of the EGO (a) before and (b) after 3h sonication. The position of the diffraction peaks of G (PDF 65-6212) is included in the lower panels for reference, respectively.

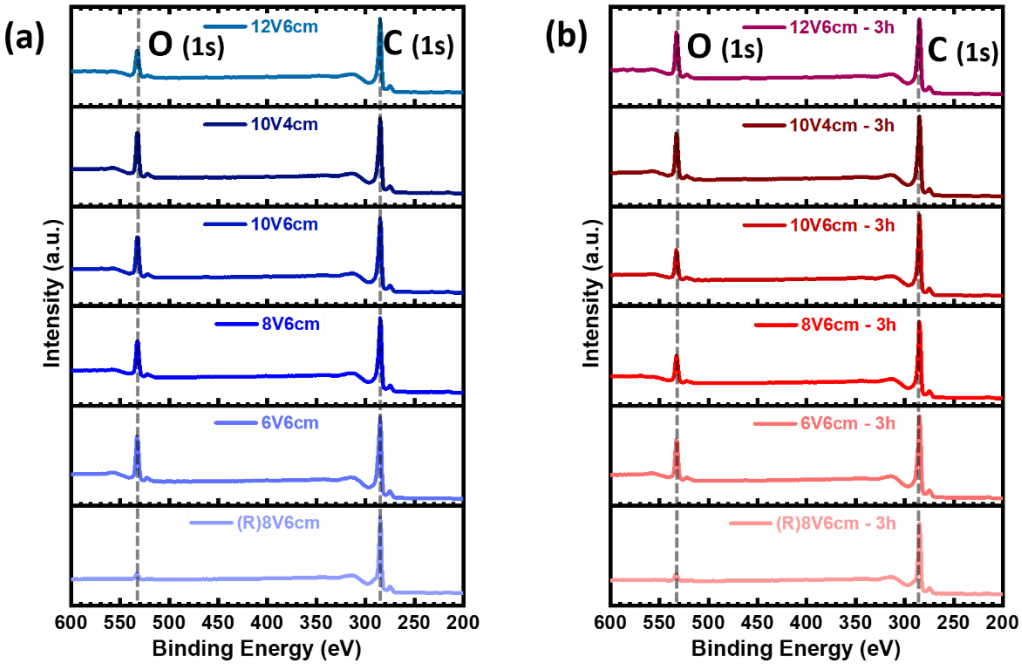

Figure S4.5. XPS survey spectra of EGOs (a) before and (b) after 3h sonication.

Table S4.3. Oxygen percentage (O at%) and C/O at% ratio determined by XPS analysis for EGO samples before and after 3h sonication.

EGO	Before 3h sonication				After 3h sonication			
	O (at%)	StDev (%)	at%C /at%O	Error	O (at%)	StDev (%)	at%C/ at%O	Error
6V6cm	15.9	0.5	5.3	0.5	15.0	0.5	5.7	0.6
8V6cm	14.1	0.7	6.1	0.6	11.7	1.0	7.5	0.7
10V6cm	16.2	0.5	5.2	0.7	12.2	0.4	7.2	0.7
12V6cm	12.4	1.0	7.1	0.9	19.1	0.3	4.2	0.4
10V4cm	17.1	0.7	4.7	0.5	16.0	0.6	5.2	0.5
(R)8V6cm	3.4	0.9	28.2	4.7	4.4	1.3	21.8	3.7

At% - atomic percentage, StDev – Standard Deviation.

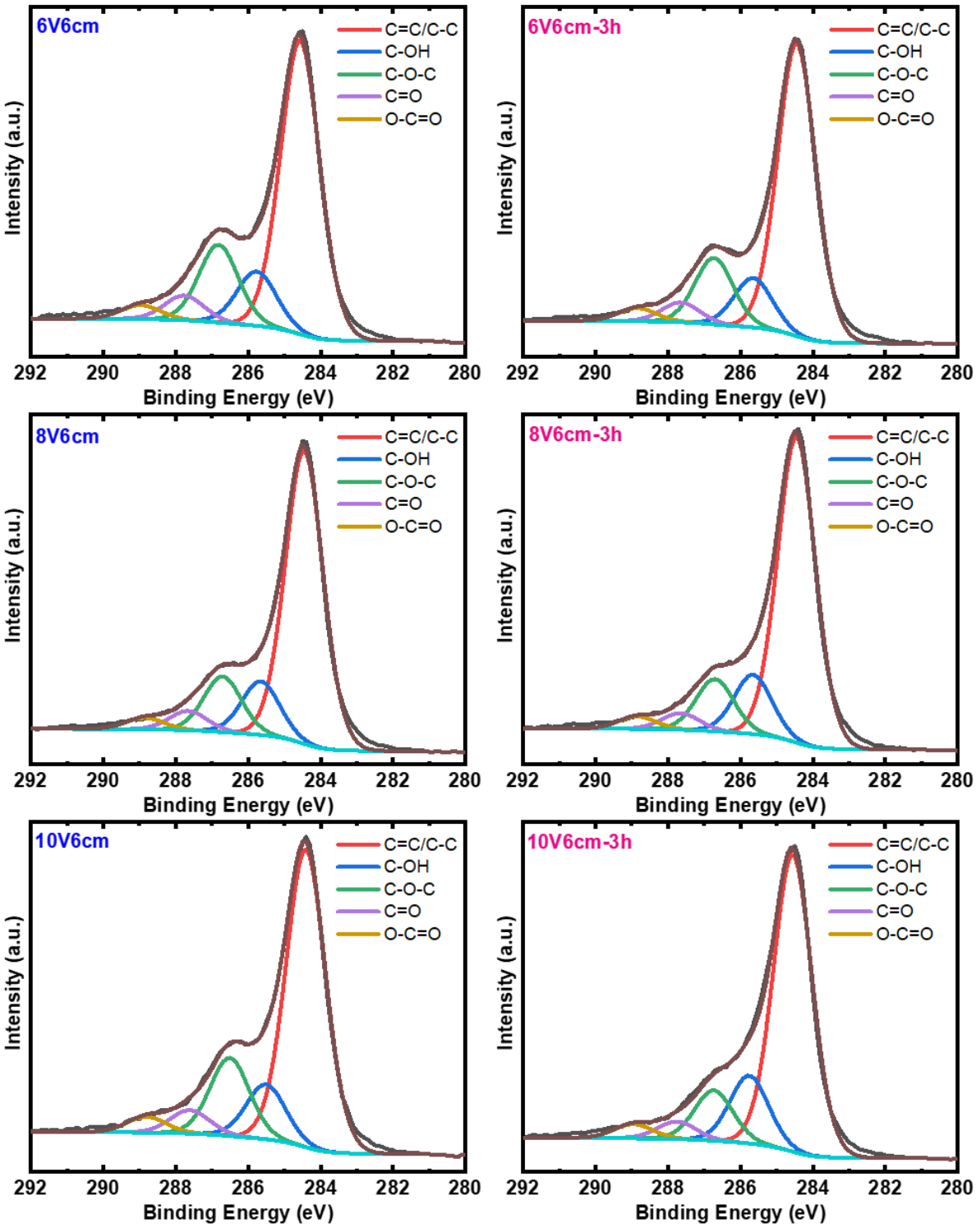
6V6cm
6V6cm-3h
8V6cm
8V6cm-3h
10V6cm
10V6cm-3h
C=C/C-C
C-OH
C-O-C
C=O
O-C=O
Intensity (a.u.)
Binding Energy (eV)
292
290
288
286
284
282
280

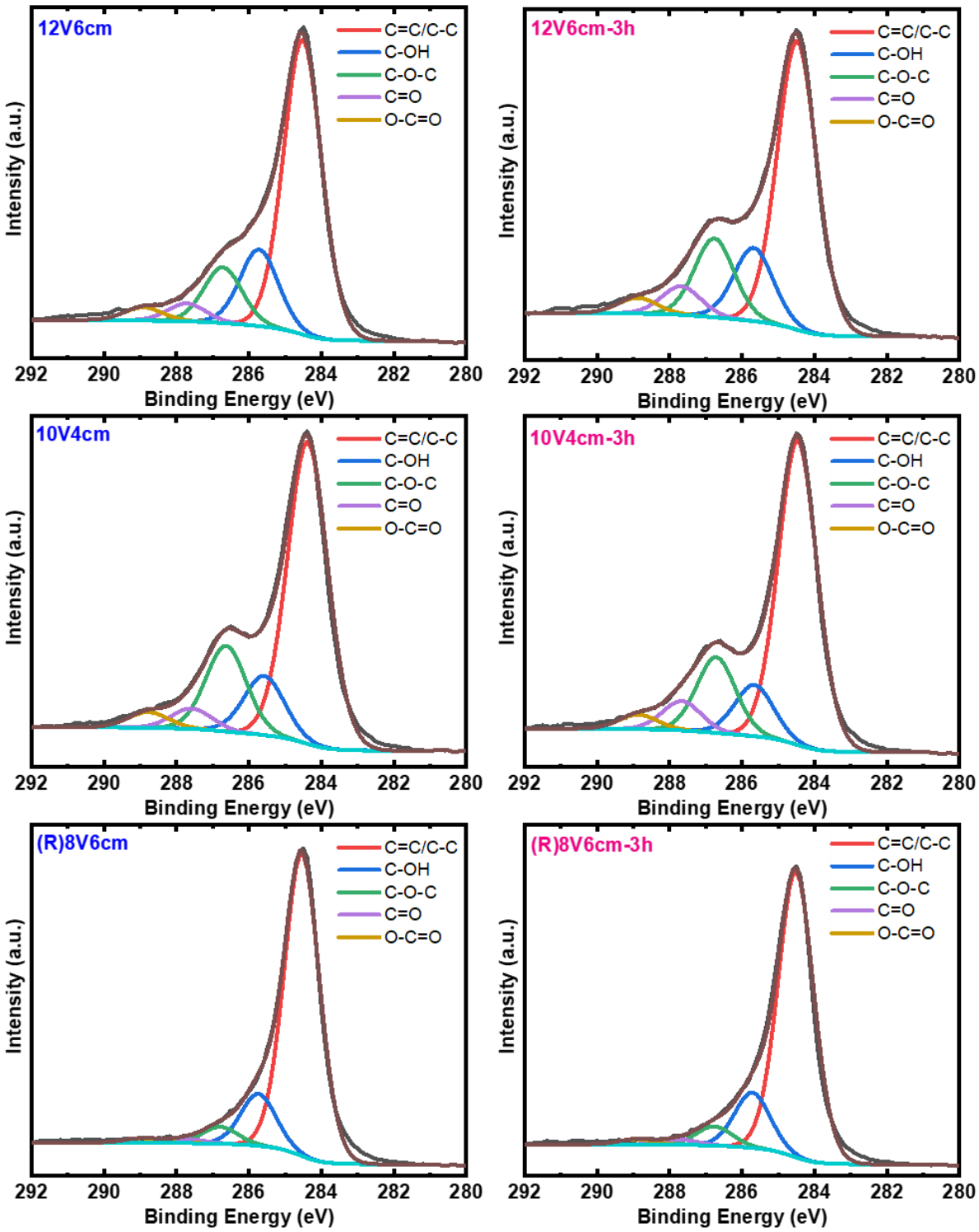

Figure S4.6. C 1s spectra of the EGOs powders before (left column) and after 3h sonication (right column).

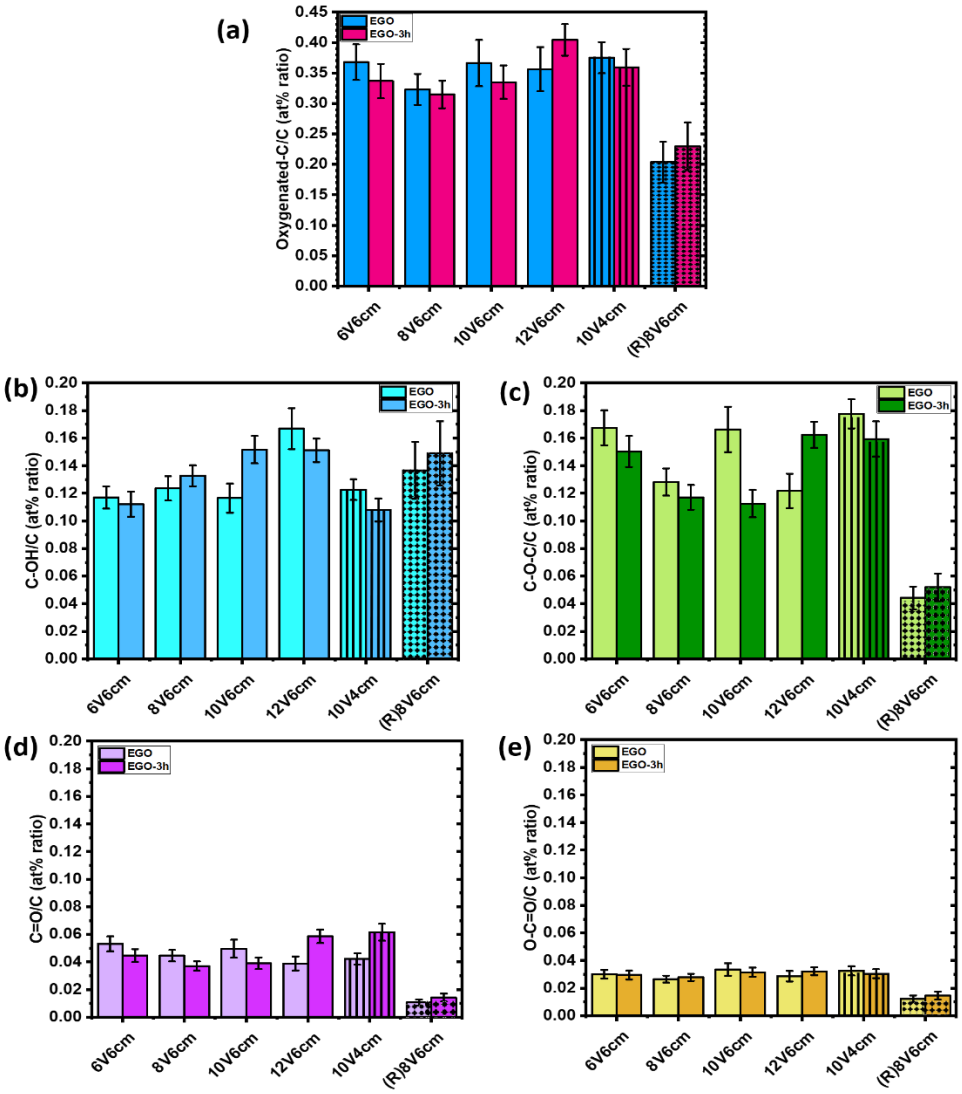

Figure S4.7. Ratios between the atomic concentrations of the carbon species composing the C 1s spectra of EGOs powders before and after 3h sonication: (a) total-oxygenated-carbon to graphitic carbon (Oxygenated-C/C); (b) C-OH to graphitic carbon (C-OH/C); (c) C-O-C to graphitic carbon (C-O-C/C); (d) C=O to graphitic carbon (C=O/C); (e) O-C=O to graphitic carbon (O-C=O/C).

During extended sonication, the EGO dispersion environment undergoes changes in the temperature and pressure, resulting in the oxidation of EGO with the increase of temperature and pressure or in the reduction of EGO due to lack of oxygen.[238] Hence the sonication process might modify the amount of oxygen-containing groups of the EGO.[239] Overall, according to Table S4.3 and **Figure S4.6** no major variations of the at% ratios before and after sonication are observed indicating that the 3 hours of sonication have no impact on the surface composition of the EGOs

prepared in this work. Only sample EGO6cm10V stands out of the trend for the (C-O-C)/C atomic ratio.

Table S4.4. A summary of recent representative studies on the synthesis of graphene materials by electrochemically anodic exfoliation of graphite.

Electrolytes	Graphite electrode	Voltage applied	Additional conditions	Properties of graphene materials				Ref.
				Number of layers	O% (%)	C/O ratio	I_D/I_G	
0.1M H_2SO_4	Graphite foil	8V	6cm, 150 min	3~7	14.1	6.1	0.55	This work
0.1M H_2SO_4	Graphite foil	8V	6cm, 150 min Reduced in 900°C for 1h	3~7	3.4	28.2	0.28	This work
0.48M H_2SO_4	Natural graphite flakes or HOPG	Alternating between ±10V	5cm, 1V for 5~10 min, 10V for 1 min	1~4	NA	NA	NA	22
0.1M H_2SO_4	Graphite foil	10V	4cm, 1h	2~4	NA	7.7	0.11	26
0.1M H_2SO_4	Graphite flakes	10V	2 min	2	7.5	12.3	0.4	21
0.1M $(NH_4)_2SO_4$	Graphite flakes	10V	3~5 min	≤ 3	5.5	17.2	0.42	20
0.5M H_2SO_4	Graphite foil	10V	2cm, 2V for 2 min then 10V for 20 min	6~8	NA	8.1	1.34	95
0.5M Na_2SO_4	Graphite foil	10V	2cm, 2V for 2 min then 10V for 20 min	6~8	NA	8.8	0.95	95
0.5M $LiClO_4$	Graphite foil	10V	2cm, 2V for 2 min then 10V for 20 min	6~8	NA	4.0	1.00	95
10M H_2SO_4	Expanded graphite	1V and 2V	1V for 10 min then 2V for 20 min	<7	3.9	7.5	0.3	105
0.5M H_2SO_4	Graphite foil	10V	3cm, 10 min, pretreatment in 1M NaOH	2~4	8.32	11	0.29	100
0.1M H_2SO_4	HOPG	1 to 10V	combination with shear field (400−74 400 s^{-1})	1~3	NA	NA	0.21~0.32	240
1M H_2SO_4	High-quality pyrolytic graphite sheet	8V	Cathodic pretreatment	3~5	NA	NA	1.1	241

NA – not available, HOPG – highly ordered pyrolytic graphite.

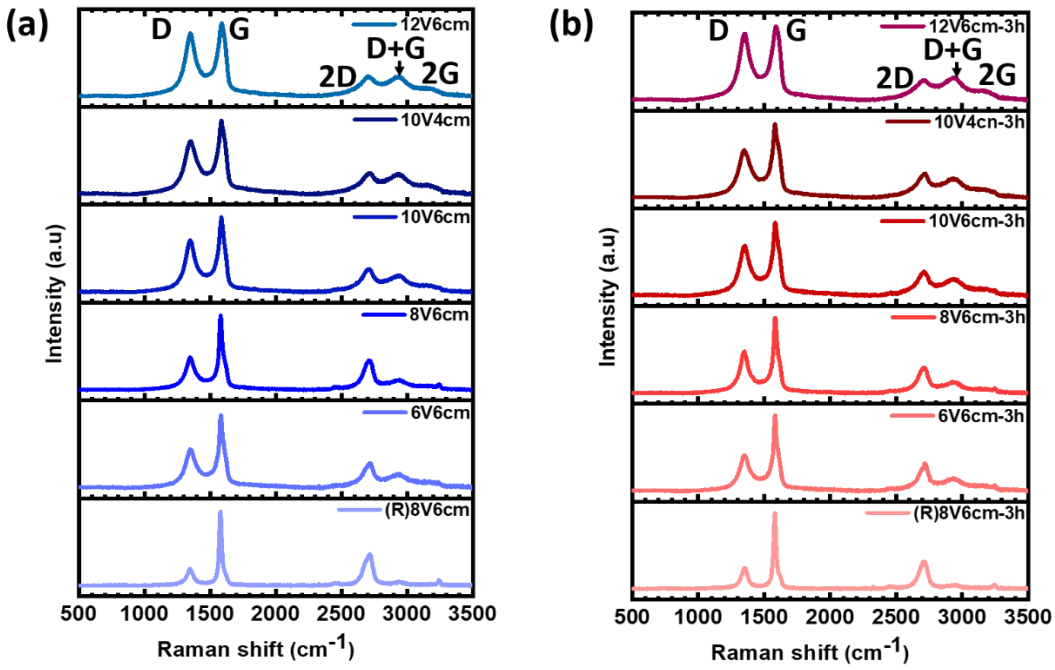

Figure S4.8. Raman spectra of the EGOs (a) before and (b) after 3h sonication.

Table S4.5. Position of the 2D bands in the Raman spectra for EGOs and EGO-3h.

EGO	Before 3h sonication		After 3h sonication	
	2D (cm^{-1})	Standard deviation (cm^{-1})	2D (cm^{-1})	Standard deviation (cm^{-1})
6V6cm	2714.3	3.4	2715.0	1.3
8V6cm	2709.5	6.0	2708.4	1.6
10V6cm	2708.8	3.4	2710.1	5.5
12V6cm	2702.9	4.4	2700.7	3.1
10V4cm	2700.7	5.8	2711.7	1.0
(R)8V6cm	2711.7	5.1	2705.1	3.1

Table S4.6. The ratio between the intensity of G (I_G) and 2D (I_{2D}) bands in the Raman spectra of EGOs and EGO-3h.

EGO	Before 3h sonication		After 3h sonication	
	I_G/I_{2D}	Standard deviation	I_G/I_{2D}	Standard deviation
6V6cm	2.7	0.1	2.7	0.1
8V6cm	2.7	0.1	3.0	0.1
10V6cm	2.8	0.1	2.8	0.1
12V6cm	3.1	0.1	2.7	0.1
10V4cm	2.8	0.1	2.6	0.1
(R)8V6cm	2.4	0.1	2.6	0.1

4.6.4. Electrochemical characterization of modified electrode and calculations

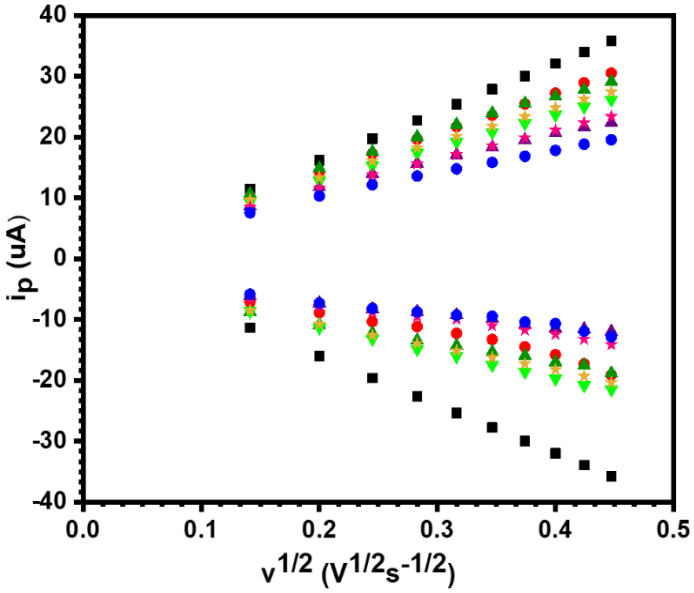

Figure S4.9. Variation of the peak current as a function of the square root of the scant rate: GCE (black square), AP/GCE (red closed circle), EGO(R)8V/AP/GCE (dark-green triangle), EGO6V/AP/GCE (purple triangle), EGO8V/AP/GCE (light-green triangle), EGO10V6cm/AP/GCE (yellow star), EGO10V4cm/AP/GCE (pink star), EGO12V/AP/GCE (blue closed circle).

The dependence of the cathodic peak current with the square root of the scant rate deviated from linearity at high scan rate. Thus, only the anodic peak currents were used to calculate the ESA value in this work.

Table S4.7. Average electrochemical surface area (ESA) values for each type of EGO-based electrode.

Electrode modified	Average slop value (X10-5)	Average A (cm2)	STDEV
GCE	7.88	0.108	0.002
GCE/AP	6.49	0.08	0.01
6V6cm/AP/C	5.02	0.069	0.005
8V6cm/AP/C	5.83	0.080	0.003
(R)8V6cm/**AP/C**	6.11	0.09	0.02
10V6cm/AP/C	6.02	0.082	0.003
10V4cm/AP/C	4.07	0.07	0.01
12V6cm/AP/C	4.73	0.065	0.003

Table S4.8. Calculation of k^0 value for one EGO 10V6cm - based electrode.

v (mV s^{-1})	ΔEp (mV)	Ψ (dimensionless)	k^0 (cm s^{-1})	Average k^0 (cm s^{-1})	Standard deviation (cm s^{-1})
200	128.8	0.301	0.128		
180	131.8	0.284	0.114		
160	126.4	0.317	0.120		
140	126.4	0.316	0.112		
120	121.5	0.351	0.115	0.114	0.007
100	119.1	0.370	0.111		
80	114.3	0.413	0.111		
60	107.0	0.494	0.115		
40	99.7	0.604	0.115		
20	92.4	0.761	0.102		

4.6.5. Results of modification of GCE with EGO film by drop-casting method

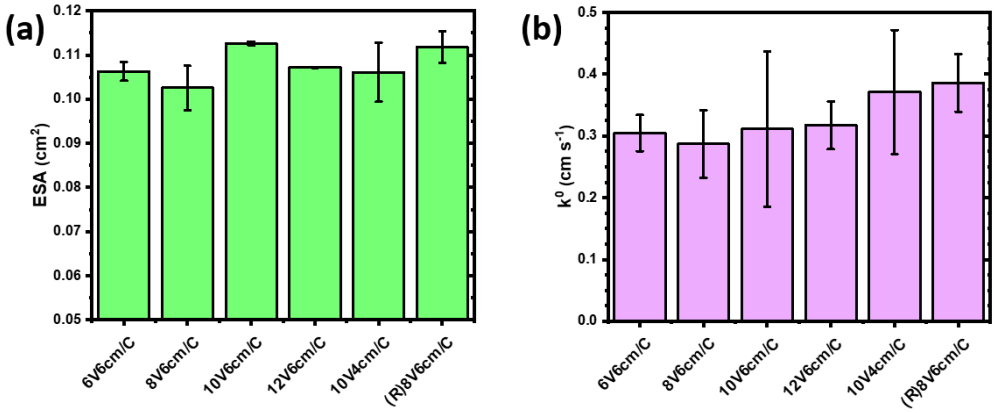

Figure S4.10. Electrochemical surface area (ESA) (a) and standard rate constant (k^0) (b) according to the modified GCE with EGOs by drop casting method.

4.7. Annex

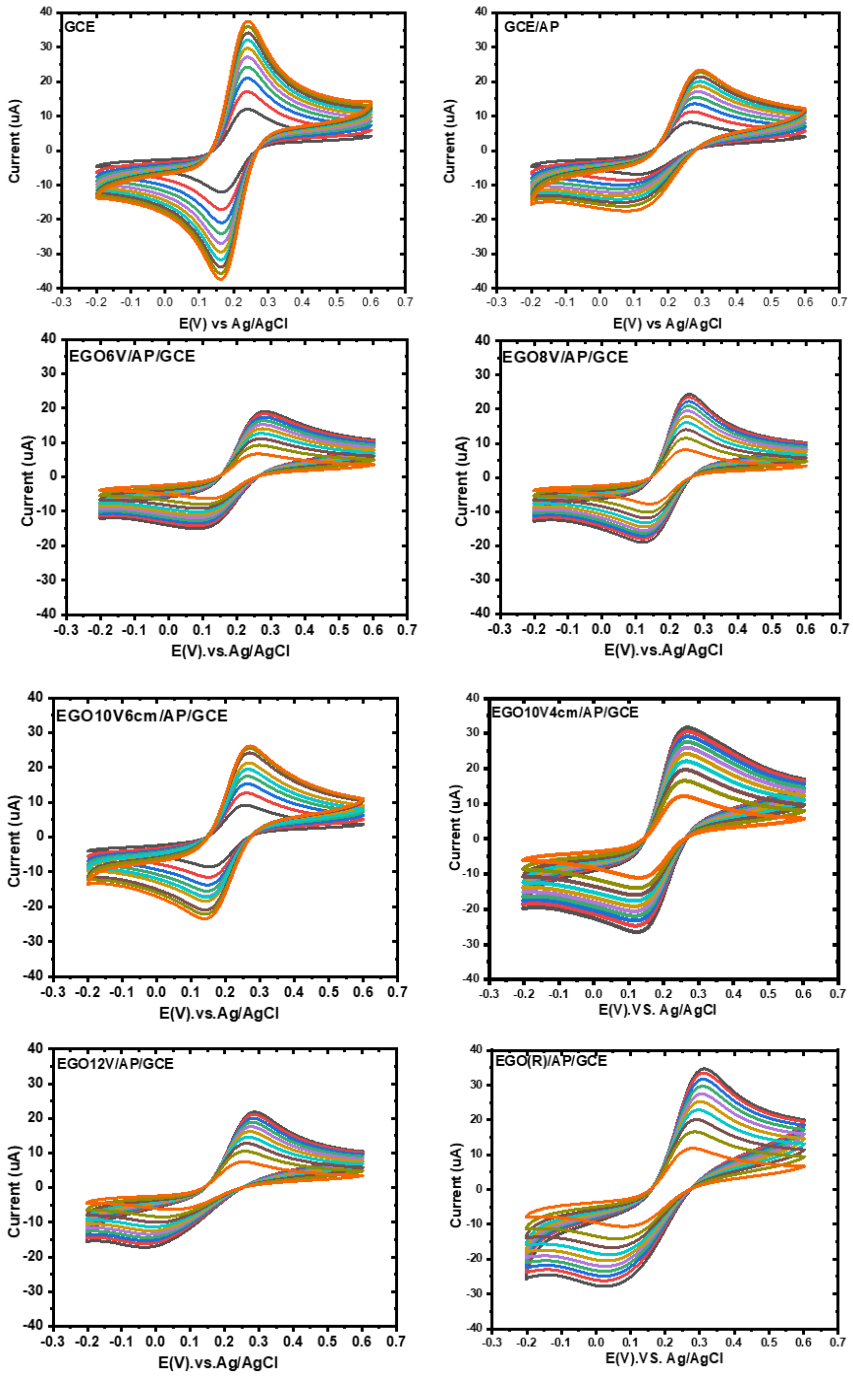

Figure A4.11. Cyclic voltammograms of the glassy carbon electrode (GCE) and the modified GCE recorded in 1 mM $[Fe(CN)_6]^{3-/4-}$ / 0.1 M KCl at different scan rate from 20 to 200 mV s^{-1}.

5. ELECTROCHEMICALLY EXFOLIATED GRAPHENE OXIDE FOR SIMPLE FABRICATION OF COCAINE APTASENSOR

OXYDE DE GRAPHÈNE EXFOLIÉ ÉLECTROCHIMIQUEMENT POUR LA FABRICATION SIMPLE DE COCAÏNE APTASENSOR

Authors:

Yuting Lei[a], Benjamin D. Ossonon[a], Pierre-Luc Trahan[b], Jiyun Chen[a], Jonathan Perreault[b*] and Ana C. Tavares[a*]

[a] Institut National de la Recherche Scientifique – Energie, Matériaux et Télécommunications (INRS-EMT), 1650 Boulevard Lionel-Boulet, J3X 1P7, Varennes, Québec, Canada

[b] Institut National de la Recherche Scientifique – Armand-Frappier Santé Biotechnologie (INRS-AFSB), 531 Boulevard des Prairies, H7V 1B7, Laval, Québec, Canada

Publication: ACS APPLIED MATERIALS & INTERFACES

Publication Date: July 13, 2023

Volume 15, Pages 35580-35589

DOI: https://doi.org/10.1021/acsami.3c03777

Contribution of authors:

This research was conceptualized and designed by Yuting Lei, Prof. Jonathan Perreault, and Prof. Ana Tavares. The EGO samples were prepared by Yuting Lei under the guidance of Dr. Benjamin D. Ossonon. Almost all the experiments were conducted by Yuting Lei. The radioactivity tests were carried out by Pierre-Luc Trahan in Prof. Jonathan Perreault's lab. Jiyun Chen assisted in drawing the scheme. All the experiment results were discussed with Dr. Prof. Jonathan Perreault and Prof. Ana Tavares. Almost all the manuscript was written by Yuting Lei, and the part on the radioactivity test was written by Pierre-Luc Trahan. The manuscript was commented on and revised by Prof. Jonathan Perreault and Prof. Ana Tavares. This work was financially supported by Prof. Jonathan Perreault and Prof. Ana Tavares' grants.

Link between articles:

Considering previous research, the EGO 10V6cm was selected for the fabrication of the electrochemical aptasensor since it has better electrochemical properties (highest ESA and k0 values). The cocaine aptamers were used to functionalize the EGO 10V6cm material through physical adsorption and covalent immobilization methods, their sensing performances were investigated and compared in this work. The study also demonstrated the effect of the electrochemical intrinsic properties of the EGO materials on the sensing performance.

5.1. Abstract

Transducers made from graphene-type materials are widely used in sensing applications. However, utilization of graphene oxide obtained from electrochemical exfoliation of graphite (EGO) has remained relatively unexplored. In this study, electrochemical cocaine aptasensors based on large-size EGO flakes were investigated. In particular, the influence of the following parameters on the sensors performance were examined: (i) aptamer's terminal group (-NH_2 vs -OH), (ii) functionalization of EGO with the aptamer via physical adsorption and covalent immobilization, and (iii) intrinsic electrochemical properties of EGO such as electrochemical surface area (ESA) and standard rate constant of electron transfer (k^0). The results demonstrate that EGO-based electrochemical aptasensors fabricated by physical adsorption with NH_2-modified aptamer have very good reproducibility, shelf-life stability, and high sensitivity for detecting cocaine with a detection limit of 50 nM. Their performance is comparable to that of the aptasensors prepared using the covalent immobilization. Additionally, it is shown that EGO materials with high ESA and k^0 can enhance the sensing performance. The fast (less than 10 minutes) and strong adsorption of the NH_2-modifed cocaine aptamer on the surface of large EGO flakes makes the fabrication of the sensing platform simple and rapid. This simple approach has the potential to simplify the fabrication of sensors.

5.2. Introduction

Generally, a biosensor consists of a transducer and a bio-receptor. For electrochemical biosensors, bio-receptors such as enzymes, antibodies, aptamers, etc. recognize the target analyte, and the electrode converts the recognition event into a measurable electrical signal. [141, 242] Graphene-based nanomaterials including graphene (G), graphene oxide (GO), and reduced GO (rGO), among others, can be used as electrode materials in transducers to improve the analytical performance of the sensor. [154-155, 243] Graphene-based materials are characterized by a

high electrical conductivity, [209, 244] high specific surface area, [31] good biocompatibility, and affinity for specific biomolecules profiting from oxygenated functional groups. [45, 59] However, the use of graphene oxides obtained by electrochemical exfoliation of graphite (named EGO) as materials for transducers is scarce, [245-248] and they have been mostly used in composite electrodes. [247-248] However, Maccaferri et al. [246] electrochemically exfoliated highly ordered pyrolytic graphite in acetonitrile with sodium perchlorate, and used the EGO modified screen-printed electrodes as amperometric sensors for morphine detection in 0.1 M phosphate-buffered solution (PBS). The electrocatalytic properties of the graphene coating combined with a suitable cleaning process conferred a high sensitivity to the sensor (LOD=2.5 ppb).

Compared with Hummers' chemical method of GO synthesis, [15, 86] the electrochemical exfoliation of graphite in an aqueous solution is more environmentally friendly, simpler, faster and inexpensive. Through this method, large-scale production of EGO materials can be achieved with different functional groups, structural defects, and tunable sheet sizes by simply adjusting the parameters such as applied voltage and/or distance between the two electrodes, or by using different electrolytes. [20, 22-23, 26, 57, 95-96, 249] With these advantages, EGO materials are ideal for industrial production of electrochemical sensors, but selecting the one that is appropriate for a particular application can be challenging. In our previous study on EGO, [23] a series of large flake size EGO materials (> 10 µm) with few layers (from 3 to ~7) were synthesized in 0.1 M H_2SO_4 under different electric fields. According to the electrochemical characterization using the $[Fe(CN)_6]^{3-/4-}$ redox probe, their electrochemical surface area (ESA) varied between 0.065 and 0.82 cm^2, while the standard rate constant of electron transfer (k^0) varied between 0.05 and 0.13 cm s^{-1}. EGO materials with few layers ($\leqslant 7$) and low density of C-O-C groups had higher ESA and k^0 values. Moreover, the EGO materials have a lower density of oxygenated functional groups (C/O > 4) [23] compared to the chemical methods (e.g. Hummers' method: C/O $\approx$ 2), [15] a property that may be beneficial to electrochemical devices. [16, 28] Hence, in addition to exploring the use of EGO materials in sensing applications, it is also important to understand how their physicochemical and electrochemical properties impact the performance of the device.

The ability to functionalize the surface of graphene-materials with aptamers and other sensing elements relies on the materials' physicochemical properties, such as surface composition and sheet size. [151-153] According to the previous literature, both physical adsorption and chemical immobilization methods are often used for antibodies and DNA. [5, 154-156] Chemical immobilization involves the formation of a stable covalent bond between the bio-receptor and the transducer surface, such as the carboxamide bond formed after the reaction between the amine and carboxyl

groups. [154, 157] The physical adsorption method uses the pi-pi stacking interactions between the DNA strands and the surface of graphene-based materials, and the electrostatic forces between the functional groups of the bio-receptor and those of the graphene-based materials. Despite the simplicity of this method, it is used less frequently, since it usually reports weaker adhesion and less control over the orientation of biomolecules, leading to lower stability and sensibility compared to chemical immobilization methods. [154, 158] Recently, Eissa et al. reported that for GO materials synthesized by modified Hummers' method, the response of microcystin-LR toxin aptasensors was found to be enhanced with increasing GO sheet size (from 0.22 to >100 µm) when physical adsorption was used. Meanwhile, small-sized GO sheets (<2.5 µm) offered better sensing performance by the covalent attachment method. [151] This study demonstrated the impact of GO flake sizes and functionalization method on the sensing performance. In other works, new materials or electrode architectures have been investigated to improve the sensitivity and stability of sensors, [250-253] But these often require laborious processes which usually result in higher, which may hamper their industrial production and wide-spread use. [254-257] It is therefore important to be able to fabricate efficient and simple sensors using simple and inexpensive methods.

In this work, we demonstrate the suitability and benefits of using EGO materials for the fabrication of electrochemical aptasensors. We investigated both physical adsorption and chemical immobilization of a cocaine aptamer [258-260] functionalized with a terminal amine group (aptamer-NH_2) on the EGO surface (having the highest ESA and k^0 values according to our previous work [23]). We show that the EGO-based cocaine aptasensors fabricated through the simple physical adsorption method and by the covalent method have identical sensing performance in terms of limit of detection and shelf-life. Control experiments with an unmodified cocaine aptamer (having -OH as the terminal group) revealed that more aptamer-NH_2 is adsorbed on EGO surface resulting in a better sensing performance. Finally, our study also confirms that the performance of the aptasensor scales with the EGOs' electrochemical intrinsic properties such ESA and k^0.

5.3. Experimental section

5.3.1. Materials.

The chemicals used in this work are listed in the supporting information (SI). The electrochemically exfoliated graphene oxides (EGOs) were synthesized according to our previous work. [23] Their physicochemical and electrochemical properties are summarized in **Tables S5.1** and **S5.2**.

5.3.2. Fabrication and electrochemical characterization of the cocaine aptasensor based on EGO.

Scheme 5.1 illustrates the procedures used to fabricate the EGO-based electrochemical cocaine aptasensor for both physical adsorption and covalent immobilization methods. First, 8 µL of EGO suspension (0.4 mg/mL sonicated for 3h) was deposited on the surface of a glassy carbon electrode (GCE, 3 mm diameter) and dried at room temperature (21±1° C). Next, the modified electrode (GCE/EGO) was incubated in the cocaine aptamer-NH_2 solution (6 µL of 1 µM cocaine aptamer in 0.05 M KCl, pH = 7), 10 minutes for the optimized time. The cocaine aptamer-NH_2 modified electrode (GCE/EGO/Apt-NH_2) was then immersed in 6 µL of 0.1% bovine serum albumin (BSA) solution, 30 minutes for the optimized time, to block the electrode's surface and to avoid nonspecific adsorption. Finally, the blocked electrode (GCE/EGO/Apt-NH_2/BSA) was incubated in 8 µL cocaine solutions of varying concentrations for 30 min for the optimized time (GCE/EGO/Apt-NH_2/BSA/Co).

For the covalent immobilization method, a supplementary step was added to the fabrication procedure. The GCE/EGO electrode was incubated in 8 µL of a 50 µM N,N,N',N'-tetramethyl (succinimido) uronium tetrafluoroborate (TSTU) and 4-dimethylaminopyridine (DMAP) solution for 1 h to form the linker (GCE/EGO/linker). [206-207] Subsequently, the electrode was incubated in the cocaine aptamer-NH_2 solution (GCE/EGO/linker/Apt-NH_2) for 10 min, the BSA solution (GCE/EGO/linker/Apt-NH_2/BSA) for 30 min, and lastly, the cocaine solution (GCE/EGO/linker/Apt-NH_2/BSA/Co) for 30 min.

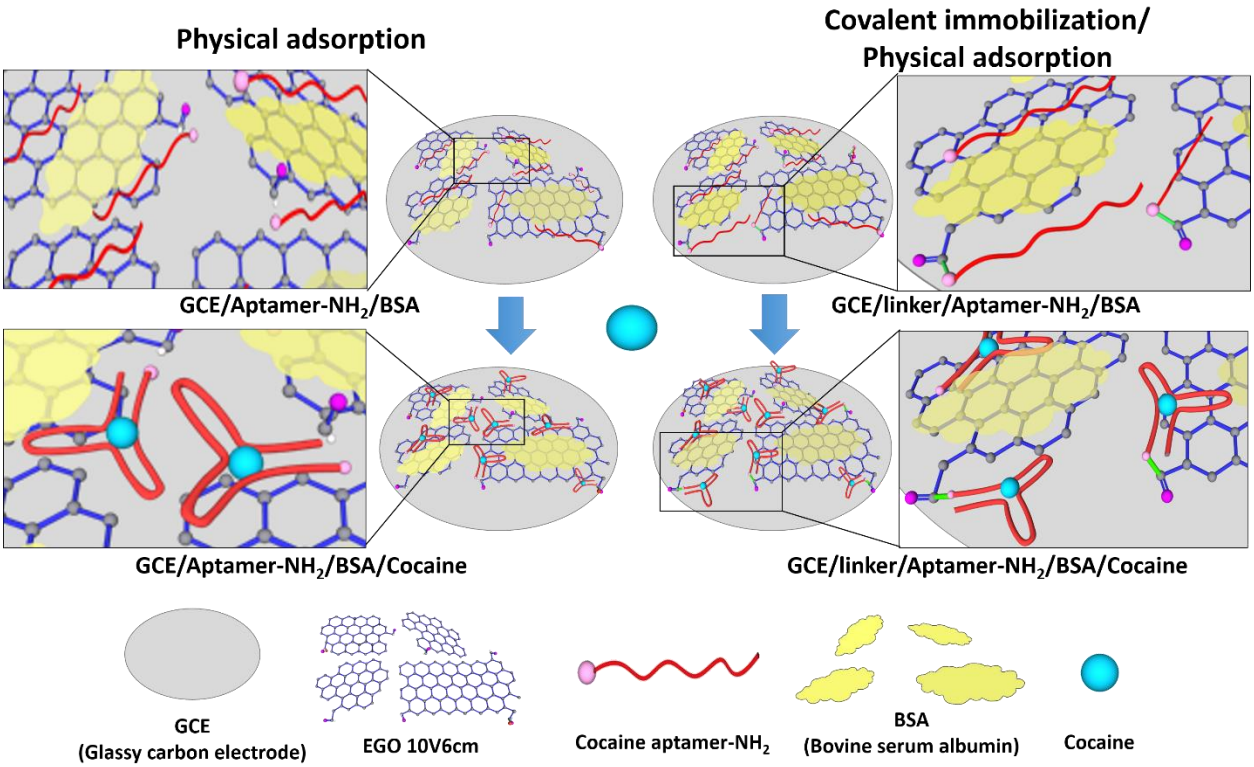

Scheme 5.1. Illustration of the electrochemical aptasensor for the detection of cocaine based on electrochemically exfoliated graphene oxide (EGO).

Before use, all the GCE electrodes were cleaned by cloth polishing with 1, 0.3 and 0.05 mm alumina particles and washed with Millipore water. The modified electrodes were also washed with Millipore water after each modification step. To follow the surface modification of the GCE, cyclic voltammograms (CVs) and square wave voltammograms (SWVs) were recorded after each step with at least three electrodes. The electrodes were also washed with Millipore water after each characterization step. A traditional three-electrode cell equipped with the bare or modified CGE as the working electrode, a Pt wire as the counter electrode, and a Ag/AgCl (1 M KCl) reference electrode was used. The GCE, Pt wire, and the reference electrode were purchased from CH Instruments. All electrochemical measurements were conducted at room temperature in the presence of 1 mM $[Fe(CN)_6]^{3-/4-}$ inner-sphere redox couple in 0.1 M KCl, which is very sensitive to the surface structure of carbon materials. [207] The CVs were recorded from -0.2 V to 0.6 V with a scan rate of 0.1V s^{-1}, and the second cycle is presented. The SWVs were recorded from -0.2 V to 0.8 V with a frequency of 25 Hz. A Metrohm Autolab potentiostat PSTAT302 controlled by NOVA 2.1.2 (Ecochemie) was used.

5.3.3. Physicochemical characterization

Physicochemical characterization of the electrodes was done by X-ray photoelectron spectroscopy (XPS) and by radioactivity tests. XPS was used to confirm the chemical attachment of the aptamer-NH_2 on the surface of the EGO flakes during the sensor fabrication. The radioactivity tests were used to verify the adhesion of the aptamer to the EGO surface after binding with cocaine. The experimental details can be found in the SI.

5.4. Results and discussion

In this work, the two approaches - physical adsorption and covalent immobilization - for the fabrication of the aptasensor with EGO materials are explored, **Scheme 5.1**. The EGO with the highest ESA and k^0 values as reported previously (named 10V6cm, **Tables S5.1 and S5.2**) [23] was chosen in this comparative study.

5.4.1. Optimization of incubation time for each step.

Figure 5.1a shows the CV recorded in 1 mM $[Fe(CN)_6]^{3-/4-}$ in 0.1 M KCl following each modification step during the fabrication of the aptasensor using the physical adsorption method. The current increased after EGO deposition on the GCE due to increases in the ESA and k^0 of the electrode. [23] Next, the current began to decrease after incubating in cocaine aptamer-NH_2 and BSA solutions, due to the surface being blocked. In the last step, the current increased once again which is ascribed to the modification of the aptamer-NH_2 configuration after binding with the cocaine molecule. [258] This configuration change exposes more electrode surface for the electron transfer with the $[Fe(CN)_6]^{3-/4-}$ redox probe. SWV, which is more sensitive compared with CV, is employed to quantify the relative variation in the peak current (Δi) after each modification step (**Figure 5.1b** and **Figure S5.1**). For better assay results, the incubation time of the cocaine aptamer-NH_2, BSA, and cocaine were optimized. The Δi for the aptamer-NH_2 modification step (GCE/EGO/Apt-NH_2) was constant after 10 minutes, indicating that the aptamer-NH_2 can be adsorbed very quickly on the EGO (**Figure 5.1c**). In the surface blocking step (GCE/EGO/Apt-NH_2/BSA), the Δi (**Figure 5.1d**) becomes constant after 30 minutes. The binding between the aptamer-NH_2 and the cocaine molecule was completed after 30 minutes (**Figure 5.1e**).

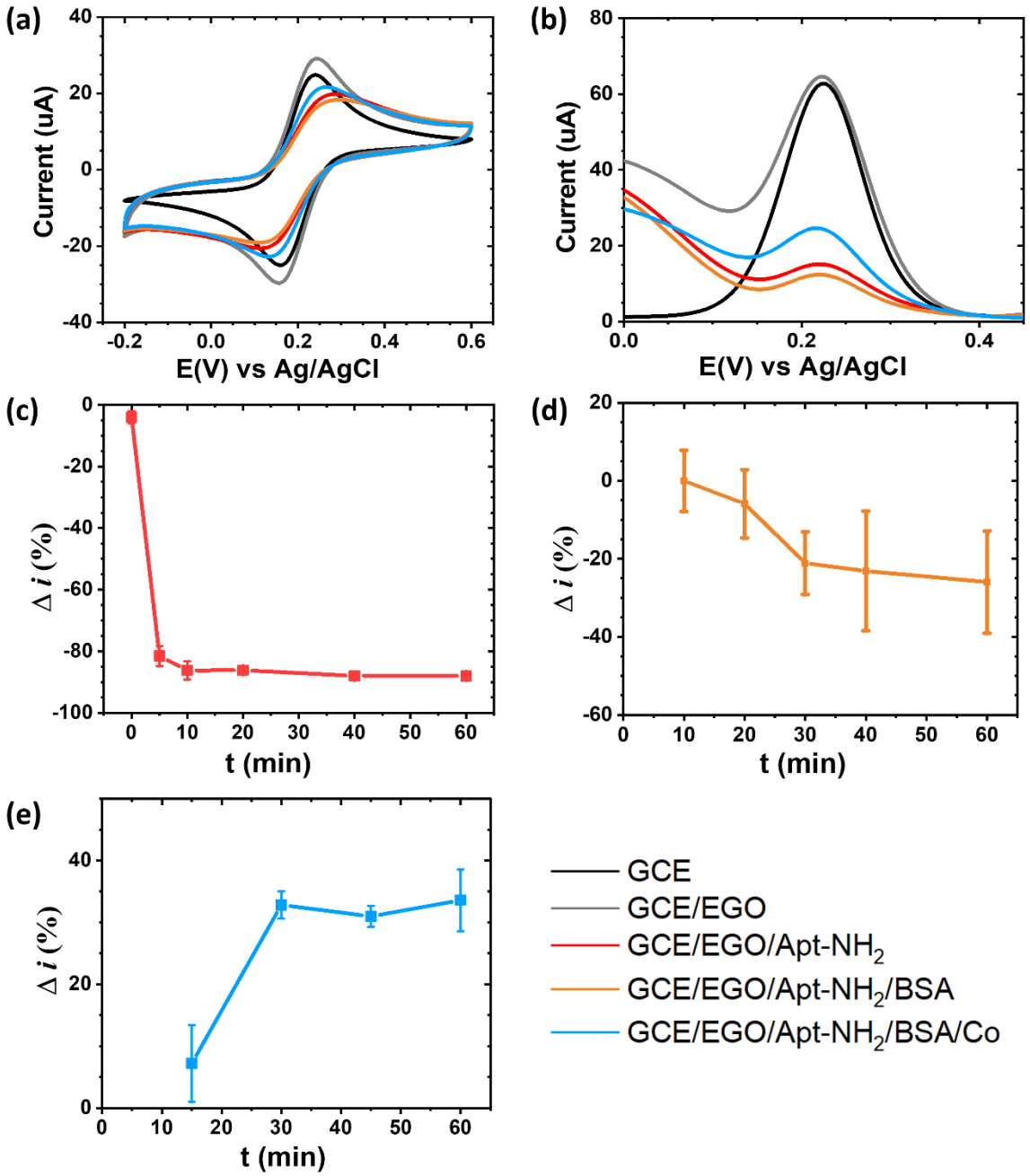

Figure 5.1. Monitoring the fabrication of the cocaine aptasensor via the physical adsorption method by (a) Cyclic voltammograms at 0.1 V s^{-1} and (b) square wave voltammograms at 25 Hz recorded in 1 mM $[Fe(CN)_6]^{3-/4-}$ / 0.1 M KCl after each modification step. Optimization of incubation time in the solutions of (c) cocaine aptamer-NH_2 (1 µM, 6 µL), (d) BSA (0.1%, 6 µL) and (e) cocaine (1 µM in H_2O, 8 µL).

5.4.2. Comparing the terminal groups of the cocaine aptamer.

For the physical adsorption method, in addition to the pi-pi stacking, there may also be electrostatic interaction between the aptamer's terminal amine group and the EGO oxygenated

functional groups. Thus, the same experiment was run to investigate the effect of this group by using an unmodified cocaine aptamer (thus having a OH terminal group, aptamer-OH). In **Figure 5.2a**, it is shown that the value of Δ*i* of the GCE/EGO electrode with aptamer-OH decreased slightly less than that of the aptamer-NH_2. However, the Δ*i* decreased dramatically after incubating in BSA, showing that the aptamer-OH covered less surface compared with the aptamer-NH_2, and that more surface has been blocked by BSA. Finally, after the detection of cocaine, the electrode having the aptamer-NH_2 showed better performance especially at low concentration of cocaine, **Figure 5.2b**. The improvement concerned both the Δ*i* amplitude as well as reproducibility. Thus, the presence of the terminal NH_2 functional group in the aptamer will improve biosensor performance, likely because the positively-charged amine groups have enhanced the electrostatic interaction with the negatively-charged EGO, resulting in more aptamers stably adsorbed on the EGO [8, 23]. Moreover, to verify if the cocaine-induced changes were triggered by aptamers released from the surface or by a conformational change of the aptamer on the surface, a radioactivity test using ^{32}P-radiolabeled aptamers-NH_2 was performed. As shown in **Figure S5.2**, aptamers were adsorbed onto the surface of EGO on two types of electrodes (GCE, screen-printed gold electrode (Au-SPE)) and on EGO freestanding films. Following aptamer functionalization (**Figure S5.2**), radioactivity can only be detected in cleaning water for Au-SPE, whereas for the two other substrates, no radioactivity is detected above background noise. This indicates a very strong binding of the aptamer to the EGO surface. After incubation with 50 µM cocaine solution or 0.05 M KCl solution, the radioactivity on the EGO/Apt-NH_2 surface seems intact since no radioactivity was detected in cleaning water (**Figure S5.3**). Therefore, no cocaine aptamers-NH_2 were released from the EGO surface after binding with cocaine. A DNase was used to try to strip the aptamers from the EGO surface, but it failed (**Figure S5.4**). These tests demonstrate once more that EGO has a strong adsorption capacity for aptamers modified with the NH_2 terminal group as well as for smaller DNA sequences. It also demonstrates the possibility of using the EGO surface on multiple substrates with no visible change in efficiency.

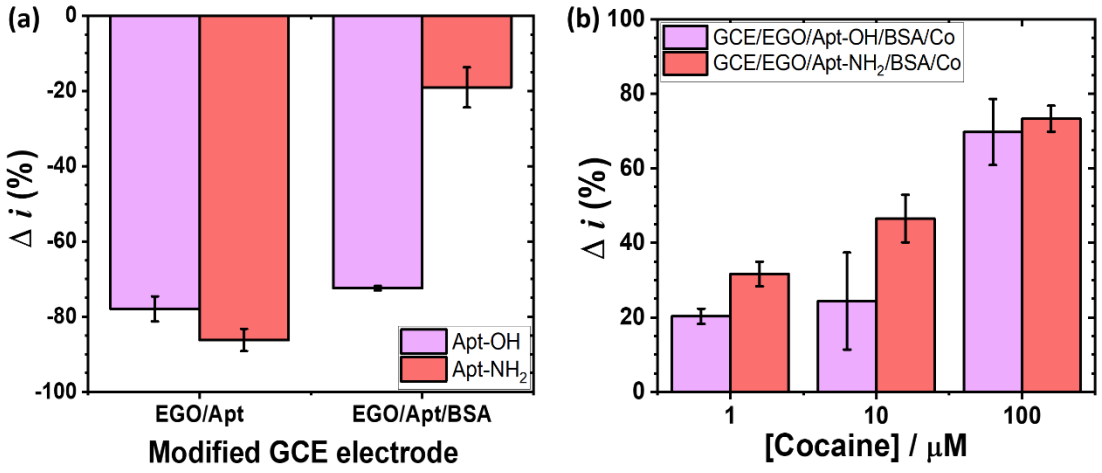

Figure 5.2. Comparison of the relative variations in the peak current (Δi) using a cocaine aptamer with terminal amine group (Apt-NH_2) and an unmodified cocaine aptamer (Apt-OH): (a) GCE/EGO electrodes modified by cocaine aptamers and BSA, and (b) detection with different cocaine concentrations.

5.4.3. Comparing the adsorption method with the covalent immobilization method.

For the covalent immobilization method, the same aptamer-NH_2 concentration and incubation time as in the physical adsorption method were used to properly compare these two methods. However, it should be noted that physical adsorption of the aptamers on the electrode surface cannot be avoided during the covalent immobilization process due to fast and strong adsorption of the aptamer-NH_2 on the EGO (see **Figures 5.1c** and **S5.2**-**S5.4**). XPS analysis was used to investigate the covalent immobilization process through the TSTU/DMAP reaction in an aqueous solution. It consists in the formation of carboxamide bonds between the carboxyl groups of EGOs and amine groups of the aptamers (see **Scheme S5.1**). [206-207] The survey spectra of the modified electrodes are shown in **Figure S5.5a**, and the low intensity peak at 400 eV indicates that there is N on the electrodes' surface. The N atom% values obtained from the quantification of the N 1s core level spectra were included in the figure. From the C 1s spectra (**Figure S5.3b-e**), the relative intensities of the C=O/C=N and O-C=O/N-C=O peaks increased after the functionalization with the linker and aptamer-NH_2. From the N 1s spectra (**Figure 5.3**), the N-(C=O) bond appeared due to the formation of the succinimidyl nitrogen of the linker in the GCE/EGO/linker electrode (**Figure 5.3a**). After incubation with the cocaine aptamer, both amine and amide bonds were observed in the GCE/EGO/linker/Apt-NH_2 electrode (**Figure 5.3b**), corresponding to the cocaine aptamers-NH_2 and the carboxamide bonds formed between the EGO and aptamers, respectively. [261-263] In comparison, the N-C and amine (C-NH_2) bonds coming from the cocaine aptamer-NH_2 were

observed for GCE/EGO/Apt-NH_2 electrode (**Figure 5.3c**), but no N-(C=O) bond was found in this case. GCE/EGO electrode (**Figure 5.3d**) shows a low intensity peak within a noisy background. Since no chemicals containing N-moieties were used in the exfoliation of the graphite foil, most likely nitrogen from air is adsorbed onto the EGO surface. [264] These results demonstrate successful electrode modification via the covalent immobilization method.

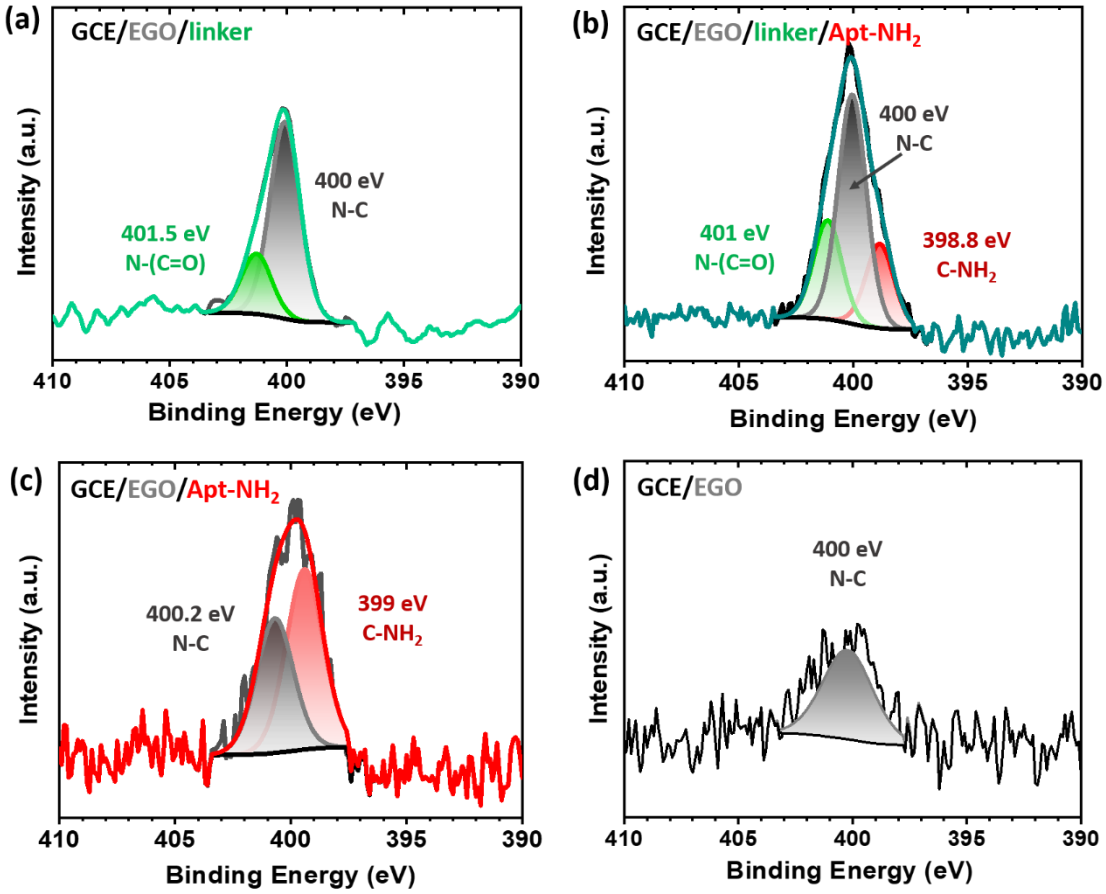

Figure 5.3. N 1s X-ray photoelectron spectra of the electrodes after (a) formation of the linker on the EGO surface; (b) reaction between the linker and the aptamer-NH_2; (c) physical adsorption of the aptamer-NH_2 on the EGO surface; (d) EGO on glassy carbon electrode.

Figure 5.4a compares the electrochemical signal, Δi, after each step of both covalent immobilization and physical adsorption methods. It can be appreciated that Δi is almost the same for both methods after functionalization with the cocaine aptamers-NH_2 and BSA. This result indicates the dominance of the physical adsorption over covalent bonding, and confirms the excellent ability of the EGO to adsorb the aptamer-NH_2 on its surface. The CV and SWV for the covalent immobilization method appear in **Figure S5.6** of the SI. For quantitative cocaine determination, the Δi was calculated after incubating in cocaine solutions of different

concentrations, as shown in **Figure S5.7**. Linear calibration curves in the log-log form were drawn in the concentration range of 0.05-100 µM (**Figure 5.4b**), and expressed by the following regression equations:

$$\log(\Delta i) = 0.192 * log\,[cocaine(nM)] + 0.928 \quad (5.1)$$

with R^2 = 0.9977 (n = 3) for the physical adsorption method, and

$$\log(\Delta i) = 0.200 * log\,[cocaine(nM)] + 0.903 \quad (5.2)$$

with R^2 = 0.9955 (n = 3) for the covalent immobilization method.

The LOD, defined as three times the standard deviation of blank/slope by the International Union of Pure and Applied Chemistry (IUPAC), [265] was calculated at roughly 50 nM for both methods. Comparing these two methods, their calibration curves and LOD are too similar to distinguish a difference between them. The results also suggest that the physical adsorption of the aptamers occurs simultaneously with the chemical functionalization and that its impact on the response of the aptasensors is dominant. This means that there is no advantage for the covalent immobilization when using large-size flakes of graphene oxide materials. This is ascribed to small amounts of carboxyl groups (O-C=O/C atom % ratio is about 4%) on the EGO flakes. [23] Meanwhile, the large flake sizes will favor the physical adsorption of aptamers, resulting in better sensor performance. [151] Additional tests were conducted where the chemical immobilization of the aptamer on EGO was extended to 20 and 40 minutes, **Figure S5.8**. But, as shown in the figure, there was no improvement in the sensor's performance.

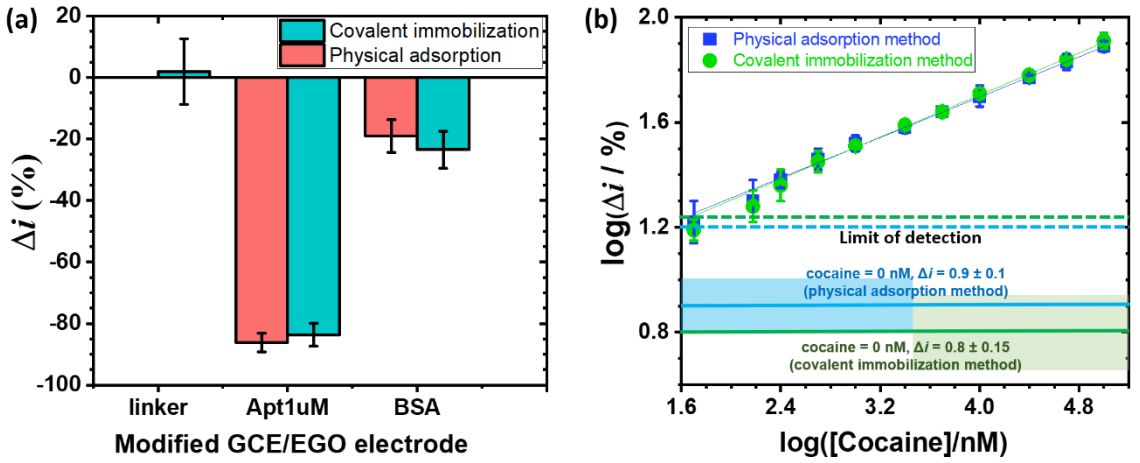

Figure 5.4. Comparison of physical adsorption and covalent immobilization methods: (a) relative variations in the peak current (Δi) of GCE/EGO electrodes modified by the linker, cocaine aptamers and blockage with BSA; (b) calibration curves of cocaine detection, where the blue and green solid lines correspond to log(Δi) when the cocaine is 0 nM for the covalent immobilization and physical adsorption methods, respectively. Blue and green dotted lines correspond to the detection limits for the covalent immobilization and physical adsorption methods, respectively.

Considering the prospective applications in clinical diagnostics and biomonitoring, a shelf-life test of the proposed EGO-based cocaine aptasensors was also performed. Thus, the constructed sensors were stored at 4° C for 14 days and then monitored with SWV in 1 mM $[Fe(CN)_6]^{3-/4-}$ / 0.1 M KCl. It was found that they maintained 98.7% and 98.4% of their initial response after 14 days for the physical adsorption and the covalent immobilization methods, respectively, **Figure 5.5**. These results show that the aptasensor based on EGO exhibited good stability, regardless of whether it was developed through the physical adsorption method or the covalent immobilization method. For a convenient comparison, SI **Table S5.3** summarizes the characteristics of the cocaine electrochemical aptasensor reported in this work together with those of other electrochemical biosensors for cocaine reported in the literature. [250-253, 258-259, 266-267] It shows that the EGO-based electrochemical sensor prepared in this work presents a good performance, and the LOD for cocaine is lower than the one required by the Canadian Society of Forensic Science Drugs and Driving Committee (DDC), at 50 ng/mL (165 nM) in the oral fluid. [268-269] Moreover, it has the advantage of being simpler and faster to prepare.

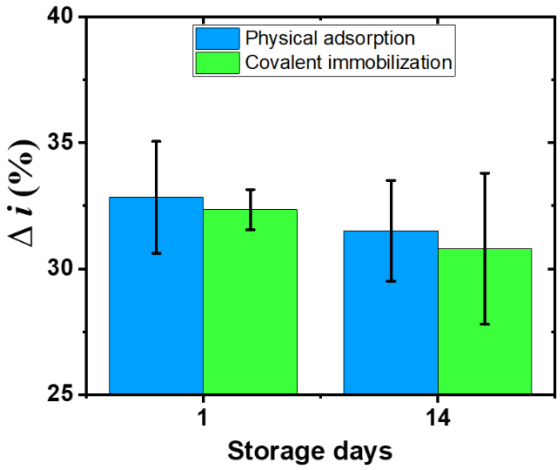

Figure 5.5. Fourteen-day shelf-life test for the detection of 1 µM cocaine.

5.4.4. Selectivity test.

As previously reported, the cocaine aptamer-NH_2 is sensitive but is not very selective. [270-271] Nevertheless, the selectivity of the proposed aptasensor prepared by physical adsorption method was examined to ensure that it does not have additional selectivity issues beyond those related to this aptamer since selectivity is one of the primary objectives when incorporating aptamers into sensors. First, two molecules whose structure are included within that of cocaine, methyl benzoate and anhydro ecgonidine methyl ester, were chosen. According to the results shown in

Figure 5.6, for the same concentration of these analytes (10 µM), the Δ*i* for methyl benzoate is barely above the detection limit, showing there is no interaction with the cocaine aptamer. The Δ*i* of anhydro ecgonidine methyl ester is about 35% with a high error, indicating the occurrence of an interaction between it and the cocaine aptamer. This is not surprising since the anhydro ecgonidine methyl ester forms the main part of the cocaine molecule. These assays were performed with Millipore water as the solvent in order to demonstrate the universality of this EGO-based aptamer sensor. However, these conditions may reduce the selectivity of the aptasensor through nonspecific electrostatic interactions. This is illustrated in **Figure S5.9** during the detection of kanamycin in Millipore water where the Δ*i* of kanamycin is tremendous (around 800%). This phenomenon is attributable to nonspecific interactions between the positively charged kanamycin and the negatively charged EGO and/or negatively charged aptamer. However, it can be avoided after changing the Millipore water by 1 mM $MgCl_2$ solution. The divalent ions modulate these interactions by neutralizing the negative charge of the phosphate groups in aptamers, greatly reducing their attraction toward positively charged amino groups in kanamycin molecules. [10] In other words, the sensing performance in terms of selectivity of this EGO-based aptasensor may be further enhanced by using high-affinity selective aptamers and by using a more optimal solvent including buffers and cations, such as Mg^{2+}, or phosphate buffer containing 1 M NaCl. [258]

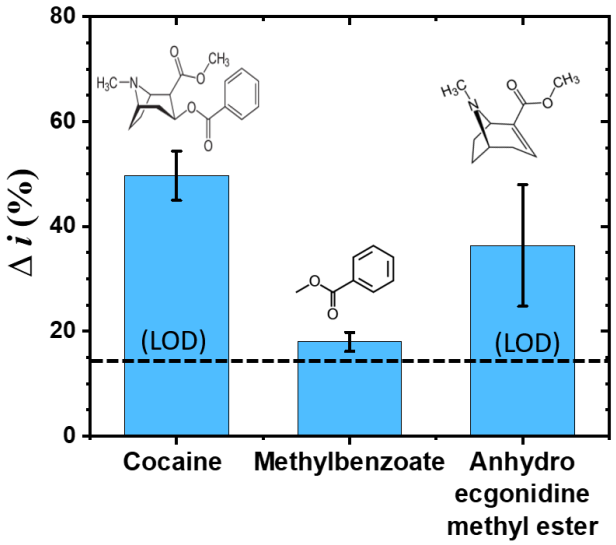

Figure 5.6. Selectivity test with different analytes (10 µM).

5.4.5. Real sample analysis.

Detection of cocaine in a human saliva sample (diluted in Millipore water) was conducted to test the applicability of the EGO-based aptasensor prepared by the physical adsorption method The

saliva samples were spiked with cocaine at various concentrations. As shown in **Table 5.1**, the detected cocaine concentrations in three tests correspond to those spiked in the samples, based on the standard curve (**Figure 5.4b**). These results confirm the suitability of our EGO and the physical adsorption method in the fabrication of reliable electrochemical biosensors.

Table 5.1. Analytical response of the EGO-based aptasensor prepared by physical adsorption method to the determination of cocaine in spiked saliva samples.

Test	Spiked Cocaine (nM)	Δ*i* (%)	Detected cocaine (nM)
1	150	22 ± 3	144 ± 56
2	1000	32 ± 3	1014 ± 289
3	10000	49 ± 0.8	9328 ± 776

5.4.6. Comparing with other EGOs.

Tuning the intrinsic electrochemical properties of the transducer's material is necessary to improve the performance of the aptasensor in terms of sensitivity. Thus, different EGOs were also used to fabricate the cocaine aptasensor through the physical adsorption method to investigate the influence of their ESA and k^0 values on the sensing performance. The EGOs were obtained by adjusting the exfoliation parameter such as the applied voltage and the distance between the electrodes, [23] and their physicochemical and electrochemical properties are summarized in **Tables S5.1 and S5.2**. Briefly, EGO (R)8V6cm was subjected to a thermal annealing at 800 °C in Ar, it has few oxygenated functional groups and can be considered as few-layer graphene. The EGO 6V6cm has more than eight layers can be considered as graphite oxide. The other EGOs are few-layers graphene oxide but have larger flake sizes All of these modified electrodes were tested under the same 1 µM concentration of cocaine. According to the Δ*i* values associated to each electrode modification step and cocaine detection (**Figure S5.10**), the different EGOs show different sensing performances. For instance, as shown in **Figure S5.10a**, the Δ*i* values of the EGO 8V6cm and 10V6cm only decreased slightly compared to other EGOs because they have higher ESA and k^0. Instead, the EGO (R)8V6cm shows the lowest sensitivity (lowest Δ*i,*) because it has the lowest k^0 compared to the other EGOs. Similarly, the EGO 6V6cm also showed a low Δ*i* because its low ESA and k^0 values. In **Figure S5.10b**, all Δ*i* values dropped significantly with the same tendency after incubation in aptamers, further proving the quick adsorption of aptamers on the EGO materials. However, the Δ*i* value of EGO 10V6cm decreased the minimum after

modification with the BSA solution (**Figure S5.10c**), indicating that there were more aptamers adsorbed on EGO 10V6cm-modified electrode, leaving less surface for BSA adsorption. Finally, the EGO 10V6cm-modified electrode presented the highest Δ*i* value after detection of 1 µM cocaine compared with other EGOs reported, [23] indicating the best sensing performance (**Figure 5.7a**). This result agrees very well with the findings in our previous work. [23] This is illustrated in **Figures 5.7b**,**c** where Δ*i* values after detection of 1 µM cocaine are seen to increase with the respective ESA and k^0 values.

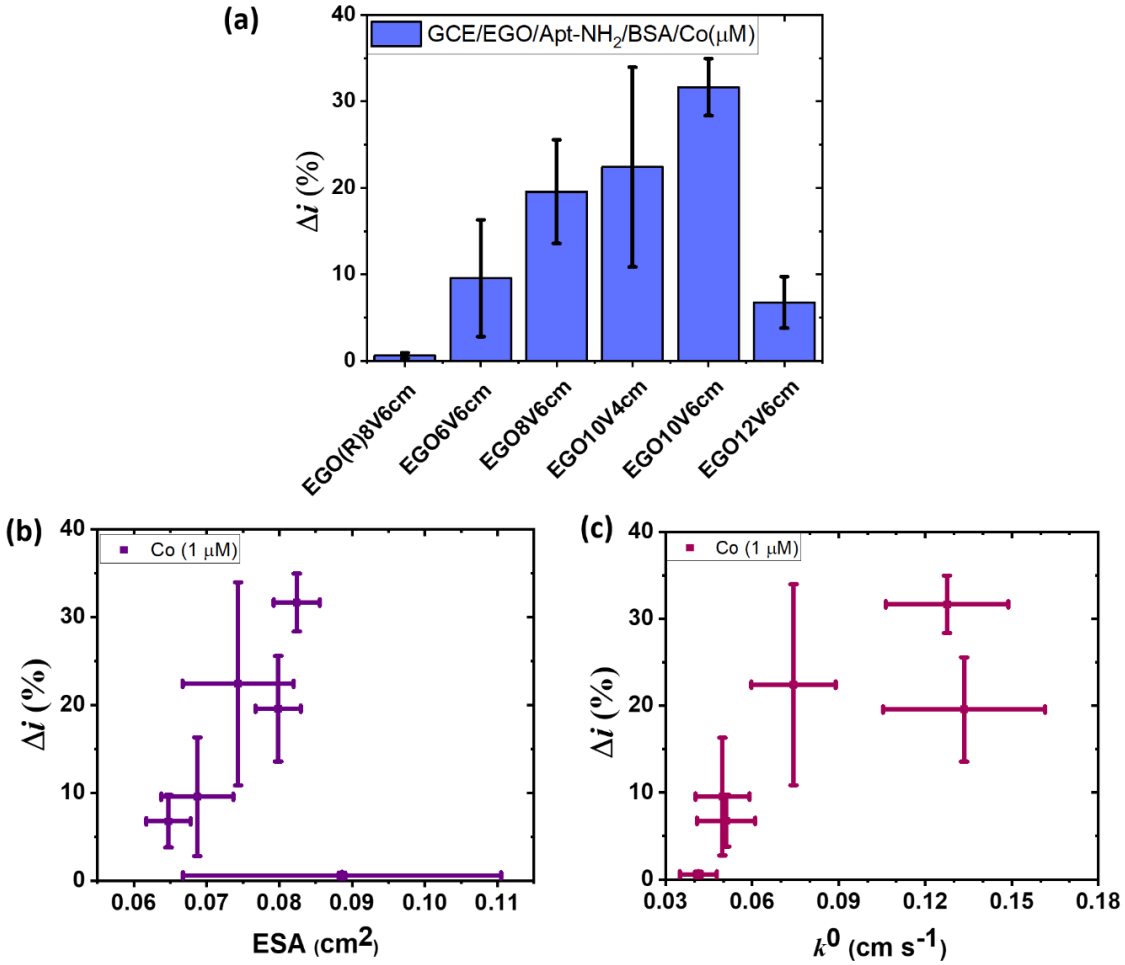

Figure 5.7. Impact of the electrochemical surface area (ESA) and electron transfer rate constant (k^0) of EGO materials on the performance of the sensors fabricated using the aptamer-NH_2 and physical adsorption method. The relative variations in the peak current (Δi) (a) after incubating GCE/EGO/Apt-NH_2/BSA electrodes in cocaine solution (8 µL, 1 µM for 30 minutes). The correlation of Δi with (b) ESA and (c) k^0 values.

5.5. Conclusion

A simple and sensitive electrochemical sensing platform based on EGO 10V6cm and published amine-modified cocaine aptamer was developed by the physical adsorption method. The cocaine

aptamers-NH_2 were adsorbed rapidly on the surface of EGO-modified GCE through physical adsorption, making the fabrication of the apta-sensing platform simple, rapid, and cost-effective, which is critical for industrial scaling. Compared with an unmodified aptamer (OH terminal group), the terminal amine group promotes the adsorption of aptamers on the EGO surface through the electrostatic interaction with the oxygenated functional groups of EGO. The proposed electrochemical cocaine aptasensor fabricated by the physical adsorption method displayed good reproducibility and shelf-life with a detection limit of 50 nM. Further, compared with other EGOs, the EGO 10V6cm leads to a better sensing performance due to its higher ESA and k^0 values, demonstrating how the electrochemical properties of materials play a crucial role. In addition, this simple EGO/aptamer-NH_2 platform, developed for the detection in an aqueous solution, is believed to be applicable to the manufacturing of similar biosensors. Its performance can be further enhanced by using sensing elements with higher affinity and selectivity, other transducer materials such as EGO flakes decorated with Au nanoparticles (for higher sensitivity by increasing electron transfer rate), [8, 272-273] and optimizing the composition of aqueous medium where the assays are performed (to minimize nonspecific interactions for higher selectivity). In the future, it is anticipated that this proposed protocol will inspire more research on electrochemically exfoliated graphene materials-based electrochemical sensors. [196]

5.6. Supporting Information

5.6.1. Materials

Electrochemically exfoliated graphene oxides (EGOs) were synthesized according to our previous work. [23] **Tables S5.1** and **S5.2** summarize the physicochemical and electrochemical properties of the EGOs.

Table S5.1. Summary of the EGOs physiochemical properties. [23]

EGOs[a]	Sheet size (µm)[b]	Number of layers[c] (typical number)	C/O[d]	(I_D/I_G)[e]
(R)8V6cm	>10	3~7	28.2 ± 4.7	0.20 ± 0.03
6V6cm	>10	>8	5.3 ± 0.5	0.51 ± 0.04
8V6cm	>10	<7 (3~4)	6.1 ± 0.6	0.46 ± 0.04
10V4cm	>10	3~7	4.7 ± 0.5	0.83 ± 0.09
10V6cm	>10	3~7	5.2 ± 0.7	0.73 ± 0.06
12V6cm	>10	<7 (3~4)	7.1 ± 0.9	0.86 ± 0.04

[a] (R) refers to an EGO that was thermally reduced in Ar at 800°C. XVYcm indicate the applied voltage (X) and the distance (Y) between the electrodes during the exfoliation of the graphite foil; [b] from scanning

electron microscope; [c] from Transmission electron microscopy; [d] from X-ray photoelectron spectroscopy; [e] from Raman spectroscopy

Table S5.2. The electrochemical surface area (ESA) and standard electron transfer rate (k^0) values of EGOs. [23]

EGOs	ESA (cm^2)	STDV	k^0 (cm s^{-1})	STDV
(R)8V6cm	0.09	0.02	0.0413	0.0064
6V6cm	0.069	0.005	0.0497	0.0094
8V6cm	0.080	0.003	0.1335	0.0281
10V4cm	0.07	0.01	0.0743	0.0146
10V6cm	0.082	0.003	0.1280	0.0212
12V6cm	0.065	0.003	0.0509	0.0101

STDV: Standard deviation

Millipore water (18.2 MΩ cm) was used for rinsing the EGO samples and to prepare all aqueous solutions. Potassium chloride (KCl, min. 99.5%) and magnesium chloride ($MgCl_2$, 99+%) were purchased from Bioshop, potassium ferricyanide ($K_3[Fe(CN)_6]$, 99+%, for analysis) from Acros, potassium hexacyanoferrate ($K_4[Fe(CN)_6]\cdot 3H_2O$, 98.5 – 102.0%) from Alfa Aesar, N,N,N',N'-tetramethyl (succinimido) uronium tetrafluoroborate (TSTU, 97%), 4-dimethylaminopyridine (DMAP, ≥99%), methyl benzoate ($C_6H_5COOCH_3$, 99%), kanamycin sulfate ($C_{18}H_{36}N_4O_{11}\ H_2O_4S$), cocaine ($C_{17}H_{21}NO_4$,1.0 mg/mL in acetonitrile), and anhydro ecgonidine methyl ester ($C_{10}H_{15}NO_2$, 1.0 mg/mL in acetonitrile) from Sigma. Bovine serum albumin (BSA, 20 mg/mL) was purchased from BioLabs. Cocaine aptamers were purchased from AlphaDNA (Montreal, Canada). The cocaine aptamer sequence was 5′- AGACAAGGAAAATCCTTCAATGAAGTGGGTCG-3′, named as Aptamer-OH (Apt-OH). The sequence of the cocaine aptamer modified with an amine group (Aptamer-NH_2, Apt-NH_2) was 5′-C6-NH_2-AGACAAGGAAAATCCTTCAATGAAGTGGGTCG-3′. [259-260, 274] Glassy carbon electrodes for microscopy and surface analysis studies (GCEmicro, 3mm) used for XPS analysis and radioactivity tests were purchased from Gaoss Union ®, from China. For real sample tests, the saliva collection device was purchased from Quantisal®.

For radiolabel analysis, T4 polynucleotide kinase (T4 PNK, 10000 units/mL), T4 polynucleotide kinase buffer 10X (700 mM Tris-HCl, 100 mM $MgCl_2$, 5 mM DTT), DNase 1 (2000 units/mL) and DNase 1 reaction buffer 10X (100 mM Tris-HCl, 25 mM $MgCl_2$, 5 mM $CaCl_2$) were purchased from New England BioLabs. Radioactive ATP (ATP-^{32}P, 20 mCi/mL) was purchased from Perkin Elmer. Foramide (CH_3NO, ≥99%), EDTA ($C_{10}H_{16}N_20_8$, ~99%), bromophenol blue ($C_{19}H_{10}Br_4O_5S$, ~90%),

xylene cyanol ($C_{25}H_{27}N_2NaO_6S_2$, ~80%), sodium chloride (NaCl, ≥99%) and sodium acetate ($C_2H_3O_2Na$, ≥99%) from Sigma were used. The sequence of the cocaine aptamer modified with an amine group was 5'- AGACAAGGAAAATCCTTCAATGAAGTGGGTCG-C6-NH_2-3'and was purchased from AlphaDNA (Montreal, Canada). Screen printed gold electrodes (DRP-220AT) were purchased from Metrohm DropSens (Canada). EGO freestanding films (EGO films) were prepared by vacuum filtration of EGO suspensions to compare with screen printed gold electrodes.

5.6.2. Characterization

5.6.2.1. X-ray photoelectron spectroscopy (XPS) analysis

XPS was performed with a VG Escalab 200i-XL equipped with a hemispherical analyzer (pass energy = 20 eV) and a multi-channel detector, applying a Twin Anode X-Ray Source at 15 kV and 20 mA. The base pressure inside the spectrometer during analysis was less than 7×10^{-10} torr. The binding energy of the C 1s peak at 284.5 eV was used as an internal standard. The core-level spectra were peak-fitted using Lorentzian and Gaussian curves after the Shirley type background subtraction, and Casa XPS software was used. Peak areas were normalized by appropriate atomic sensitivity factors.

5.6.2.2. Radioactivity test

Aptamer radiolabeling. For the radiolabeling of the cocaine aptamer, 15 pmol of aptamer has been incubated with T4 PNK for 1 h at 37 °C (1 µL of aptamer 6 µM (~110 ng), 70 mM Tris-HCl, 10 mM $MgCl_2$, 5 mM DTT, pH 7.6, 5 µCi ATP-^{32}P, T4 Polynucleotide Kinase [10 units], H_2O to 20 µL). The aptamer was then purified on an 8% denaturing polyacrylamide gel electrophoresis (8 M urea). The aptamer was loaded with a 2X loading buffer (95% formamide, 10 mM EDTA, 0.05% bromophenol blue, 0.05% xylene cyanol), and electrophoresis was done for 1 h at 500 V. The gel was then exposed on a phosphor screen for 10 min and visualized with a Typhoon™ The expected bands were then purified. The bands were eluted overnight in elution buffer (0.3 M NaCl). Supernatant was then precipitated with 0.1 volume of sodium acetate 3 M and 2 volumes of ethanol 100% at -80°C for 2 hours. A centrifugation at 21,1 G for 30 min was performed, and the supernatant was discarded. The aptamer was resuspended in 500 µL 70% ethanol, and centrifugated at 21,1 G for 10 min. The supernatant was discarded, and aptamer was resuspended in 100 µL of Milli-Q water.

Radiolabeled aptamer on EGO. 8 µL of EGO suspension was dropcasted on the surface of the Au-SPE (GCEmicro) and allowed to dry. In the latter a smaller volume was used to prevent the

suspension from overflowing from the electrode surface. Then, 8 µL of radiolabeled aptamer (6 µL for GCEmicro) were deposited onto the electrodes and left to incubate at room temperature for 10 min. The same procedure was used with 6 µL deposited onto EGO freestanding films (EGO films). The electrodes and the EGO films were then cleaned with 50 µL of Milli-Q water. Afterwards, the electrodes, the EGO films and the cleaning water were exposed on phosphor screen for 1 hour. Then, 8 µL of 50 µM cocaine (in 0.05 M KCl) and 8 µL of 0.05M KCl were dropped onto the electrodes and EGO films and incubated for 30 min at room temperature (6 µL for GCEmicro). Electrodes and EGO films were cleaned and exposed as described, as well as the liquid recovered from the surfaces. Then aptamers were stripped with DNase 1 (1 µL of DNAse 10× buffer (10 mM Tris-HCl, 2.5 mM $MgCl_2$, 0.5 mM $CaCl_2$, pH 7.6 at 25 °C), DNase 1 [2 units], Milli-Q water to 10 µL) and incubated for an hour at 37 °C. Electrodes and EGO films were cleaned and visualized as described before.

Radioactivity readings were performed with a Typhoon™ FLA 9500 (GE Healthcare Life Sciences), and analysis has been performed with Image Quant TL (Cytiva, United States).

5.6.3. Real sample test

Saliva samples were collected using Quantisal saliva collection devices. As directed by the package instructions, saliva was collected and diluted 1: 4 in Millipore water. The sample was spiked with cocaine at various concentrations (150 nM, 1 µM, and 10 µM) and subjected to detection. The samples were dropped on the GCE/EGO/Apt/BSA electrodes (EGO aptasensor developed with physical adsorption method) and left to incubate for 30 min. Then the electrodes were well-washed with Millipore water and characterized by cyclic voltammograms and square wave voltammograms as described in the experimental section. Three electrodes were tested for concentration of cocaine.

5.6.4. Supplementary Results

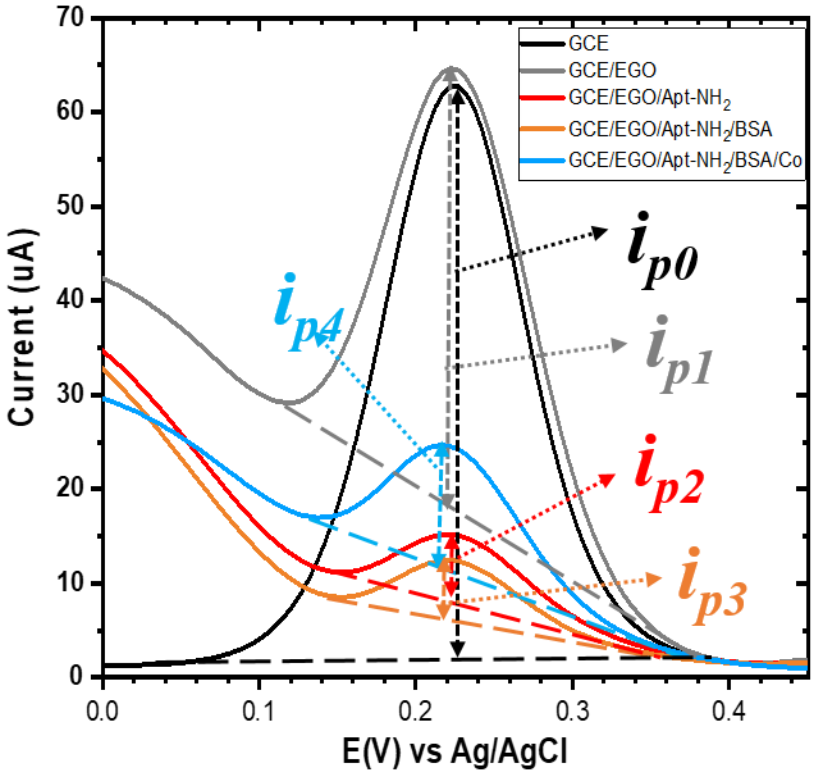

Figure S5.1. Schematic illustration of the calculation of the relative variation of the current (Δ*i*) from the square wave voltammograms recorded in the presence of 1 mM $[Fe(CN)_6]^{3-/4-}$ redox couple in 0.1 M KCl after each modification of the electrodes.

The relative variation of the current (Δ*i*) after each modification step was calculated as follows:

$\Delta \boldsymbol{i} = \frac{\boldsymbol{i_{p(n)} - i_{p(n-1)}}}{\boldsymbol{i_{p(n-1)}}}$, (*n*=1,2,3…),

where $i_p$is the peak current, and the (*n*-1) is the previous step of *n*.

The following **Figure S5.2** to **S5.4** show the results of radioactivity test of labeled cocaine aptamer-NH_2 on EGO modified electrodes (screen printed gold electrode and glassy carbon electrode) and on EGO free standing film after the functionalization, the binding to cocaine and the DNase stripping. This comparative study allows the verification of potential adsorption of the radiolabeled aptamer onto these substrates.

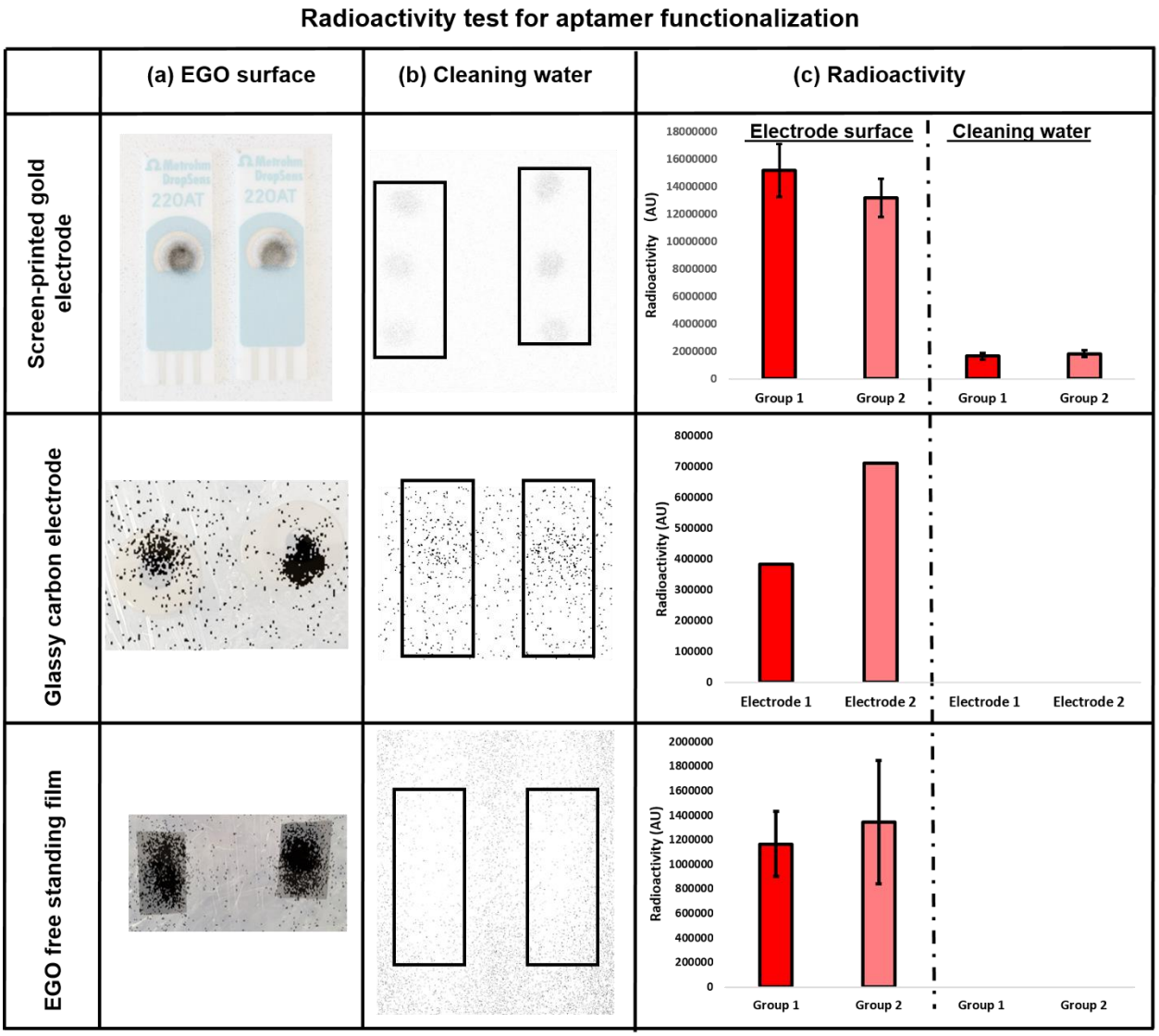

Figure S5.2. Radioactivity test of labeled cocaine aptamer-NH_2 on EGO modified electrodes (screen printed gold electrode and glassy carbon electrode) and on EGO freestanding films after functionalization. (a) Radiolabeled aptamer on EGO surface (overlay of the ^{32}P scan with pictures of electrodes and EGO film). (b) Cleaning water from electrodes and EGO freestanding films showing released radioactivity from the surface. (c) Radioactivity (arbitrary units) from both EGO surface and cleaning water.

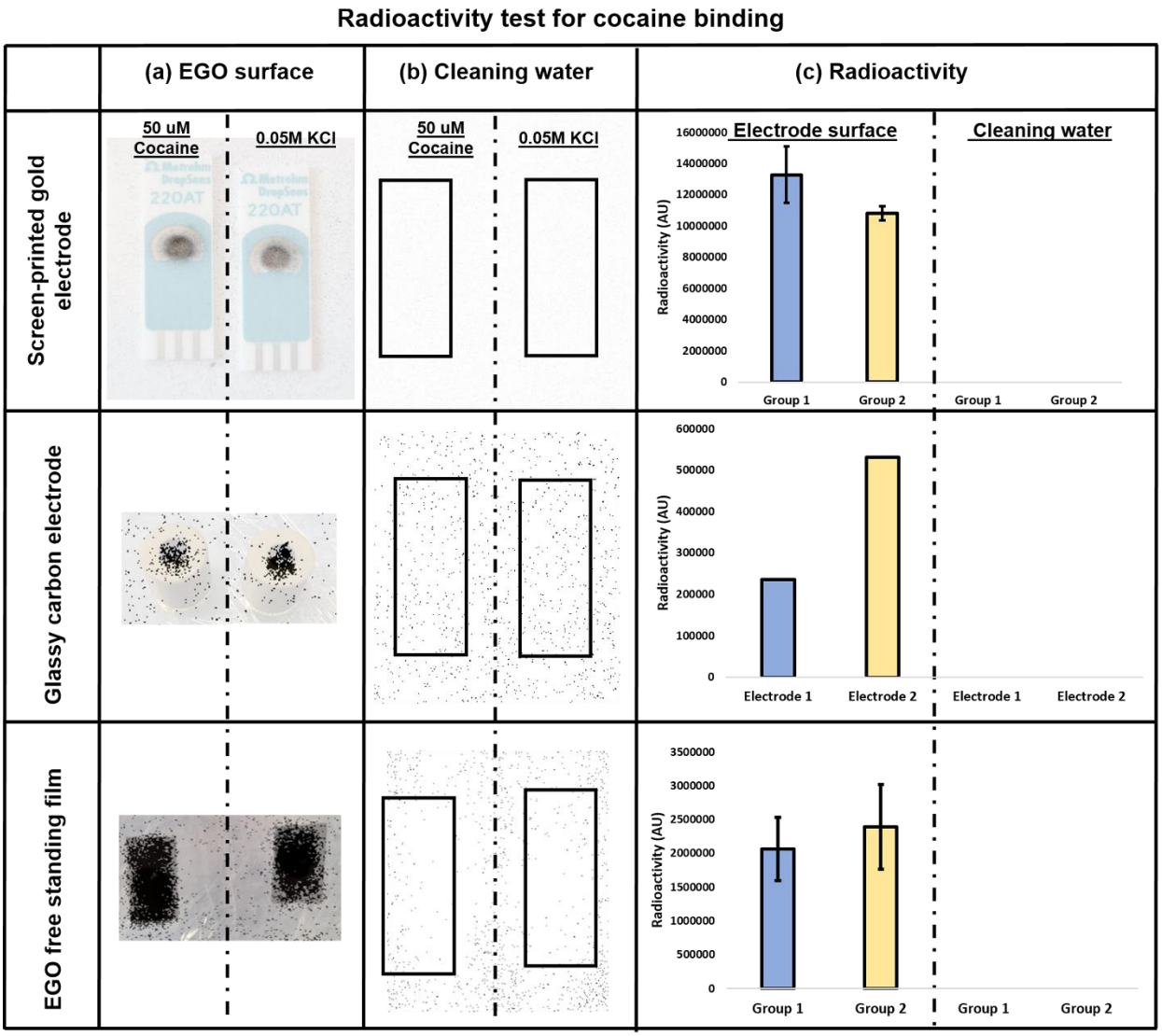

Figure S5.3. Radioactivity test of labeled cocaine aptamer-NH_2 on EGO modified electrodes (screen printed gold electrode and glassy carbon electrode) and on EGO freestanding films after binding to cocaine. (a) Radiolabeled aptamer on EGO modified electrodes and on EGO freestanding films after binding with cocaine (in 0.05 M KCl) and in 0.05 M KCl buffer (overlay of the ^{32}P scan with pictures of electrodes). (b) Cleaning water from electrodes and EGO freestanding films showing released radioactivity from the surface. (c) Radioactivity (arbitrary units) from both EGO surface and cleaning water.

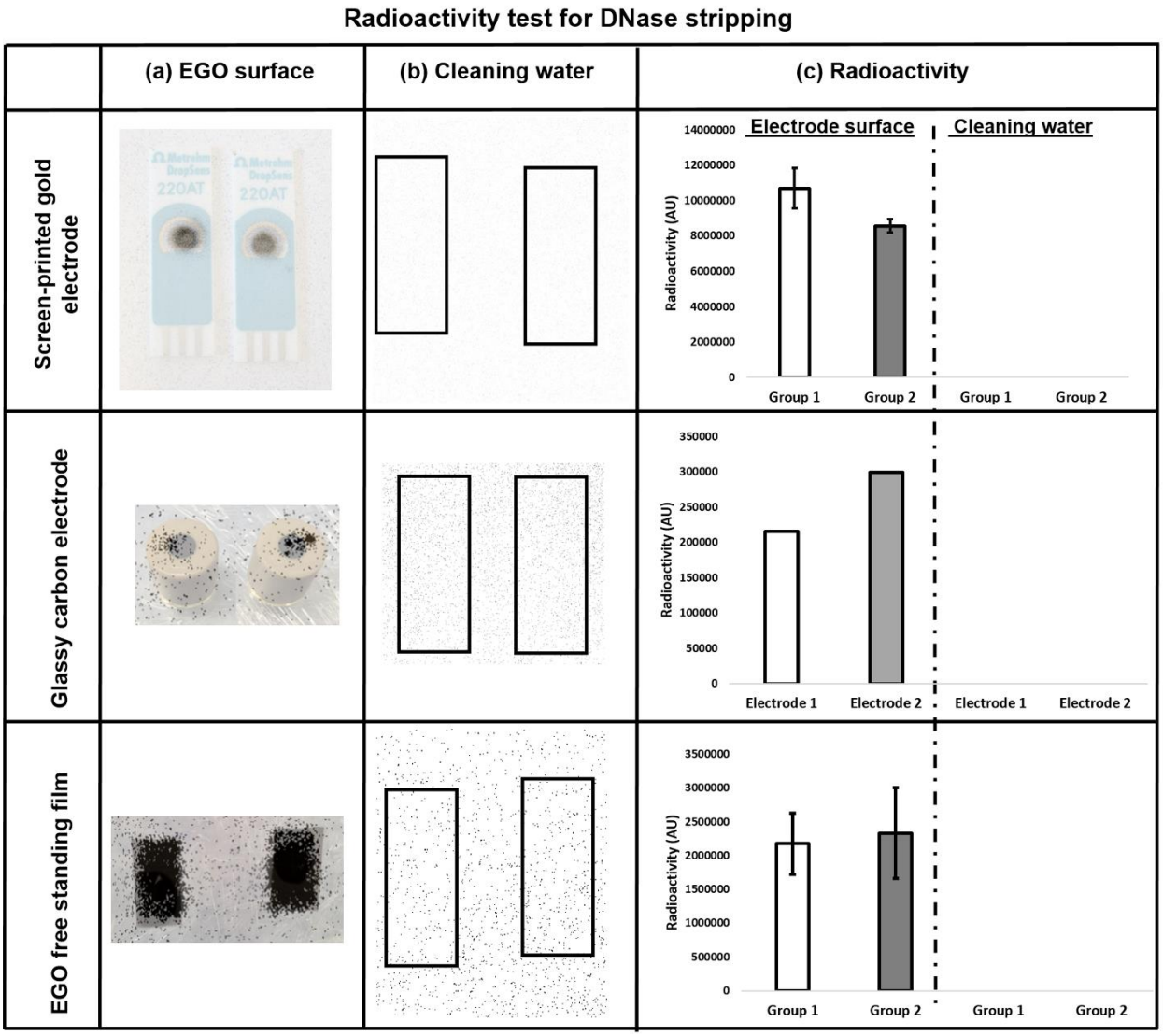

Figure S5.4. Radioactivity test of cocaine aptamer-NH_2 on EGO modified electrodes (screen printed gold electrode and glassy carbon electrode) and on EGO freestanding films after DNase stripping. (a) Radiolabeled aptamer on EGO modified electrodes and on EGO freestanding films after DNase stripping (overlay of the ^{32}P scan with pictures of electrodes). (b) Cleaning water from electrodes and EGO freestanding films showing released radioactivity from the surface. (c) Radioactivity (arbitrary units) from both electrodes and cleaning water.

It should be noted that a smaller volume of aptamer was used on the GCE to prevent the EGO ink from overflowing from the electrode surface. This can partially explain the smaller radioactivity readings compared to the two other substrates. Despite this fact, the conclusions remain the same. Only 20% of the cleaning water volume is used to the radioactivity test. The only case where radioactivity could be detected in cleaning water (and in very small quantity) was for aptamer functionalization on screen printed gold electrode. These results indicate a very strong adsorption for GCE and EGO freestanding films, whereas for screen printed gold electrode, it is still very clear that most aptamers stay on EGO surface.

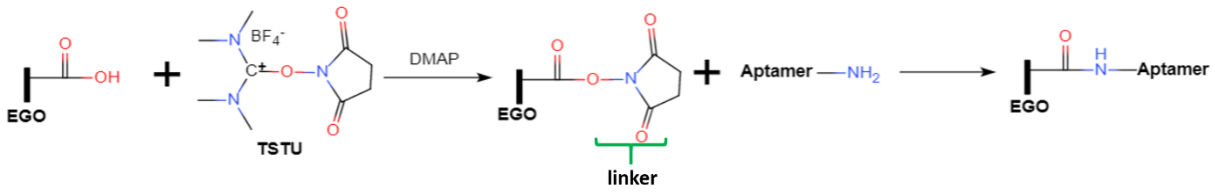

Scheme S5.1. Schematic illustration the reaction mechanism between the COOH groups of EGO and the NH2 groups of the aptamer through N,N,N',N'-tetramethyl (succinimido) uronium tetrafluoroborate (TSTU) and 4-dimethylaminopyridine (DMAP).[206-207]

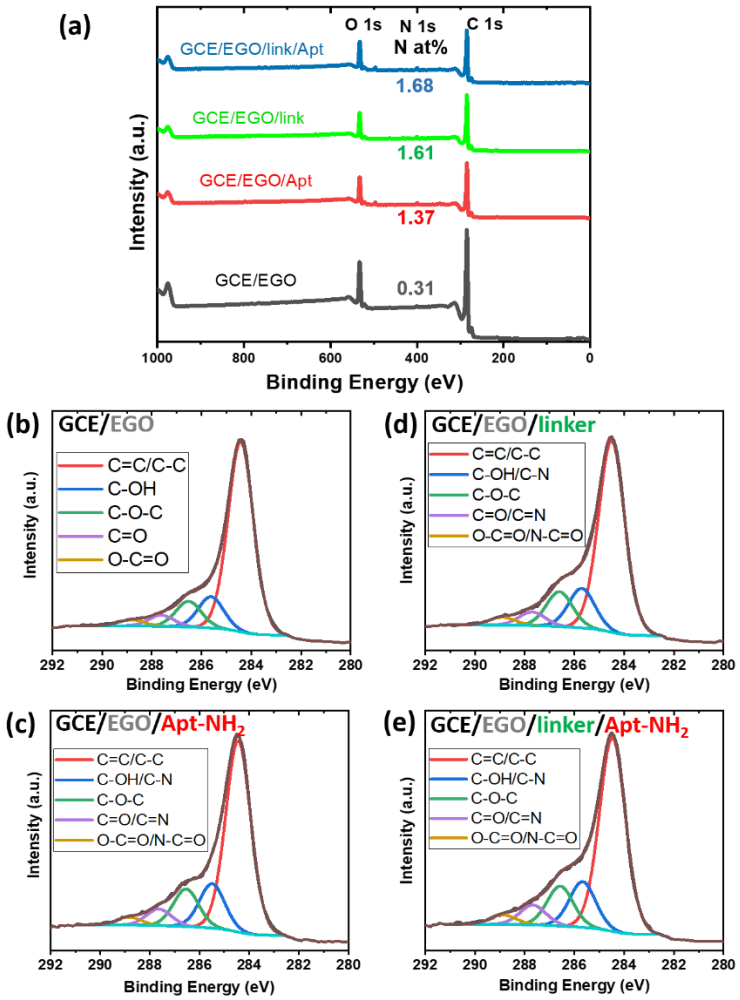

Figure S5.5. (a) XPS survey spectra of the modified electrodes. C 1s XPS spectra of the modified glassy carbon electrodes (GCE) by (b) EGO, (c) EGO/Aptamer through physical adsorption method, (d) EGO/linker and (e) EGO/linker/Aptamer through covalent immobilization method.

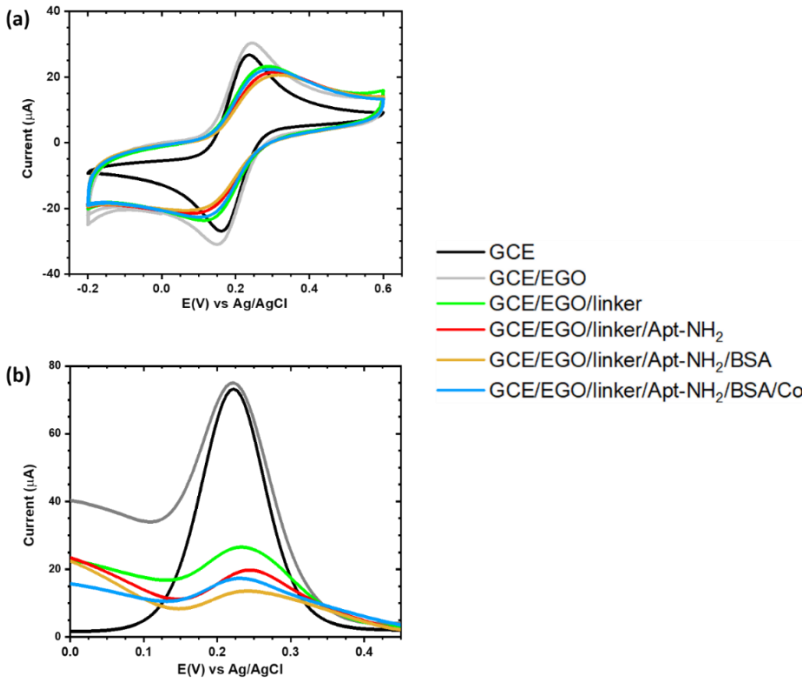

Figure S5.6. (a) Cyclic voltammograms at 0.1 V s^{-1} and (b) Square wave voltammograms at 25 Hz recorded in the presence of 1 mM $[Fe(CN)_6]^{3-/4-}$ redox couple in 0.1 M KCl of the modified electrodes by covalent immobilization method.

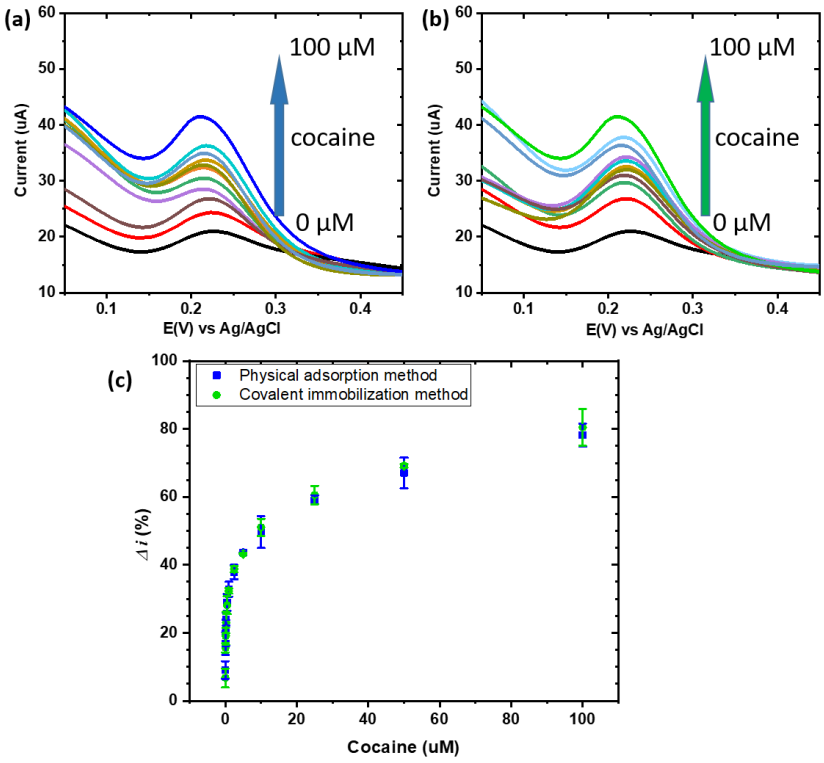

Figure S5.7. Square wave voltammograms at 25 Hz recorded in the presence of 1 mM $[Fe(CN)_6]^{3-/4-}$ redox couple in 0.1 M KCl of the modified electrodes by (a) physical adsorption method and (b) covalent immobilization method under

different concentration of cocaine; (c) the relative variation of the current (Δi) from the square wave voltammograms according to different concentration of cocaine.

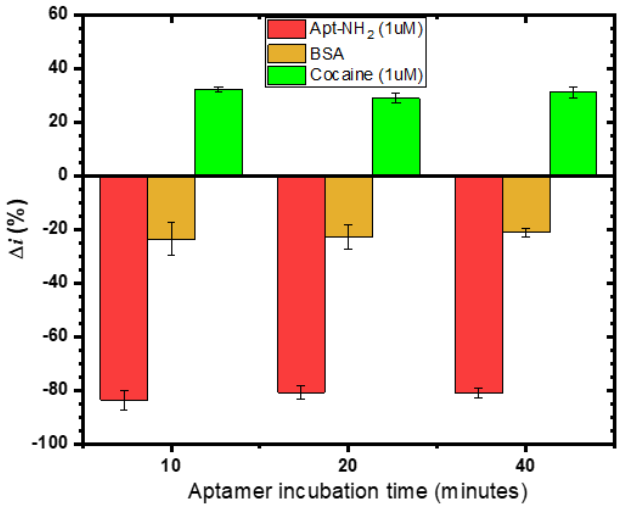

Figure S5.8. Covalent immobilization method and the influence of the aptamer incubation time: relative variations in the peak current (Δ*i*) from the square wave voltammograms recorded in the presence of 1 mM $[Fe(CN)_6]^{3-/4-}$ redox couple in 0.1 M KCl for the GCE/EGO/link electrodes incubated in cocaine aptamer (Apt-NH_2) solution, surface blockage with BSA and binding with cocaine.

Table S5.3. Comparison of performance of the electrochemical cocaine sensor proposed in this work with other methods.

Detection method	Architecture	Electrode preparation time	Cocaine incubation time / min	Buffer or solvent used	Linear range / nM	LOD / nM	Real sample	Refs
SWV	Cocaine aptamer adsorbed on EGO modified GCE	**10+30 min**	**30**	Millipore water (pH 6~6.5)	**50 - 1×10^5**	**50**	Cocaine in human saliva diluted in Millipore water	**This work**
DPV	Covalent attachment of aptamer-functionalized Au nanoparticles (NPs) onto MWCNTs/IL/Chit nanocomposite on GCE	90min+2h	45	0.1 M phosphate buffer saline (PBS, pH 7.4)	**1 – 1.1×10^4**	**0.1**	cocaine in human serum	252
DPV	Covalent immobilization of aptamer-functionalized Ag NPs on the MWCNTs/IL/Chit nanocomposite on GCE	24h+90min+ 12h	45	10 mM PBS, pH 7.4	2 - 2500	0.15	cocaine in human serum	251
DPV	Biotin-modified secondary binding aptamers on the electrochemically reduced GO and Au NPs modified screen-printed carbon electrode	Overnight + 1h	40	10 mM phosphate buffer (PB, pH 7.0)	1 - 500	1	**/**	250
DPV	Single-walled carbon nanotubes and a complementary strand of aptamer modified screen-printed gold electrode	1h+1h+2h+1 h(+1h)	**30**	10 mM PBS, pH 7.4	0.1 -10	0.136	cocaine in rat serum	253
DPV	Covalent immobilization of aptamer decorated with 2,5-dihydroxybenzoic acid on nanopore gold electrode	1h+12h+6h+ 2h	40	0.02 M PB (pH 7.0) in 1 M NaCl	50 – 3.5×10^4	21	**/**	274
CV	Au electrode surface decorated with an aptamer probe−pendant tetrahedral DNA nanostructure	Overnight+o vernight+2h	**30**	10 mM PB in 1 M NaCl (pH 7.4)	**100 - 1×10^6**	33.0	cocaine in 10% and 50% calf serum in buffer	266
DPV and EIS	GCE modified with Pt NPs and using rutin as a redox probe	24h+90min+ 12h	45	0.1 M PB, pH 7.4	1 – 1100	**0.1**	Cocaine in serum samples	267
ACV	Covalent attachment of aptamer decorated with thiol and methylene blue on Au electrode	2h+25min+3 h	**<15**	10 mM PBS buffer (in 1 M NaCl, pH 7)	/	10x1 0^3		259

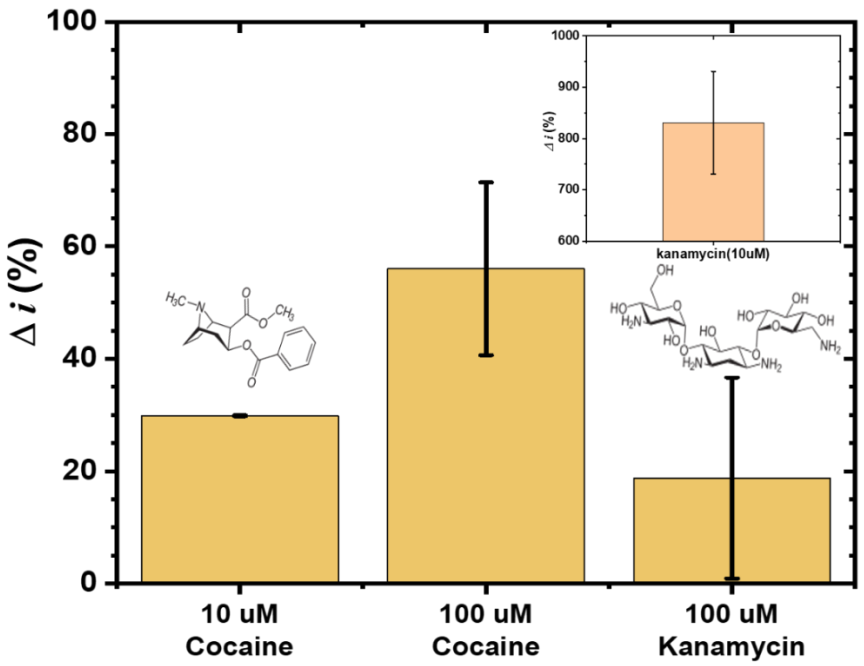

Figure S5.9. Negative control test by kanamycin in 1 mM $MgCl_2$ solution. The figure in the inside shows the negative control test by kanamycin in Millipore water.

As shown in the inset, the Δ*i* of kanamycin is several folds that of cocaine (around 800%). As mentioned in the main text, this could derive from nonspecific interactions between the positively-charged kanamycin and negative charges on the surface (EGO or aptamer). Adding 1 mM $MgCl_2$ solution allows Mg^{2+} cations to neutralize the surface charge and reduce non-specific interactions. As expected, the Δ*i* for the detection by kanamycin (in 1 mM $MgCl_2$) decreased significantly (with a large error bar) as shown in **Figure S5.9**. Although the Δ*i* for cocaine detection in 1 mM $MgCl_2$ decreased slightly compared to cocaine in water (**Figure 5.6**), the signals cannot be ignored.

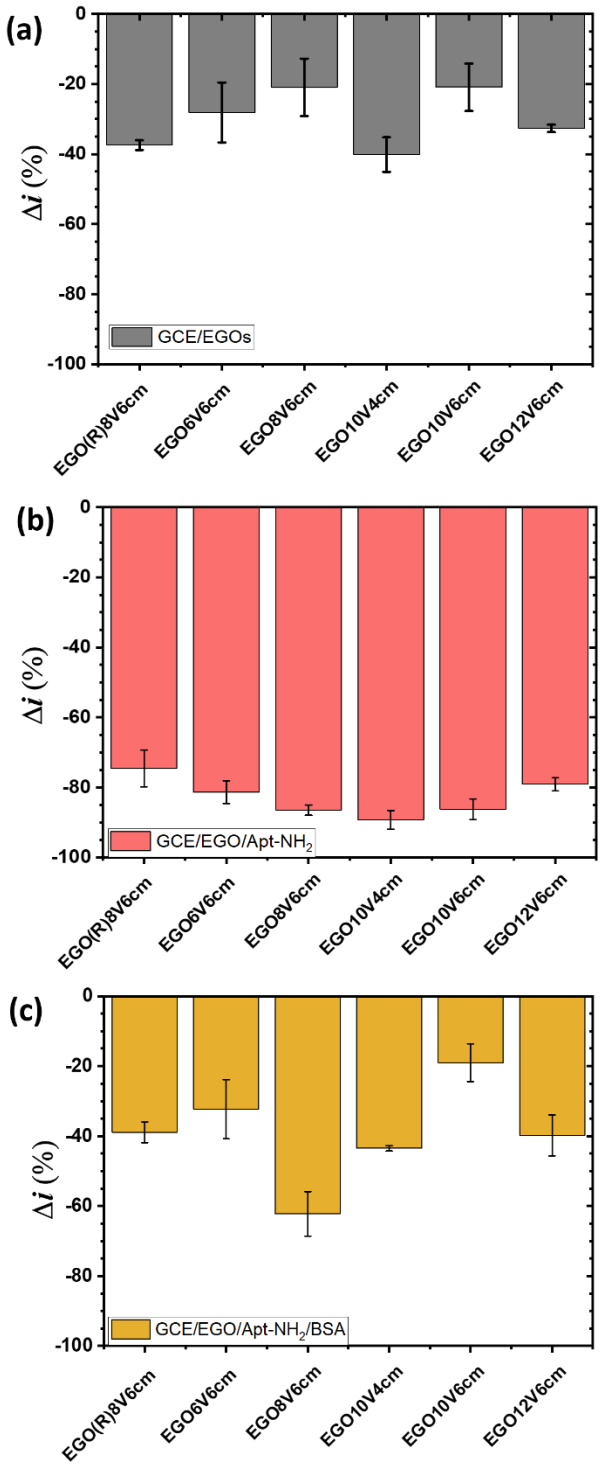

Figure S5.10. The relative variation of the current (Δ*i*) after (a) the modification of GCE with different EGOs (0.4 mg/mL sonicated for 3 hours in water); (b) incubating the GCE/EGO electrodes in cocaine aptamer solution (6 µL, 1 µM for 10 minutes); (c) incubating the GCE/EGO/Apt electrodes in BSA solution (6 µL, 0.1% for 30 minutes).

6. ONE-STEP SYNTHESIS OF AMINOBENZOIC ACID FUNCTIONALIZED GRAPHENE OXIDE BY ELECTROCHEMICAL EXFOLIATION OF GRAPHITE FOR OXYGEN REDUCTION TO HYDROGEN PEROXIDE AND SUPERCAPACITORS

SYNTHÈSE EN UNE ÉTAPE D'OXYDE DE GRAPHÈNE FONCTIONNALISÉ PAR L'ACIDE AMINOBENZOÏQUE PAR EXFOLIATION ÉLECTROCHIMIQUE DE GRAPHITE POUR LA RÉDUCTION DE L'OXYGÈNE EN PEROXYDE D'HYDROGÈNE ET EN SUPERCONDENSATEURS

Authors:

Yuting Lei [1,†], Ludmila dos Santos Madalena [2,†], Benjamin D. Ossonon [1], Fausto Eduardo Bimbi Junior [2], Jiyun Chen [1], Marcos R. V. Lanza [2] and Ana C. Tavares [1,*]

[1] Institut National de la Recherche Scientifique—Énergie Matériaux Télécommunications (INRS-EMT), 1650 Boulevard Lionel-Boulet, Varennes, QC J3X 1P7, Canada

[2] Instituto de Química de São Carlos, Universidade de São Paulo, Av. Trab. São Carlense, 400—Parque Arnold Schimidt, São Carlos 13566-590, SP, Brazil;

Publication : Molecules

Publication Date : 7 November 2022

Volume 27, Pages 7629

DOI : https://doi.org/10.3390/molecules27217629

Contribution of authors:

This research was conceptualized and designed by Yuting Lei, Dr. Benjamin D. Ossonon, and Prof. Ana Tavares. Yuting Lei prepared all samples and conducted most of the physicochemical characterizations. The performance for oxygen reduction to H2O2 was carried out by Fausto Eduardo Bimbi Junior in Prof. Marcos R. V. Lanza's lab at the University of São Paulo. Ludmila dos Santos Madalena conducted the performance for supercapacitors under the training of Dr. Benjamin D. Ossonon. XRD characterizations and analyses were performed by Jiyun Chen, who also helped draw the scheme. Yuting Lei, Jiyun Chen, Dr. Benjamin D. Ossonon, and Prof. Ana

Tavares discussed all the experiment results. The manuscript was written by Yuting Lei under the assistance of Jiyun Chen and Dr. Benjamin D. Ossonon, and it was revised by Prof. Ana Tavares. This work was financially supported by Prof. Marcos R. V. Lanza and Prof. Ana Tavares' grants.

Link between articles:

In previous work, the physical adsorption and covalent immobilization methods were used to functionalize the EGO 10V6cm with the cocaine aptamers. It was found the sensing performances were almost the same for both methods. This was probably because the EGO 10V6cm has too few COOH functional groups. Thus, we wanted EGO materials with more COOH groups to increase the amount of aptamers on their surface. Based on this concept, the one-step synthesis of aminobenzoic acid functionalized EGO materials (EGO-ABA) was investigated. However, the aptamer for the detection of methyl benzoate was found not selective. Nonetheless, EGO-ABA materials were tested for oxygen reduction reactions (ORR) and supercapacitors because of the redox properties of the aminobenzoic acid functional groups. These investigations, results, and discussions were presented in this work.

6.1. Abstract

Graphene-based materials have attracted considerable attention as promising electrocatalysts for the oxygen reduction reaction (ORR) and as electrode materials for supercapacitors. In this work, electrochemical exfoliation of graphite in the presence of 4-aminobenzoic acid (4-ABA) is used as a one-step method to prepare graphene oxide materials (EGO) functionalized with aminobenzoic acid (EGO-ABA). The EGO and EGO-ABAs materials were characterized by FT-IR spectroscopy, X-ray photoelectron spectroscopy, Raman spectroscopy, X-ray diffraction and scanning electron microscopy. It was found that the EGO-ABA materials have smaller flake size and higher density of oxygenated functional groups compared to bare EGO. The electrochemical studies showed that the EGO-ABA catalysts have higher activity for the ORR to H_2O_2 in alkaline medium compared to EGO due to their higher density of oxygenated functional groups. However, bare EGO has a higher selectivity for the 2-electron process (81%) compared to the EGO-ABA (between 64 and 72%) which was related to a lower content of carbonyl groups. The specific capacitance of the EGO-ABA materials was higher than that of EGO, with an increase by a factor of 3 for the materials prepared from exfoliation in 5 mM 4-ABA/0.1 M H_2SO_4. This electrode material also showed a remarkable cycling capability with a loss of only 19.4% after 5000 cycles at 50 mVs^{-1}.

6.2. Introduction

Graphene-based materials have been extensively investigated because of their tunable chemistry (e.g., surface functional groups and heteroatoms doping), high surface area and good electrical conductivity. [1-2] Graphene oxide (GO) materials are abundant in surface functional groups such as hydroxyl, epoxy, carbonyl and carboxyl, and can be easily functionalized with other molecules or nanoparticles to form new compounds and composites with improved properties. [8, 12, 214, 275] For these reasons GO and its composites have been used in a broad range of applications, [9-11] including (bio)sensors, [8, 12] electrogeneration of hydrogen peroxide [13-14] and supercapacitors [1].

Hydrogen peroxide (H_2O_2) is used in wastewater treatment, disinfection and pulp- and paper bleaching. [13-14, 276] The electrochemical synthesis of H_2O_2 via the oxygen reduction reaction (ORR) is considered a cleaner and more sustainable process compared to the conventional anthraquinone one. [13, 277] In alkaline medium, the reduction of O_2 to H_2O_2 occurs according to Equation (6.1). Carbon materials, such as certain types of carbon blacks, [278] oxidized carbon black, [279-280] and oxidized carbon nanotubes, [281] reduced graphene oxide (rGO) [16, 19] are active and selective for ORR to H_2O_2 in alkaline electrolytes, and their activity and selectivity have been correlated to the amount of oxygen functional groups. [16, 280-282] In addition, the carbon atoms adjacent to COOH [16, 19] and C-O-C [17, 19] were identified as the active sites with high selectivity for the 2-electron process, whereas carbons sites next to C=O were found bind too strongly to the peroxide and to promote its reduction to OH^- [280] (Equation (6.2)).

$$O_2 + H_2O + 2\,e^- \rightarrow HO_2^- + OH^- \qquad E^0 = -0.065\ V\ (vs.\ SHE) \qquad (6.1)$$

$$HO_2^- + H_2O + 2\,e^- \rightarrow 3\,OH^- \qquad E^0 = +0.867\ V\ (vs.\ SHE) \qquad (6.2)$$

Supercapacitors (SC) are charge storage systems characterized by high-power density, rapid charge–discharge, are environmentally friendly because of low CO_2 emissions and have longer cycle life than batteries. [1, 160, 283] They can be used as complementary devices to conventional batteries in applications that require peak power pulses, [160, 284] or to power stretchable and wearable electronic devices. [170] Pseudocapacitors, a specific type of SCs, are based on charge storage involving fast surface redox reactions at the electrode/electrolyte interface, [160, 169-170] and GO materials are of potential interest as electrode materials for this technology. [49] The presence of functional oxygenated groups on the GO's surface impedes the restacking of the layers and the agglomeration of the flakes, an important drawback associated with the use of graphene sheets. [31] These functional groups also improve the wettability of the electrode by the electrolyte

and can participate in reversible redox processes thus increasing the pseudocapacitance. [1, 186] However, the oxygenated functional group lowers the electrical conductivity of the GO materials so their content should be optimized. [1]

Generally, GO materials are prepared using chemical methods such as the modified Hummers method, [15] followed by a thermal treatment, [16-17] by electrochemical reduction [18] or by hydrothermal treatment [19] to partially remove the functional groups and to obtain reduced graphene oxide (rGO). Electrochemical exfoliation of graphite is an environmentally friendly and low-cost method that offers the possibility of synthesizing GO materials in few hours. [20-23] Materials, usually referred as electrochemical exfoliated graphene oxide (EGO), with different properties (amounts and types of functional groups, density of defects, number of layers, flake sizes) can be easily synthesized by varying the experimental conditions during the electrochemical exfoliation, such as applied voltage and electrolyte. [23] Compared to the chemical methods (e.g., Hummers' method: C/O $\approx$ 2), [15] the EGO materials obtained this way have a lower density of oxygenated functional groups (C/O > 4) [23] which could be of advantage for electrochemical applications. [16, 28] In addition, the method also allows the preparation of EGO-based composites [24-25] or the surface modification of EGO with other molecules in a one-step process. [26-27]

In this work, electrochemical exfoliation of graphite in 0.1 M sulfuric acid containing 4-aminobenzoic acid (4-ABA) was conducted aiming at obtaining a series of aminobenzoic acid functionalized EGO materials (EGO-ABA). Modification (electrografting) of carbon surfaces by amine oxidation is a known method, [275, 285] and 4-ABA functionalized GO materials prepared by 2 steps methods were used in sensing and membrane applications. [286-288] However, little is known of its use during the electrochemical exfoliation of graphite to obtain functional graphene oxides. Considering the simplicity of the method and the large possible combinations of electrolytes and molecular precursors, graphene-type materials with diversified structures and compositions can be obtained and their properties should be investigated. During this one-step process, graphite is electrochemically oxidized and exfoliated to form EGO sheets, while the amine groups of 4-ABA are oxidized to radicals, followed by the formation of covalent bonds between the sp^2 carbons (on the EGO basal plan) and the amine-derived radicals (**Scheme 6.1**).[275, 285, 289] As will be shown, the amount of 4-ABA in the electrolyte alters significantly the exfoliation process, the composition and flake size of the EGO-ABA materials. Their electrochemical behavior and the role of the functional groups towards the ORR and the supercapacitors are investigated. The materials obtained from exfoliation in 4-ABA/H_2SO_4 solutions with [4-ABA] = 5 and 10 mM have the highest

specific capacitance and the best activity for ORR, respectively. However, the selectivity of EGO for the 2-electron process decreases after functionalization with the aminobenzoic acid.

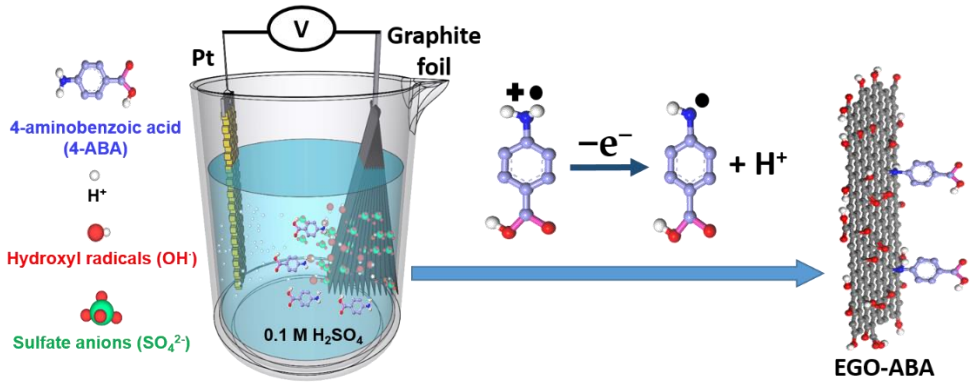

Scheme 6.1. One-step synthesis of electrochemically exfoliated and aminobenzoic acid functionalized graphene oxide (EGO-ABA). The exfoliation of graphite is carried out in 0.1 M H_2SO_4 with the presence of 4-aminobenzoic acid.

6.3. Results

6.3.1. Electrochemical Exfoliation of Graphite in the Presence of 4-Aminobenzoic Acid

In this work the electrochemical exfoliation of graphite was conducted with a two-electrode system where the graphite foil was used as the anode. The electrochemical cell was filled with 0.1 M H_2SO_4 electrolyte, and the concentration of 4-ABA was varied between 0 and 40 mM. When a potential difference is applied between the electrodes, water is reduced at the cathode generating H_2 and hydroxyl radicals are formed at the anode. These radicals attack the graphite electrode, facilitate the intercalation of ions from electrolyte within the graphitic layers, and the gases released (SO_2, CO_2) during the exfoliation assist the formation of EGO and EGO-ABA flakes. [20-21, 289]

However, the presence of 4-aminobenzoic acid (4-ABA) has a profound impact on the exfoliation process (rate and duration), including changes in color of the electrolyte. As the concentration of 4-ABA in the electrolyte increases, the lower the value of the initial current, the faster the electrolyte turns purple around graphite electrode until it finally became brown, and the longer the exfoliation time (**Table 6.1**). The reduction in the initial current value results from a higher electrolyte resistance due to the addition of 4-ABA. This translates in a lower concentration of hydroxyl radicals and in a slower intercalation of the sulfate anion between the graphite layers.

Moreover, as shown in **Scheme 6.2**, the oxidation of 4-ABA (Reaction 1) competes with the oxidation of graphite and may also slowdown the exfoliation process. While the electrolyte coloration proves that the 4-ABA is being oxidized, it also indicates that the formation of an azo compound is taking place during the exfoliation and is competing with the functionalization of 4-ABA on the basal plan of EGO (Reaction 2 and 3). [285, 290]

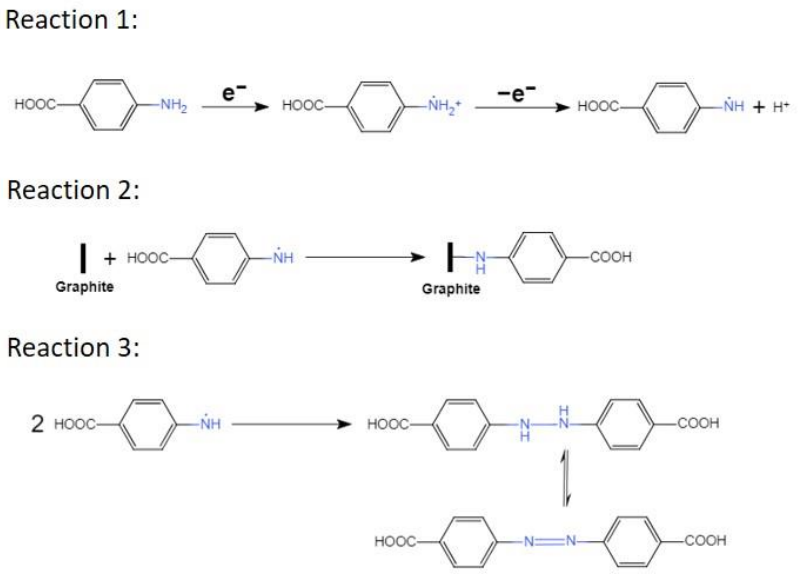

Scheme 6.2. The chemical reactions describing the grafting of aminobenzoic acid on the basal plane of the graphitic layers.

Table 6.1. Experimental observations during the synthesis of the EGO and EGO-ABA materials.

Samples	[4-ABA] (mM)	I_{ini} (A)	t_{exf} (min)	Observation
EGO	0	1.67	60	Electrolyte colorless, graphite foil completely exfoliated
EGO-ABA-5	5	1.20	180	The electrolyte first turns purple around the graphite foil and then turns all brown; graphite foil completely exfoliated
EGO-ABA-10	10	1.14	180	The electrolyte first turns purple around the graphite foil and then turns all brown; graphite foil completely exfoliated
EGO-ABA-20	20	1.06	210	The electrolyte first turns purple around the graphite foil and then turns all brown; graphite foil almost completely exfoliated
EGO-ABA-40	40	0.90	210	The electrolyte first turns purple around the graphite foil and then all brown; graphite foil was not completely exfoliated

4-ABA: 4-aminobenzoic acid; I_{ini}: initial current; t_{exf}: exfoliation time.

Figure 6.1 shows the Fourier Transform Infrared (FT-IR) spectra of the EGO, EGO-ABA-5 and EGO-ABA-20. The spectrum of EGO displays the bands associated with C-O-C (1284 cm^{-1}), C-OH (1370 cm^{-1}), C=O (1680 cm^{-1}) stretching vibration and a broadband coming from OH stretching vibration around 3000 cm^{-1}. [26, 287] The peaks corresponding to C-H aromatic bending modes (770 cm^{-1}) and N-H deformation vibration (secondary amine, at 700 cm^{-1}) appear in the spectra of EGO-ABA samples and their intensity increases with the 4-ABA concentration. [291-292] The same trend is found for the C=O band. Additionally, for EGO-ABA-20 and 40 (Supplementary **Figure S6.1a**), the peaks corresponding to C-N stretching vibration (around 1410 cm^{-1}) and to azo compounds N=N stretching vibration (1516 cm^{-1}) are observed. [293] Finally, the peaks corresponding to asymmetric and symmetric NH_2 stretching vibrations (primary amine, around 3400 cm^{-1}, see FTIR spectrum of 4-ABA in Supplementary **Figure S6.1b** are absent from the spectra of the EGO-ABAs materials. [287, 291] FT-IR analysis confirms that the EGO was functionalized with 4-ABA, and that azo compounds were formed when the concentration of 4-ABA was above 20 mM.

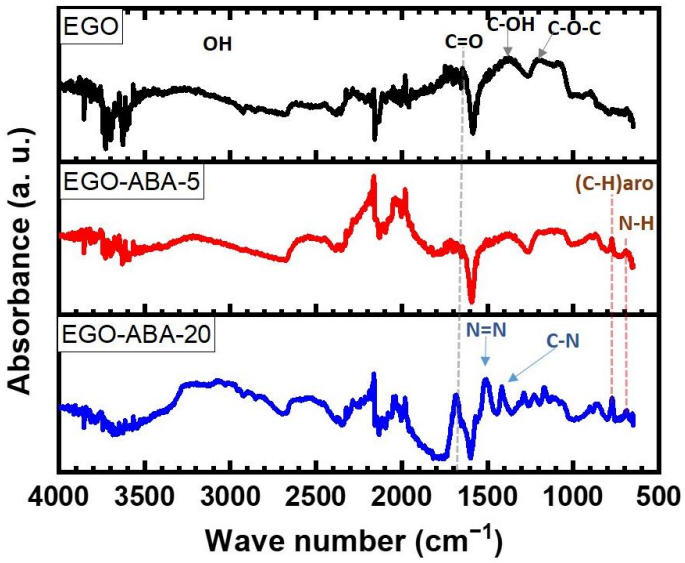

Figure 6.1. FT-IR spectra of EGO, EGO-ABA 5 and 20 materials.

To get insights on the functionalization of EGO by 4-ABA, XPS was used to analyze the surface composition of the materials. The XPS survey spectra (**Figure 6.2a**) show the expected C 1s, N 1s and O 1s peaks at 285, 400 and 532 eV, respectively; being the N 1s peak more intense for EGO-ABA-20 and EGO-ABA-40. As shown in Supplementary **Figure S6.2a**, the C 1s spectrum was deconvoluted into five peaks identified as graphitic carbon: C-C and C=C (284.5 eV), C-OH

(285.8 eV), C-O or C-N (286.8 eV), C=O (288 eV), and O-C=O (289 eV). [57, 294] Generally, the hydroxyl (C-OH) are on the basal plan and at the edges, while, the epoxy groups (C-O-C) are on the basal plan, the carbonyl (C=O) and carboxyl (O-C=O) groups are at the edges sites. [3] However, it should be noted that the grafting of 4-ABA which contains carboxyl (O-C=O) groups occurs on the basal plan of EGO. [26, 285] The N 1s spectrum (Supplementary **Figure S6.2b**) was fitted into 3 peaks: C–N (399.8 eV), N–H (401.7 eV) and =N- (398.6 eV). [294-295] The presence of =N- groups confirms that the 4-ABA underwent a side reaction leading to the formation of diazocompounds. The various functional groups and related carbon and nitrogen species were quantified, and the atomic percentages (at%) are presented in **Figure 6.2b–e**. As expected, these at% ratios increase with the increasing concentration of 4-ABA in the electrolyte, pointing for a successful functionalization of the EGO surface with 4-ABA, but reached a plateau for [4-ABA] ≥ 20 mM. However, all plots—except the one for C-OH—have an inflexion point at 10 mM of 4-ABA. Looking at **Figure 6.2d and e**, it can be concluded that most of the N species are in the form of N-C bonds with small amounts from N-H and =N- bonds. In addition, the at% ratios of other C and N-species decrease from 5 to 10 mM 4-ABA, being the C-OH/C-N species the only exception. These trends suggest that the functionalization of EGO by oxidative grafting of 4-ABA dominates up to 10 mM, after which the functionalization of EGO through physical adsorption of 4-ABA and the diazo compounds dominates. Hence, 5 to 10 mM of 4-ABA seem to be the appropriate concentration to conduct simultaneously the graphite exfoliation and 4-ABA grafting on the EGO surface, while too much 4-ABA increases the occurrence of side reactions and slows the exfoliation process.

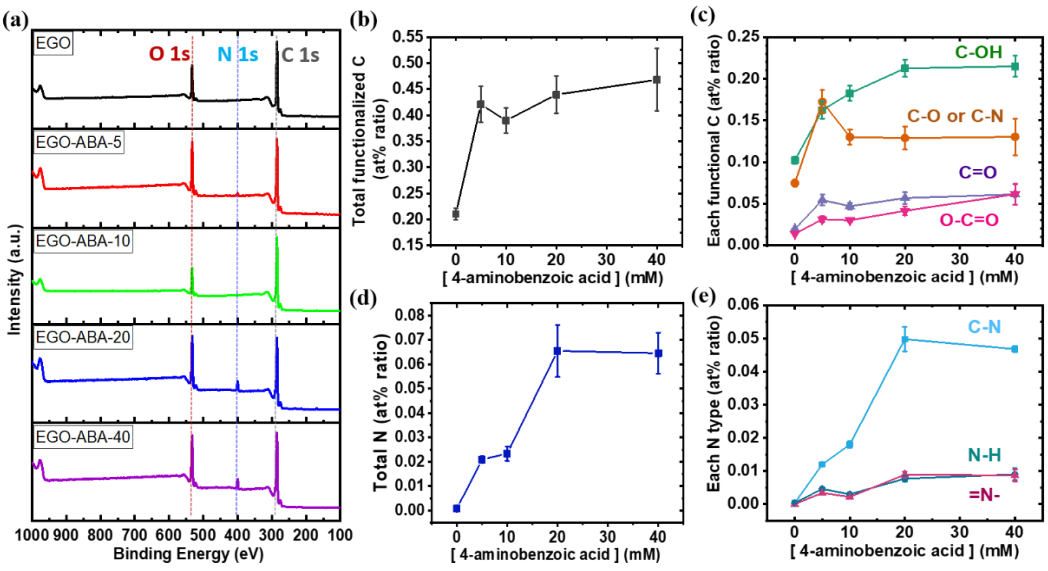

Figure 6.2. (a) XPS survey spectra; atomic percentage (at% ratio) of (b) total functionalized carbon, (c) each functional group, (d) total nitrogen and (e) each nitrogen type.

The bulk structure of EGO and EGO-ABA materials was characterized by XRD. As expected, the XRD patterns (**Figure 6.3a**) show the typical features characteristic of graphene materials with a high intensity diffraction peak at 26.5° attributed to the (002) plane of graphite. [23, 289] The position of the diffraction peak does not vary significantly with the extent of functionalization, and it corresponds to an average lattice spacing of 0.3587 nm. The lattice spacing value and the absence of the graphene oxide's diffraction peak (usually at 10°) [222] suggest that the EGO materials have a low degree of oxidation and that the 4-ABA is on the external surface of the EGO flakes. [289]

Raman spectroscopy was used to characterize the structural defects of the EGO and EGO-ABA materials in the form of free-standing films. For each sample, five Raman spectra were recorded, their average I_D/I_G ratios and representative spectra show in **Figure 6.3b**. The strong G band around 1600 cm^{-1} corresponds to the sp^2 carbon network. [226] The D band at about 1350 cm^{-1} is related to defects such as edge defects, vacancies, etc. [227] The 2D band which is related to the number of layers of graphene materials shifts from 2687 cm^{-1} to 2711 cm^{-1} (Supplementary **Table S6.1**) suggesting these samples have few layers (≤6 layers). [228] Low-intensity D + G (≈2950 cm^{-1}) and 2G (≈3248 cm^{-1}) bands were found proving that these graphene sheets are slightly oxidized. [231] Finally, the ratio between the intensity of the D and G bands (I_D/I_G) was calculated, being 0.52 ± 0.02 for EGO and varying between 0.68 ± 0.01 for EGO-ABA-5 and 0.55 ± 0.08 for EGO-ABA-40. Based on these results, it can be concluded that EGO-ABA materials have more defects than EGO, and that EGO-ABA-5 seems to have the highest number of defects. These results are consistent with the other experimental findings indicating that the oxidative grafting of 4-ABA is favored at low concentration of the amine and that the presence of 4-ABA in the electrolyte hinders the oxidation and exfoliation of graphite (**Table 6.1**).

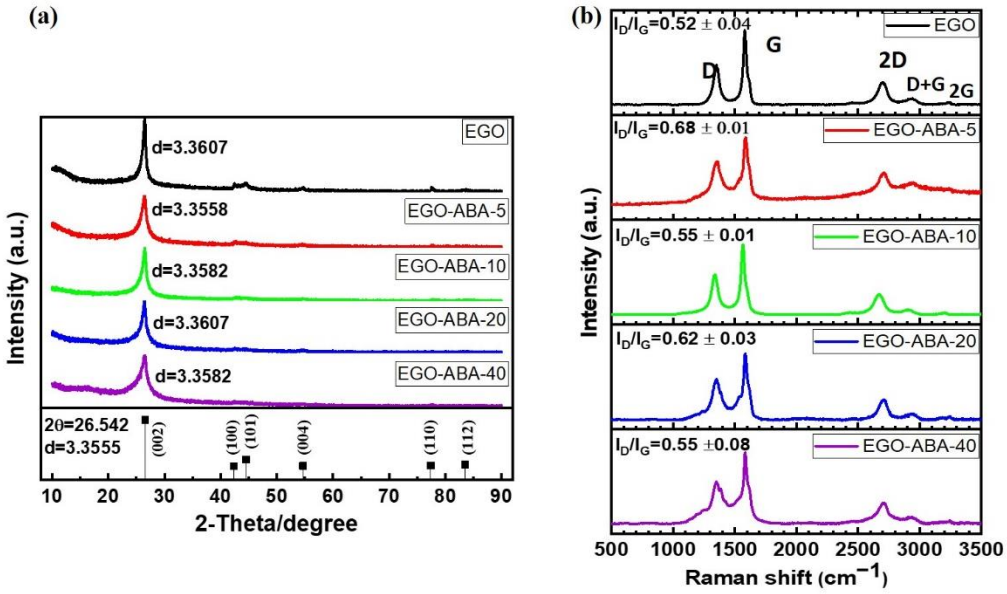

Figure 6.3. (a) The powder XRD patterns of the EGO and EGO-ABA materials. The position of the diffraction peaks of graphene (PDF 65-6212) is included in the lower panels for reference, respectively. (b) Raman spectra of the EGO and EGO-ABA materials.

All samples exhibited the typical morphology of graphene materials, [26] characterized by curled and overlapped flakes, Supplementary **Figure S6.3**. However, the sheet size of EGO is larger than that of EGO-ABA. This may be explained by the slow kinetics of exfoliation in the presence of 4-ABA, where the slow intercalation of the sulfate anions between the graphite sheets combined with the evolution of SO_2, CO_2 gases during the exfoliation [20] lead to the formation of the EGO-ABA with smaller flakes. [23]

6.3.2. Electrochemical Characterization of EGO and EGO-ABA Materials and Their Performance for the and Oxygen Reduction to Hydrogen Peroxide in 0.1 M KOH

Cyclic voltammetry (CV) in 0.1 M KOH was employed to evaluate the electrochemical behavior of EGO and EGO-ABA thin layers deposited on the surface of a glassy carbon electrode (GCE). As shown in **Figure 6.4a** and in Supplementary **Figure S6.4a**, the CV of EGO/GCE in N_2-saturated 0.1 M KOH has only one broad cathodic peak (~ −0.30 V) and one broad anodic peak (~ −0.50 V) corresponding to reversible redox reactions of oxygen functional groups; while the CVs of EGO-ABAs/GCE have an additional narrow and well defined pair of anodic and cathodic peaks (~ −0.90 V and −0.85 V, respectively) corresponding to oxidation/reduction of secondary

amine groups (-NH-). [296] This was confirmed by recording CVs of the GCE in N_2-saturated 0.1 M KOH with different concentrations of 4-ABA. As shown in Supplementary **Figure S6.4b**, no redox peaks were found indicating that 4-ABA is not electroactive in these conditions. The total voltammetric charge (Q_{total}) was plotted as a function of [4-ABA] as shown in **Figure 6.4b**. It can be appreciated that the EGO-ABA-5 based electrode has the highest Q_{total} indicating that this material has the largest electrochemical surface area. A similar trend was found for the Faradic charge ($Q_{Faradic}$) as shown in Supplementary **Figure S6.5**.

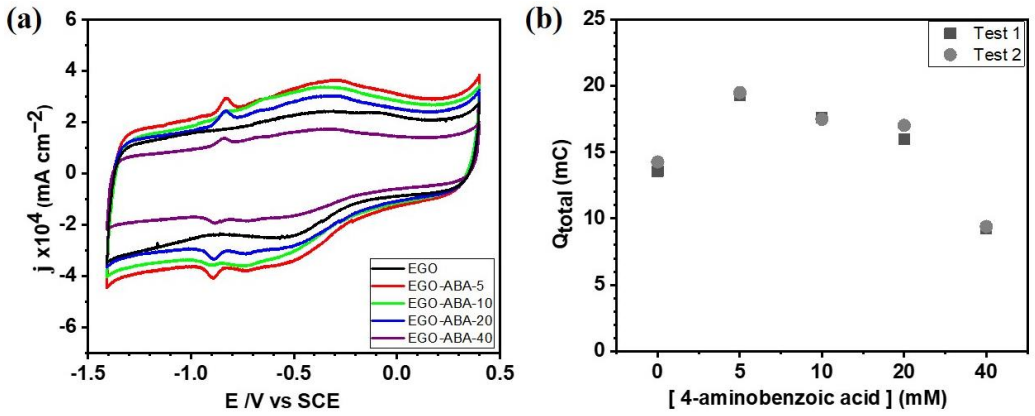

Figure 6.4. (a) Cyclic voltammetry of the EGO and EGO-ABAs modified electrodes in N_2-saturated 0.1 M KOH solution after 20 cycles, scan rate 50 mV s^{-1}. (b) The total charge (Q_{total}) calculated from the voltammograms presented in Supplementary Figure S6.4a.

To evaluate in detail, the electrocatalytic activity and selectivity of EGO and EGO-ABAs for ORR, a set of the rotating ring-disc electrode (RRDE) polarization curves were recorded in O_2 and N_2 saturated 0.1 M KOH. The background subtracted disk and ring currents are shown in the bottom and top panels, respectively, of **Figure 6.5a**. The disk currents consist of two reduction waves, the first one having a limiting current plateau between −0.50 ~ −0.85 V and the second one starting at more negative potentials (around −1.00 V). These linear sweep voltammograms (LSVs) are characteristic of carbon materials [297] and indicate that ORR is proceeding through the 2-electron process with the formation of hydroperoxide anion (Equation (6.1)) followed by a second 2-electron process leading to the formation of the hydroxyl anion (Equation (6.2)).

The onset potential, here defined as the potential necessary to reach current of −0.1 mA, is more positive for EGO-ABA compared to EGO indicating a higher ORR activity after functionalization, **Figure 6.5a** (insert). More specifically, the EGO-ABA-10 has the most positive onset potential. Moreover, the current intensity also increases from EGO to EGO-ABA-10, decreasing afterwards, confirming the highest ORR activity for this catalyst. The trend found for the activity seems to

follow the one found for $Q_{Faradic}$, which agrees with previous reports in the literature that have correlated the ORR activity to H_2O_2 of carbon materials with the content of oxygenated functional groups. [16, 280-282] The higher activity of EGO-ABA is clearly related to a higher amount of COOH, C=O and C-O-C functional groups (and density if the smaller size of the flakes is taken into consideration) compared to EGO (see **Figure 6.2**).

The selectivity of the EGO and EGO-ABA catalysts toward the electrogeneration of H_2O_2 was evaluated through the analysis of the disk and ring currents, and Equations (6.3) and (6.4) were used to estimate the number of exchanged electrons (*n*) during ORR and the peroxide species (HO_2^-) yield, respectively:

$$n_{e^-} = 4 \cdot \frac{i_d}{i_d + \frac{i_a}{N}} \qquad (6.3)$$

$$H_2O_2\ (\%) = \frac{2i_a/N}{i_d + i_a/N} \cdot 100\% \qquad (6.4)$$

where i_d and i_a, are the disc and ring current, respectively, and *N* is the collection efficiency (*N* = 0.37).

The n value is close to 2.4 for EGO and it increases up to 2.7 for EGO-ABA, **Figure 6.5b**. This indicates that the ORR proceeds predominately via $2e^-$ pathway with the production of HO_2^- on both EGO and EGO-ABA. However, and as shown in **Figure 5.6c,** the selectivity for H_2O_2 decreases significantly after the surface modification of the EGO with 4-ABA, according to the following trend: EGO (81.6%) > EGO-ABA-10 (71.2%) > EGO-ABA-5 ≈EGO-ABA-20 ≈ EGO-ABA-40 (64–66%). The high selectivity of EGO is most probably associated with the relatively low amount of C=O groups [281, 298] on large size flakes also characterized by a low density of defects on the basal plane. As the amount and density of C=O groups increases in the EGO-ABA series, the selectivity decreases.

The EGO prepared in this work has a much higher selectivity for H_2O_2 than Printex L6 (63.4% of H_2O_2 yield), [19] rGO obtained by Hummers method followed by solvothermal reduction at 150 °C (72.9%), [19] and graphene obtained by Hummers method followed by high temperature reduction at 1050 °C in Ar (55%). [297] It has however a lower selectivity than mild reduced graphene oxide (mrGO, ≈100%) prepared by the Hummers' method and reduced at 100 °C under N_2 flow [16] and oxidized carbon nanotubes (O-CNTs, 90%). [281]

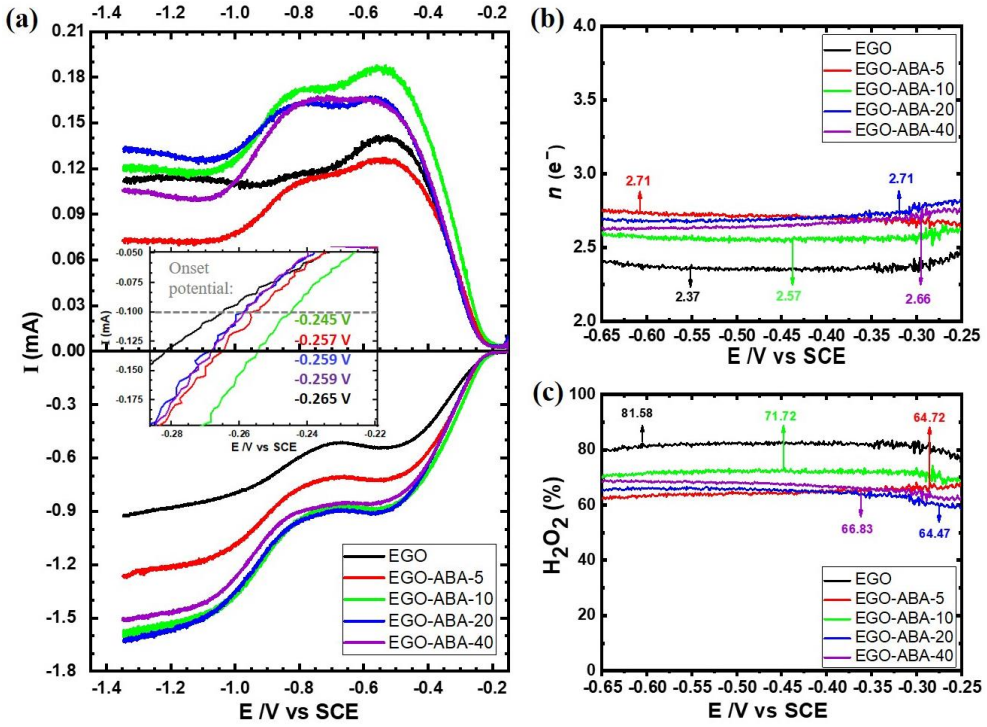

Figure 6.5. (a) Linear sweep voltammograms (LSVs) for the oxygen reduction reaction for EGO and EGO-ABA electrodes 0.1 M KOH at 5 mV s^{-1} with a rotation of 1600 rpm: disc current (bottom panel) and ring currents (top panel). The potential dependence of (b) number of transferred electrons (n) and (c) of the yield of hydroperoxide formation on EGO and EGO-COOHs based electrodes.

6.3.3. Performance of EGO and EGO-ABA Materials for Supercapacitors

Figure 6.6a shows the cyclic voltammograms of EGO and EGO-ABA electrodes in 6 M KOH collected at the scan rate of 50 mV s^{-1} from 0 to −1.15 V. The cyclic voltammogram of the Ni foam support is shown in Supplementary **Figure S6.6**. The EGO-ABA materials show a large current response with pronounced redox peaks in the potential range from −0.3 to −1 V related to the oxidation and reduction of functional groups (see Section 6.4.2). These related redox reactions can be expressed as follows: [299]

$$-\mathrm{COOH} + \mathrm{OH}^- \leftrightarrow -\mathrm{COO} + \mathrm{H_2O} + \mathrm{e}^- \qquad \text{(Reaction 4)}$$

$$>\mathrm{C\text{-}OH} + \mathrm{OH}^- \leftrightarrow >\mathrm{C{=}O} + \mathrm{H_2O} + \mathrm{e}^- \qquad \text{(Reaction 5)}$$

$$>\mathrm{C{=}O} + \mathrm{e}^- \leftrightarrow >\mathrm{C\text{-}O}^- \qquad \text{(Reaction 6)}$$

The current intensity is the highest for EGO-ABA-5 and then it decreases for EGO-ABA-10 and EGO-ABA-40. The peaks are less visible on the unmodified EGO which shows a quasi-rectangular-shaped and symmetric cyclic voltammogram typical of a double layer capacitive

behavior. First, the low content of 4-ABA in the reaction medium could lead to a uniform grafting of ABA molecules on EGO and could suppress the aggregation of the graphene oxide nanosheet and facilitate the redox reactivity, as illustrated in **Figure 6.6a** for EGO-ABA-5. Additionally, it could enhance the surface wettability and the accessible surface area of the electrode leading to a higher pseudocapacitance, as illustrated in **Figure 6.5a**. However, the excessive amount of 4-ABA during the synthesis led to the reaction between amines and the adsorption of these products on the EGO surface. This hinders the porosity path within the graphene sheets, is unfavorable to the rapid transport of electrolyte ions and even negatively affects the overall electrochemical performance of the samples, as shown in Figure 6a for EGO-ABA-40.

Cyclic voltammograms were also recorded at different scan rates (Supplementary **Figure S6.7**) to determine the specific capacitance of each electrode. **Figure 6.6b** displays the variation of specific capacitances which decrease gradually with increasing scan rate. [25] However, the capacitances of EGO and EGO-ABA-5 at 5 mV s^{-1} are lower than those at 10 and 20 mV s^{-1}, which is unusual, indicating that the electrodes' surface area is less accessible at the lowest scan rate. Other studies have reported similar trends with carbon materials and it was proposed that the structure of the materials collapses when scanning at low scan rate or charging at low current density. [300-301] Furthermore, the specific capacitances of EGO-ABA-5 and EGO-ABA-10 are much larger than that of EGO-ABA-40 and of EGO. As already observed with the voltammetric charges obtained with 0.1M KOH (**Figure 6.4b**), the capacitance of the EGO-ABA materials is higher than that of EGO and then gradually decreases with increasing of the amine concentration in the reaction medium from 5 to 40 mM. The oxygen functional groups (**Figure 6.3c**) besides participating in the fast redox processes that provide pseudocapacitance [222], play a very important role in the charging/discharging processes because they render the internal surface of graphene matrix accessible to the ions in the electrolyte. [222, 226]

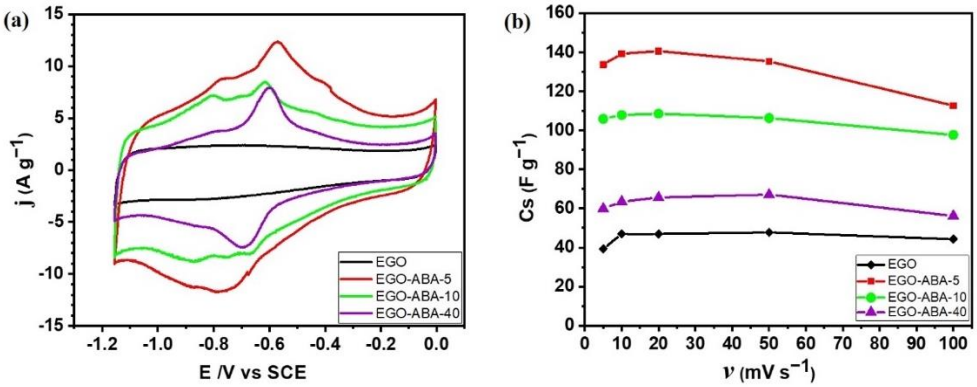

Figure 6.6. (a) Cyclic voltammograms (CV) of graphene materials, before (EGO) and after surface functionalization (EGO-ABA) collected at the scan rate of 50 mV s^{-1} from 0 to −1.15 V. (b) Specific capacitance (C_s) versus the scan rate (u) for EGO and EGO-ABA based electrodes.

Extended cycling capability is a key parameter of supercapacitors. Hence, the performance of the EGO-ABA-5 electrode was evaluated by recording up to 5000 cycles at 50 mV s^{-1}. As shown in **Figure 6.7**, the electrode retained 80.6% of the initial capacitance after 5000 cycles in 6 M KOH. This decrease of capacitance can be attributed to desorption of the non-covalently attached ABA molecules that are loosely bound to the EGO surface. [227-228] In any case, the extended cycling test demonstrates the remarkable electrochemical durability of this electrode material and its potential to be used in supercapacitors.

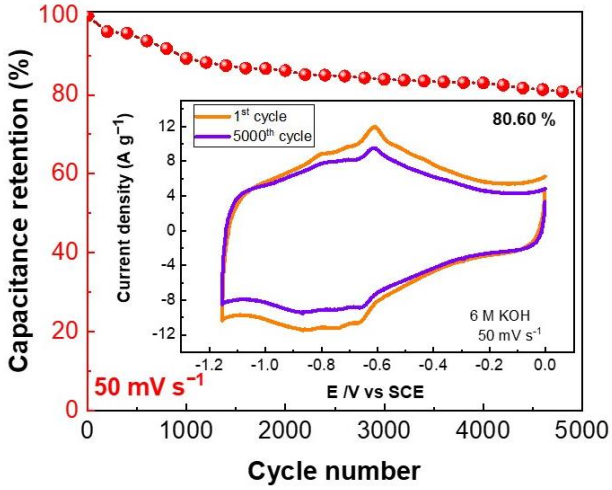

Figure 6.7. Cycling performance of the EGO-ABA-5/NF electrode at 50 mV s^{-1} for 5000 cycles; the inset shows CV curves for the 1st and 5000th cycles.

6.4. Materials and Methods

Details related to materials, instrumentation, and physicochemical characterization techniques can be found in the Supplementary.

6.4.1. Preparation of Aminobenzoic Acid Functionalized Graphene Oxide (EGO-ABA)

In a two-electrodes system, a graphite foil (5 cm × 2 cm × 0.05 cm) was used as anode and a Pt mesh (6 cm^2) was used as cathode. Both electrodes were immersed into 0.1 M H_2SO_4 electrolyte

with different concentrations of 4-aminobenzoic acid (4-ABA, 0, 5, 10, 20, 40 mM) and connected to the direct current power supply. The distance between the two electrodes was 6 cm. After applying a potential difference of 8 V, the electrochemical exfoliation of graphite started immediately. After the exfoliation, the EGO sheets were washed with Millipore water and collected by vacuum filtration through an MF-Millipore membrane filter with 0.22 µm pore size. pH paper was used to verify the presence of residual acid. After several washes with water and vacuum filtration, the pH of the colorless filtrate was found to be around 5–6, indicating that the sulfuric acid electrolyte and the adduct produced by the side reactions have been removed.

The EGO and EGO-ABA powders were then dispersed in water by ultrasonication for 90 min to maximize the exfoliation. The dispersion was freeze-dried, and the powders stored for further use. The samples are named according to the concentration of 4-aminobenzoic acid, such as EGO (0 mM of 4-ABA) and EGO-ABA-5 (5 mM of 4-ABA). **Table 6.1** summarizes the experimental observations during the synthesis of the EGO materials, including the initial current, the exfoliation time, and the color of electrolyte.

6.4.2. Preparation and Electrochemical Characterization of EGO-ABA Based Electrodes for ORR Study

Electrochemical studies in 0.1 M KOH were conducted on glassy carbon electrodes (GCE) disk and on a glassy carbon rotating disk ring electrode (RRDE) covered with EGO or EGO-ABA catalyst layers. Catalyst inks were prepared by dispersing 10 mg of EGO or EGO-ABA flakes in 525 µL isopropyl alcohol and 25 µL of 5 wt% Nafion® perfluorinated resin solution. Subsequently, the inks were sonicated for 1 h. The electrodes (diameter of 5 mm) were polished on suede with 0.3 and 0.05 µm Al_2O_3 powder, rinsed with Millipore water and washed thoroughly in an ultrasound bath. Next, the disks were covered with an appropriate volume of the catalyst ink to obtain a catalyst loading of 463.8 µgcm^{-2}, and dried in room temperature. The GCE/RRDE electrodes covered with EGO materials, a counter electrode (Pt coil), and a saturated calomel reference electrode were all housed in a single compartment electrochemical cell.

Cyclic voltammetry was first conducted on the GCE in saturated N_2 electrolyte at 50 mV s^{-1} from 0.4 V to −1.4 V vs. SCE and 20 cycles were recorded for each material. For the ORR studies, the RRDE and the following protocol were used: (i) three cyclic voltammograms from 0.4 V to −1.4 V vs. SCE were recorded at 50 mVs^{-1}; (ii) linear sweep voltammograms (LSV) between −0.10 V to −1.35 V vs. SCE were recorded in saturated N_2 electrolyte at 5 mV s^{-1} varying the rotation rate

from 1600, 900, 400, 225 to 100 rpm; (iii) saturation of the electrolyte with O_2 and the procedures (i) and (ii) were performed again. The ring potential was set at a constant value of 1.2 V vs. SCE to oxidize the H_2O_2 formed on the disc electrode, allowing for its quantification. Before the LSV experiments, the Pt ring was activated by cyclic voltammetry in saturated N_2 electrolyte at 500 mV s^{-1} (15 CV) from 0.4 V to −0.9 V vs. SCE.

In order to calculate the number of electrons involved during ORR and the percentage of electrogenerated H_2O_2, Equations (6.3) and (6.4) were used, respectively.

6.4.3. Preparation and Electrochemical Characterization of EGO-ABA Based Electrodes for Supercapacitors

Nickel foams (NF) were used as support for the fabrication of EGO and EGO-ABA electrodes. The EGO-based materials and PTFE binder (90:10 wt.% ratio, 90 mg of graphene materials and 10 mg of PTFE) were mixed in a small volume (2 mL) of ethanol under sonication until a homogenized dispersion is obtained. Then, the Ni foam (1 cm^2) was coated by simple repetitive dip-coating steps into EGO inks and dried at 60 °C under vacuum overnight. The active material loading (around 1.5–2.0 mg) was calculated from the weight difference of the nickel foam before and after coating determined by high precision weighing balance (accuracy 0.0001 mg).

The electrochemical behavior of EGO-based NF electrodes was investigated by cyclic voltammetry in a three-electrode configuration, where carbon paper (CP) and a saturated calomel electrode (SCE) were employed as counter and reference electrodes, respectively. The electrochemical studies were carried out in 6 M KOH electrolyte and the scan rate varied between 5 and 100 mV s^{-1} [208]. The specific capacitance (Cs) of EGO/NF and EGO-COOHs/NF was evaluated from the cyclic voltammograms using the cathodic voltammetric charge (Q) integrated in the 0 to −1.15 V vs. SCE potential window by using Equation (6.5): [24]

$$Cs = \frac{Q}{m\Delta V} \qquad (6.5)$$

where *Cs* is the specific capacitance (in F g^{-1}), Q is the charge (in C), ΔV is the potential window (in V), and m is the mass of active material (in g).

6.5. Conclusions

In this work, we have synthesized the aminobenzoic acid functionalized electrochemically exfoliated graphene oxide (EGO-ABA) by one-step method. The amount of 4-aminobenzoic acid (4-ABA) in the 0.1 M sulfuric acid electrolyte was varied between 0 and 40 mM during the electrochemical exfoliation of graphite to obtain EGO materials with different extents of functionalization. It was found that the presence of 4-ABA decreases the rate of exfoliation and that several reactions occur simultaneously and compete with each other: (1) electrochemical oxidation of graphite vs. oxidation of 4-ABA; (2) the formation of EGO-ABA through grafting vs. the formation of azo dye as a side product. The concentration of 4-ABA should be limited to 10 mM to favor the grafting of 4-ABA on the EGO surfaces.

By adding different concentrations of 4-ABA, the EGO-ABA materials with different amounts and types of functional groups were obtained. Additionally, the EGO-ABA materials have more functional groups, higher density of defects, and a smaller size compared to EGO.

The electrochemical performance of the EGO and EGO-ABA materials for oxygen reduction reaction (ORR) and for supercapacitors were explored in alkaline medium. The presence of the functional groups associated with smaller flake sizes increases the activity for ORR (lower onset potentials, shift of the polarization curves to more positive potentials and higher current) and the specific capacitance of the EGO. However, the non-modified EGO material has a higher selectivity for the 2-electron process compared to the EGO-ABA materials. This was attributed to a lower amount of carbonyl groups in the EGO compared to EGO-ABA. The EGO-ABA synthesized from 5 mM 4-ABA (EGO-ABA-5) has the highest specific capacitance than the other EGO-ABA materials and a remarkable cycling capability (80.6% retention of the initial capacitance after 5000 cycles at 50 mVs^{-1}). It is concluded that the EGO-ABA materials synthesized from higher concentrations of 4-ABA (20 and 40 mM) have more unreacted 4-ABA and side products adsorbed on the EGO flakes' surface hindering their electrochemical performance. Therefore, low concentration of amines should be used in this type of synthesis of EGO materials.

6.6. Supplementary

6.6.1. Materials and Instrumentation

Materials: Graphite foil (0.5 mm thick, 99.8%) and 4-aminobenzoic acid ($C_7H_7NO_2$, 99%) were purchased from Alfa Aesar. Millipore water (18.2 MΩ cm) was used for rinsing the samples of EGO materials and for preparation of all aqueous solutions. Sulfuric acid (H_2SO_4, 95.0 - 98.0%) was purchased from Sigma-Aldrich. Potassium hydroxide (>99.99%), isopropyl alcohol (99.5%)

and ethanol (91.5%) were purchased from Fisher Scientific and were used without further treatment. The 5 wt% Nafion® suspensions were purchased from Ion Power, Inc. Poly(tetrafluoroethylene) (PTFE) binder was purchased from Aldrich Chemical Company, Inc. High grade nickel foam (99.8% purity) was purchased from KUNHEWUHUA, China.

Instrumentation:

The electrochemical exfoliation of graphite was conducted with a DC Power supply (HY3005F-3) from Dr. Meter.

Scanning Electron Microscopy (SEM) images were taken with a Tescan Vega 3 microscope operating at 20.0 keV incident energy.

Fourier Transform Infrared (FT-IR) spectra of the powder samples were recorded in the region 4000–600 cm^{-1} on a Nicolet FT-IR spectrophotometer.

The bulk structure of electrochemically exfoliated graphene oxide was characterized by X-ray diffraction (XRD) on Bruker D8 X-ray diffractometer with Cu-Kα radiation (λ = 1.54178 Å).

Raman spectra were recorded on a Raman microscope (Renishaw, inVia, at University of Québec at Montreal) with a laser source of 532 nm. The laser beam was focused on the sample on a spot size of 1 μm in diameter, and at least 5 spectra were recorded for each EGO film.

X-ray photoelectron spectroscopy (XPS) was performed with a VG Escalab 200i-XL equipped with a hemispherical analyzer (pass energy = 20 eV) and a multi-channel detector, applying a Twin Anode X-Ray Source at 15 kV and 20 mA. The base pressure inside the spectrometer during analysis was less than 7 × 10-10 torr. The binding energy of the C 1s peak at 284.5 eV was used as internal standard. The core level spectra were peak-fitted using Lorentzian and Gaussian curves after the Shirley type background subtraction, and Casa XPS software. Peak areas were normalized by appropriate atomic sensitivity factors.

A Princeton applied research 273A and an Autolab PGSTAT128N potentiostats were used to conduct the electrochemical tests. A glassy carbon electrode (GCE, 5 mm of diameter, from Pine Instrument Co), a glassy carbon rotating ring disk RRDE (AFE7R9GCPT, Pine Instrument Co) and controller (AFMSRCE, Pine Instrument Co.) were used for the cyclic voltammetry and oxygen reduction studies in 0.1M KOH. The parameters of the RRDE are the following: electrode area (disk): 0.2472 cm^{-2}, ring-disk gap = 320 μm; collection efficiency = 37%; disk OD = 5.61 mm; Ring OD = 7.92 mm; Ring ID = 6.25 mm.

6.6.2. Results

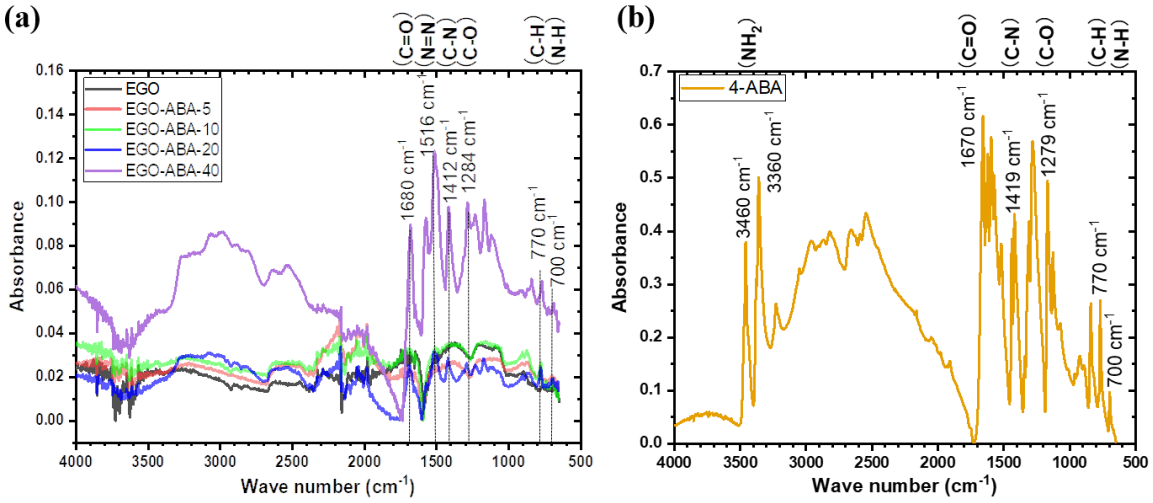

Figure S6.1. FT-IR spectra: (a) EGO and EGO-ABA materials, (b) 4-ABA.

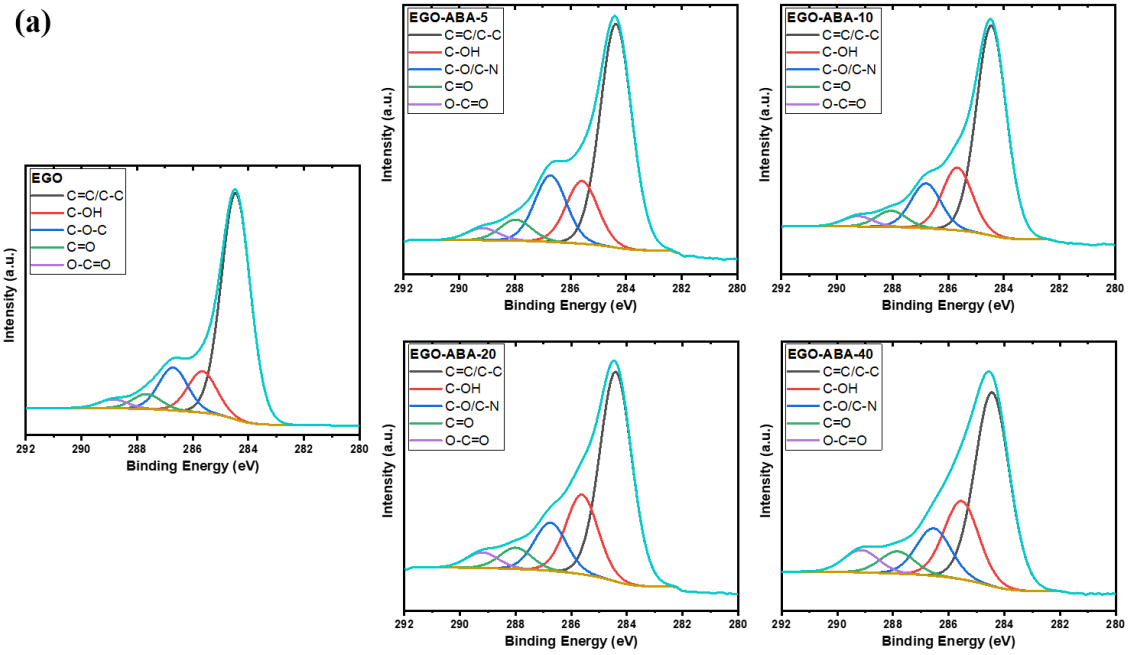

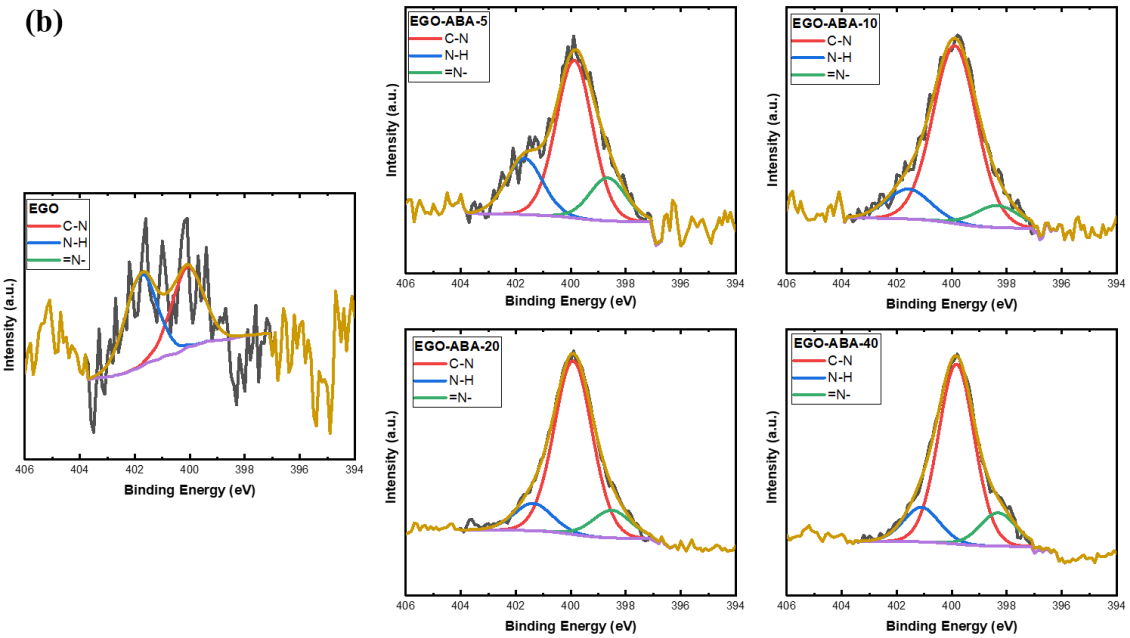

Figure S6.2. XPS spectra of C 1s (a) and N 1s (b) for EGO and EGO-ABA materials.

Table S6.1. Position of the 2D band in the Raman spectra for EGO and EGO-ABA materials.

Samples	2D (cm^{-1})	Standard deviation (cm^{-1})
EGO	2702	9
EGO-ABA-5	2705	5
EGO-ABA-10	2697	10
EGO-ABA-20	2697	5
EGO-ABA-40	2705	4

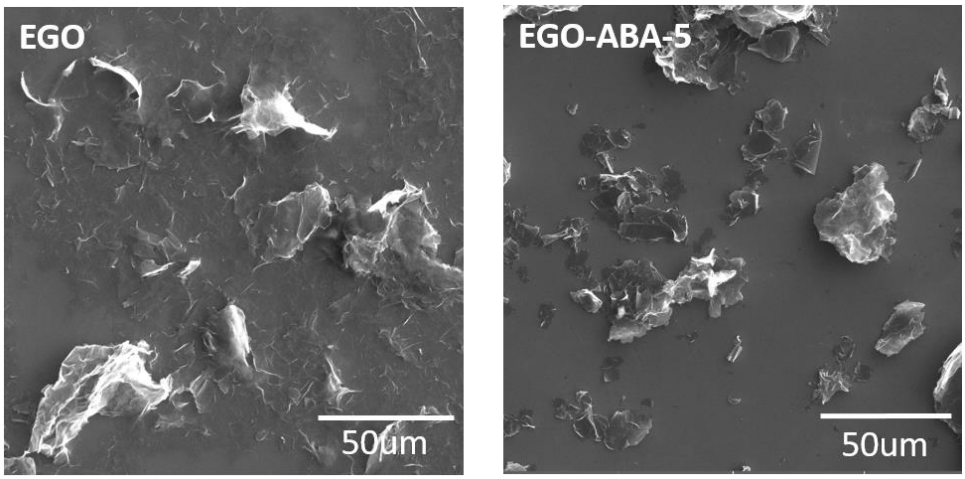

Figure S6.3. SEM images for EGO and EGO-ABA-5 materials.

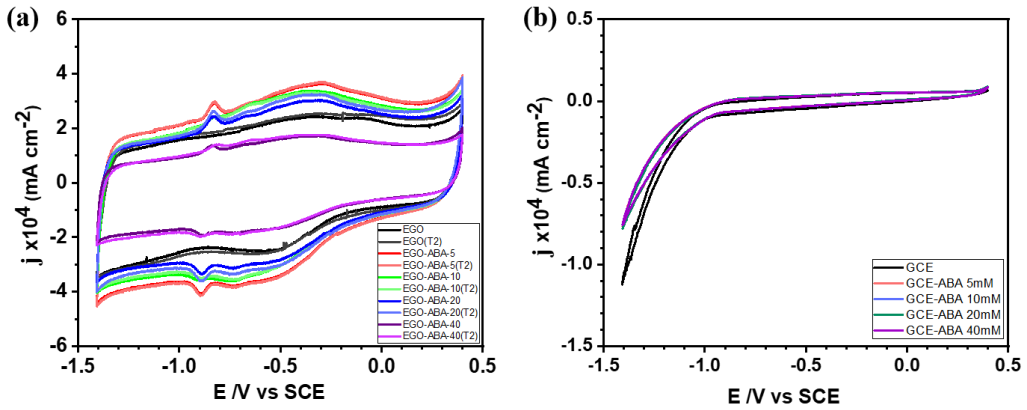

Figure S6.4. (a) Cyclic voltammetry of the EGO and EGO-ABAs modified electrodes in N_2-saturated 0.1M KOH solution after 20 cycles, scan rate 50 mV s^{-1}. (b) Cyclic voltammetry of the GCE in N_2-saturated 0.1M KOH solution with different concentration of 4-ABA after 20 cycles, scan rate 50 mV s^{-1}.

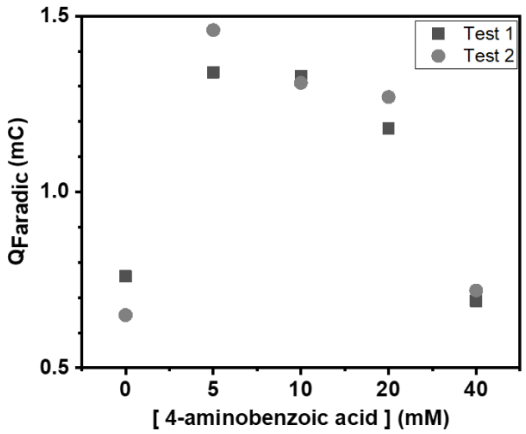

Figure S6.5. The faradic charge ($Q_{Faradic}$) for the EGO and EGO-ABA electrodes calculated from the CV recorded in N_2-saturated 0.1M KOH solution.

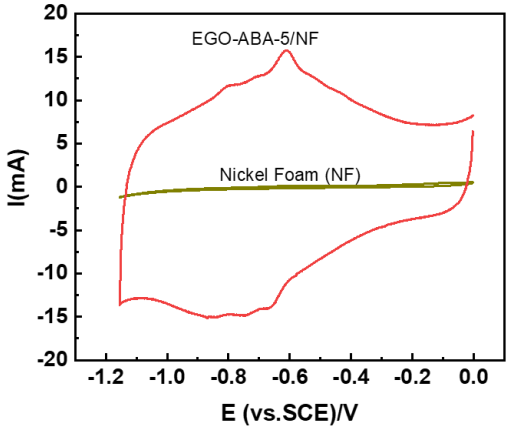

Figure S6.6. Cyclic voltammograms of Nickel foam (NF) and EGO-ABA-5/NF recorded at the scan rate of 50 mV s^{-1} from 0 to -1.15 V.

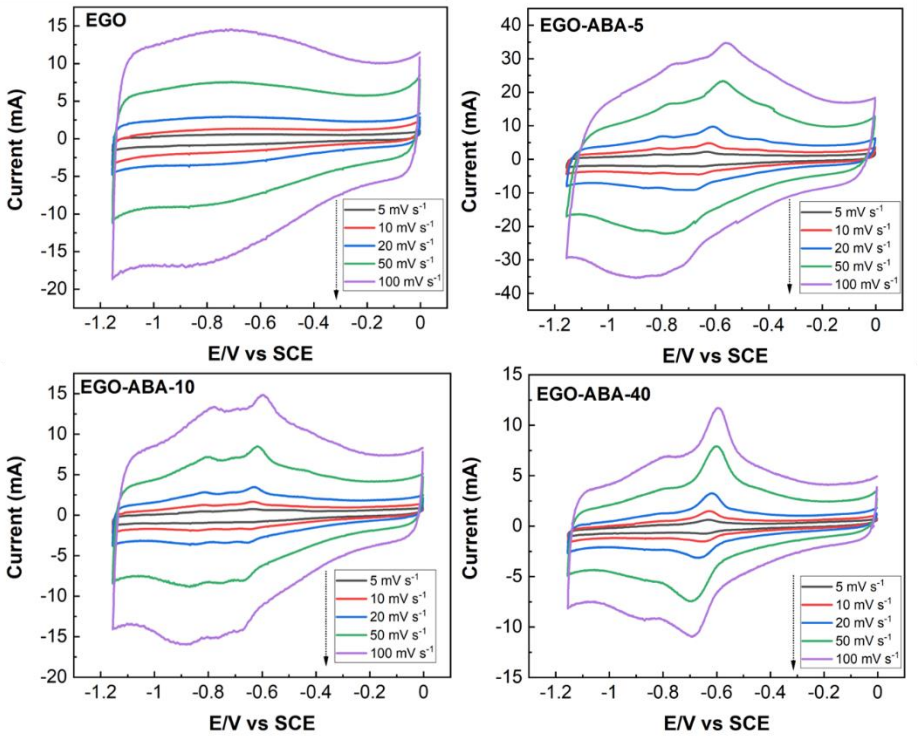

Figure S6.7. Cyclic voltammograms recorded in 6 M KOH at different scan rates for each EGO-ABA/NF electrode.

7. ONGOING AND FUTURE WORKS

In this chapter, several ongoing and future research will be discussed. As explained below, the one-step synthesis of different EGO-based materials using the electrochemical exfoliation of graphite foil was explored.

7.1. One-step synthesis of EGO with gold nanoparticles

Since graphene materials and metal nanocomposites possess a variety of characteristics and excel in a variety of applications, they have attracted more and more attention. Gold nanoparticles (Au NPs) are investigated extensively for their remarkable surface chemical properties, excellent catalytic activity, biocompatibility, and other outstanding characteristics. [302-306] In some studies, Au NPs/rGO composites have been shown to increase electrocatalytic efficiency, enhance Raman signals, etc. [307-309] In biosensor applications, several composites are used without the limitations of a single component and provide superior catalytic properties, increased specificity, or higher limit of detection (LOD). [272-273, 309] In light of these aspects, we explored the synthesis of EGO flakes decorated with Au NPs (EGO-Au NPs) using one-step electrochemical exfoliation of graphite in the presence of chloroauric acid.

As of now, six tests have been conducted, whose experimental parameters and observations are illustrated in Table 7.1. A H-type cell and a proton exchange Nafion (N117) membrane were used in these experiments. The solution of the chloroauric acid precursor was in the anode side only. More details of the experimental setup can be found in chapter 3. Because of the large separation (7 cm) between the graphite foil and Pt electrodes and because of the Nafion membrane separating the two cell compartments, the electrolyte series resistance between the two electrodes is high. Therefore, the concentration of sulfuric acid and the voltage applied are higher than the exfoliation using one single compartment cell. Also, we observed that the exfoliation time for the same size graphite foil (4.5cm x 7cm x 0.05 cm), the electrolyte temperature, and the membrane color after exfoliation varied according to the experimental conditions.

Table 7.1. Experimental parameters and observations for the synthesis of EGO-Au NP materials.

EGO-Au NPs Samples	**01M15V0 1mM**	**05M15V0 6mM**	**05M10V0 4mM**	**01M30V0 6mM**	**02M15V0 6mM**	**04M15V0 6mM**
H_2SO_4	0.1 M	0.5 M	0.5 M	0.1 M	0.2 M	0.4 M

Voltage	15V	15V	10V	30V	15V	15V
$HAuCl_4$	0.1 mM	0.6 mM	0.4 mM	0.6 mM	0.6 mM	0.6 mM
Exfoliation Time	> 6h	75 min	130 min	160 min	220 min	100 min
Temperature	/	55 °C	40 °C	60 °C	44 °C	55 °C
Membrane color	Pink	Colorless	Colorless	Pink (pale)	Colorless	Colorless

The SEM images in **Figure 7.1** show gold nanostructures in EGO-Au NP materials, especially for samples 02M15V06mM and 04M15V06mM. However, gold chloride is present in these gold nanostructures, as indicated by the XPS results (**Figure 7.2**). The TGA results (**Figure 7.3a**) demonstrate that chloride can be eliminated when the temperature reaches 300 °C. To obtain Au NPs, two samples (02M15V06mM and 04M15V06mM) with more Au nanostructure according to SEM images were reduced for one hour at 300 °C under Ar. Based on the XPS results (**Figure 7.3 b and c**), the reduced samples do not contain chloride. However, TEM characterization (**Figure 7.4**) showed that Au NPs had a non-uniform distribution of shapes and sizes. It is therefore necessary to optimize the experimental parameters to achieve uniform NP.

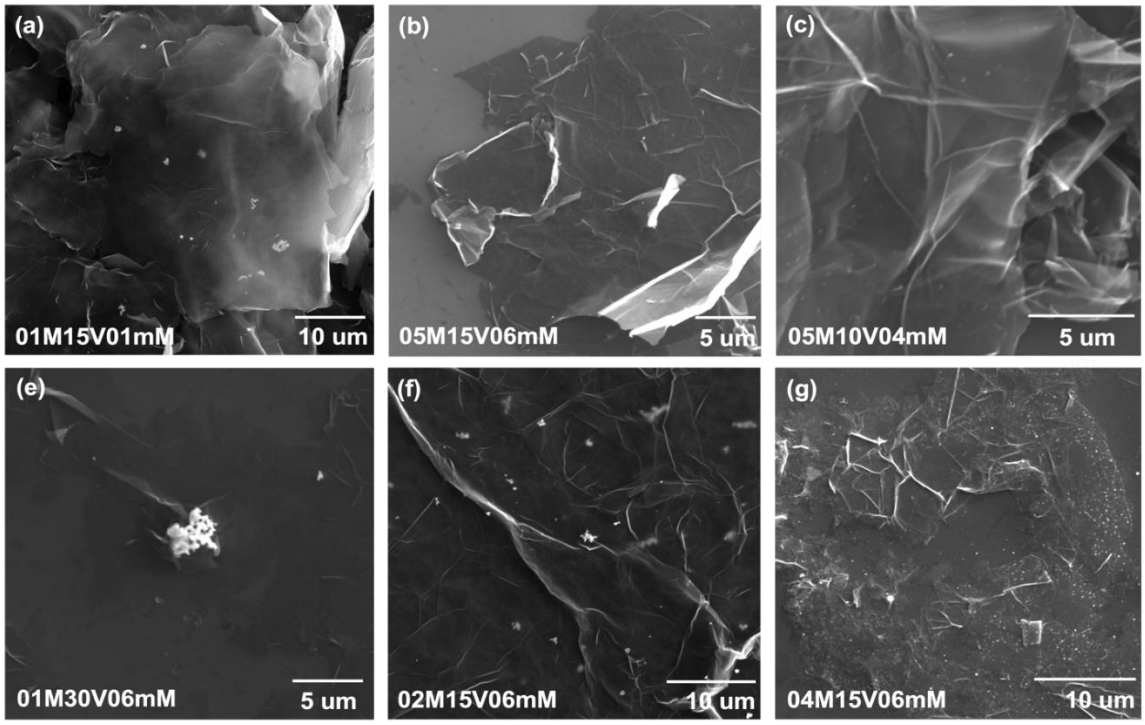

Figure 7.1. SEM images for EGO-Au NPs samples.

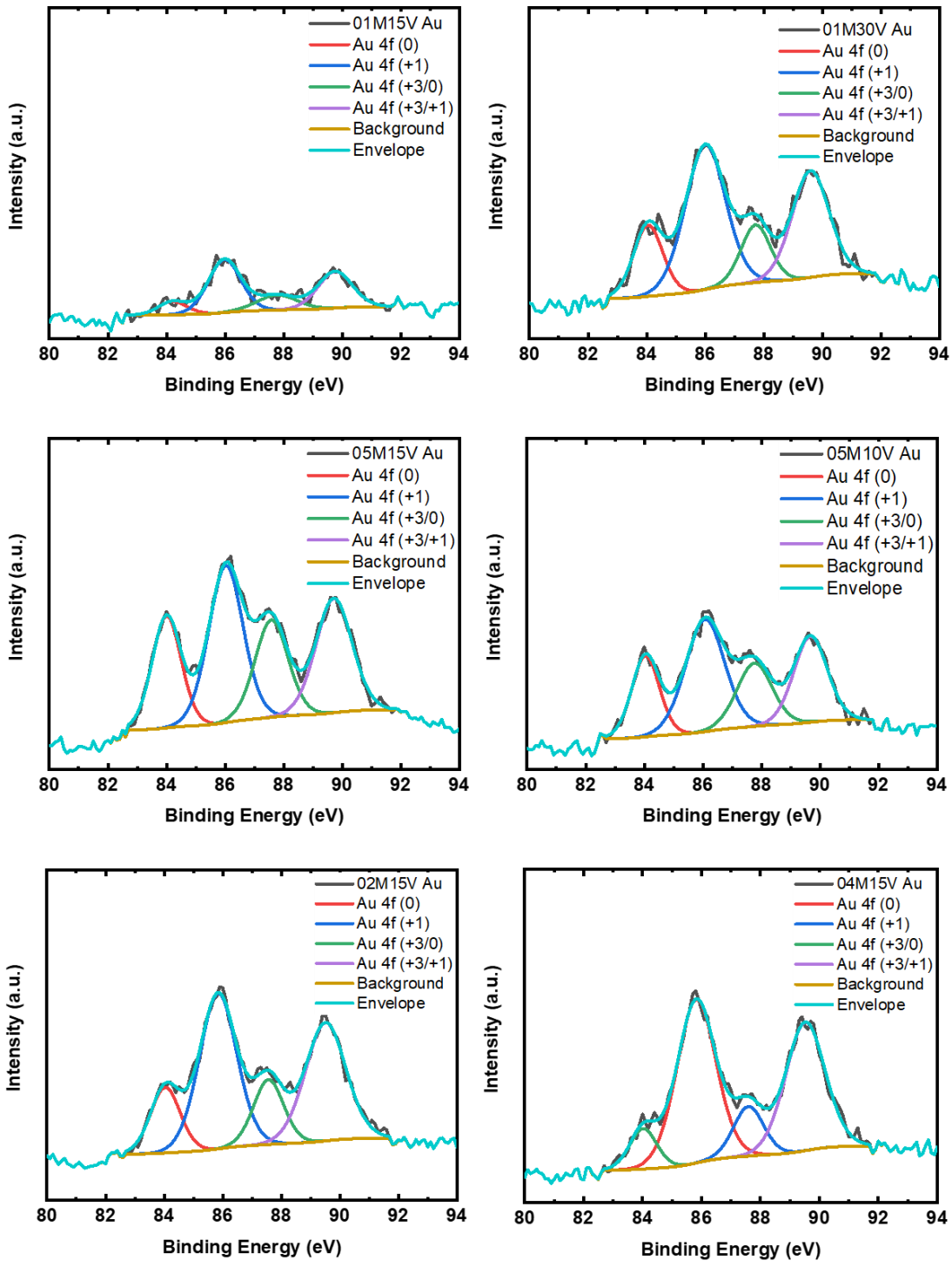

Figure 7.2. Au 4f XPS spectres of EGO-Au NPs samples.

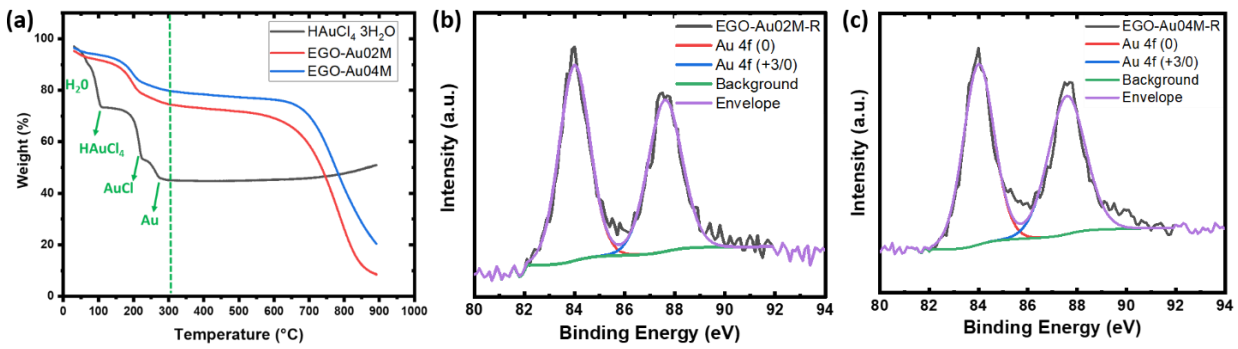

Figure 7.3. (a)TGA and Au 4f XPS spectres of reduced EGO-Au NPs 02M15V06mM (b) and 04M15V06mM (c) samples.

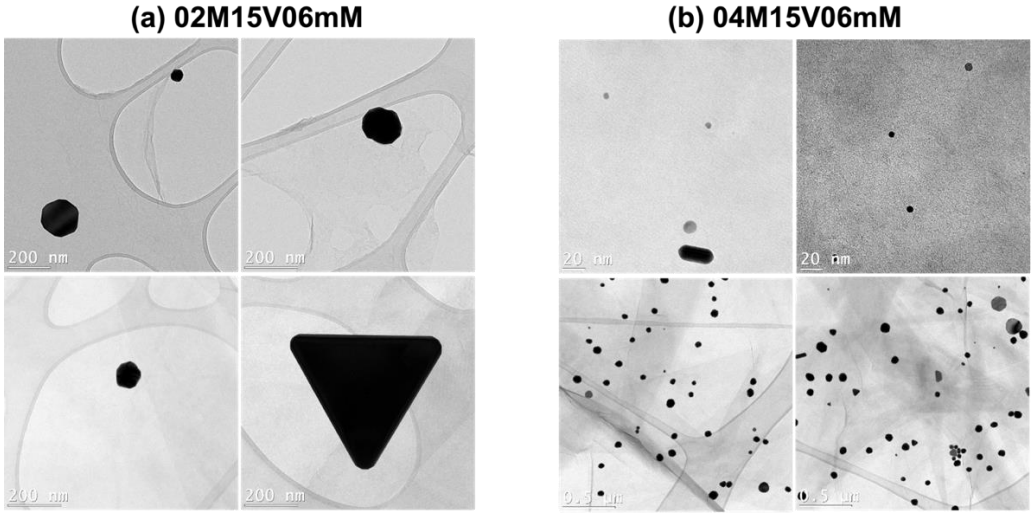

Figure 7.4. TEM images for EGO-Au NPs 02M15V6mM (a) and 04M15V06mM (b) samples.

7.2. EGO synthesis with membrane

For comparison, four EGO samples were synthesized in H-type cell by membrane and without chloroauric acid. From the XPS results (**Figure 7.5**.), membrane-based EGO (EGO-membrane) materials have a higher amount of oxygenated functional groups than ordinary EGO materials. This is likely due to the proton exchange membrane blocking hydroxide ions formed on the anode from moving across it. By doing this, the concentration of hydroxide ions increases, more $OH^{\bullet}$ radicals are formed, and more graphite and EGO sheets are oxidized. Thus, by using a different electrolysis cell and a proton exchange membrane, EGO can contain more oxygen-containing functional groups. Electrochemical exfoliation, as previously discussed, generates materials with low oxygen content, so it is crucial to design systems that produce materials with higher oxygen

content. Because it is important for some applications, including ORR, where the amount of oxygen functional groups correlates with activity and selectivity, and for supercapacitors, where the functional groups can enhance electrode wettability and contribute to reversible redox processes, thus increasing the pseudocapacitance.

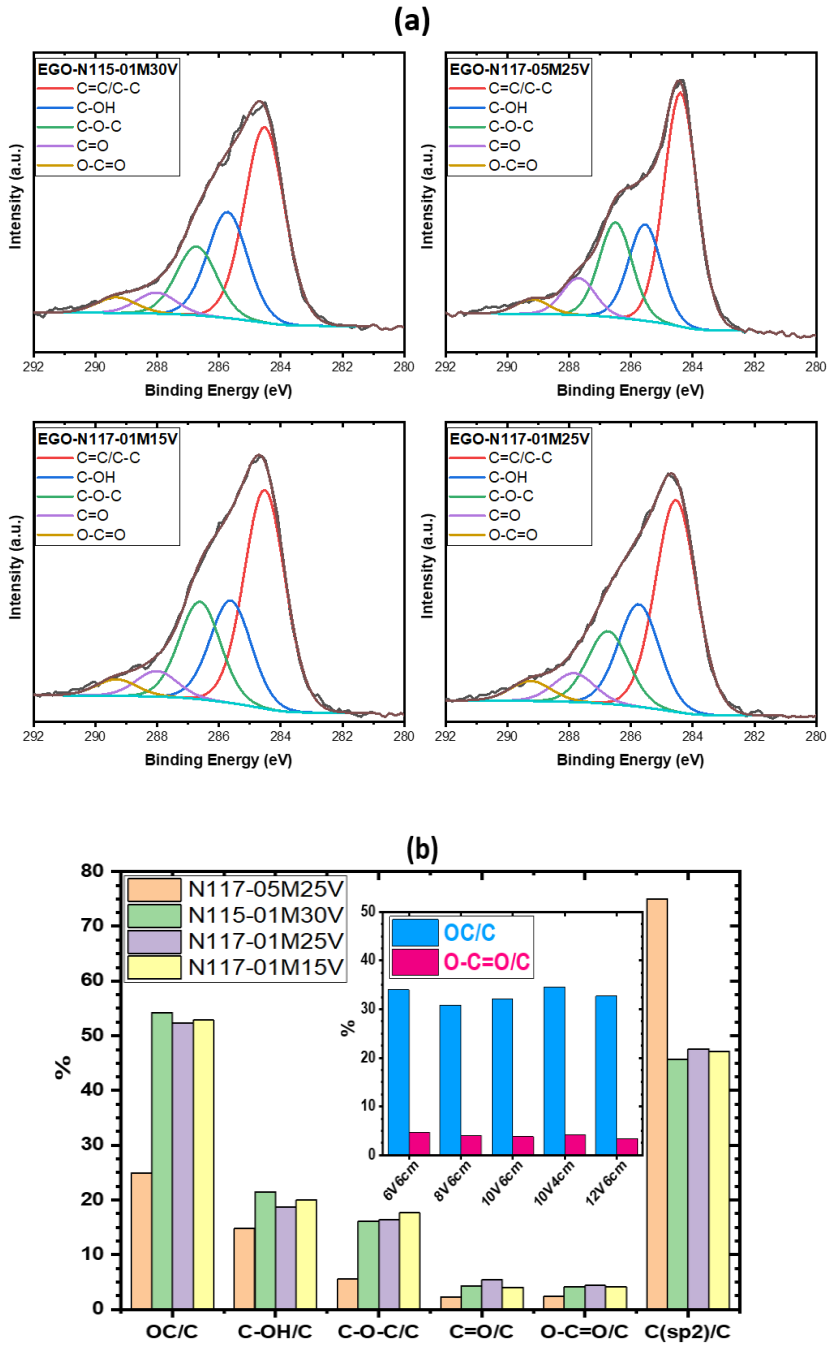

Figure 7.5. (a) C 1s XPS spectres of EGO-membrane materials. (b) Atomic percentage (at% ratio) of each functional groups (OC: all oxygenated functional groups) of the EGO-membrane materials, enclosed the at% ratio of OC and COOH of EGO materials.

7.3. Electrochemical characterization of EGO-ABA, reduced EGO-Au NPs and EGO-membrane materials

To study and compare the electrochemical properties of the EGO-ABA, reduced EGO-Au NPs and EGO-membrane materials, the amine-phenyl film modified glassy carbon electrode (GCE/AP) was immersed in their dispersion (0.05 mg/mL) for 20 minutes, and a series of CVs were recorded at different scan rates (between 20 mV/s and 200 mV/s) using $[Fe(CN)_6]^{3-/4-}$ as redox probe. The electrochemical surface area (ESA) and the standard rate constant of electron transfer (k^0) were calculated. As shown in **Figure 7.6**., materials from the EGO-ABA series have lower ESA and k^0 values than bare EGO, which may be due to its presence of more COOH functional groups that inhibit the oxidation and reduction reactions of the $[Fe(CN)_6]^{3-/4-}$ redox probe. [196] The ESA and k^0 values of EGO-membrane are the highest, possibly because they contain more oxygen-containing functional groups, and therefore more defect sites for the electron transfer. In addition, these materials disperse very well in water which facilitates their assembly on the GCE/AP electrode. According to the study presented in Chapter 5, this type of EGO is promising for biosensors, but more research is necessary. Too many functional groups decrease the electrical conductivity of the graphene materials which can be detrimental for the application. Lastly, the two reduced EGO-Au NP materials also showed a slightly higher ESA and k^0 than bare EGO due to the gold nanoparticles. Finally, as illustrated in **Figure 7.7**, the scaling relation between ESA and k^0 values holds for all EGO materials once again demonstrating the applicability of the self-assembly approach developed in Chapter 4 to characterize different materials.

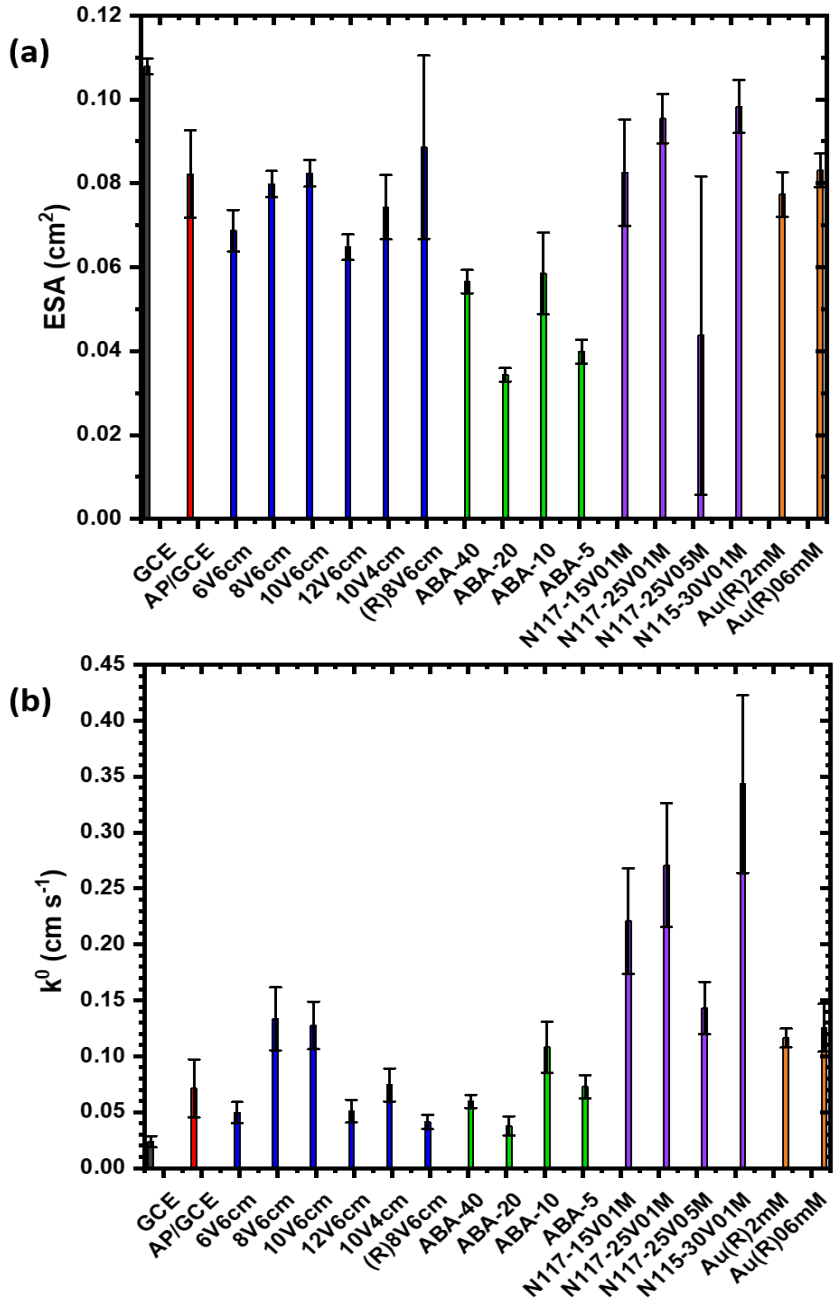

Figure 7.6. (a) Electrochemical surface area (ESA) and (b) standard rate constant (k^0) of the EGO-based electrodes.

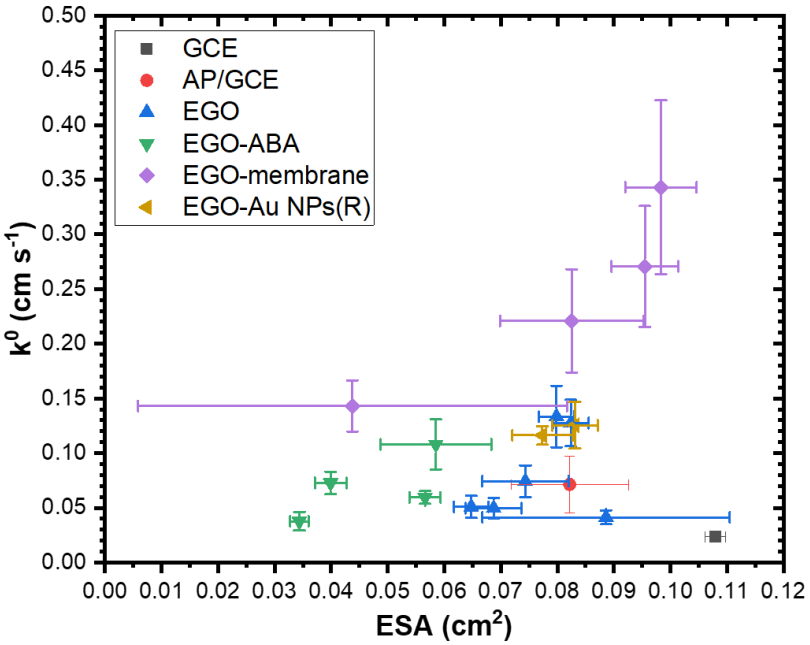

Figure 7.7. Correlation between the k^0 and ESA values.

7.4. Setting the stage for the electrochemical detection of volatile substances

There are many adverse effects of drug use on public health and safety, including overdoses, car accidents, and crime. Thus, simple and rapid detection of drug smuggling and drug use is crucial in public places, border detection, and while driving. In general, cocaine biosensors target the drug itself and certain metabolites, but detecting their volatile hydrophobic derivatives, such as cocaine derived compounds: methyl benzoate and THC (tetrahydrocannabinol), is more useful for detecting smuggling activities. In addition, the detection of volatile substances such as toxic gases or chemicals is also important for safety. Thus, developing an electrochemical sensor for the detection of volatile substances would be very beneficial. However, because of the limited electrolytes, electrochemical detection for most volatile substances is difficult since they are hydrophobic. In order to detect volatile substances, we investigated the oxidation and reduction of $[Fe(CN)_6]^{3-/4-}$ redox probe in alcohol solutions. CV and SWV measurements using a GCE were carried out in 30 vol% ethanol, methanol, and isopropanol solutions containing different concentration of $[Fe(CN)_6]^{3-/4-}$ redox probe (1 mM and 5 mM), respectively. According to **Figure 7.8**, working with alcohol solution is feasible, although the peak-to-peak separation of the CV increases and the peak current value of the CV and SWV curves decreases. This is not surprising because the conductivity of organic solutions is lower than that of aqueous solution. Larger current intensity can be obtained by increasing the concentration of $[Fe(CN)_6]^{3-/4-}$ redox probe from 1 mM

to 5 mM. When we increased the alcohol content to 35vol%, the $[Fe(CN)_6]^{3-/4-}$ redox probe began to crystallize, and no measurements were possible. Based on these results, it appears that electrochemical detection of volatile substances with $[Fe(CN)_6]^{3-/4-}$ redox probes in alcohol solutions is feasible in the future.

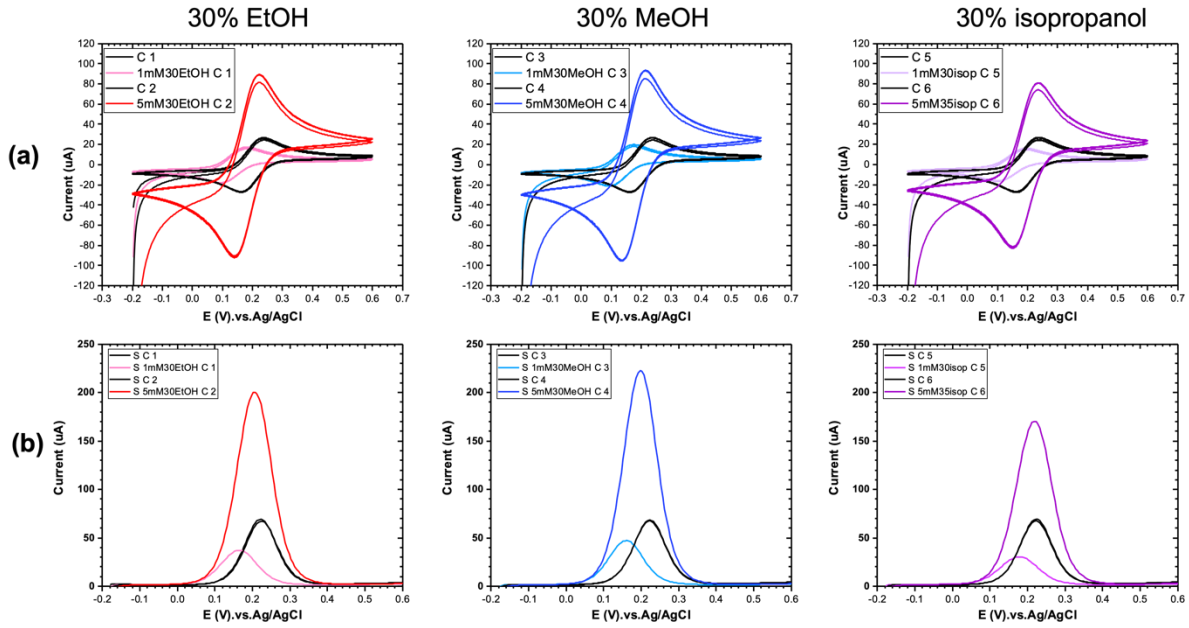

Figure 7.8. (a) CV and (b) SWV recorded in in 30% ethanol, methanol, and isopropanol solutions containing 1mM and 5mM $[Fe(CN)_6]^{3-/4-}$ redox probe, respectively.

Actually, we have tried to detect methyl benzoate based on a screen-printed carbon electrode modified by EGO 10V6cm and aptamer synthesized by Kamar Daou (co-lab of INRS-AFSB) by using 5 mM $[Fe(CN)_6]^{3-/4-}$ in 30% methanol as a redox probe. But it failed because the aptamer that was assayed is not selective, it can give the same response when detecting methyl benzoate, THC, or benzoic acid. Nevertheless, it is promising that aptasensors can be made from EGO materials using aqueous solutions and organic solvents.

8. CONCLUSION

Electrochemical exfoliation of graphite is a powerful method to synthesize GO materials, which are called electrochemically exfoliated graphene oxide (EGO). Compared to chemical methods, it is more environmentally friendly, simpler, and of lower cost. Large amounts of EGO materials with various sheet sizes, number of layers, different content and type of functional groups can be synthesized in a few hours by varying the exfoliation conditions such as graphite electrode, electrolyte, applied voltage and distance between electrodes. As there are numerous variables in the experiment, understanding the reaction mechanism in the electrochemical exfoliation process and finding suitable EGO materials for related applications can be challenging. Therefore, in this thesis, we investigated the synthesis of EGO materials under several different conditions, analyzed their physicochemical and electrochemical properties, and applied them to electrochemical biosensors and supercapacitors. Specifically, the following conclusions can be drawn.

In chapter 4, a series of EGO materials were synthesized in 0.1 M H_2SO_4, and the effect of the electric field (applied voltage divided by distance between electrodes) was examined by Raman spectroscopy and XPS. Raman spectroscopy showed that the defect density (I_D/I_G) increases with applied electric field. Results from XPS show that oxygenated functional groups located at the basal plane (C-OH and C-O-C) are strongly influenced by exfoliation conditions, and their rate depends on two different regimes: exfoliation kinetics and $OH^{\bullet}$ radical concentrations. By using the $[Fe(CN)_6]^{3-/4-}$ redox probe, the EGO materials assembled on GCE through an AP-film linker were electrochemically characterized, and the ESA and k^0 values of the EGO modified GCE electrode were found to be dependent on their intrinsic properties. The results demonstrated that a high density of C-O-C groups has a detrimental impact on ESA and k^0 values for a few layers (≤ 7 layers) EGO. When the number of layers of EGO exceeds 10, it turns into a negative parameter that affects ESA and k^0. EGO materials obtained at 8 - 10 V and 6 cm provided the highest ESA (0.08 cm^2) and the highest k^0 (0.13 cm^{-1}). Based on the platform proposed, excellent correlations can be established between graphene-type materials prepared by electrochemical exfoliation of graphite and their electrochemical, structural, and chemical properties. However, it also should be noted that the CVs of the GCE at different scan rates (from 20 to 200 mV/s) in 1 mM $[Fe(CN)_6]^{3-/4-}$ redox probe were characteristic of a reversible system (Figure A4.11). Future studies should use higher scan rates (more than 200 mV/s) to transition from a reversible to an irreversible redox process and to get more accurate k^0 values for this electrode.

In chapter 5, electrochemical aptasensors based on large-size EGO flakes synthesized in chapter 3 and an amine-modified cocaine aptamer were investigated. It was also examined how the following parameters affected the sensors' performance: 1) the terminal group of the aptamer (-NH_2 vs -OH), 2) the physical adsorption and covalent immobilization of EGO with the aptamer, and 3) EGO's intrinsic electrochemical properties like ESA and k^0. The results demonstrated the cocaine aptamer, particularly with the terminal group -NH_2, can be adsorbed rapidly (10 minutes) on the surface of EGO-modified GCE through physical adsorption method, resulting in an easy, rapid, and cost-effective way to manufacture the apta-sensing platform, which are important criteria for industrial applications. It also showed good reproducibility, shelf-life, and high sensitivity, with a detection limit of 50 nM. Additionally, a higher ESA and k^0 value of EGO 10V6cm brings better sensing performance than other EGOs, proving how electrochemical properties of materials play a crucial role in sensing performance. The simple EGO/aptamer-NH_2 platform is believed to be applicable to manufacturing similar biosensors. As the aim of this work is to use the EGO for electrochemical biosensors, we have used a published cocaine aptamer as a model for the study, and we have examined how aptamers are functionalized on EGO surfaces and the influence of EGO electrochemical properties on sensing performance. However, the binding of cocaine aptamers to cocaine and how they influence sensing performance is also an area for further study. For example, although there are two linked sites between cocaine aptamer and cocaine with varying affinity depending on buffer conditions, [310] the sensor for the detection of cocaine at 100 uM may tend to be saturated or have been saturated. Another interesting point is that, although our detection is not the lowest (50 nM), it is far less than the dissociation constant value of the aptamer (around 0.17 ~ 0.3 uM).

In chapter 6, by varying the concentration of 4-aminobenzoic acid (4-ABA) (between 0 and 40 mM) in 0.1 M H_2SO_4 electrolyte during graphite electrochemical exfoliation, different extents of aminobenzoic acid functionalized electrochemically exfoliated graphene oxide (EGO-ABA) materials were synthesized by the one-step method. FT-IR spectroscopy, XPS, Raman spectroscopy, XRD, and SEM were used to characterize EGO and EGO-ABA materials. It was found that the presence of 4-ABA reduced exfoliation rates as well as several reactions that occur simultaneously and compete: (1) electrochemical oxidation of graphite opposed to 4-ABA oxidation; (2) grafting EGO-ABA against azo dye formation. 4-ABA should be limited to 10 mM to promote grafting on EGO surfaces. Compared to bare EGO, EGO-ABA materials showed smaller flake sizes and a higher density of oxygenated functional groups. EGO and EGO-ABA materials were then tested in alkaline medium for oxygen reduction (ORR) and supercapacitors. Compared to EGO, EGO-ABA catalysts have a higher activity for ORR to H_2O_2 in alkaline medium due to

their higher density of oxygenated functional groups. However, a lower carbonyl group content of bare EGO caused it to have a greater selectivity for the 2-electron process (81% compared to 64-72% with EGO-ABA). For supercapacitors, EGO-ABA materials had an increased specific capacitance than EGO, increasing by a factor of 3 for materials prepared by exfoliating in 5 mM 4-ABA/10 mM H_2SO_4. The electrode material also showed impressive cycling capability after 5000 cycles at 50 mVs-1, with a loss of only 19.4%.

Furthermore, we present a few recent studies in chapter 7, including the synthesis of EGO-Au NP materials in one step and EGO materials with larger oxygen content by using a H-type cell and a proton exchange membrane (EGO-membrane), and the electrochemical characterization in $[Fe(CN)_6]^{3-/4-}$ redox probe in alcohol solutions.

As a result of the existing electrochemical properties test results, both EGO-Au NPs and EGO-membrane materials will be valuable in the development of biosensors. It is also worth exploring the use of the EGO-membrane materials in supercapacitors. More work is needed to fully understand the mechanism of synthesis processes and the influence of various parameters in the electrochemical exfoliation of graphite electrodes on the properties of EGO materials.

9. REFERENCE

1. Li, F.; Jiang, X.; Zhao, J.; Zhang, S., Graphene oxide: A promising nanomaterial for energy and environmental applications. *Nano Energy* **2015,** *16*, 488-515.
2. Yadav, R.; Subhash, A.; Chemmenchery, N.; Kandasubramanian, B., Graphene and Graphene Oxide for Fuel Cell Technology. *Industrial & Engineering Chemistry Research* **2018,** *57* (29), 9333-9350.
3. Lerf, A.; He, H.; Forster, M.; Klinowski, J., Structure of Graphite Oxide Revisited. *The Journal of Physical Chemistry B* **1998,** *102* (23), 4477-4482.
4. Konios, D.; Stylianakis, M. M.; Stratakis, E.; Kymakis, E., Dispersion behaviour of graphene oxide and reduced graphene oxide. *Journal of Colloid and Interface Science* **2014,** *430*, 108-112.
5. Wang, Y.; Li, Z.; Wang, J.; Li, J.; Lin, Y., Graphene and graphene oxide: biofunctionalization and applications in biotechnology. *Trends in Biotechnology* **2011,** *29* (5), 205-212.
6. Justino, C. I. L.; Gomes, A. R.; Freitas, A. C.; Duarte, A. C.; Rocha-Santos, T. A. P., Graphene based sensors and biosensors. *TrAC Trends in Analytical Chemistry* **2017,** *91*, 53-66.
7. Eissa, S.; Ng, A.; Siaj, M.; Zourob, M., Label-Free Voltammetric Aptasensor for the Sensitive Detection of Microcystin-LR Using Graphene-Modified Electrodes. *Analytical Chemistry* **2014,** *86* (15), 7551-7557.
8. Elshafey, R.; Siaj, M.; Tavares, A. C., Au nanoparticle decorated graphene nanosheets for electrochemical immunosensing of p53 antibodies for cancer prognosis. *Analyst* **2016,** *141* (9), 2733-2740.
9. Zhu, Y.; Murali, S.; Cai, W.; Li, X.; Suk, J. W.; Potts, J. R.; Ruoff, R. S., Graphene and Graphene Oxide: Synthesis, Properties, and Applications. *Advanced Materials* **2010,** *22* (35), 3906-3924.
10. Chen, D.; Feng, H.; Li, J., Graphene oxide: preparation, functionalization, and electrochemical applications. *Chemical reviews* **2012,** *112* (11), 6027-6053.
11. Suvarnaphaet, P.; Pechprasarn, S., Graphene-Based Materials for Biosensors: A Review. *Sensors* **2017,** *17* (10), 2161.
12. Chang, J.; Zhou, G.; Christensen, E. R.; Heideman, R.; Chen, J., Graphene-based sensors for detection of heavy metals in water: a review. *Analytical and Bioanalytical Chemistry* **2014,** *406* (16), 3957-3975.
13. Wang, N.; Ma, S.; Zuo, P.; Duan, J.; Hou, B., Recent Progress of Electrochemical Production of Hydrogen Peroxide by Two-Electron Oxygen Reduction Reaction. *Advanced Science* **2021,** *8* (15), 2100076.
14. Brillas, E.; Sirés, I.; Oturan, M. A., Electro-Fenton process and related electrochemical technologies based on Fenton's reaction chemistry. *Chemical reviews* **2009,** *109* (12), 6570-6631.
15. Hummers, W. S.; Offeman, R. E., Preparation of Graphitic Oxide. *Journal of the American Chemical Society* **1958,** *80* (6), 1339-1339.
16. Kim, H. W.; Ross, M. B.; Kornienko, N.; Zhang, L.; Guo, J.; Yang, P.; McCloskey, B. D., Efficient hydrogen peroxide generation using reduced graphene oxide-based oxygen reduction electrocatalysts. *Nature Catalysis* **2018,** *1* (4), 282-290.
17. Zhao, B.; Liu, P.; Jiang, Y.; Pan, D.; Tao, H.; Song, J.; Fang, T.; Xu, W., Supercapacitor performances of thermally reduced graphene oxide. *Journal of power sources* **2012,** *198*, 423-427.
18. Yang, J.; Gunasekaran, S., Electrochemically reduced graphene oxide sheets for use in high performance supercapacitors. *Carbon* **2013,** *51*, 36-44.
19. Carneiro, J. F.; Paulo, M. J.; Siaj, M.; Tavares, A. C.; Lanza, M. R., Nb2O5 nanoparticles supported on reduced graphene oxide sheets as electrocatalyst for the H2O2 electrogeneration. *Journal of Catalysis* **2015,** *332*, 51-61.
20. Parvez, K.; Wu, Z.-S.; Li, R.; Liu, X.; Graf, R.; Feng, X.; Müllen, K., Exfoliation of Graphite into Graphene in Aqueous Solutions of Inorganic Salts. *Journal of the American Chemical Society* **2014,** *136* (16), 6083-6091.

21. Parvez, K.; Li, R.; Puniredd, S. R.; Hernandez, Y.; Hinkel, F.; Wang, S.; Feng, X.; Müllen, K., Electrochemically Exfoliated Graphene as Solution-Processable, Highly Conductive Electrodes for Organic Electronics. *ACS Nano* **2013,** *7* (4), 3598-3606.
22. Su, C.-Y.; Lu, A.-Y.; Xu, Y.; Chen, F.-R.; Khlobystov, A. N.; Li, L.-J., High-Quality Thin Graphene Films from Fast Electrochemical Exfoliation. *ACS Nano* **2011,** *5* (3), 2332-2339.
23. Lei, Y.; Ossonon, B. D.; Chen, J.; Perreault, J.; Tavares, A. C., Electrochemical characterization of graphene-type materials obtained by electrochemical exfoliation of graphite. *Journal of Electroanalytical Chemistry* **2021,** *887*, 115084.
24. Ossonon, B. D.; Tavares, A. C., Innovative approach for the synthesis of graphene/MnO2 nanocomposites and their electrochemical behavior. *Electrochemical Science Advances* **2021**, 2100029.
25. Aghamohammadi, H.; Eslami-Farsani, R.; Torabian, M.; Amousa, N., Recent advances in one-pot functionalization of graphene using electrochemical exfoliation of graphite: A review study. *Synthetic Metals* **2020,** *269*, 116549.
26. Ossonon, B. D.; Bélanger, D., Functionalization of graphene sheets by the diazonium chemistry during electrochemical exfoliation of graphite. *Carbon* **2017,** *111*, 83-93.
27. Liu, F.; Wang, C.; Sui, X.; Riaz, M. A.; Xu, M.; Wei, L.; Chen, Y., Synthesis of graphene materials by electrochemical exfoliation: Recent progress and future potential. *Carbon Energy* **2019,** *1* (2), 173-199.
28. Tarcan, R.; Todor-Boer, O.; Petrovai, I.; Leordean, C.; Astilean, S.; Botiz, I., Reduced graphene oxide today. *Journal of Materials Chemistry C* **2020,** *8* (4), 1198-1224.
29. Compton, O. C.; Nguyen, S. T., Graphene Oxide, Highly Reduced Graphene Oxide, and Graphene: Versatile Building Blocks for Carbon-Based Materials. *Small* **2010,** *6* (6), 711-723.
30. Novoselov, K. S.; Geim, A. K.; Morozov, S. V.; Jiang, D.-e.; Zhang, Y.; Dubonos, S. V.; Grigorieva, I. V.; Firsov, A. A., Electric field effect in atomically thin carbon films. *science* **2004,** *306* (5696), 666-669.
31. Stoller, M. D.; Park, S.; Zhu, Y.; An, J.; Ruoff, R. S., Graphene-based ultracapacitors. *Nano letters* **2008,** *8* (10), 3498-3502.
32. Lee, C.; Wei, X.; Kysar, J. W.; Hone, J., Measurement of the Elastic Properties and Intrinsic Strength of Monolayer Graphene. *Science* **2008,** *321* (5887), 385-388.
33. Li, X.; Zhu, Y.; Cai, W.; Borysiak, M.; Han, B.; Chen, D.; Piner, R. D.; Colombo, L.; Ruoff, R. S., Transfer of large-area graphene films for high-performance transparent conductive electrodes. *Nano letters* **2009,** *9* (12), 4359-4363.
34. Balandin, A. A.; Ghosh, S.; Bao, W.; Calizo, I.; Teweldebrhan, D.; Miao, F.; Lau, C. N., Superior Thermal Conductivity of Single-Layer Graphene. *Nano Letters* **2008,** *8* (3), 902-907.
35. Bolotin, K. I.; Sikes, K. J.; Jiang, Z.; Klima, M.; Fudenberg, G.; Hone, J.; Kim, P.; Stormer, H. L., Ultrahigh electron mobility in suspended graphene. *Solid state communications* **2008,** *146* (9-10), 351-355.
36. Moser, J.; Barreiro, A.; Bachtold, A., Current-induced cleaning of graphene. *Applied Physics Letters* **2007,** *91* (16), 163513.
37. Sanchez, V. C.; Jachak, A.; Hurt, R. H.; Kane, A. B., Biological Interactions of Graphene-Family Nanomaterials: An Interdisciplinary Review. *Chemical Research in Toxicology* **2012,** *25* (1), 15-34.
38. Eda, G.; Fanchini, G.; Chhowalla, M., Large-area ultrathin films of reduced graphene oxide as a transparent and flexible electronic material. *Nature nanotechnology* **2008,** *3* (5), 270-274.
39. Li, X.; Wang, X.; Zhang, L.; Lee, S.; Dai, H., Chemically derived, ultrasmooth graphene nanoribbon semiconductors. *science* **2008,** *319* (5867), 1229-1232.
40. Zhang, Y.; Gao, Z.; Song, N.; He, J.; Li, X., Graphene and its derivatives in lithium–sulfur batteries. *Materials today energy* **2018,** *9*, 319-335.
41. Zhang, Y.; Xia, X.; Liu, B.; Deng, S.; Xie, D.; Liu, Q.; Wang, Y.; Wu, J.; Wang, X.; Tu, J., Multiscale graphene‐based materials for applications in sodium ion batteries. *Advanced Energy Materials* **2019,** *9* (8), 1803342.

42. Dai, C.; Sun, G.; Hu, L.; Xiao, Y.; Zhang, Z.; Qu, L., Recent progress in graphene-based electrodes for flexible batteries. *InfoMat* **2020,** *2* (3), 509-526.
43. Zhang, Q.; Wu, Z.; Li, N.; Pu, Y.; Wang, B.; Zhang, T.; Tao, J., Advanced review of graphene-based nanomaterials in drug delivery systems: Synthesis, modification, toxicity and application. *Materials Science and Engineering: C* **2017,** *77*, 1363-1375.
44. Liu, J.; Dong, J.; Zhang, T.; Peng, Q., Graphene-based nanomaterials and their potentials in advanced drug delivery and cancer therapy. *Journal of Controlled Release* **2018,** *286*, 64-73.
45. Lee, J.; Kim, J.; Kim, S.; Min, D.-H., Biosensors based on graphene oxide and its biomedical application. *Advanced Drug Delivery Reviews* **2016,** *105*, 275-287.
46. Rowley-Neale, S. J.; Randviir, E. P.; Dena, A. S. A.; Banks, C. E., An overview of recent applications of reduced graphene oxide as a basis of electroanalytical sensing platforms. *Applied Materials Today* **2018,** *10*, 218-226.
47. Ke, Q.; Wang, J., Graphene-based materials for supercapacitor electrodes–A review. *Journal of Materiomics* **2016,** *2* (1), 37-54.
48. Yang, Z.; Tian, J.; Yin, Z.; Cui, C.; Qian, W.; Wei, F., Carbon nanotube-and graphene-based nanomaterials and applications in high-voltage supercapacitor: A review. *Carbon* **2019,** *141*, 467-480.
49. Korkmaz, S.; Kariper, İ. A., Graphene and graphene oxide based aerogels: Synthesis, characteristics and supercapacitor applications. *Journal of Energy Storage* **2020,** *27*, 101038.
50. Ruoff, R., Calling all chemists. *Nature Nanotechnology* **2008,** *3* (1), 10-11.
51. Rao, C. e. N. e. R.; Sood, A. e. K.; Subrahmanyam, K. e. S.; Govindaraj, A., Graphene: the new two-dimensional nanomaterial. *Angewandte Chemie International Edition* **2009,** *48* (42), 7752-7777.
52. Geim, A. K.; Novoselov, K. S., The rise of graphene. *Nature Materials* **2007,** *6* (3), 183-191.
53. Iijima, S., Helical microtubules of graphitic carbon. *Nature* **1991,** *354* (6348), 56-58.
54. Kroto, H. W.; Heath, J. R.; O'Brien, S. C.; Curl, R. F.; Smalley, R. E., C60: Buckminsterfullerene. *Nature* **1985,** *318* (6042), 162-163.
55. Choi, W.; Lee, J.-w., *Graphene: synthesis and applications*. CRC press: 2011.
56. Shinohara, H.; Tiwari, A., *Graphene: an introduction to the fundamentals and industrial applications*. John Wiley & Sons: 2015.
57. Ossonon, B. D.; Bélanger, D., Synthesis and characterization of sulfophenyl-functionalized reduced graphene oxide sheets. *RSC advances* **2017,** *7* (44), 27224-27234.
58. Das, S.; Sudhagar, P.; Kang, Y. S.; Choi, W., Synthesis and characterization of graphene. *Carbon Nanomaterials for Advanced Energy Systems: Advances in Materials Synthesis and Device Applications* **2015**, 85-131.
59. Deng, X.; Tang, H.; Jiang, J., Recent progress in graphene-material-based optical sensors. *Analytical and Bioanalytical Chemistry* **2014,** *406* (27), 6903-6916.
60. Bai, J.; Hong, W.; Bai, H., Electrochemically reduced graphene oxide: Preparation, composites, and applications. *Carbon* **2022**.
61. Agarwal, V.; Zetterlund, P. B., Strategies for reduction of graphene oxide–A comprehensive review. *Chemical Engineering Journal* **2021,** *405*, 127018.
62. Chua, C. K.; Pumera, M., Chemical reduction of graphene oxide: a synthetic chemistry viewpoint. *Chemical Society Reviews* **2014,** *43* (1), 291-312.
63. Guo, S.; Dong, S., Graphene nanosheet: synthesis, molecular engineering, thin film, hybrids, and energy and analytical applications. *Chemical Society Reviews* **2011,** *40* (5), 2644-2672.
64. Novoselov, K. S.; Colombo, L.; Gellert, P.; Schwab, M.; Kim, K., A roadmap for graphene. *nature* **2012,** *490* (7419), 192-200.
65. Ciesielski, A.; Samorì, P., Graphene via sonication assisted liquid-phase exfoliation. *Chemical Society Reviews* **2014,** *43* (1), 381-398.
66. Liang, X.; Chang, A. S.; Zhang, Y.; Harteneck, B. D.; Choo, H.; Olynick, D. L.; Cabrini, S., Electrostatic force assisted exfoliation of prepatterned few-layer graphenes into device sites. *Nano letters* **2009,** *9* (1), 467-472.

67. Ci, L.; Song, L.; Jariwala, D.; Elias, A. L.; Gao, W.; Terrones, M.; Ajayan, P. M., Graphene shape control by multistage cutting and transfer. *Advanced Materials* **2009,** *21* (44), 4487-4491.
68. Viculis, L. M.; Mack, J. J.; Mayer, O. M.; Hahn, H. T.; Kaner, R. B., Intercalation and exfoliation routes to graphite nanoplatelets. *Journal of Materials Chemistry* **2005,** *15* (9), 974-978.
69. Park, S.; Ruoff, R. S., Chemical methods for the production of graphenes. *Nature nanotechnology* **2009,** *4* (4), 217-224.
70. Hummers Jr, W. S.; Offeman, R. E., Preparation of graphitic oxide. *Journal of the american chemical society* **1958,** *80* (6), 1339-1339.
71. Staudenmaier, L., Verfahren zur darstellung der graphitsäure. *Berichte der deutschen chemischen Gesellschaft* **1898,** *31* (2), 1481-1487.
72. Lin, Z.; Waller, G.; Liu, Y.; Liu, M.; Wong, C. P., Facile synthesis of nitrogen-doped graphene via pyrolysis of graphene oxide and urea, and its electrocatalytic activity toward the oxygen-reduction reaction. *Advanced Energy Materials* **2012,** *2* (7), 884-888.
73. De Heer, W. A.; Berger, C.; Wu, X.; First, P. N.; Conrad, E. H.; Li, X.; Li, T.; Sprinkle, M.; Hass, J.; Sadowski, M. L., Epitaxial graphene. *Solid state communications* **2007,** *143* (1-2), 92-100.
74. Li, X.; Cai, W.; An, J.; Kim, S.; Nah, J.; Yang, D.; Piner, R.; Velamakanni, A.; Jung, I.; Tutuc, E., Large-area synthesis of high-quality and uniform graphene films on copper foils. *science* **2009,** *324* (5932), 1312-1314.
75. Obraztsov, A.; Obraztsova, E.; Tyurnina, A.; Zolotukhin, A., Chemical vapor deposition of thin graphite films of nanometer thickness. *Carbon* **2007,** *45* (10), 2017-2021.
76. Bhuyan, M. S. A.; Uddin, M. N.; Islam, M. M.; Bipasha, F. A.; Hossain, S. S., Synthesis of graphene. *International Nano Letters* **2016,** *6*, 65-83.
77. Munoz, R.; Gómez-Aleixandre, C., Review of CVD synthesis of graphene. *Chemical Vapor Deposition* **2013,** *19* (10-11-12), 297-322.
78. Reina, A.; Jia, X.; Ho, J.; Nezich, D.; Son, H.; Bulovic, V.; Dresselhaus, M. S.; Kong, J., Large Area, Few-Layer Graphene Films on Arbitrary Substrates by Chemical Vapor Deposition. *Nano Letters* **2009,** *9* (1), 30-35.
79. Yu, Q.; Lian, J.; Siriponglert, S.; Li, H.; Chen, Y. P.; Pei, S.-S., Graphene segregated on Ni surfaces and transferred to insulators. *Applied Physics Letters* **2008,** *93* (11), 113103.
80. Wei, D.; Liu, Y.; Wang, Y.; Zhang, H.; Huang, L.; Yu, G., Synthesis of N-Doped Graphene by Chemical Vapor Deposition and Its Electrical Properties. *Nano Letters* **2009,** *9* (5), 1752-1758.
81. Lang, B., A LEED study of the deposition of carbon on platinum crystal surfaces. *Surface Science* **1975,** *53* (1), 317-329.
82. Vallés, C.; Drummond, C.; Saadaoui, H.; Furtado, C. A.; He, M.; Roubeau, O.; Ortolani, L.; Monthioux, M.; Pénicaud, A., Solutions of Negatively Charged Graphene Sheets and Ribbons. *Journal of the American Chemical Society* **2008,** *130* (47), 15802-15804.
83. Brodie, B. C., XIII. On the atomic weight of graphite. *Philosophical Transactions of the Royal Society of London* **1859,** *149*, 249-259.
84. Krishnamoorthy, K.; Veerapandian, M.; Yun, K.; Kim, S.-J., The chemical and structural analysis of graphene oxide with different degrees of oxidation. *Carbon* **2013,** *53*, 38-49.
85. Botas, C.; Álvarez, P.; Blanco, P.; Granda, M.; Blanco, C.; Santamaría, R.; Romasanta, L. J.; Verdejo, R.; López-Manchado, M. A.; Menéndez, R., Graphene materials with different structures prepared from the same graphite by the Hummers and Brodie methods. *Carbon* **2013,** *65*, 156-164.
86. Dreyer, D. R.; Park, S.; Bielawski, C. W.; Ruoff, R. S., The chemistry of graphene oxide. *Chemical Society Reviews* **2010,** *39* (1), 228-240.
87. Adetayo, A.; Runsewe, D., Synthesis and Fabrication of Graphene and Graphene Oxide: A Review. *Open Journal of Composite Materials* **2019,** *09*, 207-229.
88. Marcano, D. C.; Kosynkin, D. V.; Berlin, J. M.; Sinitskii, A.; Sun, Z.; Slesarev, A.; Alemany, L. B.; Lu, W.; Tour, J. M., Improved Synthesis of Graphene Oxide. *ACS Nano* **2010,** *4* (8), 4806-4814.

89. Wei, D.; Grande, L.; Chundi, V.; White, R.; Bower, C.; Andrew, P.; Ryhänen, T., Graphene from electrochemical exfoliation and its direct applications in enhanced energy storage devices. *Chemical communications* **2012,** *48* (9), 1239-1241.
90. Hernandez, Y.; Nicolosi, V.; Lotya, M.; Blighe, F. M.; Sun, Z.; De, S.; McGovern, I. T.; Holland, B.; Byrne, M.; Gun'Ko, Y. K., High-yield production of graphene by liquid-phase exfoliation of graphite. *Nature nanotechnology* **2008,** *3* (9), 563-568.
91. Low, C.; Walsh, F.; Chakrabarti, M.; Hashim, M.; Hussain, M., Electrochemical approaches to the production of graphene flakes and their potential applications. *Carbon* **2013,** *54*, 1-21.
92. Liu, J.; Poh, C. K.; Zhan, D.; Lai, L.; Lim, S. H.; Wang, L.; Liu, X.; Gopal Sahoo, N.; Li, C.; Shen, Z.; Lin, J., Improved synthesis of graphene flakes from the multiple electrochemical exfoliation of graphite rod. *Nano Energy* **2013,** *2* (3), 377-386.
93. Yu, P.; Lowe, S. E.; Simon, G. P.; Zhong, Y. L., Electrochemical exfoliation of graphite and production of functional graphene. *Current opinion in colloid & interface science* **2015,** *20* (5-6), 329-338.
94. Wang, J.; Manga, K. K.; Bao, Q.; Loh, K. P., High-yield synthesis of few-layer graphene flakes through electrochemical expansion of graphite in propylene carbonate electrolyte. *Journal of the American Chemical Society* **2011,** *133* (23), 8888-8891.
95. Ambrosi, A.; Pumera, M., Electrochemically Exfoliated Graphene and Graphene Oxide for Energy Storage and Electrochemistry Applications. *Chemistry – A European Journal* **2016,** *22* (1), 153-159.
96. Lei, Y.; Madalena, L. d. S.; Ossonon, B. D.; Junior, F. E. B.; Chen, J.; Lanza, M. R.; Tavares, A. C., One-Step Synthesis of Aminobenzoic Acid Functionalized Graphene Oxide by Electrochemical Exfoliation of Graphite for Oxygen Reduction to Hydrogen Peroxide and Supercapacitors. *Molecules* **2022,** *27* (21), 7629.
97. Munuera, J.; Paredes, J.; Villar-Rodil, S.; Ayán-Varela, M.; Pagán, A.; Aznar-Cervantes, S.; Cenis, J.; Martínez-Alonso, A.; Tascón, J., High quality, low oxygen content and biocompatible graphene nanosheets obtained by anodic exfoliation of different graphite types. *Carbon* **2015,** *94*, 729-739.
98. Sevilla, M.; Ferrero, G. A.; Fuertes, A. B., Aqueous dispersions of graphene from electrochemically exfoliated graphite. *Chemistry–A European Journal* **2016,** *22* (48), 17351-17358.
99. Chen, K.; Xue, D.; Komarneni, S., Nanoclay assisted electrochemical exfoliation of pencil core to high conductive graphene thin-film electrode. *Journal of colloid and interface science* **2017,** *487*, 156-161.
100. Huang, X.; Li, S.; Qi, Z.; Zhang, W.; Ye, W.; Fang, Y., Low defect concentration few-layer graphene using a two-step electrochemical exfoliation. *Nanotechnology* **2015,** *26* (10), 105602.
101. MK, P. K.; Shanthini, S.; Srivastava, C., Electrochemical exfoliation of graphite for producing graphene using saccharin. *Rsc Advances* **2015,** *5* (66), 53865-53869.
102. Liang, Z.; Chen, J.; Tian, W.; Liu, Y.; Chen, M.; Cao, D., Preparation of multi-function graphene materials through electrode-distance controlled electrochemical exfoliation. *Nanotechnology* **2022,** *33* (37), 375601.
103. Abdelkader, A. M.; Kinloch, I. A.; Dryfe, R. A., Continuous electrochemical exfoliation of micrometer-sized graphene using synergistic ion intercalations and organic solvents. *ACS applied materials & interfaces* **2014,** *6* (3), 1632-1639.
104. Zhou, M.; Tang, J.; Cheng, Q.; Xu, G.; Cui, P.; Qin, L.-C., Few-layer graphene obtained by electrochemical exfoliation of graphite cathode. *Chemical Physics Letters* **2013,** *572*, 61-65.
105. Wu, L.; Li, W.; Li, P.; Liao, S.; Qiu, S.; Chen, M.; Guo, Y.; Li, Q.; Zhu, C.; Liu, L., Powder, Paper and Foam of Few-Layer Graphene Prepared in High Yield by Electrochemical Intercalation Exfoliation of Expanded Graphite. *Small* **2014,** *10* (7), 1421-1429.
106. Liu, J.; Poh, C. K.; Zhan, D.; Lai, L.; Lim, S. H.; Wang, L.; Liu, X.; Sahoo, N. G.; Li, C.; Shen, Z., Improved synthesis of graphene flakes from the multiple electrochemical exfoliation of graphite rod. *Nano energy* **2013,** *2* (3), 377-386.

107. Liu, J.; Yang, H.; Zhen, S. G.; Poh, C. K.; Chaurasia, A.; Luo, J.; Wu, X.; Yeow, E. K. L.; Sahoo, N. G.; Lin, J., A green approach to the synthesis of high-quality graphene oxide flakes via electrochemical exfoliation of pencil core. *Rsc Advances* **2013,** *3* (29), 11745-11750.
108. Imran, H.; Manikandan, P. N.; Dharuman, V., Facile and green synthesis of graphene oxide by electrical exfoliation of pencil graphite and gold nanoparticle for non-enzymatic simultaneous sensing of ascorbic acid, dopamine and uric acid. *RSC Advances* **2015,** *5* (78), 63513-63520.
109. Rao, K. S.; Senthilnathan, J.; Liu, Y.-F.; Yoshimura, M., Role of peroxide ions in formation of graphene nanosheets by electrochemical exfoliation of graphite. *Scientific reports* **2014,** *4* (1), 4237.
110. Tripathi, P.; Patel, C.; Prakash, R.; Shaz, M.; Srivastava, O., Synthesis of high-quality graphene through electrochemical exfoliation of graphite in alkaline electrolyte. *arXiv preprint arXiv:1310.7371* **2013**.
111. Fan, X.; Peng, W.; Li, Y.; Li, X.; Wang, S.; Zhang, G.; Zhang, F., Deoxygenation of exfoliated graphite oxide under alkaline conditions: a green route to graphene preparation. *Advanced Materials* **2008,** *20* (23), 4490-4493.
112. Munuera, J.; Paredes, J.; Villar-Rodil, S.; Castro-Muñiz, A.; Martínez-Alonso, A.; Tascón, J., High quality, low-oxidized graphene via anodic exfoliation with table salt as an efficient oxidation-preventing co-electrolyte for water/oil remediation and capacitive energy storage applications. *Applied Materials Today* **2018,** *11*, 246-254.
113. Ejigu, A.; Fujisawa, K.; Spencer, B. F.; Wang, B.; Terrones, M.; Kinloch, I. A.; Dryfe, R. A., On the role of transition metal salts during electrochemical exfoliation of graphite: antioxidants or metal oxide decorators for energy storage applications. *Advanced Functional Materials* **2018,** *28* (48), 1804357.
114. Munuera, J.; Paredes, J.; Enterría, M.; Pagán, A.; Villar-Rodil, S.; Pereira, M.; Martins, J.; Figueiredo, J. L.; Cenis, J.; Martínez-Alonso, A., Electrochemical exfoliation of graphite in aqueous sodium halide electrolytes toward low oxygen content graphene for energy and environmental applications. *ACS applied materials & interfaces* **2017,** *9* (28), 24085-24099.
115. Shang, N. G.; Papakonstantinou, P.; Sharma, S.; Lubarsky, G.; Li, M.; McNeill, D. W.; Quinn, A. J.; Zhou, W.; Blackley, R., Controllable selective exfoliation of high-quality graphene nanosheets and nanodots by ionic liquid assisted grinding. *Chemical Communications* **2012,** *48* (13), 1877-1879.
116. Lu, J.; Yang, J.-x.; Wang, J.; Lim, A.; Wang, S.; Loh, K. P., One-pot synthesis of fluorescent carbon nanoribbons, nanoparticles, and graphene by the exfoliation of graphite in ionic liquids. *ACS nano* **2009,** *3* (8), 2367-2375.
117. Liu, N.; Luo, F.; Wu, H.; Liu, Y.; Zhang, C.; Chen, J., One-step ionic-liquid-assisted electrochemical synthesis of ionic-liquid-functionalized graphene sheets directly from graphite. *Advanced Functional Materials* **2008,** *18* (10), 1518-1525.
118. Munuera, J.; Paredes, J.; Villar-Rodil, S.; Ayán-Varela, M.; Martínez-Alonso, A.; Tascón, J., Electrolytic exfoliation of graphite in water with multifunctional electrolytes: en route towards high quality, oxide-free graphene flakes. *Nanoscale* **2016,** *8* (5), 2982-2998.
119. Li, C.; Xu, Y.-T.; Zhao, B.; Jiang, L.; Chen, S.-G.; Xu, J.-B.; Fu, X.-Z.; Sun, R.; Wong, C.-P., Flexible graphene electrothermal films made from electrochemically exfoliated graphite. *Journal of materials science* **2016,** *51*, 1043-1051.
120. Hamra, A.; Lim, H.; Chee, W.; Huang, N., Electro-exfoliating graphene from graphite for direct fabrication of supercapacitor. *Applied Surface Science* **2016,** *360*, 213-223.
121. Coroş, M.; Pogăcean, F.; Roşu, M.-C.; Socaci, C.; Borodi, G.; Mageruşan, L.; Biriş, A. R.; Pruneanu, S., Simple and cost-effective synthesis of graphene by electrochemical exfoliation of graphite rods. *Rsc Advances* **2016,** *6* (4), 2651-2661.
122. Sahoo, S. K.; Mallik, A., Synthesis and characterization of conductive few layered graphene nanosheets using an anionic electrochemical intercalation and exfoliation technique. *Journal of materials chemistry c* **2015,** *3* (41), 10870-10878.
123. Abdelkader, A.; Kinloch, I.; Dryfe, R. A., High-yield electro-oxidative preparation of graphene oxide. *Chemical Communications* **2014,** *50* (61), 8402-8404.

124. Zhou, F.; Huang, H.; Xiao, C.; Zheng, S.; Shi, X.; Qin, J.; Fu, Q.; Bao, X.; Feng, X.; Müllen, K., Electrochemically scalable production of fluorine-modified graphene for flexible and high-energy ionogel-based microsupercapacitors. *Journal of the American Chemical Society* **2018,** *140* (26), 8198-8205.
125. Yen, P.-J.; Ting, C.-C.; Chiu, Y.-C.; Tseng, T.-Y.; Hsu, Y.-J.; Wu, W.-W.; Wei, K.-H., Facile production of graphene nanosheets comprising nitrogen-doping through in situ cathodic plasma formation during electrochemical exfoliation. *Journal of Materials Chemistry C* **2017,** *5* (10), 2597-2602.
126. Kakaei, K.; Balavandi, A., Hierarchically porous fluorine-doped graphene nanosheets as efficient metal-free electrocatalyst for oxygen reduction in gas diffusion electrode. *Journal of colloid and interface science* **2017,** *490*, 819-824.
127. Thirumal, V.; Pandurangan, A.; Jayakumar, D.; Ilangovan, R., Modified solar power: electrochemical synthesis of Nitrogen doped few layer graphene for supercapacitor applications. *Journal of Materials Science: Materials in Electronics* **2016,** *27*, 3410-3419.
128. Gu, S.-Y.; Hsieh, C.-T.; Yuan, J.-Y.; Hsueh, J.-H.; Gandomi, Y. A., Amino-functionalization of graphene nanosheets by electrochemical exfoliation technique. *Diamond and Related Materials* **2018,** *87*, 99-106.
129. Yang, Y.; Shi, W.; Zhang, R.; Luan, C.; Zeng, Q.; Wang, C.; Li, S.; Huang, Z.; Liao, H.; Ji, X., Electrochemical exfoliation of graphite into nitrogen-doped graphene in glycine solution and its energy storage properties. *Electrochimica Acta* **2016,** *204*, 100-107.
130. Mooste, M.; Kibena-Põldsepp, E.; Ossonon, B. D.; Bélanger, D.; Tammeveski, K., Oxygen reduction on graphene sheets functionalised by anthraquinone diazonium compound during electrochemical exfoliation of graphite. *Electrochimica Acta* **2018,** *267*, 246-254.
131. Ejigu, A.; Kinloch, I. A.; Dryfe, R. A., Single stage simultaneous electrochemical exfoliation and functionalization of graphene. *ACS applied materials & interfaces* **2017,** *9* (1), 710-721.
132. Ossonon, B. D.; Tavares, A. C., Innovative approach for the synthesis of graphene/MnO2 nanocomposites and their electrochemical behavior. *Electrochemical Science Advances* **2022,** *2* (4), 2100029.
133. Wang, J.; Zhang, H.; Wang, C.; Zhang, Y.; Wang, J.; Zhao, H.; Cheng, M.; Li, A.; Wang, J., Co-synthesis of atomic Fe and few-layer graphene towards superior ORR electrocatalyst. *Energy Storage Materials* **2018,** *12*, 1-7.
134. Ejigu, A.; Miller, B.; Kinloch, I. A.; Dryfe, R. A., Optimisation of electrolytic solvents for simultaneous electrochemical exfoliation and functionalisation of graphene with metal nanostructures. *Carbon* **2018,** *128*, 257-266.
135. Zhao, B.; Jiang, L.; Zeng, X.; Zhang, K.; Yuen, M. M.; Xu, J.-B.; Fu, X.-Z.; Sun, R.; Wong, C.-P., A highly thermally conductive electrode for lithium ion batteries. *Journal of Materials Chemistry A* **2016,** *4* (38), 14595-14604.
136. Hsieh, Y.-P.; Chiang, W.-Y.; Tsai, S.-L.; Hofmann, M., Scalable production of graphene with tunable and stable doping by electrochemical intercalation and exfoliation. *Physical Chemistry Chemical Physics* **2015,** *18* (1), 339-343.
137. Ananthanarayanan, A.; Wang, X.; Routh, P.; Sana, B.; Lim, S.; Kim, D. H.; Lim, K. H.; Li, J.; Chen, P., Facile synthesis of graphene quantum dots from 3D graphene and their application for Fe3+ sensing. *Advanced Functional Materials* **2014,** *24* (20), 3021-3026.
138. Lu, X.; Cai, M.; Wu, X.; Zhang, Y.; Li, S.; Liao, S.; Lu, X., Controllable Synthesis of 2D Materials by Electrochemical Exfoliation for Energy Storage and Conversion Application. *Small* **2022**, 2206702.
139. Rajendran, J.; Reshetilov, A. N.; Sundramoorthy, A. K., An electrochemically exfoliated graphene/poly (3, 4-ethylenedioxythiophene) nanocomposite-based electrochemical sensor for the detection of nicotine. *Materials Advances* **2021,** *2* (10), 3336-3345.
140. CHAPTER 1 - Sensor Fundamentals. In *Sensor Technology Handbook*, Wilson, J. S., Ed. Newnes: Burlington, 2005; pp 1-20.

141. Lee, Y. H.; Mutharasan, R., CHAPTER 6 - Biosensors. In *Sensor Technology Handbook*, Wilson, J. S., Ed. Newnes: Burlington, 2005; pp 161-180.
142. Grieshaber, D.; MacKenzie, R.; Vörös, J.; Reimhult, E., Electrochemical Biosensors - Sensor Principles and Architectures. *Sensors* **2008,** *8* (3), 1400-1458.
143. McCreery, R. L., Advanced Carbon Electrode Materials for Molecular Electrochemistry. *Chemical Reviews* **2008,** *108* (7), 2646-2687.
144. Son, M. H.; Park, S. W.; Sagong, H. Y.; Jung, Y. K., Recent Advances in Electrochemical and Optical Biosensors for Cancer Biomarker Detection. *BioChip Journal* **2022**.
145. Ellington, A. D.; Szostak, J. W., In vitro selection of RNA molecules that bind specific ligands. *Nature* **1990,** *346* (6287), 818-822.
146. Mascini, M.; Palchetti, I.; Tombelli, S., Nucleic Acid and Peptide Aptamers: Fundamentals and Bioanalytical Aspects. *Angewandte Chemie International Edition* **2012,** *51* (6), 1316-1332.
147. Li, Y.; Qi, H.; Peng, Y.; Yang, J.; Zhang, C., Electrogenerated chemiluminescence aptamer-based biosensor for the determination of cocaine. *Electrochemistry Communications* **2007,** *9* (10), 2571-2575.
148. Mokhtarzadeh, A.; Ezzati Nazhad Dolatabadi, J.; Abnous, K.; de la Guardia, M.; Ramezani, M., Nanomaterial-based cocaine aptasensors. *Biosensors and Bioelectronics* **2015,** *68*, 95-106.
149. Khoshnevisan, K.; Maleki, H.; Honarvarfard, E.; Baharifar, H.; Gholami, M.; Faridbod, F.; Larijani, B.; Faridi Majidi, R.; Khorramizadeh, M. R., Nanomaterial based electrochemical sensing of the biomarker serotonin: a comprehensive review. *Microchimica Acta* **2019,** *186*, 1-21.
150. Allen, M. J.; Tung, V. C.; Kaner, R. B., Honeycomb carbon: a review of graphene. *Chemical reviews* **2010,** *110* (1), 132-145.
151. Eissa, S.; N'diaye, J.; Brisebois, P.; Izquierdo, R.; Tavares, A. C.; Siaj, M., Probing the influence of graphene oxide sheets size on the performance of label-free electrochemical biosensors. *Scientific Reports* **2020,** *10* (1), 13612.
152. Akhavan, O.; Ghaderi, E.; Rahighi, R., Toward single-DNA electrochemical biosensing by graphene nanowalls. *ACS nano* **2012,** *6* (4), 2904-2916.
153. Mohanty, N.; Berry, V., Graphene-Based Single-Bacterium Resolution Biodevice and DNA Transistor: Interfacing Graphene Derivatives with Nanoscale and Microscale Biocomponents. *Nano Letters* **2008,** *8* (12), 4469-4476.
154. Peña-Bahamonde, J.; Nguyen, H. N.; Fanourakis, S. K.; Rodrigues, D. F., Recent advances in graphene-based biosensor technology with applications in life sciences. *Journal of Nanobiotechnology* **2018,** *16* (1), 75.
155. Yang, Y.; Asiri, A. M.; Tang, Z.; Du, D.; Lin, Y., Graphene based materials for biomedical applications. *Materials Today* **2013,** *16* (10), 365-373.
156. Du, D.; Yang, Y.; Lin, Y., Graphene-based materials for biosensing and bioimaging. *MRS Bulletin* **2012,** *37* (12), 1290-1296.
157. Zhang, H.; Li, Z.-f.; Snyder, A.; Xie, J.; Stanciu, L. A., Functionalized graphene oxide for the fabrication of paraoxon biosensors. *Analytica Chimica Acta* **2014,** *827*, 86-94.
158. Hirsh, S. L.; Bilek, M. M. M.; Nosworthy, N. J.; Kondyurin, A.; dos Remedios, C. G.; McKenzie, D. R., A Comparison of Covalent Immobilization and Physical Adsorption of a Cellulase Enzyme Mixture. *Langmuir* **2010,** *26* (17), 14380-14388.
159. Mkhoyan, K. A.; Contryman, A. W.; Silcox, J.; Stewart, D. A.; Eda, G.; Mattevi, C.; Miller, S.; Chhowalla, M., Atomic and electronic structure of graphene-oxide. *Nano letters* **2009,** *9* (3), 1058-1063.
160. Simon, P.; Gogotsi, Y., Materials for electrochemical capacitors. *Nature materials* **2008,** *7* (11), 845-854.
161. Jeffery, D. J., Capacitors, capacitance, and dielectrics. **2008**.
162. Miller, J. R.; Simon, P., Electrochemical capacitors for energy management. *science* **2008,** *321* (5889), 651-652.
163. Pandolfo, A. G.; Hollenkamp, A. F., Carbon properties and their role in supercapacitors. *Journal of power sources* **2006,** *157* (1), 11-27.

164. Tehrani, Z.; Thomas, D. J.; Korochkina, T.; Phillips, C. O.; Lupo, D.; Lehtimäki, S.; O'Mahony, J.; Gethin, D. T., Large-area printed supercapacitor technology for low-cost domestic green energy storage. *Energy* **2017,** *118*, 1313-1321.
165. Jiang, Y.; Liu, J., Definitions of pseudocapacitive materials: a brief review. *Energy & Environmental Materials* **2019,** *2* (1), 30-37.
166. Pandolfo, T.; Ruiz, V.; Sivakkumar, S.; Nerkar, J., Supercapacitors: Materials, Systems, and Applications. *Australia: John Wiley & Sons* **2013**, 69-75.
167. Wang, F.; Xiao, S.; Hou, Y.; Hu, C.; Liu, L.; Wu, Y., Electrode materials for aqueous asymmetric supercapacitors. *Rsc Advances* **2013,** *3* (32), 13059-13084.
168. Aravindan, V.; Gnanaraj, J.; Lee, Y.-S.; Madhavi, S., Insertion-type electrodes for nonaqueous Li-ion capacitors. *Chemical reviews* **2014,** *114* (23), 11619-11635.
169. Wang, F.; Wu, X.; Yuan, X.; Liu, Z.; Zhang, Y.; Fu, L.; Zhu, Y.; Zhou, Q.; Wu, Y.; Huang, W., Latest advances in supercapacitors: from new electrode materials to novel device designs. *Chemical Society Reviews* **2017,** *46* (22), 6816-6854.
170. Liu, L.; Niu, Z.; Chen, J., Unconventional supercapacitors from nanocarbon-based electrode materials to device configurations. *Chemical Society Reviews* **2016,** *45* (15), 4340-4363.
171. Shao, Y.; El-Kady, M. F.; Sun, J.; Li, Y.; Zhang, Q.; Zhu, M.; Wang, H.; Dunn, B.; Kaner, R. B., Design and Mechanisms of Asymmetric Supercapacitors. *Chemical Reviews* **2018,** *118* (18), 9233-9280.
172. Zhang, L. L.; Zhao, X., Carbon-based materials as supercapacitor electrodes. *Chemical Society Reviews* **2009,** *38* (9), 2520-2531.
173. Conway, B.; Supercapacitors, I. E., Scientific fundamentals and technological applications. *Electrochemical Supercapacitors* **1999,** *698*.
174. Trasatti, S.; Buzzanca, G., Ruthenium dioxide: A new interesting electrode material. Solid state structure and electrochemical behaviour. *Journal of electroanalytical chemistry and interfacial electrochemistry* **1971,** *29* (2), A1-A5.
175. Augustyn, V.; Simon, P.; Dunn, B., Pseudocapacitive oxide materials for high-rate electrochemical energy storage. *Energy & Environmental Science* **2014,** *7* (5), 1597-1614.
176. Long, J., To Be or not to Be pseudocapacitive. *J. Electrochem. Soc.* **2015,** *162*, A5185-A5189.
177. Conway, B., Two-dimensional and quasi-two-dimensional isotherms for Li intercalation and upd processes at surfaces. *Electrochimica acta* **1993,** *38* (9), 1249-1258.
178. Sudha, V.; Sangaranarayanan, M., Underpotential deposition of metals: structural and thermodynamic considerations. *The Journal of Physical Chemistry B* **2002,** *106* (10), 2699-2707.
179. Bi, R.-R.; Wu, X.-L.; Cao, F.-F.; Jiang, L.-Y.; Guo, Y.-G.; Wan, L.-J., Highly dispersed RuO2 nanoparticles on carbon nanotubes: facile synthesis and enhanced supercapacitance performance. *The Journal of Physical Chemistry C* **2010,** *114* (6), 2448-2451.
180. Kong, L.; Zhang, C.; Zhang, S.; Wang, J.; Cai, R.; Lv, C.; Qiao, W.; Ling, L.; Long, D., High-power and high-energy asymmetric supercapacitors based on Li+-intercalation into a T-Nb 2 O 5/graphene pseudocapacitive electrode. *Journal of Materials Chemistry A* **2014,** *2* (42), 17962-17970.
181. Bandaru, P.; Yamada, H.; Narayanan, R.; Hoefer, M., Charge transfer and storage in nanostructures. *Materials Science and Engineering: R: Reports* **2015,** *96*, 1-69.
182. Permatasari, F. A.; Irham, M. A.; Bisri, S. Z.; Iskandar, F., Carbon-Based Quantum Dots for Supercapacitors: Recent Advances and Future Challenges. *Nanomaterials* **2021,** *11* (1), 91.
183. Ke, Q.; Wang, J., Graphene-based materials for supercapacitor electrodes – A review. *Journal of Materiomics* **2016,** *2* (1), 37-54.
184. Lemine, A. S.; Zagho, M. M.; Altahtamouni, T. M.; Bensalah, N., Graphene a promising electrode material for supercapacitors—A review. *International Journal of Energy Research* **2018,** *42* (14), 4284-4300.
185. Yang, W.; Ni, M.; Ren, X.; Tian, Y.; Li, N.; Su, Y.; Zhang, X., Graphene in Supercapacitor Applications. *Current Opinion in Colloid & Interface Science* **2015,** *20* (5), 416-428.

186. Zhang, W.; Zhang, Y.; Tian, Y.; Yang, Z.; Xiao, Q.; Guo, X.; Jing, L.; Zhao, Y.; Yan, Y.; Feng, J., Insight into the capacitive properties of reduced graphene oxide. *ACS applied materials & interfaces* **2014,** *6* (4), 2248-2254.
187. Zabihinpour, M.; Ghenaatian, H., A novel multilayered architecture of graphene oxide nanosheets for high supercapacitive performance electrode material. *Synthetic metals* **2013,** *175*, 62-67.
188. Yang, J.; Jo, M. R.; Kang, M.; Huh, Y. S.; Jung, H.; Kang, Y.-M., Rapid and controllable synthesis of nitrogen doped reduced graphene oxide using microwave-assisted hydrothermal reaction for high power-density supercapacitors. *Carbon* **2014,** *73*, 106-113.
189. Akhtar, K.; Khan, S. A.; Khan, S. B.; Asiri, A. M., Scanning Electron Microscopy: Principle and Applications in Nanomaterials Characterization. In *Handbook of Materials Characterization*, Sharma, S. K., Ed. Springer International Publishing: Cham, 2018; pp 113-145.
190. Szynkowska, M. I., MICROSCOPY TECHNIQUES | Scanning Electron Microscopy. In *Encyclopedia of Analytical Science (Second Edition)*, Worsfold, P.; Townshend, A.; Poole, C., Eds. Elsevier: Oxford, 2005; pp 134-143.
191. Kannan, M., Transmission electron microscope—Principle, components and applications. *A textbook on fundamentals and applications of nanotechnology* **2018**, 93-102.
192. Soumia, S. A.; Messali, Z.; Ouahabi, A.; Trepout, S.; Messaoudi, C.; Marco, S., Nonparametric Denoising Methods Based on Contourlet Transform with Sharp Frequency Localization: Application to Low Exposure Time Electron Microscopy Images. *Entropy* **2015,** *17*, 3461-3478.
193. Epp, J., 4 - X-ray diffraction (XRD) techniques for materials characterization. In *Materials Characterization Using Nondestructive Evaluation (NDE) Methods*, Hübschen, G.; Altpeter, I.; Tschuncky, R.; Herrmann, H.-G., Eds. Woodhead Publishing: 2016; pp 81-124.
194. Nasir, S.; Hussein, M.; Zainal, Z.; Yusof, N.; Zobir, S.; Alibe, I., Potential Valorization of By-product Materials from Oil Palm: A review of Alternative and Sustainable Carbon Sources for Carbon-based Nanomaterials Synthesis. *Bioresources* **2018,** *14*.
195. Guy, O. J.; Walker, K.-A. D., Chapter 4 - Graphene Functionalization for Biosensor Applications. In *Silicon Carbide Biotechnology (Second Edition)*, Saddow, S. E., Ed. Elsevier: 2016; pp 85-141.
196. Baranton, S.; Bélanger, D., Electrochemical derivatization of carbon surface by reduction of in situ generated diazonium cations. *The Journal of Physical Chemistry B* **2005,** *109* (51), 24401-24410.
197. Taghizadeh, A.; Leffers, U.; Pedersen, T. G.; Thygesen, K. S., A library of ab initio Raman spectra for automated identification of 2D materials. *Nature Communications* **2020,** *11* (1), 3011.
198. Wu, J.-B.; Lin, M.-L.; Cong, X.; Liu, H.-N.; Tan, P.-H., Raman spectroscopy of graphene-based materials and its applications in related devices. *Chemical Society Reviews* **2018,** *47* (5), 1822-1873.
199. Undavalli, V. K.; Ling, C.; Khandelwal, B., Chapter 6 - Impact of alternative fuels and properties on elastomer compatibility. In *Aviation Fuels*, Khandelwal, B., Ed. Academic Press: 2021; pp 113-132.
200. Savinell, R. F.; Zeller, R. L.; Adams, J. A., Electrochemically Active Surface Area: Voltammetric Charge Correlations for Ruthenium and Iridium Dioxide Electrodes. *Journal of The Electrochemical Society* **1990,** *137* (2), 489-494.
201. Klingler, R. J.; Kochi, J. K., Electron-transfer kinetics from cyclic voltammetry. Quantitative description of electrochemical reversibility. *The Journal of Physical Chemistry* **1981,** *85* (12), 1731-1741.
202. Zoski, C. G., *Handbook of electrochemistry*. Elsevier: 2006.
203. Konopka, S. J.; McDuffie, B., Diffusion coefficients of ferri- and ferrocyanide ions in aqueous media, using twin-electrode thin-layer electrochemistry. *Analytical Chemistry* **1970,** *42* (14), 1741-1746.
204. Nicholson, R. S., Theory and Application of Cyclic Voltammetry for Measurement of Electrode Reaction Kinetics. *Analytical Chemistry* **1965,** *37* (11), 1351-1355.
205. Lavagnini, I.; Antiochia, R.; Magno, F., An Extended Method for the Practical Evaluation of the Standard Rate Constant from Cyclic Voltammetric Data. *Electroanalysis* **2004,** *16* (6), 505-506.
206. Bannwarth, W.; Knorr, R., Formation of carboxamides with N, N, N′, N′-tetramethyl (succinimido) uronium tetrafluoroborate in aqueous/organic solvent systems. *Tetrahedron letters* **1991,** *32* (9), 1157-1160.

207. Cline, K. K.; McDermott, M. T.; McCreery, R. L., Anomalously Slow Electron Transfer at Ordered Graphite Electrodes: Influence of Electronic Factors and Reactive Sites. *The Journal of Physical Chemistry* **1994,** *98* (20), 5314-5319.
208. Gilliam, R. J.; Graydon, J. W.; Kirk, D. W.; Thorpe, S. J., A review of specific conductivities of potassium hydroxide solutions for various concentrations and temperatures. *International Journal of Hydrogen Energy* **2007,** *32* (3), 359-364.
209. Novoselov, K. S.; Geim, A. K.; Morozov, S. V.; Jiang, D.; Zhang, Y.; Dubonos, S. V.; Grigorieva, I. V.; Firsov, A. A., Electric Field Effect in Atomically Thin Carbon Films. *Science* **2004,** *306* (5696), 666-669.
210. Ismach, A.; Druzgalski, C.; Penwell, S.; Schwartzberg, A.; Zheng, M.; Javey, A.; Bokor, J.; Zhang, Y., Direct chemical vapor deposition of graphene on dielectric surfaces. *Nano Lett* **2010,** *10* (5), 1542-8.
211. Ji, X.; Banks, C. E.; Crossley, A.; Compton, R. G., Oxygenated Edge Plane Sites Slow the Electron Transfer of the Ferro-/Ferricyanide Redox Couple at Graphite Electrodes. *ChemPhysChem* **2006,** *7* (6), 1337-1344.
212. Davies, T. J.; Hyde, M. E.; Compton, R. G., Nanotrench Arrays Reveal Insight into Graphite Electrochemistry. *Angewandte Chemie International Edition* **2005,** *44* (32), 5121-5126.
213. Kampouris, D. K.; Banks, C. E., Exploring the physicoelectrochemical properties of graphene. *Chemical Communications* **2010,** *46* (47), 8986-8988.
214. Ambrosi, A.; Bonanni, A.; Sofer, Z.; Cross, J. S.; Pumera, M., Electrochemistry at Chemically Modified Graphenes. *Chemistry – A European Journal* **2011,** *17* (38), 10763-10770.
215. Pumera, M.; Sasaki, T.; Iwai, H., Relationship between Carbon Nanotube Structure and Electrochemical Behavior: Heterogeneous Electron Transfer at Electrochemically Activated Carbon Nanotubes. *Chemistry – An Asian Journal* **2008,** *3* (12), 2046-2055.
216. Chou, A.; Böcking, T.; Singh, N. K.; Gooding, J. J., Demonstration of the importance of oxygenated species at the ends of carbon nanotubes for their favourable electrochemical properties. *Chemical Communications* **2005,** (7), 842-844.
217. Chen, L.; Tang, Y.; Wang, K.; Liu, C.; Luo, S., Direct electrodeposition of reduced graphene oxide on glassy carbon electrode and its electrochemical application. *Electrochemistry Communications* **2011,** *13* (2), 133-137.
218. Raj, M. A.; John, S. A., Fabrication of Electrochemically Reduced Graphene Oxide Films on Glassy Carbon Electrode by Self-Assembly Method and Their Electrocatalytic Application. *The Journal of Physical Chemistry C* **2013,** *117* (8), 4326-4335.
219. Robinson, J. T.; Perkins, F. K.; Snow, E. S.; Wei, Z.; Sheehan, P. E., Reduced Graphene Oxide Molecular Sensors. *Nano Letters* **2008,** *8* (10), 3137-3140.
220. Elshafey, R.; Brisebois, P.; Abdulkarim, H.; Izquierdo, R.; Tavares, A. C.; Siaj, M., Effect of & x11c; raphene Oxide Sheet Size on the Response of a Label-Free Voltammetric Immunosensor for Cancer Marker VEGF. *ELECTROANALYSIS* **2020**.
221. Menanteau, T.; Dias, M. n.; Levillain, E.; Downard, A. J.; Breton, T., Electrografting via diazonium chemistry: the key role of the aryl substituent in the layer growth mechanism. *The Journal of Physical Chemistry C* **2016,** *120* (8), 4423-4429.
222. Feng, H.; Cheng, R.; Zhao, X.; Duan, X.; Li, J., A low-temperature method to produce highly reduced graphene oxide. *Nature Communications* **2013,** *4* (1), 1539.
223. Oturan, N.; Oturan, M. A., Electro-Fenton process: Background, new developments, and applications. In *Electrochemical Water and Wastewater Treatment*, Elsevier: 2018; pp 193-221.
224. Yang, D.; Velamakanni, A.; Bozoklu, G.; Park, S.; Stoller, M.; Piner, R. D.; Stankovich, S.; Jung, I.; Field, D. A.; Ventrice, C. A.; Ruoff, R. S., Chemical analysis of graphene oxide films after heat and chemical treatments by X-ray photoelectron and Micro-Raman spectroscopy. *Carbon* **2009,** *47* (1), 145-152.

225. Ganguly, A.; Sharma, S.; Papakonstantinou, P.; Hamilton, J., Probing the Thermal Deoxygenation of Graphene Oxide Using High-Resolution In Situ X-ray-Based Spectroscopies. *The Journal of Physical Chemistry C* **2011,** *115* (34), 17009-17019.
226. Tuinstra, F.; Koenig, J. L., Raman Spectrum of Graphite. *The Journal of Chemical Physics* **1970,** *53* (3), 1126-1130.
227. Krishnamoorthy, K.; Veerapandian, M.; Yun, K.; Kim, S. J., The chemical and structural analysis of graphene oxide with different degrees of oxidation. *Carbon* **2013,** *53*, 38-49.
228. Graf, D.; Molitor, F.; Ensslin, K.; Stampfer, C.; Jungen, A.; Hierold, C.; Wirtz, L., Spatially Resolved Raman Spectroscopy of Single- and Few-Layer Graphene. *Nano Letters* **2007,** *7* (2), 238-242.
229. Ferrari, A. C.; Meyer, J.; Scardaci, V.; Casiraghi, C.; Lazzeri, M.; Mauri, F.; Piscanec, S.; Jiang, D.; Novoselov, K.; Roth, S., Raman spectrum of graphene and graphene layers. *Physical review letters* **2006,** *97* (18), 187401.
230. Prikhod'ko, N.; Mansurov, Z.; Auelkhankyzy, M.; Lesbaev, B.; Nazhipkyzy, M.; Smagulova, G., Flame synthesis of graphene layers at low pressure. *Russian Journal of Physical Chemistry B* **2015,** *9* (5), 743-747.
231. Pimenta, M. A.; Dresselhaus, G.; Dresselhaus, M. S.; Cançado, L. G.; Jorio, A.; Saito, R., Studying disorder in graphite-based systems by Raman spectroscopy. *Physical Chemistry Chemical Physics* **2007,** *9* (11), 1276-1290.
232. Lucchese, M. M.; Stavale, F.; Ferreira, E. H. M.; Vilani, C.; Moutinho, M. V. O.; Capaz, R. B.; Achete, C. A.; Jorio, A., Quantifying ion-induced defects and Raman relaxation length in graphene. *Carbon* **2010,** *48* (5), 1592-1597.
233. Baranton, S.; Bélanger, D., In situ generation of diazonium cations in organic electrolyte for electrochemical modification of electrode surface. *Electrochimica Acta* **2008,** *53* (23), 6961-6967.
234. Zouaoui, N.; Ossonon, B. D.; Fan, M.; Mayilukila, D.; Garbarino, S.; de Silveira, G.; Botton, G. A.; Guay, D.; Tavares, A. C., Electroreduction of CO 2 to formate on amine modified Pb electrodes. *Journal of Materials Chemistry A* **2019,** *7* (18), 11272-11281.
235. Tang, L.; Wang, Y.; Li, Y.; Feng, H.; Lu, J.; Li, J., Preparation, Structure, and Electrochemical Properties of Reduced Graphene Sheet Films. *Advanced Functional Materials* **2009,** *19* (17), 2782-2789.
236. Randviir, E. P.; Brownson, D. A.; Metters, J. P.; Kadara, R. O.; Banks, C. E., The fabrication, characterisation and electrochemical investigation of screen-printed graphene electrodes. *Physical Chemistry Chemical Physics* **2014,** *16* (10), 4598-4611.
237. Bryson, A., The Effects of m-Substituents on the pKa Values of Anilines, and on the Stretching Frequencies of the N-H Bonds. *Journal of the American Chemical Society* **1960,** *82* (18), 4858-4862.
238. Compton, O. C.; An, Z.; Putz, K. W.; Hong, B. J.; Hauser, B. G.; Catherine Brinson, L.; Nguyen, S. T., Additive-free hydrogelation of graphene oxide by ultrasonication. *Carbon* **2012,** *50* (10), 3399-3406.
239. Oh, W.-C., The effect of thermal and ultrasonic treatment on formation of graphene oxide nanosheets. *Journal of The Korean Physical Society - J KOREAN PHYS SOC* **2010,** *56*.
240. Shinde, D. B.; Brenker, J.; Easton, C. D.; Tabor, R. F.; Neild, A.; Majumder, M., Shear Assisted Electrochemical Exfoliation of Graphite to Graphene. *Langmuir* **2016,** *32* (14), 3552-3559.
241. Sahoo, S. K.; Ratha, S.; Rout, C. S.; Mallik, A., Physicochemical properties and supercapacitor behavior of electrochemically synthesized few layered graphene nanosheets. *Journal of Solid State Electrochemistry* **2016,** *20* (12), 3415-3428.
242. Lee, Y. H.; Mutharasan, R., CHAPTER 1 - Sensor Fundamentals. In *Sensor Technology Handbook*, Wilson, J. S., Ed. Newnes: Burlington, 2005; pp 1-20.
243. Coroş, M.; Pruneanu, S.; Stefan-van Staden, R.-I., Review—Recent Progress in the Graphene-Based Electrochemical Sensors and Biosensors. *Journal of The Electrochemical Society* **2019,** *167* (3), 037528.
244. Kim, H. W.; Park, H.; Roh, J. S.; Shin, J. E.; Lee, T. H.; Zhang, L.; Cho, Y. H.; Yoon, H. W.; Bukas, V. J.; Guo, J., Carbon defect characterization of nitrogen-doped reduced graphene oxide

electrocatalysts for the two-electron oxygen reduction reaction. *Chemistry of Materials* **2019,** *31* (11), 3967-3973.
245. Kirchner, E.-M.; Hirsch, T., Recent developments in carbon-based two-dimensional materials: synthesis and modification aspects for electrochemical sensors. *Microchimica Acta* **2020,** *187* (8), 441.
246. Maccaferri, G.; Terzi, F.; Xia, Z.; Vulcano, F.; Liscio, A.; Palermo, V.; Zanardi, C., Highly sensitive amperometric sensor for morphine detection based on electrochemically exfoliated graphene oxide. Application in screening tests of urine samples. *Sensors and Actuators B: Chemical* **2019,** *281*, 739-745.
247. Habibi, B.; Pashazadeh, S.; Saghatforoush, L. A.; Pashazadeh, A., Direct electrochemical synthesis of the copper based metal-organic framework on/in the heteroatoms doped graphene/pencil graphite electrode: Highly sensitive and selective electrochemical sensor for sertraline hydrochloride. *Journal of Electroanalytical Chemistry* **2021,** *888*, 115210.
248. Rajendran, J.; Reshetilov, A. N.; Sundramoorthy, A. K., An electrochemically exfoliated graphene/poly(3,4-ethylenedioxythiophene) nanocomposite-based electrochemical sensor for the detection of nicotine. *Materials Advances* **2021,** *2* (10), 3336-3345.
249. Vázquez, A. R.; Neumann, C.; Borrelli, M.; Shi, H.; Kluge, M.; Abdel-Haq, W.; Lohe, M. R.; Gröber, C.; Röpert, A.; Turchanin, A., Scalable one-step production of electrochemically exfoliated graphene decorated with transition metal oxides for high-performance supercapacitors. *Nanoscale* **2021,** *13* (37), 15859-15868.
250. Jiang, B.; Wang, M.; Chen, Y.; Xie, J.; Xiang, Y., Highly sensitive electrochemical detection of cocaine on graphene/AuNP modified electrode via catalytic redox-recycling amplification. *Biosensors and Bioelectronics* **2012,** *32* (1), 305-308.
251. Roushani, M.; Shahdost-fard, F., A novel ultrasensitive aptasensor based on silver nanoparticles measured via enhanced voltammetric response of electrochemical reduction of riboflavin as redox probe for cocaine detection. *Sensors and Actuators B: Chemical* **2015,** *207*, 764-771.
252. Roushani, M.; Shahdost-fard, F., A highly selective and sensitive cocaine aptasensor based on covalent attachment of the aptamer-functionalized AuNPs onto nanocomposite as the support platform. *Analytica Chimica Acta* **2015,** *853*, 214-221.
253. Taghdisi, S. M.; Danesh, N. M.; Emrani, A. S.; Ramezani, M.; Abnous, K., A novel electrochemical aptasensor based on single-walled carbon nanotubes, gold electrode and complimentary strand of aptamer for ultrasensitive detection of cocaine. *Biosensors and Bioelectronics* **2015,** *73*, 245-250.
254. Yu, X.; Zhang, W.; Zhang, P.; Su, Z., Fabrication technologies and sensing applications of graphene-based composite films: Advances and challenges. *Biosensors and Bioelectronics* **2017,** *89*, 72-84.
255. Mohan, V. B.; Lau, K.-t.; Hui, D.; Bhattacharyya, D., Graphene-based materials and their composites: A review on production, applications and product limitations. *Composites Part B: Engineering* **2018,** *142*, 200-220.
256. Paladiya, C.; Kiani, A., Nano structured sensing surface: Significance in sensor fabrication. *Sensors and Actuators B: Chemical* **2018,** *268*, 494-511.
257. Kong, W.; Kum, H.; Bae, S.-H.; Shim, J.; Kim, H.; Kong, L.; Meng, Y.; Wang, K.; Kim, C.; Kim, J., Path towards graphene commercialization from lab to market. *Nature Nanotechnology* **2019,** *14* (10), 927-938.
258. Tavakkoli, N.; Soltani, N.; Mohammadi, F., A nanoporous gold-based electrochemical aptasensor for sensitive detection of cocaine. *RSC Adv* **2019,** *9* (25), 14296-14301.
259. Baker, B. R.; Lai, R. Y.; Wood, M. S.; Doctor, E. H.; Heeger, A. J.; Plaxco, K. W., An electronic, aptamer-based small-molecule sensor for the rapid, label-free detection of cocaine in adulterated samples and biological fluids. *Journal of the American Chemical Society* **2006,** *128* (10), 3138-3139.
260. Stojanovic, M. N.; de Prada, P.; Landry, D. W., Aptamer-Based Folding Fluorescent Sensor for Cocaine. *Journal of the American Chemical Society* **2001,** *123* (21), 4928-4931.

261. Gouget-Laemmel, A. C.; Yang, J.; Lodhi, M. A.; Siriwardena, A.; Aureau, D.; Boukherroub, R.; Chazalviel, J. N.; Ozanam, F.; Szunerits, S., Functionalization of Azide-Terminated Silicon Surfaces with Glycans Using Click Chemistry: XPS and FTIR Study. *The Journal of Physical Chemistry C* **2013,** *117* (1), 368-375.
262. Peñas-Sanjuán, A.; López-Garzón, R.; Domingo-García, M.; López-Garzón, F. J.; Melguizo, M.; Pérez-Mendoza, M., An efficient procedure to bond nanostructured nitrogen functionalities to carbon surfaces. *Carbon* **2012,** *50* (11), 3977-3986.
263. Lim, C. Y.; Owens, N. A.; Wampler, R. D.; Ying, Y.; Granger, J. H.; Porter, M. D.; Takahashi, M.; Shimazu, K., Succinimidyl Ester Surface Chemistry: Implications of the Competition between Aminolysis and Hydrolysis on Covalent Protein Immobilization. *Langmuir* **2014,** *30* (43), 12868-12878.
264. Zhang, G.; Sebastián, D.; Zhang, X.; Wei, Q.; Lo Vecchio, C.; Zhang, J.; Baglio, V.; Wang, W.; Sun, S.; Aricò, A. S.; Tavares, A. C., Engineering of a Low-Cost, Highly Active, and Durable Tantalate–Graphene Hybrid Electrocatalyst for Oxygen Reduction. *Advanced Energy Materials* **2020,** *10* (24), 2000075.
265. Long, G. L.; Winefordner, J. D., Limit of detection. A closer look at the IUPAC definition. *Analytical Chemistry* **1983,** *55* (7), 712A-724A.
266. Wen, Y.; Pei, H.; Wan, Y.; Su, Y.; Huang, Q.; Song, S.; Fan, C., DNA Nanostructure-Decorated Surfaces for Enhanced Aptamer-Target Binding and Electrochemical Cocaine Sensors. *Analytical Chemistry* **2011,** *83* (19), 7418-7423.
267. Roushani, M.; Shahdost-fard, F., An aptasensor for voltammetric and impedimetric determination of cocaine based on a glassy carbon electrode modified with platinum nanoparticles and using rutin as a redox probe. *Microchimica Acta* **2016,** *183* (1), 185-193.
268. Ismail, M.; Stevenson, D.; Costa, C.; Webb, R.; de Puit, M.; Bailey, M., Noninvasive Detection of Cocaine and Heroin Use with Single Fingerprints: Determination of an Environmental Cutoff. *Clinical Chemistry* **2018,** *64* (6), 909-917.
269. Amy Peaire, A. F., D'Arcy Smith, Doug Beirness, Edith Viel, Heather Copley, Report on Drug Screening Equipment. **2018,** (Canadian Society of Forensic Sciences Drugs and Driving Committee), 5.
270. Sachan, A.; Ilgu, M.; Kempema, A.; Kraus, G. A.; Nilsen-Hamilton, M., Specificity and Ligand Affinities of the Cocaine Aptamer: Impact of Structural Features and Physiological NaCl. *Analytical Chemistry* **2016,** *88* (15), 7715-7723.
271. Reinstein, O.; Yoo, M.; Han, C.; Palmo, T.; Beckham, S. A.; Wilce, M. C.; Johnson, P. E., Quinine binding by the cocaine-binding aptamer. Thermodynamic and hydrodynamic analysis of high-affinity binding of an off-target ligand. *Biochemistry* **2013,** *52* (48), 8652-8662.
272. Akbari jonous, Z.; Shayeh, J. S.; Yazdian, F.; Yadegari, A.; Hashemi, M.; Omidi, M., An electrochemical biosensor for prostate cancer biomarker detection using graphene oxide–gold nanostructures. *Engineering in life sciences* **2019,** *19* (3), 206-216.
273. Pothipor, C.; Jakmunee, J.; Bamrungsap, S.; Ounnunkad, K., An electrochemical biosensor for simultaneous detection of breast cancer clinically related microRNAs based on a gold nanoparticles/graphene quantum dots/graphene oxide film. *Analyst* **2021,** *146* (12), 4000-4009.
274. Tavakkoli, N.; Soltani, N.; Mohammadi, F., A nanoporous gold-based electrochemical aptasensor for sensitive detection of cocaine. *RSC advances* **2019,** *9* (25), 14296-14301.
275. Morales-Martínez, D.; González, F. J., A mechanistic approach to the electrografting of carbon surfaces and electrochemical properties of the grafted films – A critical review. *Electrochimica Acta* **2022,** *425*, 140693.
276. Hage, R.; Lienke, A., Applications of transition-metal catalysts to textile and wood-pulp bleaching. *Angewandte Chemie International Edition* **2006,** *45* (2), 206-222.
277. Šljukić, B.; Banks, C.; Compton, R., An overview of the electrochemical reduction of oxygen at carbon-based modified electrodes. *Journal of the Iranian Chemical Society* **2005,** *2* (1), 1-25.
278. Assumpção, M.; De Souza, R.; Rascio, D.; Silva, J.; Calegaro, M.; Gaubeur, I.; Paixão, T.; Hammer, P.; Lanza, M.; Santos, M. C. d., A comparative study of the electrogeneration of hydrogen peroxide using Vulcan and Printex carbon supports. *Carbon* **2011,** *49* (8), 2842-2851.

279. Zhang, H.; Li, Y.; Zhao, Y.; Li, G.; Zhang, F., Carbon Black Oxidized by Air Calcination for Enhanced H2O2 Generation and Effective Organics Degradation. *ACS Applied Materials & Interfaces* **2019,** *11* (31), 27846-27853.
280. Wu, K.-H.; Wang, D.; Lu, X.; Zhang, X.; Xie, Z.; Liu, Y.; Su, B.-J.; Chen, J.-M.; Su, D.-S.; Qi, W.; Guo, S., Highly Selective Hydrogen Peroxide Electrosynthesis on Carbon: In Situ Interface Engineering with Surfactants. *Chem* **2020,** *6* (6), 1443-1458.
281. Lu, Z.; Chen, G.; Siahrostami, S.; Chen, Z.; Liu, K.; Xie, J.; Liao, L.; Wu, T.; Lin, D.; Liu, Y.; Jaramillo, T. F.; Nørskov, J. K.; Cui, Y., High-efficiency oxygen reduction to hydrogen peroxide catalysed by oxidized carbon materials. *Nature Catalysis* **2018,** *1* (2), 156-162.
282. Kim, H. W.; Park, H.; Roh, J. S.; Shin, J. E.; Lee, T. H.; Zhang, L.; Cho, Y. H.; Yoon, H. W.; Bukas, V. J.; Guo, J.; Park, H. B.; Han, T. H.; McCloskey, B. D., Carbon Defect Characterization of Nitrogen-Doped Reduced Graphene Oxide Electrocatalysts for the Two-Electron Oxygen Reduction Reaction. *Chemistry of Materials* **2019,** *31* (11), 3967-3973.
283. Wang, K.; Guo, Y.; Zhang, Q., Metal–Organic Frameworks Constructed from Iron-Series Elements for Supercapacitors. *Small Structures* **2022,** *3* (5), 2100115.
284. Wang, K.; Li, Q.; Ren, Z.; Li, C.; Chu, Y.; Wang, Z.; Zhang, M.; Wu, H.; Zhang, Q., 2D Metal–Organic Frameworks (MOFs) for High-Performance BatCap Hybrid Devices. *Small* **2020,** *16* (30), 2001987.
285. Bélanger, D.; Pinson, J., Electrografting: a powerful method for surface modification. *Chemical Society Reviews* **2011,** *40* (7), 3995-4048.
286. Shi, L.; Wang, Z.; Yang, G.; Yang, H.; Zhao, F., A novel electrochemical immunosensor for aflatoxin B1 based on Au nanoparticles-poly 4-aminobenzoic acid supported graphene. *Applied Surface Science* **2020,** *527*, 146934.
287. Ahmad, N.; Kausar, A.; Muhammad, B., An investigation on 4-aminobenzoic acid modified polyvinyl chloride/graphene oxide and PVC/graphene oxide based nanocomposite membranes. *Journal of Plastic Film & Sheeting* **2015,** *32* (4), 419-448.
288. Zhu, W.; Huang, H.; Gao, X.; Ma, H., Electrochemical behavior and voltammetric determination of acetaminophen based on glassy carbon electrodes modified with poly(4-aminobenzoic acid)/electrochemically reduced graphene oxide composite films. *Materials Science and Engineering: C* **2014,** *45*, 21-28.
289. Begum, H.; Ahmed, M. S.; Kim, Y.-B., Nitrogen-rich graphitic-carbon@graphene as a metal-free electrocatalyst for oxygen reduction reaction. *Scientific Reports* **2020,** *10* (1), 12431.
290. Adenier, A.; Chehimi, M. M.; Gallardo, I.; Pinson, J.; Vilà, N., Electrochemical oxidation of aliphatic amines and their attachment to carbon and metal surfaces. *Langmuir* **2004,** *20* (19), 8243-8253.
291. Samsonowicz, M.; Hrynaszkiewicz, T.; Świsłocka, R.; Regulska, E.; Lewandowski, W., Experimental and theoretical IR, Raman, NMR spectra of 2-, 3-and 4-aminobenzoic acids. *Journal of Molecular Structure* **2005,** *744*, 345-352.
292. Stewart, J. E., Vibrational spectra of primary and secondary aliphatic amines. *The Journal of Chemical Physics* **1959,** *30* (5), 1259-1265.
293. Cinar, M.; Coruh, A.; Karabacak, M., A comparative study of selected disperse azo dye derivatives based on spectroscopic (FT-IR, NMR and UV–Vis) and nonlinear optical behaviors. *Spectrochimica Acta Part A: Molecular and Biomolecular Spectroscopy* **2014,** *122*, 682-689.
294. Liu, S.; Tian, J.; Wang, L.; Zhang, Y.; Qin, X.; Luo, Y.; Asiri, A. M.; Al-Youbi, A. O.; Sun, X., Hydrothermal Treatment of Grass: A Low-Cost, Green Route to Nitrogen-Doped, Carbon-Rich, Photoluminescent Polymer Nanodots as an Effective Fluorescent Sensing Platform for Label-Free Detection of Cu(II) Ions. *Advanced Materials* **2012,** *24* (15), 2037-2041.
295. Wu, J.; Wang, W.; Wang, Z., Porphin-Based Carbon Dots for "Turn Off–On" Phosphate Sensing and Cell Imaging. *Nanomaterials* **2020,** *10*, 326.
296. Choi, H.-J.; Jeon, I.-Y.; Kang, S.-W.; Baek, J.-B., Electrochemical activity of a polyaniline/polyaniline-grafted multiwalled carbon nanotube mixture produced by a simple suspension polymerization. *Electrochimica Acta* **2011,** *56* (27), 10023-10031.

297. Zhang, G.; Wei, Q.; Yang, X.; Tavares, A. C.; Sun, S., RRDE experiments on noble-metal and noble-metal-free catalysts: Impact of loading on the activity and selectivity of oxygen reduction reaction in alkaline solution. *Applied Catalysis B: Environmental* **2017,** *206*, 115-126.
298. San Roman, D.; Krishnamurthy, D.; Garg, R.; Hafiz, H.; Lamparski, M.; Nuhfer, N. T.; Meunier, V.; Viswanathan, V.; Cohen-Karni, T., Engineering three-dimensional (3D) out-of-plane graphene edge sites for highly selective two-electron oxygen reduction electrocatalysis. *ACS Catalysis* **2020,** *10* (3), 1993-2008.
299. Ramachandran, R.; Saranya, M.; Velmurugan, V.; Raghupathy, B. P.; Jeong, S. K.; Grace, A. N., Effect of reducing agent on graphene synthesis and its influence on charge storage towards supercapacitor applications. *Applied Energy* **2015,** *153*, 22-31.
300. Sridhar, D.; Meunier, J.-L.; Omanovic, S., Directly grown carbon nano-fibers on nickel foam as binder-free long-lasting supercapacitor electrodes. *Materials Chemistry and Physics* **2019,** *223*, 434-440.
301. Sridhar, D.; Yu, H.; Meunier, J.-L.; Omanovic, S., Carbon nano-fiber forest foundation for ruthenium oxide pseudo-electrochemical capacitors. *Materials Advances* **2020,** *1* (2), 215-227.
302. Connor, E. E.; Mwamuka, J.; Gole, A.; Murphy, C. J.; Wyatt, M. D., Gold Nanoparticles Are Taken Up by Human Cells but Do Not Cause Acute Cytotoxicity. *Small* **2005,** *1* (3), 325-327.
303. Han, J.; Liu, Y.; Guo, R., Facile Synthesis of Highly Stable Gold Nanoparticles and Their Unexpected Excellent Catalytic Activity for Suzuki−Miyaura Cross-Coupling Reaction in Water. *Journal of the American Chemical Society* **2009,** *131* (6), 2060-2061.
304. Muszynski, R.; Seger, B.; Kamat, P. V., Decorating Graphene Sheets with Gold Nanoparticles. *The Journal of Physical Chemistry C* **2008,** *112* (14), 5263-5266.
305. Osváth, Z.; Deák, A.; Kertész, K.; Molnár, G.; Vértesy, G.; Zámbó, D.; Hwang, C.; Biró, L. P., The structure and properties of graphene on gold nanoparticles. *Nanoscale* **2015,** *7* (12), 5503-5509.
306. Zhang, F.; Wang, S.; Liu, J., Gold Nanoparticles Adsorb DNA and Aptamer Probes Too Strongly and a Comparison with Graphene Oxide for Biosensing. *Analytical Chemistry* **2019,** *91* (22), 14743-14750.
307. Govindhan, M.; Amiri, M.; Chen, A., Au nanoparticle/graphene nanocomposite as a platform for the sensitive detection of NADH in human urine. *Biosensors and Bioelectronics* **2015,** *66*, 474-480.
308. Kasztelan, M.; Słoniewska, A.; Gorzkowski, M.; Lewera, A.; Pałys, B.; Zoladek, S., Ammonia modified graphene oxide – Gold nanoparticles composite as a substrate for surface enhanced Raman spectroscopy. *Applied Surface Science* **2021,** *554*, 149060.
309. Sadeghi, Z.; Shirkani, H., Highly sensitive mid-infrared SPR biosensor for a wide range of biomolecules and biological cells based on graphene-gold grating. *Physica E: Low-dimensional Systems and Nanostructures* **2020,** *119*, 114005.
310. Neves, M. A. D.; Slavkovic, S.; Churcher, Z. R.; Johnson, P. E., Salt-mediated two-site ligand binding by the cocaine-binding aptamer. *Nucleic Acids Research* **2016,** *45* (3), 1041-1048.